

01. 19.7

## Journal of Polymer Science

## Part A-1: Polymer Chemistry

## Contents

IRVING KUNTZ and W. R. KROLL: Polymerization of Epoxides with Dialkylaluminum Acetylacetonate Catalyst Systems.....	1601
RICHARD G. GRISKEY and GEORGE N. FOSTER: Melting Behavior of Ethylene Copolymers and Branched Polyethylenes.....	1623
G. G. MAHER, J. A. DOUGLAS, C. R. RUSSELL, and C. E. RIST: Crosslinking of Starch Xanthate. II. Reaction with Polyacrolein.....	1637
KYOICHIRO SHIBATANI and KIYOSHI FUJII: Reaction of Poly(vinyl Alcohol) with Formaldehyde and Polymer Stereoregularity. Model Compounds.....	1647
F. T. OSBORNE, S. OMI, V. STANNETT, and E. P. STAHEL: Radiation-Induced Solution Polymerization of Styrene in an Engineering Flow System.....	1657
M. IZU and K. F. O'DRISCOLL: Copolymerization with Depropagation. IV. Computer Simulation of Copolymerization with Reversibility.....	1675
M. IZU and K. F. O'DRISCOLL: Copolymerization with Depropagation. V. Copolymerization of $\alpha$ -Methylstyrene and Methyl Methacrylate between Their Ceiling Temperatures.....	1687
KYOICHIRO SHIBATANI, YUZURU FUJIWARA, and KIYOSHI FUJII: High-Resolution Proton Magnetic Resonance and Infrared Spectra of Poly(vinyl Formal) and Its Model Compounds.....	1693
J. P. J. HIGGINS and K. E. WEALE: Effect of High Pressures on the Cyclopolymerization of Acrylic Anhydride.....	1705
A. G. PRAMANIK and P. K. CHOUDHURY: Polyelectrolyte Behavior and Macromolecular Properties of Sodium Amylopectin Xanthate in Dilute Solution...	1713
HOWARD C. HAAS, MONIS J. MANNING, and MARTIN H. MACH: Synthetic Thermally Reversible Gel Systems. V.....	1725
F. GUTMANN: Carrier Mobility and Long-Range Order in Disordered Systems. II.	1731
JOHN N. MAJERUS: Influence of Torsional Stiffness upon Temperature Response of a Polymeric Chain.....	1737
JAN W. H. FABER and W. F. FOWLER, JR.: Substituent Effects in Free Radical Polymerization of Substituted Styrenes with Acrylates and Methacrylates...	1777
K. VENKATARAO and M. SANTAPPA: Molecular Weight Distribution in Polyacrylamide Prepared by a Photochemical Method.....	1785
I. H. COOPES: Helix Formation and Formaldehyde Crosslinking in Gelatin Solutions.....	1793
D. A. KANGAS: Polymerization of Sodium 2-Sulfoethyl Methacrylate in Aqueous Solution.....	1813
KATSUKIYO ITO: Termination Rate Constants in Radical Polymerization.....	1823

(continued inside)

Journal of Polymer Science      Part A-1: Polymer Chemistry

Board of Editors: H. Mark • C. G. Overberger • T. G. Fox

Advisory Editors:

R. M. Fuoss • J. J. Hermans • H. W. Melville • G. Smets

Editor: C. G. Overberger

Associate Editor: E. M. Pearce

Advisory Board:

T. Alfrey, Jr.	E. M. Fettes	C. S. Marvel	W. H. Sharkey
W. J. Bailey	N. D. Field	F. R. Mayo	W. R. Sorenson
D. S. Ballantine	F. C. Foster	R. B. Mesrobian	V. T. Stannett
M. B. Birenbaum	H. N. Friedlander	H. Morawetz	J. K. Stille
F. A. Bovey	K. C. Frisch	M. Morton	M. Szwarc
J. W. Breitenbach	N. G. Gaylord	S. Murahashi	A. V. Tobolsky
W. J. Burlant	W. E. Gibbs	G. Natta	E. J. Vandenberg
G. B. Butler	A. R. Gilbert	K. F. O'Driscoll	L. A. Wall
S. Bywater	J. E. Guillet	S. Okamura	F. X. Werber
T. W. Campbell	H. C. Haas	P. Pino	O. Wichterle
W. L. Carrick	J. P. Kennedy	C. C. Price	F. H. Winslow
H. W. Coover, Jr.	W. Kern	B. Rånby	M. Wismer
F. Danusso	J. Lal	J. H. Saunders	E. A. Youngman
F. R. Eirich	R. W. Lenz	C. Schuerch	

Contents (continued), Vol. 8

BUNZO EDA, KEICHI NUNOME, and MACHIO IWASAKI: Electron Spin Resonance Studies on Graft Copolymerization of Gaseous Styrene onto Preirradiated Polypropylene. I. Preirradiation in the Presence of Oxygen.....	1831
J. PRESTON and R. W. SMITH: Poly(4,4'-dipiperidyl)amides.....	1841
MASANAO OYA, KEIKICHI UNO, and YOSHIO IWAKURA: Kinetics of Polymerization of <i>N</i> -Carboxy Amino Acid Anhydride in Dimethyl Sulfoxide.....	1851
JAMES R. HOYLAND: Studies on Monomer Reactivity Ratios. III. Comparison of Various Mathematical Models.....	1863
V. S. NANDA and S. C. JAIN: Statistical Study of the Effect of Variation of Bimolecular Rate Constant in Condensation Polymerization.....	1871

(continued on inside back cover)

The Journal of Polymer Science is published in four sections as follows: Part A-1, Polymer Chemistry, monthly; Part A-2, Polymer Physics, monthly; Part B, Polymer Letters, monthly; Part C, Polymer Symposia, irregular.

Published monthly by Interscience Publishers, a Division of John Wiley & Sons, Inc., covering one volume annually. Publication Office at 20th and Northampton Sts., Easton, Pa. 18042. Executive, Editorial, and Circulation Offices at 605 Third Avenue, New York, N. Y. 10016. Second-class postage paid at Easton, Pa. Subscription price, \$325.00 per volume (including Parts A-2, B, and C). Foreign postage \$15.00 per volume (including Parts A-2, B, and C).

Copyright © 1970 by John Wiley & Sons, Inc. All rights reserved. No part of this publication may be reproduced by any means, nor transmitted, nor translated into a machine language without the written permission of the publisher.

## Polymerization of Epoxides with Dialkylaluminum Acetylacetonate Catalyst Systems\*

IRVING KUNTZ and W. R. KROLL, *Esso Research and Engineering Company Linden, New Jersey 07036*

### Synopsis

Catalyst systems for the polymerization of epichlorohydrin, propylene oxide, and allyl glycidyl ether have been prepared from pure, separately synthesized dialkylaluminum acetylacetonates ( $R_2Alacac$ ). Adding small amounts of water to  $R_2Alacac$  gives a catalyst system with enhanced activity. An even more active catalyst system for yielding high molecular weight, epichlorohydrin-containing polymers is obtained when another organometallic compound is added to the  $R_2Alacac$ -0.5 water components. The  $R_2Alacac$ -0.5 water- $R_2Zn$  system has been studied in detail. Variation in the molar proportion of water and structural changes in the chelate structure of the  $R_2Alacac$  component have been examined. Results indicate that the bis-chelate structure,  $acac(R)-Al-O-Al(R)acac$ , plays a major role in catalyst formation. A bimetallic catalyst species containing aluminum and zinc atoms is proposed, with zinc functioning primarily in monomer coordination and with aluminum involved primarily in polymer chain growth.

### INTRODUCTION

Organoaluminum compounds have frequently been used as components of catalyst systems for the polymerization of epoxides. The polymerization of propylene oxide with  $(CH_3)_3Al$ , with water as cocatalyst, has been studied in detail.<sup>1,2</sup>  $(C_2H_5)_3Al$ -water catalysts have been used to polymerize epichlorohydrin.<sup>3,4</sup> Vandenberg has reported his detailed studies of the polymerization of several epoxides using alkylaluminum-water catalyst systems.<sup>5</sup> One of the systems he describes is composed of 1.0  $R_3Al$ -0.5 water-0.5 acetylacetonate, although similar catalyst systems with equal molar amounts of  $R_3Al$  and the diketone have been employed.<sup>5</sup> In this communication we describe our results in using pure dialkylaluminum acetylacetonates,  $R_2Alacac$ , separately synthesized, as the starting material for the preparation of catalyst systems for the polymerization of propylene oxide (PO), epichlorohydrin (ECH), and allyl glycidyl ether (AGE). Experiments have been carried out with  $R_2Alacac$ -water, and with systems in which another organometallic compound was used in addition to these components.

\* Presented in part before the Akron Polymer Group, Akron, Ohio, Feb. 7, 1969 and the 4th International Conference on Organometallic Chemistry, Bristol, England, July 27-August 1, 1969, *Abstracts*, p. 8.

## EXPERIMENTAL

## Materials

**Bis(isobutyl)aluminum Acetylacetonate, Bis(ethyl)aluminum Acetylacetonate, and Bis(methyl)aluminum Acetylacetonate (I).** These were synthesized by the procedure described by Kroll and Naegele.<sup>6</sup>

**Dichloroaluminum Acetylacetonate (Cl<sub>2</sub>Alacac).** Aluminum chloride (13.3 g) and Al(acac)<sub>3</sub> (16.2 g) with 40 ml of chloroform were charged to a ball mill and reacted for 7 hr. The soluble products were isolated by centrifugation followed by vacuum distillation, bp 92–93°C/0.001 mm. The product crystallized on standing, mp 79–81°C. Infrared and NMR analyses agreed with the assigned structure.

ANAL. Calcd for C<sub>9</sub>H<sub>7</sub>Cl<sub>2</sub>O<sub>2</sub>Al: Cl, 36.0%; Al, 13.8%. Found: Cl, 35.7%; Al, 13.8%.

**1,3-Diphenyl-1,3-propanedionato-bis(methyl)aluminum (II).** A solution of dibenzoylmethane (23.7 g, 0.11 mole) in toluene (80 ml) was slowly added with stirring to an equal molar amount of (CH<sub>3</sub>)<sub>3</sub>Al in the same volume of toluene at –5°C. The addition was completed over one hour and the reaction mixture then allowed to warm to room temperature. An NMR spectrum of a portion of the solution showed that II had been formed. Removal of the solvent gave the product as a bright yellow powder (28 g) which was recrystallized from benzene, mp 126–129°C.

ANAL. Calcd for C<sub>17</sub>H<sub>17</sub>O<sub>2</sub>Al: Al, 9.6%. Found: Al, 9.6%.

**1,1,1,5,5,5-Hexafluoro-2,4-pentanedionato-bis(methyl)aluminum (III).** A solution of (CH<sub>3</sub>)<sub>3</sub>Al (7.2 g) in *n*-pentane (100 ml) was cooled to –40°C. A solution of 1,1,1,5,5,5-hexafluoro-2,4-pentanedione (20.4 g) in 100 ml pentane was slowly added. After 1 hr the reaction mixture was allowed to warm to room temperature, the pentane was then removed by distillation, and the residue distilled at reduced pressure. III was a yellow liquid with bp 55°C/153 mm. The NMR pattern agreed with the assigned structure.

ANAL. Calcd for C<sub>7</sub>H<sub>7</sub>F<sub>6</sub>O<sub>2</sub>Al: Al, 10.2%. Found: Al, 10.1%.

**Monomers and Solvents.** Benzene was distilled from calcium hydride immediately before use. Propylene oxide (3 liters) was refluxed over KOH (200 g) for 2 hr and distilled immediately; standing over KOH overnight was avoided. The distilled material was stored over CaH<sub>2</sub>, and a portion distilled from fresh CaH<sub>2</sub> immediately before use. The boiling point was carefully watched, and no material with a boiling point greater than 36°C was used. Epichlorohydrin, reagent-grade material was distilled through a 25-cm column, the first 25% of distillate being rejected. Purity by gas chromatography was at least 99.7%, and  $n_D^{20}$  1.4386 ± 0.0002.

Allyl glycidyl ether (1 allyloxy-2,3-epoxypropane) was practical grade, and was distilled at 60°C/13 mm,  $n_D^{20}$  1.4548. (Caution should be ob-

served that no light boiling material is present. We have found it necessary at times to reject up to 20% of the original material.) Diethylzinc was prepared by dilution of the commercial pure material with benzene to form a 1 *M* solution. Aluminum alkyl solutions were prepared similarly. Water was distilled water which was redistilled from an all glass apparatus.

### Polymerization

Polymerizations were carried out in glass bottles which were filled in a glove box under nitrogen. Charges were prepared in the sequence solvent, monomer,  $R_2Alacac$ , water,  $R_2Zn$  (or other organometallic) as rapidly as possible. Water was added with a Hamilton syringe. Polymerizations at elevated temperatures were carried out in a water tumbling bath in which the bottles were completely immersed. The polymeric products were isolated by precipitation into boiling water, and then dried in the vacuum oven at 40°C. In those cases where thoroughly deashed products were desired, they were treated with an excess of methanol for 24 hr, then added to a Waring Blendor with 10% hydrochloric acid-ice water, rinsed with water, and finally dried *in vacuo*.

### Polymer Characterization

Polymer solubilities were generally determined on a 2-g sample at the boiling point of the solvent in a Kumagawa apparatus (Kontes Glass Co., Cat. No. K-58610). In certain cases room temperature solubilities were determined. Inherent viscosities were determined in benzene at 25°C for PO polymers and in 1-chloronaphthalene at 135°C for ECH-containing polymers.

NMR spectra were determined at 60 MHz by using the Varian A-60 instrument. Solutions were prepared in benzene, either benzene or cyclopentane being used as an internal standard. The x-ray crystallinity measurements were made on polymer films by using a Philips diffractometer equipped with a scintillation counter and a pulse height discriminator. A curved crystal monochromator was used in the diffracted beam. Per cent crystallinity values were calculated as described by Jones.<sup>7</sup>

## RESULTS

### Effect of Catalyst Components

Table I shows the results of PO polymerization experiments with the use of  $iBu_2Alacac$ . Several conclusions can be drawn from the data. When  $iBu_2Alacac$  alone is used to initiate the polymerization, the conversion to polymer is the same as in the similar experiment with  $Et_3Al$ , but the inherent viscosity of the product is higher for the former system. Using  $iBu_2Alacac$  and  $Et_3Al$  in equal molar amounts does not increase the yield of polymer. Both the  $iBu_2Alacac$ -water and  $Et_3Al$ -water systems show a marked increase in conversion compared to the organometallic alone. The

catalyst system  $i\text{Bu}_2\text{Alacac}$ -water- $\text{Et}_3\text{Al}$ , in 1:0.5:1 molar proportions gives the highest yield of polymer with the highest inherent viscosity. With this system no heterogeneity is visible. The polymerization charge is originally water-white in color and crystal clear. At higher conversion levels the charge is yellow but still clear and transparent.

TABLE I  
Polymerization of Propylene Oxide with  $i\text{Bu}_2\text{Alacac}$  and  $\text{Et}_3\text{Al}$ <sup>a</sup>

$i\text{Bu}_2\text{Alacac}$ , mmole	Water, mmole	$\text{Et}_3\text{Al}$ , mmole	Conversion to polymer, % <sup>b</sup>	Inherent viscosity dl/g <sup>b,c</sup>
3.6	—	—	6 (8)	4.50
—	—	3.6	8	1.78
3.6	1.8	—	62 (74)	4.42
3.6	1.8	3.6	88 (88)	5.79
3.6	—	3.6	7 (6)	5.20
—	1.8	3.6	55 (47)	2.07 (2.79)

<sup>a</sup> Monomer, 0.36 mole; benzene solvent, 2 volumes/volume monomer; 50°C, 20 hr.

<sup>b</sup> Parenthetical values are for duplicate experiments.

<sup>c</sup> In benzene at 25°C.

The data in Table II where  $\text{Et}_2\text{Zn}$  was used with the  $i\text{Bu}_2\text{Alacac}$  are qualitatively similar to those when  $\text{Et}_3\text{Al}$  was employed. Diethylzinc alone is inactive, while  $\text{Et}_3\text{Al}$  does show some activity. When used with water,  $\text{Et}_2\text{Zn}$  is less active than  $\text{Et}_3\text{Al}$ . One different observation is that  $i\text{Bu}_2\text{Alacac}$ - $\text{Et}_2\text{Zn}$  does give a significant yield of polymer, about five times the yield observed with the corresponding  $\text{Et}_3\text{Al}$  system. The three-component catalyst system,  $\text{R}_2\text{Alacac}$ -water- $\text{Et}_2\text{Zn}$  gives about the same conversion to polymer as the corresponding system with  $\text{Et}_3\text{Al}$  but the inherent viscosity of the polymer obtained was significantly lower in this case.

TABLE II  
Polymerization of Propylene Oxide with  $i\text{Bu}_2\text{Alacac}$  and  $\text{Et}_2\text{Zn}$ <sup>a</sup>

$i\text{Bu}_2\text{Alacac}$ , mmole	Water, mmole	$\text{Et}_2\text{Zn}$ , mmole	Conversion to polymer, %	Inherent viscosity, dl/g <sup>b</sup>
3.6	—	—	6 (8)	4.50
—	—	3.6	0	—
—	1.8	3.6	21	3.92
3.6	1.8	3.6	94	2.70
3.6	1.8	—	62 (74)	4.42
3.6	—	3.6	36 (30)	1.75

<sup>a</sup> Conditions as in Table I.

<sup>b</sup> In benzene, 25°C.

Table III shows the results obtained when the various components of the catalyst systems described so far are used singly and in various combinations to terpolymerize ECH, PO, and AGE. In these experiments

$i\text{Bu}_2\text{Alacac}$  alone was inactive in terpolymerization; with  $i\text{Bu}_2\text{Alacac}$ -water a small yield of terpolymer was obtained.  $\text{Et}_2\text{Zn}$  alone or with water is inactive for the preparation of terpolymer; the  $\text{Et}_2\text{Zn}$ -water catalyst is effective for the preparation of copolymers of PO but ECH is an epoxide more difficult to polymerize. When  $\text{Et}_2\text{Zn}$  is used with  $i\text{Bu}_2\text{Alacac}$ , a small yield of terpolymer is obtained. When the three components are used ( $i\text{Bu}_2\text{Alacac}$ , water, and  $\text{Et}_2\text{Zn}$ ), a major increase in polymer yield is obtained and a terpolymer of significantly higher inherent viscosity is obtained. This three-component system has been studied in some detail.

TABLE III  
Effect of Catalyst Components in Terpolymerization<sup>a</sup>

$i\text{Bu}_2\text{Alacac}$ , mmole	Water, mmole	$\text{Et}_2\text{Zn}$ , mmole	Conversion to polymer, %	Inherent viscosity, dl/g <sup>b</sup>
3.6	—	—	0	—
—	—	3.6	0	—
3.6	1.8	—	5	1.43
—	1.8	3.6	0	—
3.6	1.8	3.6	26	4.15
3.6	—	3.6	3	2.12

<sup>a</sup> Polymerization of 0.2 mole epichlorohydrin, 0.1 mole propylene oxide, and 0.018 mole allyl glycidyl ether in 50 ml benzene at 50°C for 20 hr.

<sup>b</sup> Determined at 135°C in 1-chloronaphthalene, concentration 0.1 g/dl.

$\text{Cl}_2\text{Alacac}$  was used in a set of terpolymerization experiments, under conditions similar to those described in Table III. When used alone, with half a molar equivalent of water, or with an equal molar amount of  $\text{Et}_2\text{Zn}$ , no conversion to polymer was observed.

### Effect of Alkyl Component

Other organometallic compounds were substituted for  $\text{Et}_2\text{Zn}$  in making up the  $\text{R}_2\text{Alacac}$ -water- $\text{Et}_2\text{Zn}$  catalyst system in a limited series of experiments. Figure 1 shows the results obtained when various organometallic compounds were used with  $i\text{Bu}_2\text{Alacac}$  and  $\text{Et}_2\text{Alacac}$ . In these terpolymerization experiments the molar ratio of  $\text{R}_2\text{Alacac}$  to water was 1:0.5, and the organometallic under test was used in a molar amount equal to the  $\text{R}_2\text{Alacac}$  component. With regard to relative activity in producing polymer several trends can be distinguished from these experiments. In the organoaluminum series the trialkylaluminums are more reactive than the alkylaluminum dihalides. The  $i\text{Bu}_3\text{Al}$  derivative is most reactive among the alkylaluminum compounds tested. Grignard reagents are inactive, while  $\text{Et}_2\text{Cd}$  shows good activity. We find it convenient to refer to the organometallic compound, used in conjunction with the  $\text{R}_2\text{Alacac}$ -water components, as a cocatalyst.

Although Figure 1 shows that many cocatalyst components may be used to produce good yields of terpolymer, there are real differences in the nature

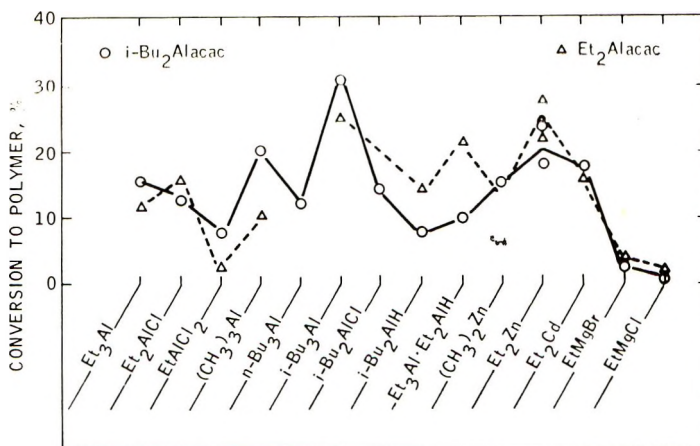


Fig. 1. Varied cocatalysts used with the R<sub>2</sub>Alacac-water catalyst. Terpolymerization experiments as described in Fig. 2. 3.6 mmole R<sub>2</sub>Alacac, 1.8 mmole water, 3.6 mmole of the organometallic tested.

of the polymer produced. This is shown by the data in Table IV, where the ECH-AGE copolymers obtained by using Et<sub>3</sub>Al contain almost half as much ether-soluble as ether-insoluble product; the ether-soluble material is of very low molecular weight as indicated by the inherent viscosity value. The experiment with Et<sub>2</sub>Zn gives almost no ether-soluble product, and the inherent viscosity of the ether-insoluble polymer it does produce is significantly higher than that produced by Et<sub>3</sub>Al.

The data in Table V show results for the homopolymerization of epichlorohydrin. It is seen that a polymer with higher inherent viscosity is obtained with Et<sub>2</sub>Zn as cocatalyst than when Et<sub>3</sub>Al is used. The extraction with boiling acetone indicates that a less soluble product is obtained with Et<sub>2</sub>Zn than with Et<sub>3</sub>Al.

These data show that in the preparation of ECH copolymers or terpolymers, the use of Et<sub>2</sub>Zn as the cocatalyst component in addition to R<sub>2</sub>Alacac-

TABLE IV  
Effect of Cocatalyst on ECH Copolymer Type<sup>a</sup>

iBu <sub>2</sub> - Alacac, mmole	Water, mmole	Et <sub>3</sub> Al, mmole	Et <sub>2</sub> Zn, mmole	Ether-soluble polymer		Ether-insoluble polymer	
				Yield, % <sup>b</sup>	Inherent viscosity, dl/g <sup>c</sup>	Yield, % <sup>b</sup>	Inherent viscosity, dl/g <sup>c</sup>
7.2	3.6	7.2	—	21	0.03	45	2.7
7.2	3.6	—	7.2	3	—	51	4.8

<sup>a</sup> 0.32 mole ECH, 0.019 mole AGE, 50 ml benzene.

<sup>b</sup> After 20 hr at 50°C.

<sup>c</sup> In 1-chloronaphthalene, 135°C.



TABLE V  
Effect of Cocatalyst on ECH Homopolymer Type<sup>a</sup>

iBu <sub>2</sub> Alacac, mmole	Water, mmole	Et <sub>3</sub> Al, mmole	Et <sub>2</sub> Zn, mmole	Polymer yield, % <sup>b</sup>	Inherent viscosity, dl/g <sup>c</sup>	Acetone solubility, wt-% <sup>d</sup>
3.6	1.8	3.6	—	72	2.25	33
3.6	1.8	—	3.6	74	3.26	11

<sup>a</sup> 0.32 mole ECH, 50 ml benzene.

<sup>b</sup> After 20 hr at 50°C.

<sup>c</sup> In 1-chloronaphthalene at 135°C.

<sup>d</sup> Determined in a Kumagawa apparatus at the boiling point.

water always seems to yield a higher molecular weight, less soluble product than is obtained with Et<sub>3</sub>Al.

### Effect of Water Concentration

The data in Tables I-III show how marked an effect water has on polymer yield and molecular weight. Terpolymerization experiments were

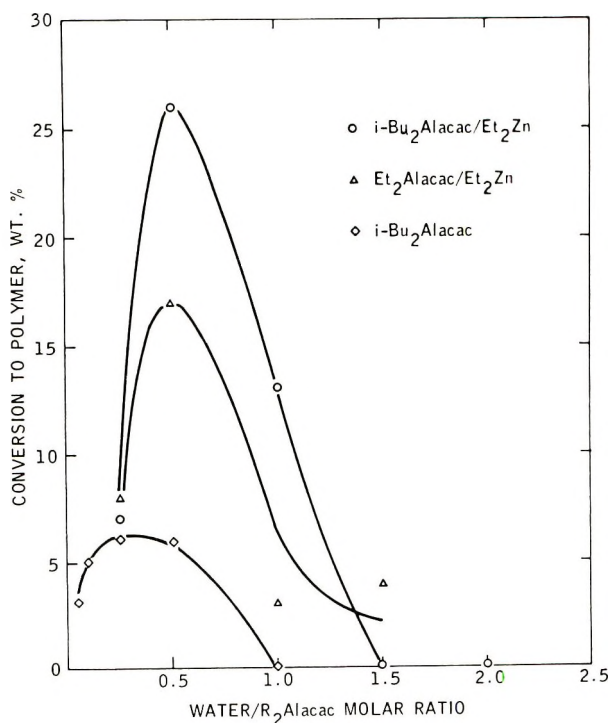


Fig. 2. Effect of water concentration on catalyst activity. Experiments were carried out with 3.6 mmole of R<sub>2</sub>Alacac and Et<sub>2</sub>Zn and varied amounts of water. Terpolymerization of 0.2 mole ECH, 0.1 mole PO, and 0.018 mole of AGE were carried out in 50 ml benzene at 50°C for 22 hr. Diamond data points were for the iBu<sub>2</sub>Alacac-water catalyst.

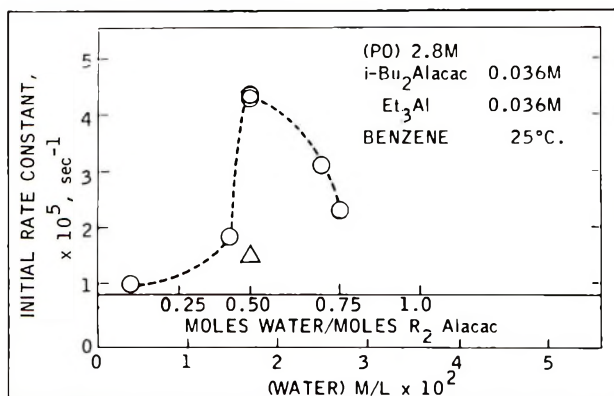


Fig. 3. Rate constants as a function of water concentration. Dilatometric initial pseudo-first-order rate constants at 25°C. Reactant concentrations were PO 2.8 *M*, *i*Bu<sub>2</sub>Alacac 0.036 *M*, Et<sub>3</sub>Al 0.036 *M* in benzene. The triangle data point is for an experiment where ECH was used instead of PO.

carried out to determine the water concentration necessary for maximum catalyst activity. The results of several series of experiments are shown in Figure 2. In one series of experiments R<sub>2</sub>Alacac and Et<sub>2</sub>Zn were used in equal molar concentrations and the concentration of water was varied. One set of experiments was carried out with Et<sub>2</sub>Alacac, another with *i*Bu<sub>2</sub>Alacac. In another series of experiments no Et<sub>2</sub>Zn was used, and the role of water in the *i*Bu<sub>2</sub>Alacac–water catalyst system was studied.

Figure 2 shows the marked sensitivity to water concentration in the terpolymerization of ECH–PO–AGE with the R<sub>2</sub>Alacac–Et<sub>2</sub>Zn–water system. With both *i*Bu<sub>2</sub>Alacac and Et<sub>2</sub>Alacac systems the maximum conversion to polymer was observed when the molar proportions were 1:1:0.5. With the *i*Bu<sub>2</sub>Alacac–water catalyst system the sensitivity to water concentration is less, and when the molar ratio of *i*Bu<sub>2</sub>Alacac–water was in the range of 1:0.125 to 1:0.6 the conversion levels were experimentally indistinguishable.

A similar dependency on water concentration was seen in another series of experiments. The kinetics of the polymerization of PO at 25°C with the *i*Bu<sub>2</sub>Alacac–Et<sub>3</sub>Al–water catalyst system were measured by using dilatometric techniques. Only initial rates were considered and with constant monomer, *i*Bu<sub>2</sub>Alacac and Et<sub>3</sub>Al concentrations pseudo-first-order rate constants were calculated as the concentration of water was varied. These experiments were carried out by using a very dilute standard solution of water in benzene to adjust to the desired water concentration. The results of these experiments are collected in Table VI and also are shown in Figure 3. The curve shows a fourfold increase in rate constant as the molar ratio of water to R<sub>2</sub>Alacac is increased from 0.1 to 0.5. Maximum rate constant is observed when the water:R<sub>2</sub>Alacac ratio is 0.5. Note that the fact that Et<sub>3</sub>Al was used as cocatalyst in these experiments, instead of the Et<sub>2</sub>Zn used for the data presented in Figure 1, has not changed the

dependency on water concentration. These proportions of water are such that many metal-carbon bonds must remain the active catalyst. We will discuss this point in more detail later.

The triangular data point in Figure 3 shows the rate constant obtained when ECH at the same molar concentration was substituted for PO. The rate constant is approximately  $1/4$  that observed for propylene oxide.

TABLE VI  
Kinetic Study of  $i\text{Bu}_2\text{Alacac-Et}_2\text{Al-Water}$  Catalyst<sup>a</sup>

[Water], $\times 10^2, M$	Molar ratio water/ $R_2\text{Alacac}$	$k \times 10^5$ $\text{sec}^{-1b}$
0.36	0.10	0.98
1.4	0.39	1.7
1.8	0.50	4.3
1.8	0.50	4.4
2.5	0.69	3.1
2.7	0.75	2.3

<sup>a</sup> PO 2.8  $M$  in benzene, 25°C,  $i\text{Bu}_2\text{Alacac}$  0.036  $M$ ,  $\text{Et}_2\text{Al}$  0.036  $M$ .

<sup>b</sup> Initial pseudo-first-order rate constant.

Some other qualitative observations with regard to water in this catalyst system are of interest. In our experience, when we prepared a catalyst from  $\text{Et}_2\text{Zn}$ -water some white insoluble material was always produced. With the three-component catalyst system, where the order of mixing was solvent, monomers,  $R_2\text{Alacac}$ , water,  $\text{Et}_2\text{Zn}$ , no heterogeneity was observed.

### Catalyst Stoichiometry Studies

The  $R_2\text{Alacac-water-R}_2\text{Zn}$  catalyst systems previously discussed have used  $R_2\text{Alacac}$  and  $\text{Et}_2\text{Zn}$  at one equal molar concentration. In an attempt to elucidate the stoichiometry involved in catalyst formation a series of experiments were carried out in which two concentrations of  $i\text{Bu}_2\text{Alacac}$  and  $\text{Et}_2\text{Zn}$  were employed and three different levels of water. The results obtained in this series of ECH homopolymerizations are shown in Figure 4. Random replicate experiments carried out in these studies are shown on the figure, and give an indication of the precision of our results.

We are fully aware of the experimental problems involved in precisely controlling the small amounts of water used in this series of experiments, and those used in the previous studies of the role of water in catalyst formation. Caution should be used in interpreting these results. However, in the experiments shown in Figure 4 if the ECH monomer and benzene solvent each contained 10 ppm of water, they would contribute 0.04 mmole of water in addition to that added, at the 100 ppm level they would add 0.4 mmole of water in addition to that deliberately added. If present, these additional amounts of water would still permit certain conclusions to be drawn.

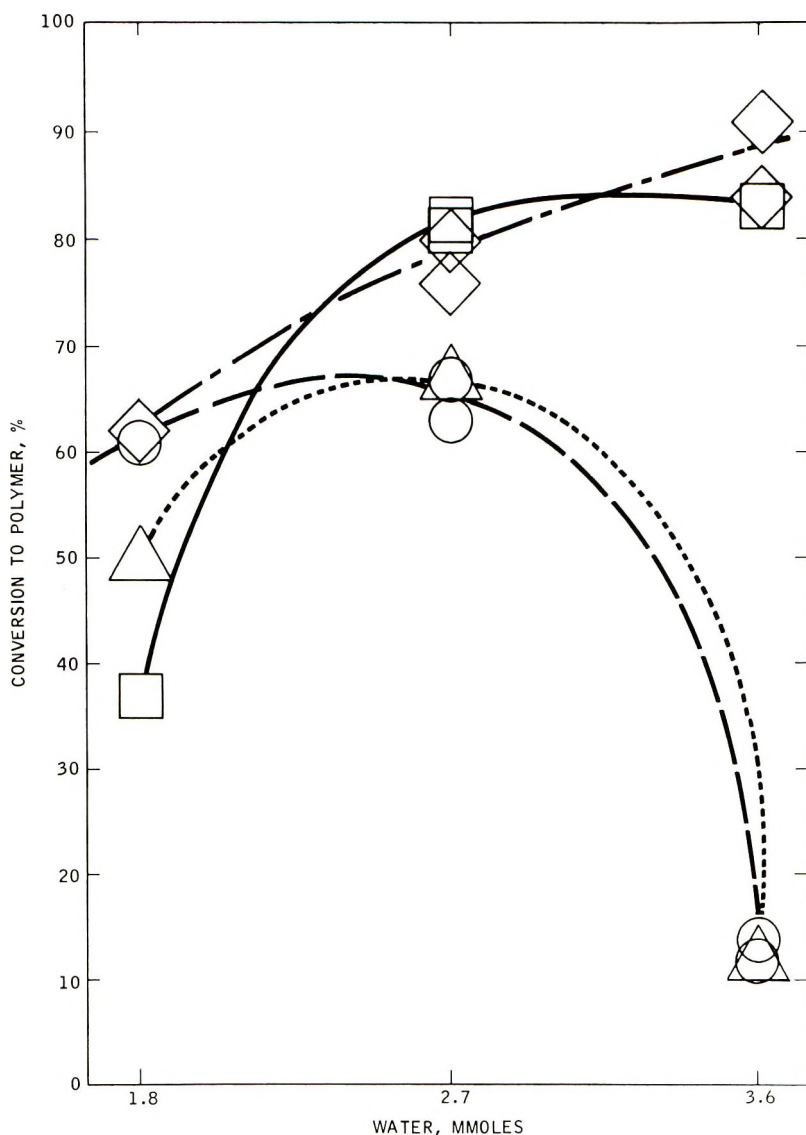


Fig. 4. Catalyst Stoichiometry Studies. ECH (0.32 mole) homopolymerizations in benzene (50 ml) at 50°C for 20 hr. Water concentrations as shown, (□) 3.6 mmole  $\text{Et}_2\text{Zn}$ , 5.4 mmole  $i\text{Bu}_2\text{Alacac}$ ; (○) 3.6 mmole  $\text{Et}_2\text{Zn}$ , 3.6 mmole  $i\text{Bu}_2\text{Alacac}$ ; (Δ) 5.4 mmole  $\text{Et}_2\text{Zn}$ , 3.6 mmole  $i\text{Bu}_2\text{Alacac}$ ; (◇) 5.4 mmole  $\text{Et}_2\text{Zn}$ , 5.4 mmole  $i\text{Bu}_2\text{Alacac}$ .

The data show that when the molar amount of water is equal to that of the  $i\text{Bu}_2\text{Alacac}$ , as in the 3.6  $i\text{Bu}_2\text{Alacac}$ -3.6 water-3.6  $\text{Et}_2\text{Zn}$  and 3.6  $i\text{Bu}_2\text{Alacac}$ -3.6 water-5.4  $\text{Et}_2\text{Zn}$  experiments, (numbers are millimoles of reagent), catalyst systems of low activity are obtained.

The absolute concentration level of the reagents has an effect. The system 5.4  $i\text{Bu}_2\text{Alacac}$ -2.7 water-5.4  $\text{Et}_2\text{Zn}$  gives a higher yield of polymer

than the 3.6-1.8-3.6 ratio system, although the molar ratio of the components is the same in both cases.

The level of  $\text{Et}_2\text{Zn}$  has less effect than the  $i\text{Bu}_2\text{Alacac}$  concentration. Figure 5 where the abscissa is expressed as the water/ $i\text{Bu}_2\text{Alacac}$  ratio, shows the pattern which indicates the primary role of  $i\text{Bu}_2\text{Alacac}$  concentration. A similar graph in terms of the water/ $\text{Et}_2\text{Zn}$  ratio is less regular. These results show that  $\text{R}_2\text{Alacac}$  and water concentrations play the primary role in determining polymerization activity.

The ECH homopolymers prepared in the experiments shown in Figure 4 had inherent viscosities from 4.3 to 6.9 dl/g; 58% of the samples had inherent viscosities from 5.2 to 5.5 dl/g. The x-ray crystallinity values varied from 35 to 47%; 61% of the samples had crystallinity values between 39 and 43%.

### Specific Structure Effects

Various experiments permit conclusions to be made regarding specific structure effects in the  $\text{R}_2\text{Alacac}-\text{Et}_2\text{Zn}$ -water catalyst system. Terpolymerization experiments have been carried out with the use of  $(\text{CH}_3)_2\text{Alacac}$ ,  $\text{Et}_2\text{Alacac}$ ,  $i\text{Bu}_2\text{Alacac}$ , and  $\text{Cl}_2\text{Alacac}$  as the  $\text{R}_2\text{Alacac}$  catalyst component. The  $(\text{CH}_3)_2\text{Alacac}$  and  $i\text{Bu}_2\text{Alacac}$  were very similar in their catalyst behavior. Generally, the  $\text{Et}_2\text{Alacac}$  compound was less active. The  $\text{Cl}_2\text{Alacac}$  compound was completely inactive. These results show that polymerization activity demands a C-Al bond in the starting chelate.

Most of our experiments were carried out with the conventional acetylacetonate derivative. However, experiments were also carried out in which the chelate moiety was varied for a series of dimethylaluminum derivatives. In this series  $(\text{CH}_3)_2\text{Alacac}$ , I, the hexafluoro derivative, III, and the diphenyl analog, II were studied. The steric features for I and III should be very similar. Literature studies of metal chelates show that the hexafluorodiketone derivative is a stronger electron withdrawing group than the corresponding hydrogen containing diketone.<sup>8</sup> Guided by chelate stability constants for simple metal derivatives,<sup>8</sup> we would estimate the electropositive nature of aluminum to decrease in the sequence  $\text{III} > \text{I} > \text{II}$ .

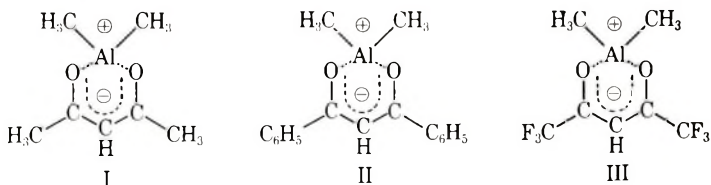


Table VII shows the results with the three chelates in the homopolymerization of ECH with the use of chelate-0.5 water catalyst systems. The hexafluoro compound, III, gives high yields of product but of very low molecular weight (as indicated by solubility on extraction with benzene, and inherent viscosity); it behaves very much like the  $\text{Et}_2\text{Al}$ -water catalyst, often considered cationic in nature.<sup>9</sup> The conventional  $(\text{CH}_3)_2$ -

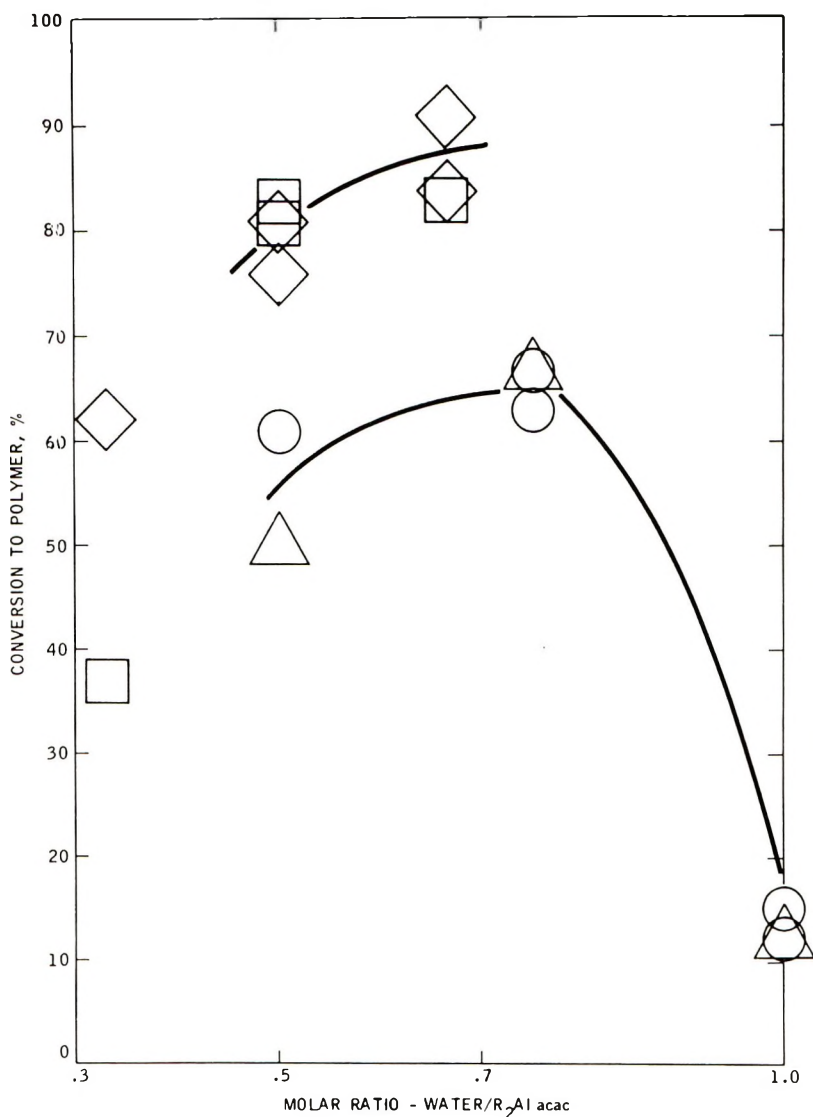


Fig. 5. Catalyst Activity As Function of Water/R<sub>2</sub>Al acac Ratio. Polymerization conditions and data point as discussed in Figure 4.

Alacac catalyst, I, shows the low solubility and high inherent viscosity shown in the earlier results; the product is essentially insoluble in benzene. The diphenyl analog, II, is similar to I, but shows a higher conversion to polymer.

Table VIII shows results for the chelate—0.5 water—Et<sub>2</sub>Zn catalyst system. The variation in conversion to polymer is reduced in these experiments. However, again the fluoro compound, III, gives a completely benzene-soluble product of low inherent viscosity. The diphenyl deriv-

TABLE VII  
Chelate Structure Effects in ECH Homopolymerizations with  
Chelate-Water Catalyst Systems<sup>a</sup>

	Chelate			
	Et <sub>3</sub> Al	III	II	I
Relative conversion to polymer	14	11	1.3	1.0
Polymer solubility, % <sup>b</sup>				
Benzene	80	100	—	5
Acetone	95	—	60	35
Inherent viscosity, dl/g				
Total polymer				
Benzene, 25°C	0.15	0.24	—	—
1-Chloronaphthalene, 135°C	0.40	—	2.2	4.3
Fractions <sup>c</sup>				
Acetone-soluble	0.19	—	0.47	2.2
Acetone-insoluble	0.84	—	2.8	2.8

<sup>a</sup> 1.8 mmoles chelate (or R<sub>3</sub>Al), 0.9 mmoles water; 0.16 mmole ECH, 25 benzene, 50°C, 21.5 hr.

<sup>b</sup> Extracted continuously at the boiling point in a Kumagawa apparatus, 24 hr.

<sup>c</sup> In 1-chloronaphthalene at 135°C, 0.05 g/dl concentration.

TABLE VIII  
Chelate Structure Effects in ECH Homopolymerization with Chelate-Water-Et<sub>2</sub>Zn  
Catalyst System<sup>a</sup>

	Chelate		
	III	II	I
Relative conversion to polymer (I in Table VII equal 1.0)	12	7.0	5.0
Polymer solubility, %			
Benzene	97	—	—
Acetone	—	60	40
Inherent viscosity, dl/g			
Total polymer			
Benzene, 25°C	0.25	—	—
1-Chloronaphthalene, 135°C	—	2.6	1.9
Fractions <sup>b</sup>			
Acetone-soluble	—	0.55	0.16
Acetone-insoluble	—	2.6	2.3

<sup>a</sup> 1.8 mmole chelate, 1.8 mmole Et<sub>2</sub>Zn, 0.9 mmole water; polymerization under same conditions as for Table VII.

<sup>b</sup> In 1-chloronaphthalene, 135°C, 0.05 g/dl concentration.

ative, II, and I give poly(ECH) which is largely insoluble in acetone. II, while giving higher conversion to polymer, seems to give a more acetone-soluble product than I.

#### Polymerization Rate and Temperature Effects

Experiments were carried out to study the polymerization rate with a ECH-PO-AGE monomer feed. Replicate charges were prepared and

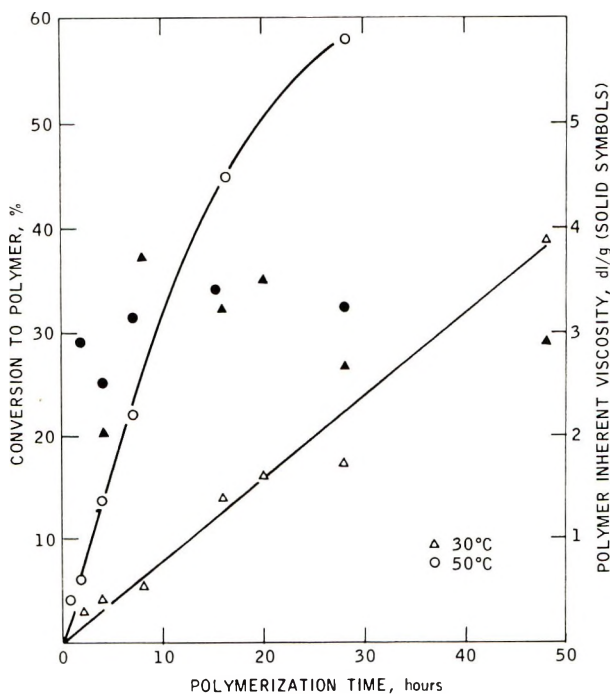


Fig. 6. Terpolymerization Rates and Inherent Viscosity. Molar concentrations in benzene were ECH 2.9, PO 1.45, AGE 0.26,  $i\text{Bu}_2\text{Alacac}$  0.052,  $\text{Et}_2\text{Zn}$  0.052, water 0.026; conversion at ( $\Delta$ ) 30°C and ( $\circ$ ) 50°C; inherent viscosities determined at 135°C in 1-chloronaphthalene for the ( $\blacktriangle$ ) 30°C and ( $\bullet$ ) 50°C polymer.

reacted for various times at 30 and 50°C. These results are shown in Figure 6. From these data, an estimate of the enthalpy of polymerization would be 14 kcal/mole.

The inherent viscosity of the various samples was determined, and results are shown in Figure 6. At both temperatures polymers of high inherent viscosity were obtained at low conversions; the inherent viscosity of the polymer produced is not particularly sensitive to conversion level.

### Nonterminated Polymerizations

Experiments were carried out to determine if the  $\text{R}_2\text{Alacac-R}_2\text{Zn}$ -water catalyst system gave long-lived polymerization species. Several replicate monomer charges were prepared and reacted so that complete conversions to polymer took place. One of the replicate charges was then terminated, fresh monomer was then added to the others, time was allowed for further polymerization, and the process then repeated.

Figure 7 shows the results of these experiments and indicates the catalyst systems being studied are long-lived. Fresh PO monomer added 102 hr after the reaction was started was completely converted to polymer. The intrinsic viscosity measurements shown for the three charges show that while conversion to polymer is complete the monomer added in the



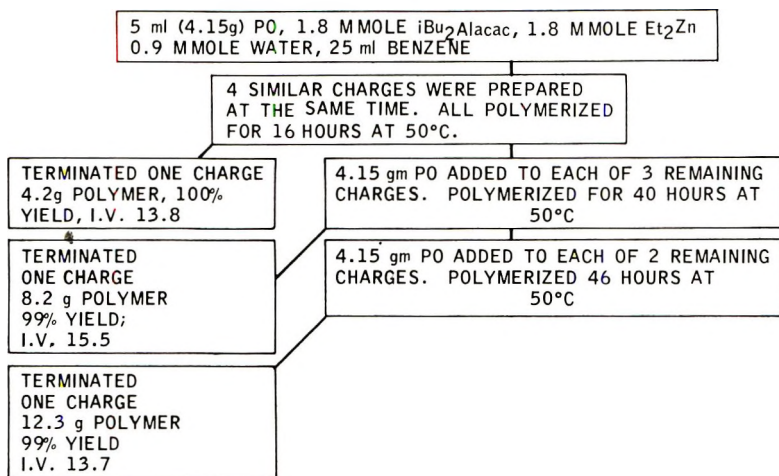


Fig. 7. Nonterminated polymerizations. See discussion in text.

later stages was not incorporated into the same macromolecules; if it were the intrinsic viscosity should continually increase.

This point was confirmed in experiments in which ECH was the monomer added in one of the later stages of an experiment started with PO. If the monomer was incorporated into "living" macromolecules, all polymer should have the same composition. Fractionation by solubility of the polymer of this experiment gave fractions with significant variation in chlorine content. We conclude from these experiments that we are deal-

TABLE IX  
X-Ray Examination of ECH-PO-AGE Terpolymers<sup>a</sup>

$(\text{ECH})_{.60}(\text{PO})_{.35}(\text{AGE})_{.05}$		$(\text{ECH})_{.60}(\text{PO})_{.35}(\text{AGE})_{.06}$		$(\text{ECH})_{.60}(\text{PO})_{.39}(\text{AGE})_{.01}$		Poly(ECH) <sup>b</sup>	
<i>d</i>	Relative intensity	<i>d</i>	Relative intensity	<i>d</i>	Relative intensity	<i>d</i>	Relative intensity
spacings, Å	<i>I</i>	spacings, Å	<i>I</i>	spacings, Å	<i>I</i>	spacings, Å	<i>I</i>
9.3	16	9.19	4.2	9.46	5.4		
7.1	0.8						
4.67	1.7						
4.54	2.6	4.50	2.1	4.55	7.9	4.57	57
3.113	11	3.099	2.1	3.11	4.2	3.86	14
				3.039	1.3	3.13	15
2.818	1.5	2.73	1.2	2.83	1.0	3.05	12
2.6	1.2	2.47	1.04	2.5	1.0		
Crystallinity, %	8.7		3.5		8.1		36

<sup>a</sup> Subscripts indicate copolymer stoichiometry.

<sup>b</sup> Isida has reported<sup>10</sup> 4.5 Å strong, 3.83 Å medium, and 3.09 Å weak.

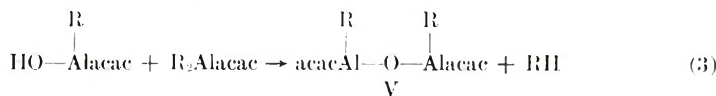
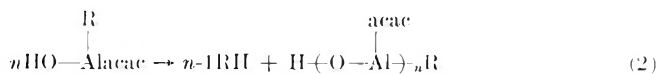
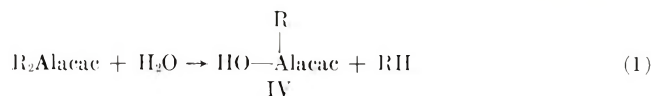
ing with long-lived catalyst species but that chain transfer or termination can take place to a considerable degree.

### Polymer Structure

A detailed analysis of the copolymerization behavior observed and characterization of the polymers obtained with the catalyst systems described in this publication is the subject of another planned publication. However, several features of the polymers and copolymers prepared can be described here. The ECH polymers prepared with the  $R_2Alacac-R_2Zn$ -water catalyst show crystallinity to the x-ray, as previously mentioned. The degree of crystallinity parallels the solubility behavior of the polymer; the insoluble residue from a Kumagawa extraction shows a higher x-ray crystallinity than the starting whole polymer. Fractionation of ECH containing copolymers and chlorine analysis of the fractions indicates that the various molecular weight components are compositionally homogeneous. Table IX shows x-ray results for various homo- and copolymers.

### DISCUSSION

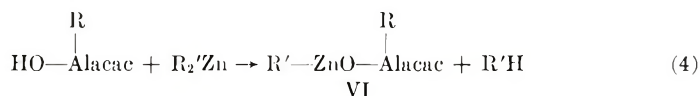
The details of the active catalyst species derived from organometallic compounds which are effective for the polymerization of epoxides to high molecular weight polymers are not clearly known.<sup>11</sup> Our observations permit us to make certain conclusions regarding the chemical pathways which lead to the active catalyst species in the system we have studied. Considering first the  $R_2Alacac$ -water system, we observed that polymerization took place if the ratio water/ $R_2Alacac$  ratio was less than one. The reaction between  $R_2Alacac$  and an equal molar amount of water is shown in eq. (1). Our observations indicate that if all the  $R_2Alacac$  is converted



to IV, inactive polymerization systems are obtained. IV may react further as shown in eq. (2). If less than a molar equivalent of water is present, then the production of the bridged chelate structure V becomes possible. We conclude that structure V is a necessary precursor for active catalyst production in the  $R_2Alacac$ -water system.

With the  $R_2Alacac$ -water- $R_2Zn$  system we found that a controlling parameter was the water/ $R_2Alacac$  ratio, independent of the amount of  $R_2Zn$  present. When the water/ $R_2Alacac$  ratio was unity, low conversion

to polymer was observed; under such conditions we would anticipate the production of VI. We conclude that VI is not involved in formation of the most active catalyst species.



Rather, our observations indicate that V is still an essential feature for active catalyst production in the  $\text{R}_2\text{Alacac}$ -water- $\text{Et}_2\text{Zn}$  system, and that the  $\text{Et}_2\text{Zn}$  modifies the basic structural features of the  $\text{R}_2\text{Alacac}$ -water system. This hypothesis was tested in experiments in which  $\text{iBu}_2\text{Alacac}$  was prereacted with half a molar equivalent of water for several hours, then  $\text{Et}_2\text{Zn}$  and ECH monomer were added and polymerization then carried out. In another experiment  $\text{Et}_2\text{Zn}$  was reacted with water in the first step. These experiments are shown in Figure 8. The results obtained support the hypothesis; prereacting  $\text{iBu}_2\text{Alacac}$  under conditions to form the bis-chelate structure V, and then adding  $\text{Et}_2\text{Zn}$  gives a yield of polymer essentially identical to those obtained in a conventional polymerization (A and C in Fig. 8). Reacting  $\text{Et}_2\text{Zn}$  with water under conditions to form  $\text{RZn-OZnR}$  type derivatives and then adding  $\text{R}_2\text{Alacac}$  gives a catalyst system of low activity.

The incorporation of the  $\text{R}_2\text{Zn}$  component in the active catalyst species, we believe, involves the oxygen atom of the Al-O-Al bridge. Constructing a Stuart-Briegleb model of  $\text{R}_2\text{Alacac}$  shows this oxygen atom to be available

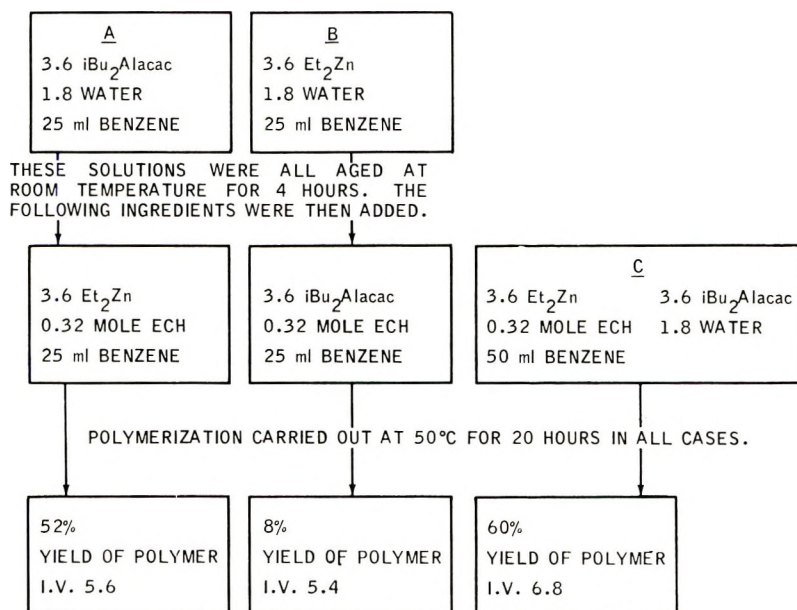


Fig. 8. Aging experiments with water. The numbers refer to the amount of the catalyst components in millimoles.

for coordination (Fig. 9). The ability of dialkylzinc compounds to form coordination complexes with ethers is well known.<sup>12</sup>

Based on previous work we believe the acetylacetonate chelate structure persists in the active catalyst species.<sup>6</sup> In the present work we have examined the NMR spectra of equal molar mixtures of  $(\text{CH}_3)_2\text{Alacac}$  and  $(\text{CH}_3)_2\text{Zn}$ , and of  $i\text{Bu}_2\text{Alacac}$  and  $\text{Et}_2\text{Zn}$ , in benzene. As shown in Table X the NMR spectra showed a one-to-one correspondence between the peaks in the mixture and of those of the individual components. Further, the peaks of the 3-hydrogen and the methyl groups of the chelate ring showed no

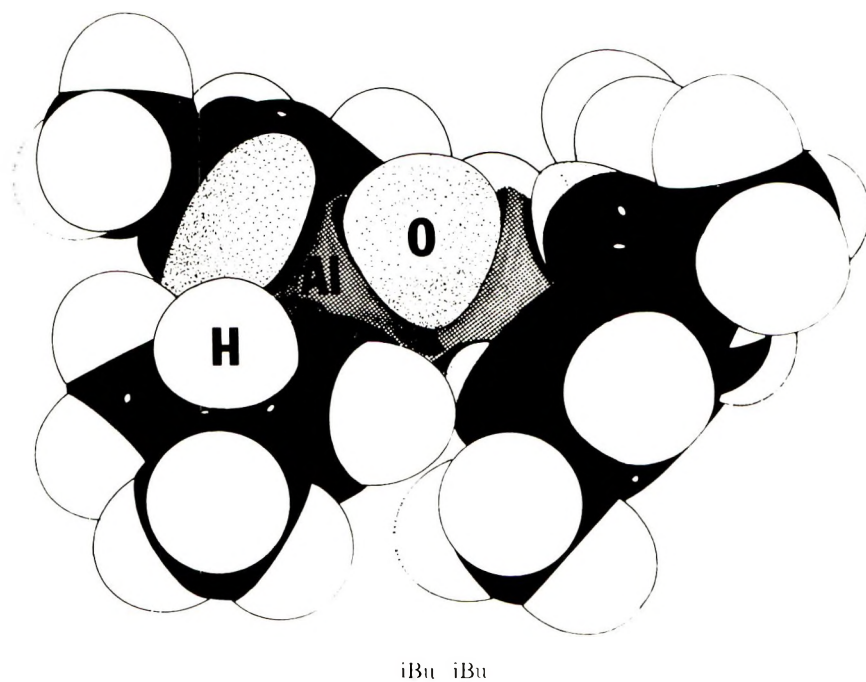
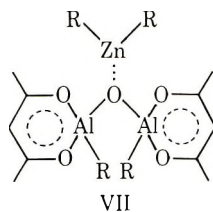


Fig. 9. Stuart Briegleb Model of  $\text{acac-Al-O-Alacac}$ . In the sketch of the model the individual carbon atoms have not been shown.

change in multiplicity. Both peaks were singlets in the mixture as in the individual components; if ring opening of the chelate had occurred, the resulting structure would have led to splitting of these resonances.

We conclude that structure VII plays an important role in the formation of the active catalyst species. The effect of varied concentrations of  $\text{R}_2\text{Zn}$  is in the amount of VII formed. V must compete for  $\text{R}_2\text{Zn}$  with the large amount of epoxide monomer present in the coordination reaction to form VII. Increasing concentration of  $\text{R}_2\text{Zn}$  should increase the amount of VII present.



Vandenberg early recognized that two or more metal atoms must be involved in the active catalyst species.<sup>5</sup> Price and Spector have come to the same conclusion.<sup>13</sup> We believe structure VII is the precursor of such a species with the  $R_2Alacac$ -water- $R_2Zn$  catalyst system.

Polymerization takes place by a coordination mechanism.<sup>5</sup> Two mechanistic processes can be identified: epoxide monomer coordination and an anionic ring-opening displacement reaction by the macromolecular alkoxy fragment bound to metal.

We believe that in the  $R_2Alacac$ -water- $R_2Zn$  catalyst system a separation of chemical function can take place. Under our conditions we found the  $Et_2Zn$ -water catalyst system ineffective for preparing interpolymers of ECH. Therefore, we speculate that in the active catalyst species zinc atoms may play a major role in monomer coordination, and aluminum a major role in chain growth. Schematically, we can formulate this mechanism for propagation as shown in eq. (5), where OR is a polymer residue, and five-coordinate aluminum is involved.

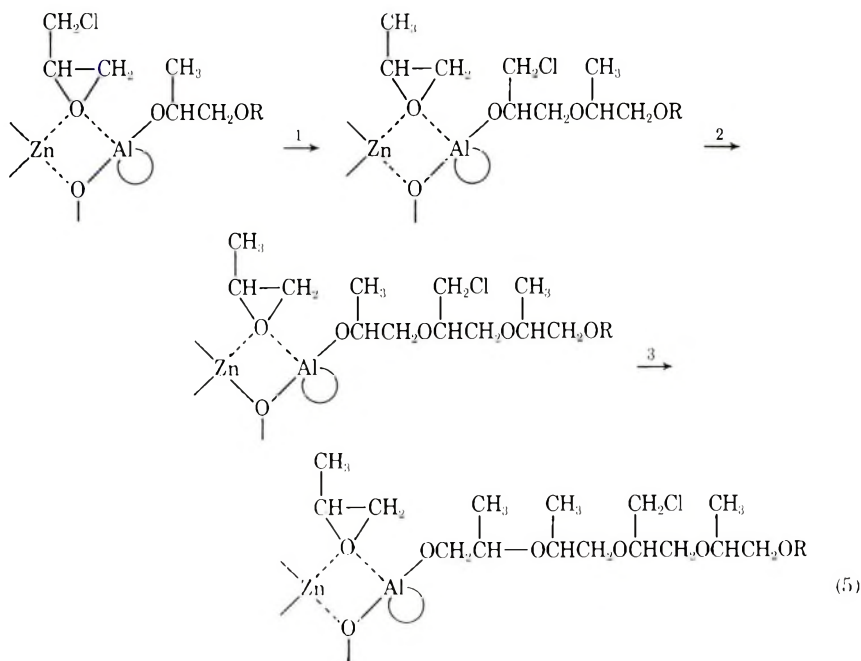


TABLE X  
 NMR Chemical Shifts in Benzene\*

Sample	Chemical shift, ppm			
	Chelate			
	3-H	CH <sub>3</sub>	CH <sub>3</sub> -Al	CH <sub>3</sub> -Zn
(CH <sub>3</sub> ) <sub>2</sub> Zn	—	—	—	-2.1
(CH <sub>3</sub> ) <sub>2</sub> Alacac <sup>b</sup>	+3.5	+0.033	-1.8	—
(CH <sub>3</sub> ) <sub>2</sub> Alacac/(CH <sub>3</sub> ) <sub>2</sub> Zn, 1/1	+3.5	+0.010	-1.8	-2.1

\* Chemical shifts are for 0.5 *M* solutions relative to cyclopentane as internal standard, + downfield from cyclopentane, - upfield.

<sup>b</sup> Determined with TMS as internal standard. Converted with the use of 1.48 ppm as the chemical shift value for cyclopentane in benzene.

The equation shows the separation of mechanistic function we have discussed; the growing polyether residue remaining bonded to aluminum, and the zinc atom primarily involved in epoxide monomer coordination. This differs from the situation where the catalyst is derived from a single organometallic compound where there is an alternation in the chemical function the metal atoms perform.

The inactivity of Cl<sub>2</sub>Alacac for polymerization suggests that the initiation step involves the reaction of alkyl group on aluminum with epoxide to form the first OR fragment bound to aluminum.

Research by Vandenberg and Price has shown that epoxides polymerize with inversion of configuration of the ring-opened carbon atom.<sup>5,14</sup> Another common feature of epoxide polymerizations shown by these researchers is that head-to-head and tail-to-tail positional isomerization are significant features in the enchainment process, in addition to the anticipated head-to-tail polymer structure.<sup>5,15,16</sup> We believe such features characterize the catalyst system described in this paper; step 3 of eq. (5) shows the production of a head-to-head polymer residue.

The acetylacetonate structure in the active catalyst species reduces the electropositive nature of aluminum, and defines certain steric parameters for the active site. Changing the chelate structure affects both these features. The incorporation of R<sub>2</sub>Zn into the active catalyst species appears to affect polymerization activity and the details of the propagation and chain-breaking processes.

We would like to thank Drs. W. J. Ristey and Z. W. Wilchinsky for the x-ray polymer characterization data and Dr. E. J. Vandenberg for making his manuscript available to us before publication.

## References

1. R. O. Colclough and K. Wilkinson, in *Macromolecular Chemistry, Paris 1963* (*J. Polym. Sci. C*, **4**), M. Magot, Ed., Interscience, New York, 1964, p. 311.
2. R. O. Colclough, G. Gee, and A. H. Jagger, *J. Polym. Sci.*, **48**, 273 (1960).
3. T. Saegusa, T. Ueshima, and S. Tomita, *Makromol. Chem.*, **107**, 131 (1967).
4. M. Dimonie and I. Gavut, *Eur. Polym. J.*, **1968**, 541.

5. E. J. Vandenberg, *J. Polym. Sci. A-1*, **7**, 525 (1969).
6. W. R. Kroll and W. Naegele, in *Proceedings of the 1967 International Symposium: Decomposition of Organometallic Compounds to Refractory Ceramics, Metals, and Metal Alloys*, University of Dayton Press, Dayton, 1968, p. 307; *J. Organometal. Chem.*, **19**, 439 (1969).
7. A. T. Jones, *Polymer*, **6**, 249 (1965).
8. R. L. Lintvedt and H. F. Holtzclaw, *J. Amer. Chem. Soc.*, **88**, 2713 (1966).
9. T. Ueshima, T. Fujii, T. Saegusa, and J. Furukawa, *Makromol. Chem.*, **98**, 58 (1966).
10. S. Isida, *Bull. Chem. Soc. Japan*, **33**, 727 (1960).
11. A. E. Gurgiolio, *Rev. Macromol. Chem.*, **1**, 39 (1966).
12. G. E. Coates and K. Wade, *Organometallic Compounds*, 3rd ed., Vol. I, Methuen, London, 1967, p. 132.
13. C. C. Price and R. Spector, *J. Amer. Chem. Soc.*, **87**, 2069 (1965).
14. C. C. Price and R. Spector, *J. Amer. Chem. Soc.*, **88**, 4171 (1966).
15. C. C. Price and A. L. Tumulo, *J. Polym. Sci. A-1*, **5**, 175 (1967).
16. C. C. Price, R. Spector, and A. L. Tumulo, *J. Polym. Sci. A-1*, **5**, 407 (1967).

Received December 24, 1969

Revised January 16, 1970

## Melting Behavior of Ethylene Copolymers and Branched Polyethylenes

RICHARD G. GRISKEY and GEORGE N. FOSTER,\* *Newark College of Engineering, Newark, New Jersey 07102*

### Synopsis

Prior research on the melting behavior of ethylene copolymers and branched polyethylenes could not be effectively evaluated since there were large differences in the levels of comonomer contents. The present research was undertaken to determine additional data so that an overall evaluation could be made. A consideration of the experimental data of the present work and earlier research data showed that methyl side groups caused less diffuse melting and less melting point depression than either ethyl groups or polyethylene branches. In addition, it was found that the Flory equation can be used to describe the relation of melting point depression to foreign group concentration for propylene copolymers. The equation did not hold for 1-butene-ethylene copolymers or branched polyethylenes. For these materials the Wunderlich modification of the Flory equation applied. Activity values for both 1-butene-ethylene copolymers and branched polyethylenes gave a common correlation with foreign groups. Enthalpy and entropy fusion data for ethylene copolymers and branched polyethylenes were also determined. It was also shown that good agreement was found between crystallinities for these materials determined independently by differential thermal analysis and x-ray analysis.

### INTRODUCTION

Differential thermal analysis has been widely applied to polymers during the past few years since it provides a rapid, convenient technique for studying endothermic and exothermic changes such as first and second order transitions. In particular, investigations have considered kinetics of crystallization,<sup>1</sup> effects of diluents on polymer melting behavior,<sup>2</sup> epoxide curing reactions,<sup>3</sup> oxidation of polyethylene,<sup>4</sup> as well as studies of first- and second-order transitions.<sup>5-14</sup>

A specific area of interest has been the effect of copolymerization and branching on the behavior of polyethylene. Ke<sup>6</sup> studied propylene and 1-butene copolymer systems of low comonomer content. Wunderlich and co-workers<sup>11-13</sup> considered higher ranges of comonomer content as well as branched systems.

The differences in level of comonomer content between the studies of Ke<sup>6</sup> and those of Wunderlich<sup>11-13</sup> precluded comparison of their results. The present work was undertaken to effect such a comparison by studying ethylene-propylene, and ethylene-1-butane copolymers with comonomer

\* Present address: Union Carbide Company, Bound Brook, New Jersey 08805.



TABLE I  
Polyethylene and Polypropylene Samples Used in this Work

Polymer	Code	Density (@23°C) g/cm <sup>3</sup>	Weight		Melt index g/10 min	Melt viscosity poise	Methyl or ethyl per 100 C	Vinyl per 2000 C	<i>trans</i> -Unsat- uration per 2000 C	Vinyl- idene per 2000 C	Carbonyl per 2000 C
			average molecular weight	Number average molecular weight							
Polyethylene	PE 77	0.9218	550,000	31,000	0.16	62.0	2.0	0.08	0.04	0.29	0.05
Polyethylene	PE 78	0.9232	225,000	16,000	19.9	0.24	2.0	0.09	0.03	0.31	0.01
Polyethylene	PE 79	0.919	500,000	18,000	3.3	1.85	2.0	0.04	0.01	0.25	0.01
Polyethylene	PE 80	0.9228	500,000	22,000	1.06	7.3	1.8	0.00	0.03	0.25	0.005
Polyethylene	PE 82	0.9188	800,000	55,000	0.21	31.0	2.1	0.05	0.02	0.27	0.005
Polyethylene	PE 84	0.9523	175,000	31,000	0.57	7.0	0.14	1.53	0.08	0.09	0.005
Polypropylene	PP 1	0.9063	300,000	25,000	1.21	1.25 × 10 <sup>6</sup>	33.3				

contents ranging from those of Ke's work to the studies of Wunderlich. In addition, several branched polyethylenes were also studied. The present study also considered the behavior of enthalpy and entropy of fusion in ethylene copolymer and branched ethylene systems.

## EXPERIMENTAL

### Materials

The polymers used in the present study were obtained from E. I. duPont De Nemours and Company (linear and branched polyethylenes, polypropylene), Phillips Petroleum Company (ethylene-propylene and ethylene-1-butene copolymers), and Enjay Plastics Company (polypropylene). Tables I and II give the characteristics of the samples used in the present work.

TABLE II  
Copolymer Samples Used in this Work

Polymer	Code	Density (23°C) g/cm <sup>3</sup>	Melt index, g/10 min.	Methyl or ethyl per 100°C
Et/Pr copolymer	EP 1	0.950	0.3	0.4
Et/Pr copolymer	EP 2	0.941	0.6	1.1
Et/Pr copolymer	EP 3	0.924	0.6	2.6
Et/Bt-1 copolymer	EB 1	0.952	0.8	0.3
Et/Bt-1 copolymer	EB 2	0.939	0.8	0.7
Et/Bt-1 copolymer	EB 3	0.928	0.8	1.1

### Procedure

Individual differential thermal analysis devices have varied somewhat in design. Most devices<sup>8,10,15-18</sup> have certain parts in common. These are: sample and reference cells, furnace, temperature-sensing elements with amplification and  $x-y$  recording systems and a linear temperature programming system.

Figure 1 shows the apparatus used in the present study. Figure 2 depicts the circuit used with the device.

Cylindrical samples,  $\frac{1}{4}$  in. in diameter and  $\frac{1}{2}$  in. in length, were prepared by using a compression mold. The samples were inserted into stainless steel sample cells which were lined with Teflon FEP film. The purpose of the film was to prevent the sample from adhering to the cell walls and also to provide a tight fit for the sample. A matched reference cell was filled with 14-mesh alumina.

A heating rate of 2.4°C/min was used in this work. The variation in heating rate was generally less than  $\pm 0.2^\circ\text{C}/\text{min}$ . Variations greater than this did not alter the data appreciably. The 2.4°C/min heating rate is one which is fast enough to minimize recrystallization and yet slow enough as to not shift recorded transition temperatures.<sup>11,15</sup>

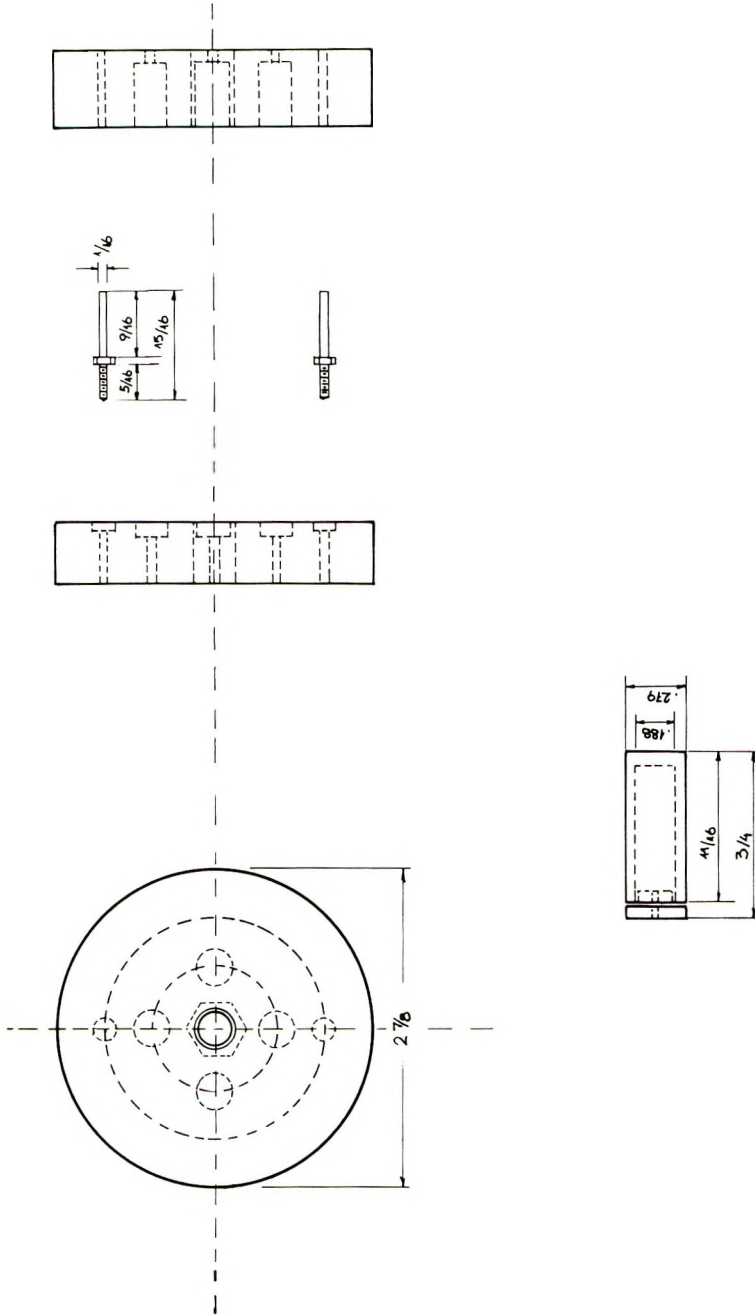


Fig. 1. Differential thermal analysis cells and molders.

In an experimental run, iron-constantan thermocouples were passed through the cell holder lids and cell covers into a centered  $\frac{1}{4}$ -in. deep hole in the sample and standard. The apparatus was then assembled. All samples were first heated to 20 or 30°C above their melting point and then slowly cooled to room temperature at a rate about  $\frac{1}{10}$  the heating rate used in the studies. This procedure was in agreement with that recommended by Wunderlich.<sup>11</sup> It was found to give reproducible thermograms for all samples.

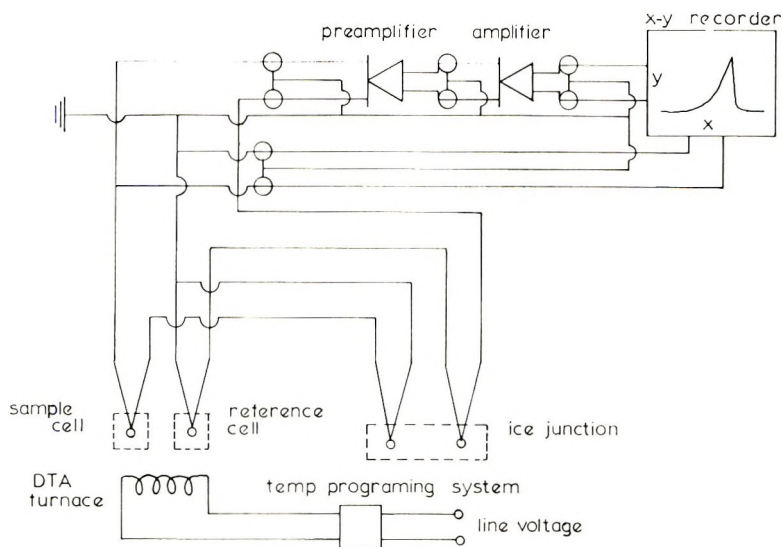


Fig. 2. Differential thermal analysis circuit.

When the sample had cooled to ambient conditions, the electronic units were carefully zeroed, and then the heating element was set to give the predetermined rate of heating. When the temperature reached 100°C above the sample melting point, the furnace was turned off and the apparatus cooled and disassembled.

## RESULTS

Thermograms for the polymers studied in the present work are given in Figures 3-5. The thermograms were analyzed by using the procedures recommended by Strella.<sup>17,18</sup> The various temperatures derived from the thermograms are given in Table III. Also shown in Table III are enthalpies and entropies of fusion as well as estimates of crystallinity from differential thermal analysis data. These quantities were also determined by the procedures recommended by Strella.<sup>17,18</sup> The apparatus was calibrated for the enthalpy calculations by using benzoic acid as a standard. Entropies were calculated by dividing the enthalpies of melting by melting temperatures.

TABLE III  
Summary of Experimental Data

Polymer	Initial Melting temperature, °C	Melting point, °C	Enthalpy of fusion, cal/g	Entropy of fusion eu/g	Crystallinity by DTA, %	$N_A$ from eq (2) and (3)	$N_A$ from data and eq (3)
PE 77	81.1	112.4	28.6	0.0743	49.1	0.924	0.962
PE 78	81.4	113.4	25.6	0.0662	43.3	0.926	0.966
PE 79	76.4	113.8	33.0	0.0853	38.7	0.930	0.971
PE 80	77.4	114.3	32.5	0.0839	49.8	0.900	0.964
PE 82	77.1	110.9	32.9	0.0857	49.7	0.910	0.956
PE 84	88.2	134.0	62.6	0.154	91.5	0.986	0.986
EP 1	78.7	130.0	60.5	0.150	88.4	0.986	0.987
EP 2	72.1	125.7	50.2	0.126	73.4	0.974	0.977
EP 3	70.6	120.8	31.3	0.0796	44.2	0.958	0.968
EB 1	75.1	130.0	58.7	0.146	85.7	0.974	0.987
EB 2	78.4	128.7	48.3	0.120	70.5	0.970	0.977
EB 3	66.0	124.6	34.8	0.0876	50.8	0.951	0.975
PP 1	138.5	169.5	25.2	0.0566	—	—	—
PP 2	124.6	167.7	17.1	0.0388	—	—	—

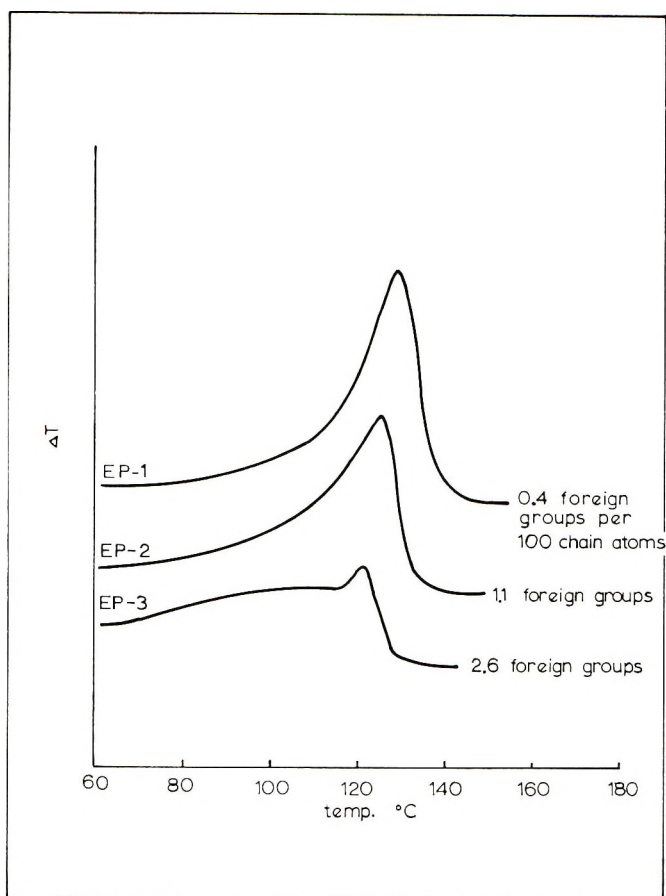


Fig. 3. Thermograms for ethylene-propylene copolymers.

## DISCUSSION

The data in the present study cannot be directly compared to earlier research since nearly all of the materials had not been studied previously. The only exception was a branched polyethylene (PE 80) that was studied earlier by Wunderlich.<sup>13</sup> The melting temperatures compared to within 0.5°C. A direct comparison of the thermograms was not possible, since the  $\Delta T$  axis units were not given in Wunderlich's work. The thermograms did, however, appear to be similar.

Generally all of the thermograms derived in the present work are as sharp and well-defined as those reported by other researchers. In this qualitative sense it would appear that these data are acceptable.

A number of conclusions can be drawn from the thermograms. First, increasing comonomer content or branches causes more diffuse melting as well as greater depression of the melting temperature (see Figs. 3-5).

Furthermore, it appears that the butene groups (Fig. 4) and polyethylene branches (Fig. 5) had more pronounced effects than the ethylene groups (Fig. 3).

Insight into these results can be drawn by considering crystallinity and melting (nondifferential thermal analysis) studies by Reding.<sup>20,21</sup> This work showed that butene groups disrupted crystallinity more effectively

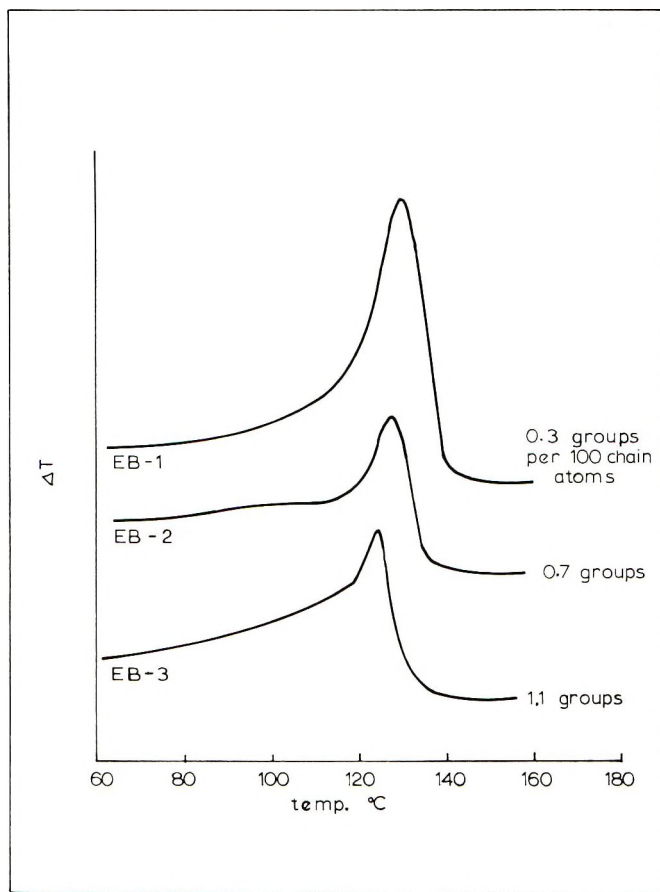


Fig. 4. Thermograms for ethylene-1-butene copolymers.

than propylene. In addition, the branched polyethylenes also apparently had greater crystallinity disruptions than the ethylene-propylene copolymers.

Although direct thermogram comparison could not be made to the work of Ke<sup>6</sup> and Wunderlich<sup>11,13</sup> there was a method for comparing their data to that of the present work. Figures 6 and 7 compare the low comonomer work of Ke<sup>6</sup> and the much higher comonomer content data of Wunderlich<sup>11,13</sup> to the present work which overlapped the earlier data. Melting points

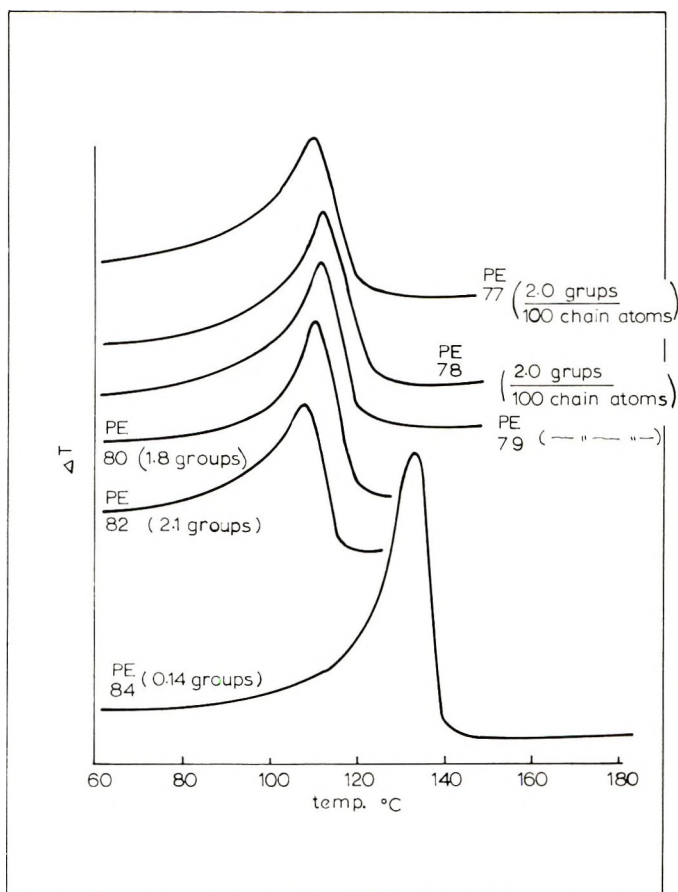


Fig. 5. Thermograms for branched polyethylenes.

from all of these data are plotted in Figures 6 and 7 together with the theoretical temperature depression predicted by Flory.<sup>23</sup>

$$(1/T_m) - (1/T_m^\circ) = -(R/\Delta H_u) \ln X_A \quad (1)$$

where  $T_m^\circ$  and  $T_m$  are the melting temperatures of the unbranched and branched polymers,  $R$  the gas constant,  $H_u$  the heat of fusion per repeating unit, and  $X_A$  the mole fraction of crystallizable units.

In Figure 6 the ethylene-propylene copolymers seem to follow the theoretical prediction of Flory. All ethylene-propylene copolymer data (those of Ke,<sup>6</sup> Wunderlich,<sup>11,13</sup> and the present work) can therefore be fairly represented by the Flory equation.

In Figure 7 it is apparent that this is not the case for ethylene-1-butene copolymers and branched polyethylenes. This deviation suggested that the values used for  $X_A$  based directly on foreign groups present is not correct in the case of the butene copolymers and branched polyethylenes. Con-



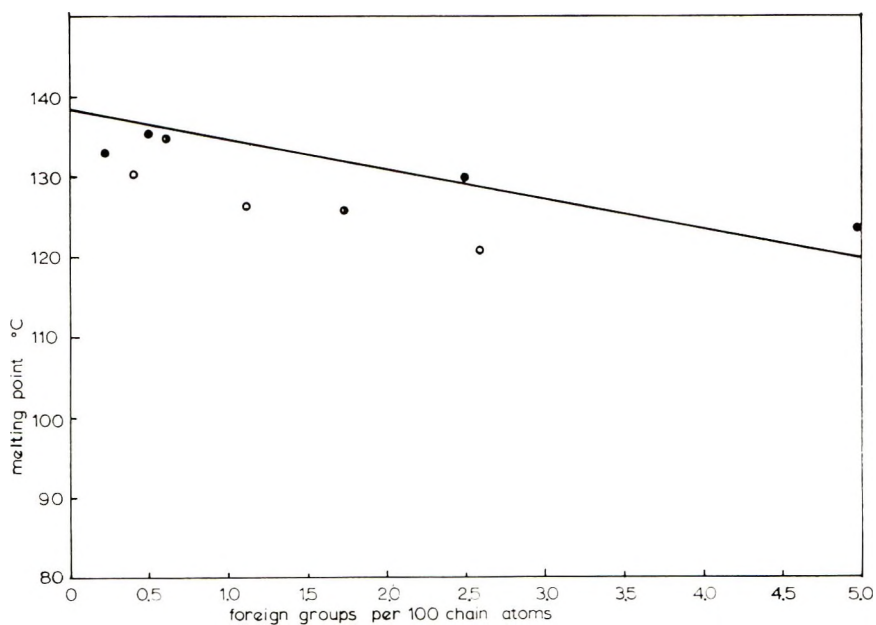


Fig. 6. Melting point depression for ethylene-propylene copolymers: (○) this work; (●) data of Wunderlich and Bodily;<sup>13</sup> (●) data of Ke;<sup>6</sup> (—) Flory theory.<sup>23</sup>

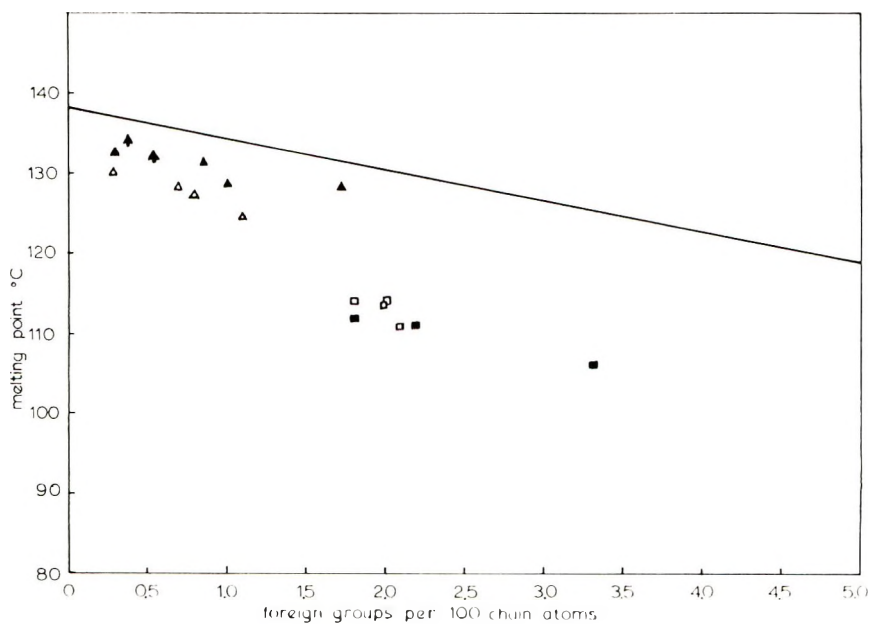


Fig. 7. Melting point depression for ethylene-1-butene copolymers and branched polyethylenes: (Δ) butene copolymers; (□) branched polyethylenes; (▲) butene copolymers;<sup>13</sup> (■) branched polyethylenes;<sup>13</sup> (Δ) butene copolymers.<sup>6</sup>

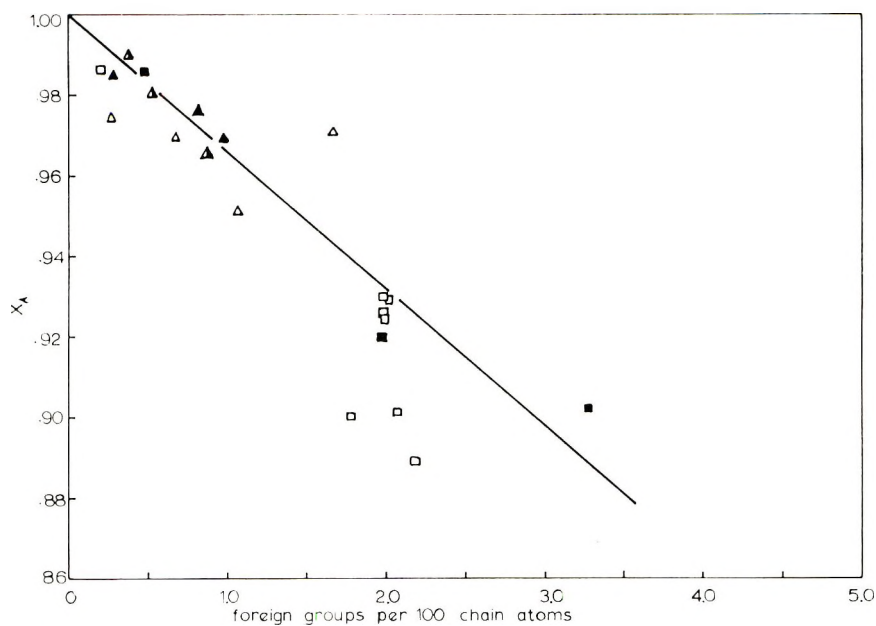


Fig. 8.  $X_A$  values for ethylene-1-butene copolymers and branched polyethylenes vs. foreign group concentration. ■ Symbols as in Fig. 7.

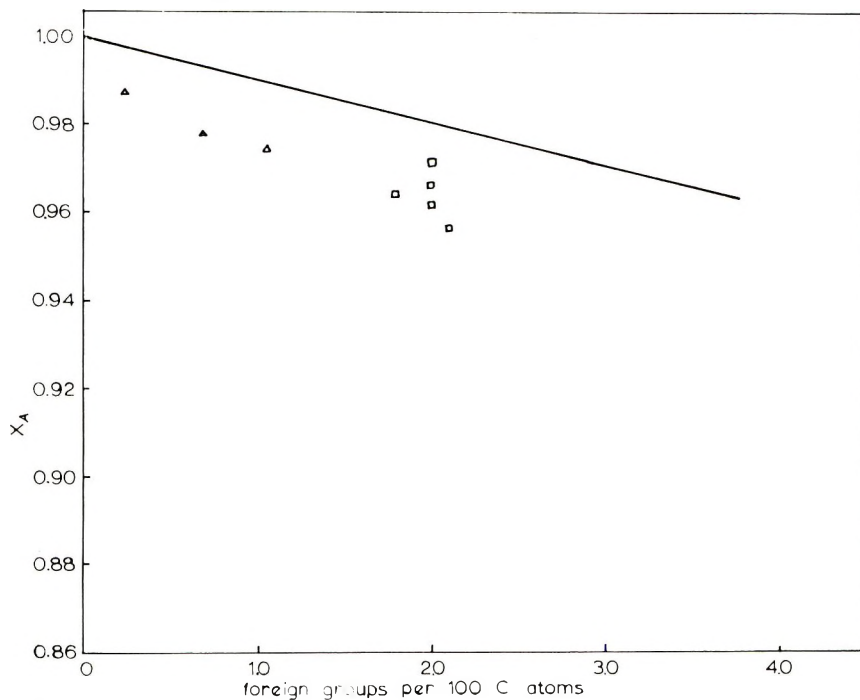


Fig. 9.  $X_A$  values for ethylene-1-butene copolymers and branched polyethylenes computed from experimental heat of fusion data; ( $\Delta$ ) ethylene-1-butene copolymers; ( $\square$ ) branched polyethylenes; (—) Flory theory.<sup>23</sup>

sequently the approach used earlier by Wunderlich<sup>13,15</sup> was employed. This technique involved calculating new  $X_A$  values by using the expressions:<sup>13,23</sup>

$$\Delta H_u = 54.6 + 0.1716T - 6.36 \times 10^{-4}T^2 \text{ cal/g} \quad (2)$$

$$M_A^\circ \Delta H_u [(1/T_m) - (1/T_m^\circ)] = -R \ln X_A \quad (3)$$

where  $M_A^\circ$  is the average molecular weight of the chain units and  $X_A$  is now considered to be an activity rather than a mole fraction.

Figure 8 compares  $X_A$  values for ethylene-1-butene copolymers and branched polyethylenes. These values were calculated from melting point depression data from the present work as well as data of Ke<sup>6</sup> and Wunderlich.<sup>11,13</sup> The line through the data is that proposed by Wunderlich<sup>13</sup> for branched polyethylenes. As can be seen, however, it also fits the ethylene-1-butene data. Wunderlich postulated a somewhat different correlation for ethylene-1-butene copolymers based only on his data. The present correlation is based not only on these data but also those of Ke<sup>6</sup> and the present work. It would therefore seem that the correlation line of Figure 8 is more proper for ethylene-1-butene copolymers than that proposed earlier by Wunderlich.<sup>13</sup>

The results in Figure 8 show that the larger side groups (polyethylene branches, 1-butene side groups) have a greater disruptive effect than that predicted on the basis of the mole fractions of these groups. They also show that the polyethylenes (with random branching) behave in a similar manner to the 1-butene side groups. This would also indicate that the polyethylene branches are most likely longer than methyl groups.

The data of the present work were also studied in another manner.  $X_A$  values were calculated from eq. (3) by using the enthalpy of fusion data determined in the present study instead of using eq. (2). The resultant  $X_A$  values are plotted in Figure 9. The line shown in the plot is the theoretical prediction of Flory based on mole fraction. As can be seen the data for ethylene-1-butene and branched polyethylene deviate only slightly from the Flory equation. This would indicate that Flory's equation more closely represents melting point data when actual fusion enthalpy values for the respective polymers are used.

This result and the relatively small scatter for the experimental data plotted in Figure 9 would also seem to indicate that the enthalpy of fusion data presented in Table III are reliable. An additional favorable point is that the enthalpy of fusion for polypropylene (25.2 cal/g) determined in the present work by differential analysis compared favorably to that determined calorimetrically (25.0 cal/g) by Dole.<sup>24</sup>

One other item in Table III deserves mention: the crystallinities estimated from the differential thermal analysis data. Figure 10 compares these values to correlation lines determined by x-ray studies by earlier investigators. In Figure 10 ethylene-1-butene data from the present work are compared to the crystallinity-foreign group relations determined by Wunderlich.<sup>13</sup> As can be seen, the agreement is excellent. In Figure 10 a

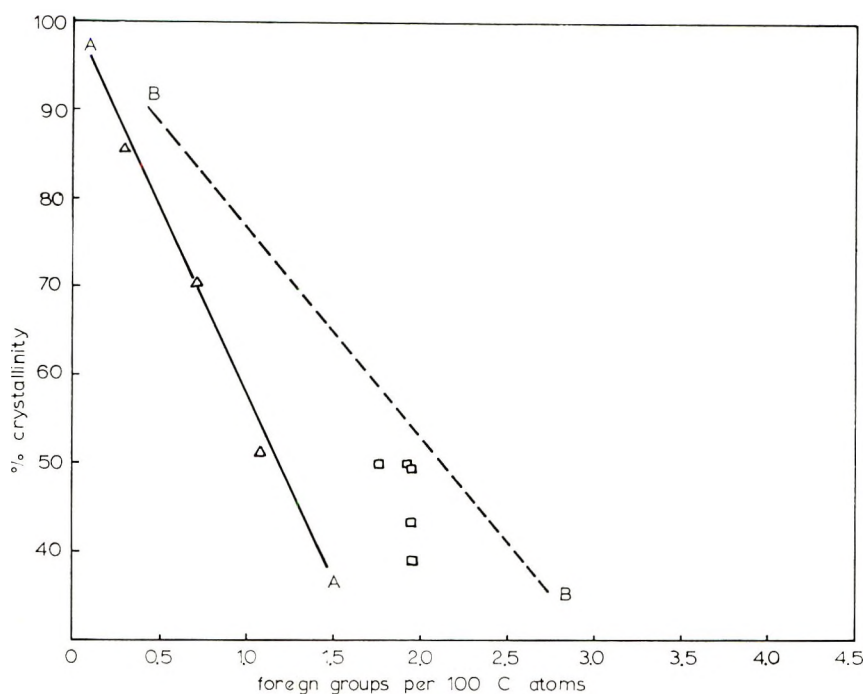


Fig. 10. Comparison of crystallinities computed from DTA data with X-ray values: ( $\Delta$ ) ethylene-1-butene data estimated by DTA (this work); ( $\square$ ) branched polyethylenes estimated by DTA (this work); (A) ethylene-1-butene, x-ray data;<sup>13</sup> (B) branched polyethylenes, x-ray data.<sup>13</sup>

similar comparison is also made for the estimates for the branched polyethylene and the relation determined with x-ray measurements by Wunderlich.<sup>13</sup> The agreement while not as good as for the ethylene-1-butene case is still adequate. The overall conclusion is that differential thermal analysis data when treated as proposed by Stella<sup>17,18</sup> can give excellent estimates of crystallinity.

In summary the following conclusions can be reached.

(1) Methyl side groups, as in ethylene-propylene copolymers, cause less diffuse melting and less depression of melting points than either ethyl groups (ethylene-1-butene copolymers) or branched polyethylenes.

(2) The melting point depression behavior of ethylene-propylene copolymers can be described by the Flory equation<sup>23</sup> by using foreign group concentration (i.e., per 100 carbon atoms) as a mole fraction.

(3) Melting point depression behavior of both ethylene-1-butene copolymers and branched polyethylenes cannot be described by the Flory equation. Instead, the Wunderlich modification<sup>13</sup> of Flory's equation must be used.

(4) Activity values ( $X_A$ ), per the Wunderlich modification, gave a common correlation with foreign groups per 100 carbon atoms for both ethylene-1-butene copolymers and branched polyethylene.

(5) Enthalpy and entropy of fusion data were determined for ethylene-propylene copolymers, ethylene-1-butene copolymers, and branched polyethylenes.

(6) Crystallinities estimated from differential thermal analysis data correlated with published x-ray crystallinity data.

Grateful acknowledgment is made to the National Science Foundation for support of this work by means of Grant GP 2099.

### References

1. J. Boor and J. C. Mitchell, *J. Polym. Sci. A*, **1**, 59 (1963).
2. B. Ke, *J. Polym. Sci.*, **50**, 79 (1961).
3. H. C. Anderson, *Anal. Chem.* **32**, 1592 (1960).
4. A. Rudin, H. P. Schreiber, and M. H. Waldman, *Ind. Eng. Chem.*, **53**, 137 (1961).
5. B. Ke, *J. Polym. Sci.*, **42**, 15 (1960).
6. B. Ke, *J. Polym. Sci.*, **61**, 47 (1962).
7. B. Ke, and A. N. Sisko, *J. Polym. Sci.*, **50**, 87 (1961).
8. I. Masakazu, *J. Polym. Sci. A*, **1**, 2697 (1963).
9. I. Masakazu, *J. Polym. Sci. A*, **1**, 3427 (1963).
10. C. B. Murphy, J. H. Palm, D. D. Doyle, and E. M. Curtiss *Mod. Plastics*, **28**, 447 (1958).
11. B. Wunderlich, and D. Poland, *J. Polym. Sci. A*, **1**, 357 (1963).
12. B. Wunderlich, *Polymer*, **5**, 611 (1964).
13. B. Wunderlich and D. Bodily, *J. Polym. Sci. A-2*, **4**, 25 (1966).
14. B. Wunderlich and T. Arakawa, *J. Polym. Sci. A-2*, **4**, 53 (1966).
15. B. Wunderlich and W. H. Kashdan, *J. Polym. Sci.*, **50**, 71 (1961).
16. B. Ke, *J. Polym. Sci. A*, **1**, 1453 (1963).
17. S. Strella, *J. Appl. Polym. Sci.*, **7**, 1281 (1962).
18. S. Strella, *J. Appl. Polym. Sci.*, **7**, 569 (1963).
19. W. Cooper and R. K. Smith, *J. Polym. Sci. A*, **1**, 159 (1963).
20. F. P. Reding, *J. Polym. Sci.*, **32**, 487 (1958).
21. F. P. Reding, *J. Polym. Sci.*, **21**, 157 (1956).
22. R. G. Quynn, J. L. Riley, D. A. Young, and H. D. Noether, *J. Appl. Polym. Sci.*, **2**, 166 (1959).
23. P. J. Flory, *Trans. Faraday Soc.*, **51**, 848 (1955).
24. M. Dole and B. Wunderlich, *J. Polym. Sci.*, **34**, 201 (1957).
25. M. Dole and R. W. Wilkinson, *J. Polym. Sci.*, **58**, 1089 (1962).

Received December 30, 1969

Revised February 10, 1970

## Crosslinking of Starch Xanthate. II. Reaction with Polyacrolein

G. G. MAHER, J. A. DOUGLAS, C. R. RUSSELL, and C. E. RIST,  
Northern Regional Research Laboratory, Northern Utilization Research and  
Development Division, Agricultural Research Service, U. S. Department of  
Agriculture, Peoria, Illinois 61604

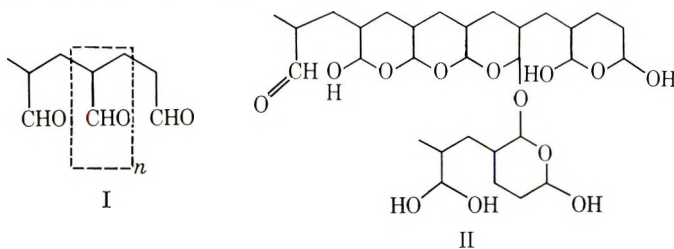
### Synopsis

The reaction between polyacrolein bisulfite adduct and sodium starch xanthate in aqueous alkali gives a rapid viscosity increase and subsequent gelation. The magnitude and pattern of the viscosity development depend on the degree of substitution of the starch xanthates in the range of 0.12 to 0.45, varying from around 5000 cP centipoises (nongelling) for the lowest to more than 100 000 cP for the highest. The viscosity patterns developed with the more highly substituted xanthates show a minimum valley after a 20-30-min reaction. Analytical and spectral analyses of solid materials obtained from the ethanol precipitation of the gels indicate that the product is a monothiocarbonate stemming from the elimination of sodium hydrogen sulfide between a xanthate group of the starch and a hydroxyl group of the polyacrolein adduct. A hydrated form of polyacrolein does not react with starch xanthate under the same aqueous alkaline conditions.

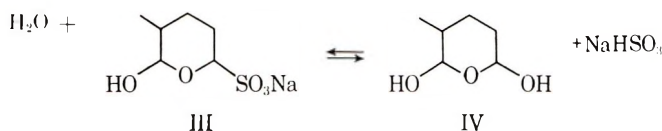
### INTRODUCTION

Sodium starch xanthate (also simply termed starch xanthate here) reacts with polyethylenimine to give a definitive product, a thiourethane that crosslinks the two polymeric reactants.<sup>1</sup> This material has been found to have a potential industrial utility. In similar studies we investigated the reaction between starch xanthate and the commercially available polyacroleins, the Aldomers. (Shell Chemical Company tradename.)

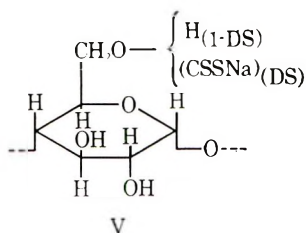
Polyacrolein, formed by the free-radical polymerization of acrolein, is visualized as a polyaldehyde (I) which, in the presence of water, spontaneously forms a fused tetrahydropyran structure (II) wherein some cross-linking can exist, Aldomer 110.<sup>2</sup> (Shell Chemical Company tradename.)



Although the tetrahydropyran form is quite water-insoluble, it does react with aqueous sodium bisulfite or with sulfur dioxide in alkaline water to produce a readily water-soluble bisulfite adduct (III), Aldomer 110B. The adduct does not shift to any significant extent in water solution into the hydrated form of polyacrolein (IV) if the carbon:sulfur atomic ratio in the adduct is 6:1.<sup>2,3</sup>



Polyacroleins in forms I, II, III, and IV are stable towards oxidation, and infrared studies show there are few free aldehyde groups. Nevertheless, the polyacroleins do readily and completely engage in many of the reactions of a typical aldehyde compound. Also, the presence of hydroxyl groups, which are hemiacetallike, account for the ability of the polyacroleins to form acetals, mercaptals, and Knoevenagel condensation products. A third reaction of the polyacroleins involves the active hydrogen (alpha to the carbon holding hydroxyl) which is an acidic hydrogen.<sup>2,4</sup> Since xanthates are known to react with aldehydes<sup>5,6</sup> and with compounds containing an active hydrogen, as in the amines,<sup>1</sup> then polyacroleins might react with starch xanthate (V).



## EXPERIMENTAL

### Materials

The starch xanthates were prepared from commercial, pearl, corn starch (Corn Products Company, Argo, Illinois) by a continuous process.<sup>7,8</sup> They were stored at 5°C as aqueous solutions of the sodium salt, pH 11.5. The solutions contained 10–13% of the sodium starch xanthate. Because starch xanthate decomposition becomes significant in regard to degree of substitution after several weeks in storage under these conditions, experimentation was done within that period. The xanthate solutions were analyzed for starch by a cuprimetric method and for xanthate groups by an acidimetric method, and the sodium starch xanthate content and the degree of substitution (DS) were calculated, based on the anhydroglucose unit, as previously described.<sup>7</sup> In addition, the starch xanthates were precipitated by ethanol and washed as described below, and the resulting powders

were analyzed for sulfur content by the method of White.<sup>9</sup> The DS for the sodium starch xanthate was also calculated from this sulfur content. The DS values obtained by the two methods are compared later.

The polyacroleins were commercial development items (Shell Chemical Company, Industrial Chemicals Division, New York, New York). Aldomer 110 was the hydrated form of polyacrolein, a white powder with 15% moisture and 1.5 equivalents of free and combined carbonyl per 100 g, insoluble in water or ethanol. Aldomer 110B was the NaHSO<sub>3</sub> adduct, a water solution of 18.6 or 19.3% content of a solid with a 6:1 C:S atomic ratio. This solution had less than 0.01 equivalent of free HSO<sub>3</sub><sup>-</sup> per 100 g and a Brookfield Viscometer viscosity of 1000–2000 cP (Model LVF, No. 4 spindle at 6 rpm). The solids in solution precipitated when ethanol was added.

Other chemicals used were reagent grade.

### Viscometry of the Reaction

To 7.5 g of the sodium starch xanthate solution in a glass vial (95 × 25 mm), 5 ml of water was added. A weighed amount of the Aldomer 110B solution was diluted with about 20 ml of water and the mixture added to the vial. The quantity of solid polyacrolein sodium bisulfite adduct (assumed molecular weight for III, 216.19) was twice that calculated for the reaction of 1 mole of the adduct with 1 mole of xanthate group. The total amount of water used was such as to give the same concentration of base starch

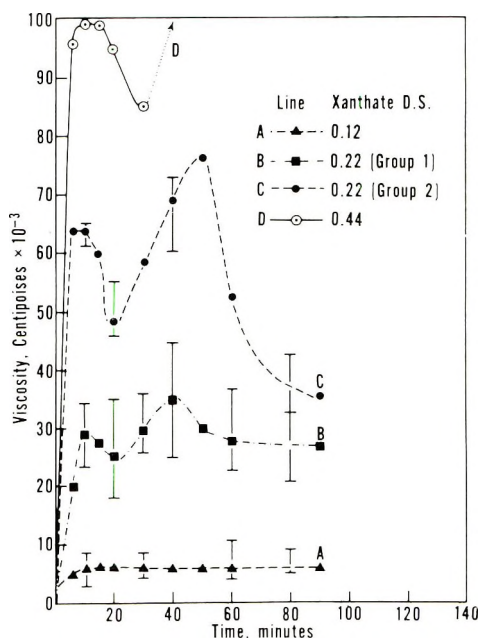


Fig. 1. Viscosity development in the reaction of polyacrolein bisulfite adduct and sodium starch xanthate in alkaline water.



TABLE I  
Preparation and Analytical Data on Solid Products from a Sodium Starch Xanthate and Polyacrolein Bisulfite Reaction

Xanthate no.	Xanthate DS		Xanthate age when used, days	Molar ratio polyacrolein: xanthate <sup>a</sup>	Product analysis		
	By titration	By precipitation			Calculated S content for monothiocarbonate, %		Anal. S content, %
					From titration DS	From precipitation DS	
468	0.12		7	2:1	3.98		3.01
469	0.23		2	2:1	6.66		5.96
470	0.48		6	2:1	10.76		9.83
472	0.12	0.09	7	2:1	3.98	3.20	3.58
473	0.22	0.14	2	2:1	6.44	4.66	5.71
474	0.42	0.37	2	2:1	9.95	9.21	10.04
472	0.12	0.09	14	2:1	3.98	3.20	3.81
473	0.22	0.14	14	2:1	6.44	4.66	5.77
474	0.42	0.37	14	2:1	9.95	9.21	10.00
482	0.22	0.16	3	1:1	6.44	5.03	4.96
483	0.50	0.44	7	1:1	11.01	10.21	10.09

<sup>a</sup> Moles of polyacrolein (as a unit weight of 216.19 g) per mole of xanthate group in the sodium starch xanthate.

solids in all reactions under comparison and to eliminate starch concentration as a factor in any viscosity differences observed. After gentle manual shaking (to avoid incorporating air bubbles unduly), the stoppered vials were allowed to stand at room conditions. The viscosity of the reaction mixtures was determined with the Brookfield viscometer (No. 4 spindle at 6 rpm) as time progressed. Viscosities are plotted in Figure 1.

Comparable reaction mixtures were made (although heterogeneous) with Aldomer 110 and starch xanthate solutions. Several "blank" reaction mixtures were also studied for viscosity development. One blank was a mixture of 7.5 g of the starch xanthate solution and an appropriate volume of water. Another was a water solution of Aldomer 110B and gelatinized starch (gelatinization being effected by the same amount of NaOH solution as used in the xanthate preparation), the concentrations of each polymer being comparable to those present in the reactions. The third was a water solution of the same amount of Aldomer 110B, and quantities of CS<sub>2</sub> and NaOH equivalent to the excess of these reagents used in preparing the average amount of sodium starch xanthate present in the reactions.

To test the possibility that an aldehyde group would react with the starch xanthate under similar conditions, equimolar mixtures were made with benzaldehyde (a little methanol had to be added to make a homogeneous medium). Also, alkaline reaction mixtures were made with potassium ethyl xanthate and benzaldehyde sodium bisulfite adduct.

### Ethanol Precipitation of Reaction Solids

The reaction mixture, about 30 ml, was poured into 150 ml of 95% ethanol. The white precipitate that formed was separated by centrifugation and washed in the tube several times each with ethanol and then ether. The resulting powders were allowed to air-dry at room temperature and then dried to constant weight *in vacuo* over P<sub>2</sub>O<sub>5</sub> at room temperature. Drying under vacuum at 110°C decomposed the product with considerable loss of sulfur. The dried products were analyzed for sulfur content (Table I).

KBr mull disks were used to obtain infrared spectra with a Perkin-Elmer 621 spectrophotometer. However, the products were too insoluble for getting good ultraviolet spectra; only end absorption at 206–208 m $\mu$  and a trace of xanthate absorption at 306 m $\mu$  were observed when a Perkin-Elmer 202 spectrophotometer was used with quartz cells.

## RESULTS AND DISCUSSION

The reaction between polyacrolein sodium bisulfite adduct and sodium starch xanthate in water, pH 10–11, is rapid. In only a few minutes, the viscosity begins to rise appreciably. The extent and pattern of viscosity development vary with the DS of the starch xanthate, as shown in Figure 1. Each curve represents an average determination with three or four different xanthate preparations of the approximate DS given. The vertical bars

represent the range in viscosity found with the different preparations at the particular points. Whereas viscosity curves with different batches of the xanthates of higher DS could vary from one another by as much as 10 000 cP, repeated reaction viscosity determinations with any one xanthate preparation gave curves varying from each other by no more than 5,000 cP. Thus the viscosity development with xanthates of around 0.12 DS is almost negligible, although it is significantly greater than the viscosity of 1000–2500 cP found in any of the "blank" reaction mixtures prepared.

For the 0.22 DS xanthate two curves are shown, and these represent a range of two groups into which all xanthates at this DS level fell. The curves have the same general shape, with "valleys" at the 20-min point, so that their only apparent difference is the magnitude of the viscosity. The viscosity curves for the 0.44 DS xanthate also have the same general shape, but the valley point comes at a longer reaction time, 30 min or slightly more. The very high viscosity, more than 100 000 cP, obtained with the xanthates of high DS is noteworthy.

No explanation is at hand for the appearance of the valleys in these viscosity curves. No visibly observable event correlating with this time point took place in the reaction mixtures. Since a separate reaction mixture was used for each viscosity determination point, it does not seem likely that the valleys are artifacts of the method of determining the viscosity. Differences between the viscosity curves are not due to any age differences in the xanthates since that possibility was checked by observing the reaction of several xanthate preparations when fresh and after 6-days' storage, and finding no notable change in viscosity development.

Whereas the reaction mixtures with 0.12 DS xanthate remain fluid, those with the 0.22 and 0.44 DS xanthates become firm gels when the viscosity reaches 20 000–30 000 cP. These rigid gels do not show any tendency to weep or exude liquid. They can be removed from the reaction vial in one piece. When left to dry in the air at room conditions, they become hard, brittle, green, and glasslike.

When the reaction mixtures were stirred into ethanol after about 30 min of reaction, which corresponds roughly to the time at which the viscosity development had passed through its minimum valley point and was again rising, solid, white products were precipitated. Data on the preparation and analysis of these solids appear in Table I. It will be noted that the DS of the starting xanthate as found by ethanol precipitation and sulfur determination is always somewhat lower than the DS found by titration. Evidently, titration gives an erroneously high value, or the xanthate preparations contain some oligosaccharide xanthates of very low molecular weight formed in the strong alkali medium, which are not precipitable by ethanol. From the sulfur content found in the solid products precipitated from the reaction mixtures by ethanol, it is apparent that the reaction involves the loss of NaHS from the two polymeric reactants. The products resulting from a 2:1 molar ratio of polyacrolein

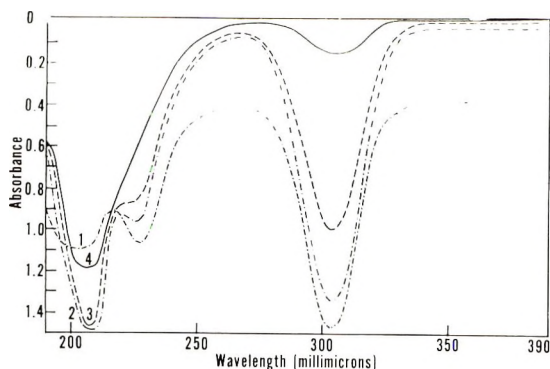
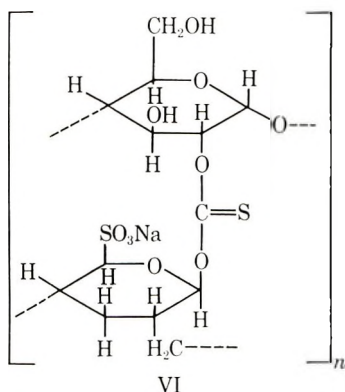


Fig. 2. Ultraviolet absorption spectra of gels and precipitated solid products in the polyacrolein bisulfite adduct and sodium starch xanthate (0.22 DS) reaction: (1) precipitated starch xanthate, 0.22 DS; (2) polyacrolein bisulfite-starch xanthate reaction gel, 2 min; (3) polyacrolein bisulfite-starch xanthate reaction gel, 120 min; (4) polyacrolein bisulfite-starch xanthate precipitated reaction product.

bisulfite adduct or xanthate group contain more sulfur than calculated for a compound with a DS assumed to be the same as that found by precipitation of the original xanthate, because the excess bisulfite adduct also is precipitated by ethanol. However, when the molar ratio is 1:1, the precipitated solid has the theoretical amount of sulfur for a product with the DS of the precipitated original starch xanthate. Most likely the elimination of NaHS originates between the  $-\text{C}(\text{S})\text{SNa}$  of the xanthate and the  $\text{HO}-$  of the polyacrolein, resulting in product VI, a thionocarbonate of symmetrical, potential structure.



Absorption spectra support the preceding proposals on product formation and structure. Although the precipitated products were somewhat too water-insoluble to give good ultraviolet spectra, monitoring the progressive formation of the reaction gel, which is water-soluble, showed a rapid decline of typical starch xanthate absorption at 226 and 303  $m\mu$ . If the precipitated products were merely a coprecipitate of the two reactants, it should show a typical xanthate absorption curve as precipitated sodium

starch xanthate does in water (Fig. 2). No xanthate is formed on the polyacrolein hydroxyl group by *trans*-xanthation, or from excess  $\text{CS}_2$  and  $\text{NaOH}$ , since the blank reaction of the inorganic reagents and the bisulfite adducts does not exhibit xanthate ultraviolet absorption, but rather tri-thiocarbonate absorption with  $\lambda_{\text{max}}$  at 198 and 328  $\text{m}\mu$ .

Infrared spectra confirm the presence of the starch structure and the polyacrolein structure in the product (Fig. 3). The polyacrolein absorption appears at 5.87, 6.15, and 6.43  $\mu$ , the starch absorption at 6.63  $\mu$  and in the 8–10  $\mu$  region, and both polymeric materials contribute to the 6.9–7.7  $\mu$  area. The presence of the 5.87  $\mu$  carbonyl band in the product spectrum

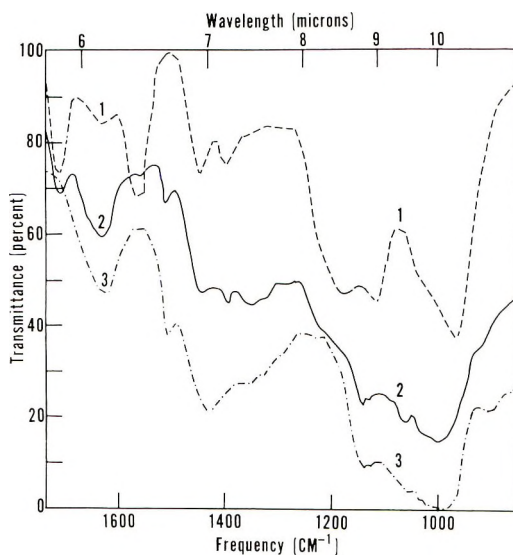
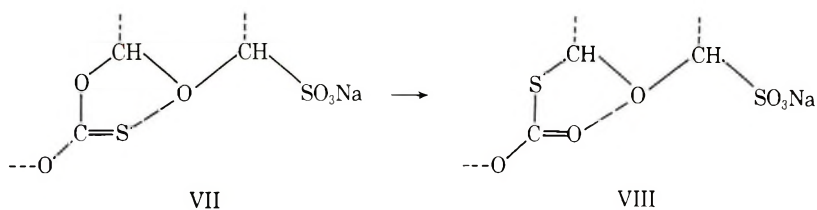


Fig. 3. Infrared absorption spectra of precipitated solid products in the polyacrolein bisulfite adduct and sodium starch xanthate reaction: (1) polyacrolein bisulfite adduct, precipitated; (2) polyacrolein bisulfite-starch xanthate precipitated reaction product, 0.22 DS; (3) precipitated starch xanthate, 0.22 DS.

indicates that the carbonyl group does not react with the xanthate, which inactivity is in agreement with observations of others that aldehyde reacts with xanthate only under acidic pH conditions.<sup>5,6</sup> The failure of aldehyde to react with xanthate in basic environment was also deduced because polyacrolein itself (Aklomer 110) and starch xanthate did not react and because the blank reaction mixture of benzaldehyde with starch xanthate in alkaline, aqueous methanol showed only a nondiminishing xanthate ultraviolet spectrum over a long reaction time. Nor did a reaction proceed in the benzaldehyde bisulfite and ethyl xanthate blank. The large absorption band at 6.1  $\mu$  in the spectra may be due in part to tenaciously adsorbed water. The bands at 6.15 and 6.43  $\mu$  are somewhat typical of polyacroleins, the former, being attributed to  $-\text{C}=\text{C}-$  groups,<sup>10</sup> and the latter, to the carboxylate ion formed from a Cannizzaro reaction in the presence of alkali.<sup>11</sup>



Possibly the grouping VII in the reaction product presents an anchimeric situation that permits a rearrangement to a monothiocarbonate (thiocarbonate) VIII.

Such rearrangements are known with thionocarbonates.<sup>12-14</sup> This structure would contribute to the carbonyl absorption in the infrared. Perhaps the valley in the viscosity development curves correlates with the rearrangement.

Unlike the crosslinked, solid product in the reaction gel formed by sodium starch xanthate and polyethylenimines,<sup>1</sup> the crosslinked monothiocarbonate cannot be precipitated from an alkaline water solution of its gel form by lowering the pH to neutral or even as low as 4.5 with hydrochloric acid. The drop in pH produces a colloidal, turbid suspension. However, when such manipulations of pH are done with mixtures of wood cellulose pulp suspensions and the solution of monothiocarbonate gel, analyses for sulfur content in dry paper mats resulting indicate about 33% of the possible monothiocarbonate is incorporated with the cellulose. This 33% stands in some contrast to the 100% precipitation of the starch polyethylenimino thiourethane material in paper mats similarly prepared.

T. R. Naffziger, W. L. Williams, and L. D. Miller prepared the starch xanthates. M. D. Swanson, B. R. Heaton, and C. E. McGrew conducted analyses.

Mention of trade or manufacturer's name should not be construed as a recommendation or endorsement by the U.S. Department of Agriculture over those not mentioned.

### References

1. G. G. Maher, C. R. Russell, and C. E. Rist, *Stärke*, **19**, 354 (1967).
2. R. C. Schulz, *Angew. Chem. Int. Ed.*, **3**, 416 (1964).
3. T. L. Dawson and F. J. Welch, *J. Amer. Chem. Soc.*, **86**, 4791 (1964).
4. E. Bergman, W. T. Tsatsos, and R. F. Fischer, *J. Polym. Sci. A*, **3**, 3485 (1965).
5. B. A. Thumm and S. Tryon, *J. Org. Chem.*, **29**, 2999 (1964).
6. L. H. Phifer and L. B. Ticknor, *J. Appl. Polym. Sci.*, **9**, 1055 (1965).
7. C. L. Swanson, T. R. Naffziger, C. R. Russell, B. T. Hofreiter, and C. E. Rist, *Ind. Eng. Chem. Prod. Res. Develop.*, **3**, 22 (1964).
8. W. M. Doane, C. R. Russell, and C. E. Rist, *Stärke*, **17**, 77 (1965).
9. D. C. White, *Mikrochim. Acta*, **807** (1962).
10. R. C. Schulz, G. Wegner, and W. Kern, in *Macromolecular Chemistry Prague 1965* (*J. Polym. Sci. C*, **16**), O. Wichterle and B. Sedláček, Eds., Interscience, New York, 1967, p. 989.
11. E. Bäder, K.-H. Rink, and H. Trautwein, *Makromol. Chem.*, **92**, 198 (1966).
12. D. L. Garmaise, A. Uchiyama, and A. F. McKay, *J. Org. Chem.*, **27**, 4509 (1962).
13. D. L. Garmaise and G. Y. Paris, *J. Org. Chem.*, **31**, 2003 (1966).
14. T. Taguchi, Y. Kawazoe, and M. Nakao, *Tetrahedron Letters*, **131** (1963).

Received June 9, 1969

Revised August 29, 1969

## Reaction of Poly(vinyl Alcohol) with Formaldehyde and Polymer Stereoregularity. Model Compounds.

KYOICHIRO SHIBATANI and KIYOSHI FUJII,  
Central Research Laboratories, Kurashiki Rayon Company,  
Sakazu, Kurashiki, Okayama, Japan

### Synopsis

The reaction of stereoisomers of pentane-2,4-diol and heptane-2,4,6-triol with formaldehyde was investigated as a model for the formalization reaction of poly(vinyl alcohol) in order to determine effect of the stereochemical configuration of the polyol molecules on the reaction. The isotactic (*meso*) diol portion reacted with formaldehyde to give *cis* formal several times faster than did the syndiotactic (*dl*) diol portion to give *trans*-formal at 30–80°C. In the reaction of heterotactic (*meso-dl*) triol which provides both the isotactic and syndiotactic diol portions in a molecule, the proportion of *trans*-formal in the total formal decreased as the reaction proceeded. This shows that the formation of *cis*-formal is also favored thermodynamically to a greater extent, and hence the intramolecular migration of *trans*-formal to *cis*-formal did occur during the reaction. The rates of hydrolysis of formals of the diols were compared with those of the triols in order to see the effect of a hydroxyl group adjacent to the formal ring on the reaction. No appreciable rate difference was observed between the dimer and trimer models both in *cis*- and *trans*-formals. Therefore it was deduced from these results that the increase of the rate of hydrolysis of poly(vinyl formal) with the increase of hydroxyl groups along the polymer chain is a characteristic of macromolecules that is not observed in the low molecular weight models.

### INTRODUCTION

The neighboring-group effect is one of the interesting aspects of the polymer reaction, and a number of reactions have been studied from the stereochemical point of view. Of these, acetalization of poly(vinyl alcohol) (PVA), along with hydrolyses of methacrylic polymers, has been most extensively studied.

In acetalization of PVA, the difference in reactivity between *meso* and *dl* diol portions of the polymer and between the *cis*- and *trans*-acetals obtained has been a major subject of investigation, and quantitative information on this problem is being accumulated.<sup>1-5</sup> It was recently disclosed that *cis*- and *trans*-formals were clearly distinguishable on the basis of the proton magnetic resonance spectrum, and this made it possible for us to follow the change of the polymer structure during formalization.<sup>4</sup> In the present paper, formalization of the stereoisomers of pentane-2,4-diol and of heptane-2,4,6-triol is studied in comparison with the reaction of the polymer which was reported in a preceding paper.<sup>5</sup> Undoubtedly this

comparison would lead to a better understanding of the reaction mechanism. Of these trimer models, heterotactic triol (*meso-dl*) is unique, in that it can form either *cis*- or *trans*-formal depending on the diol portion participating in the reaction. Therefore it was hoped that a study of the reaction of this triol might provide a useful information on the reaction of conventional (atactic) PVA.

In hydrolysis of poly(vinyl formal), it has been reported<sup>6,7</sup> that the rate of the reaction increased with the increase of hydroxyl groups in the polymer as in the hydrolysis of poly(vinyl acetate).<sup>8,9</sup> In order to see the effect of a hydroxyl group adjacent to the formal ring on the reaction, the present study included a comparison of hydrolyses of formals of the diols with those of the triols.

### EXPERIMENTAL

Pentane-2,4-diol and heptane-2,4,6-triol were synthesized and separated into the respective stereoisomers by column chromatography as reported previously.<sup>10,11</sup> The reaction of these polyols with formaldehyde was carried out in an aqueous medium in the presence of hydrochloric acid as catalyst. The rate of the reaction was followed by titrating the remaining formaldehyde by sodium bisulfite and iodine solutions.<sup>12a</sup> The rate constant of the reaction  $k$  was calculated by the equation:

$$dx/dt = k(a - x)(f - x) - k'x(b + x) \quad (1)$$

where  $a$ ,  $b$ , and  $f$  are the initial concentrations of polyols, water, and formaldehyde respectively, and  $x$  is the concentration of formaldehyde consumed during reaction time,  $t$  hours, and  $k'$  is the rate constant of the reverse reaction (hydrolysis). All formaldehyde ( $x$ ) was assumed to be consumed in the intramolecular formal formation leading to a *m*-dioxane ring and no intermolecular formal formation was taken into account in the above equation. This seemed to be a sound assumption on the basis of the finding of Kawase<sup>13</sup> that the formation of intermolecular formal was essentially negligible in formalization of PVA as long as the reaction system was homogeneous and that the crosslinking (inter-PVA formal) formed in the heterogeneous reaction was highly unstable to hydrolysis. Other problems in the kinetic treatment of the formal formation will be discussed later.

The equilibrium constant of the reaction of the diol was obtained by the equilibrium hydrolysis of the formals.<sup>2</sup> The *cis*- and *trans*-formals were separated by preparative gas chromatography with the use of dioctyl phthalate as a liquid phase and were subjected to the equilibrium hydrolysis. The equilibrium constant  $K$  was calculated by eq. (2):

$$K = k/k' = [(c - y)(b - y)]/y^2 \quad (2)$$

where  $c$  is the initial concentration of the formal (4,6-dimethyl-1,3-dioxane) and  $y$  is the concentration of formaldehyde freed at equilibrium.



The *cis/trans* ratio in formals obtained from the heterotactic triol was determined by the NMR spectrum<sup>4</sup> and gas chromatography.<sup>3</sup>

The rate of hydrolysis of the formals was measured in an experiment with the use of 1% (w/v) formal and 0.1 *N* hydrochloric acid at 60°C. The plot of the amount of formaldehyde liberated and the reaction time gave straight lines, and the rate constant  $k'$  was calculated from the slope.

## RESULTS

Representative time-conversion curves of the reaction of the triols with formaldehyde are shown in Figure 1. In this example, the reaction was carried out with the use of 10 wt-% triol and 0.69 mole/kg of formaldehyde (equimolar to the triol) in the presence of 0.1 *N* hydrochloric acid at 60°C. Obviously the isotactic molecule is reacting much faster than the syndiotactic. Thus a large difference was observed in the rate of acetal formation as well as in the reverse reaction.<sup>1</sup> From these data, the rate constant  $k$  (in kg/mole-hr), and the equilibrium constant  $K$  were estimated for each triol by using the eqs. (1) and (2).

$$k_{\text{I}} = 0.75 \pm 0.02$$

$$k_{\text{H}} = 0.45 \pm 0.04$$

$$k_{\text{S}} = 0.11 \pm 0.04$$

$$K_{\text{I}} = 3550$$

$$K_{\text{H}} = 1770$$

$$K_{\text{S}} = 190$$

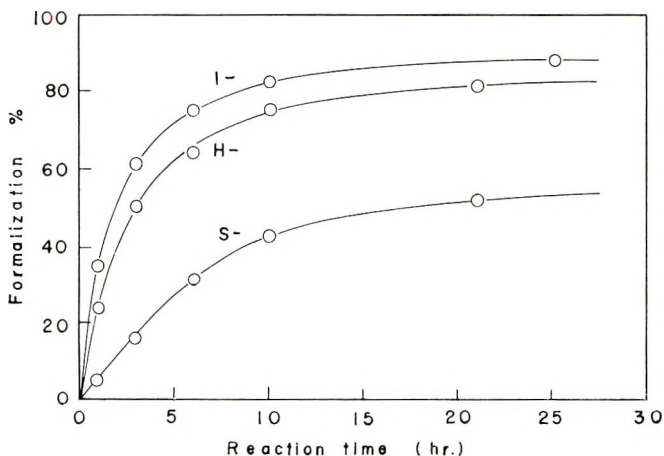


Fig. 1. Reaction of three isomeric heptane-2,4,6-triols with formaldehyde. Concentrations of HCl and the triol were 0.1 *N* and 10 wt-% respectively, and the equivalent formaldehyde to the triol was used in the reaction. The reaction temperature was 60°C.

TABLE I  
Rate and Equilibrium Constants of Reaction of Pentane-2,4-diol with  
Formaldehyde at 0.1 *N* Hydrochloric Acid

Isomer	Temperature, °C	$k$ , kg <sup>-1</sup> mole-hr	$K \times 10^{-2}$
<i>meso</i> diol	30		103.5 ± 1.0
	40	$(7.3 \pm 0.1) \times 10^{-2}$	76.0 ± 1.0
	50		59.0 ± 3.0
	60	$(5.7 \pm 0.5) \times 10^{-1}$	48.4 ± 1.0
	80	3.9 ± 0.1	35.2 ± 1.0
<i>dl</i> diol	30		2.65 ± 0.10
	40	$(0.8 \pm 0.1) \times 10^{-2}$	2.07 ± 0.10
	50		1.75 ± 0.10
	60	$(1.0 \pm 0.5) \times 10^{-1}$	1.56 ± 0.05
	80	0.9 ± 0.1	1.31 ± 0.10

The *meso* and *dl* pentane-2,4-diols were formalized at various temperatures using the same reagent concentrations as above, except that 0.87 mole/kg of formaldehyde (equimolar to the diol) was used. The equilibrium hydrolysis of *cis*- and *trans*-formals was also carried out at various temperatures at various acid concentrations from 0.1 to 2.0 *N* and initial concentrations of formal from 0.3 to 0.7 mole/kg. The reaction was carried on for three days to two weeks to complete the equilibrium. The rate and equilibrium constants thus obtained are summarized in Table I. From these data, the activation energy  $E_{\ddagger}$  and enthalpy  $H$  of the reaction were obtained by using the Arrhenius and van't Hoff equations, respectively.

$$d \ln k/dt = E_{\ddagger}/RT^2$$

The plots in Figure 2 yield

$$E_{\ddagger} = 20.0 \text{ kcal/mole}$$

$$E_{\ddagger} = 24.9 \text{ kcal/mole}$$

$$d \ln K/dt = H/RT^2$$

The plots in Figure 3 yield

$$H_I = -4.6 \text{ kcal/mole}$$

$$H_S = -3.0 \text{ kcal/mole}$$

The reaction of heterotactic triol was carried out at temperatures of 40, 60, and 80°C by use of the same reagent concentrations as in the diols, and changes of the relative amounts of *cis*- and *trans*-formals during the reaction were examined by the NMR spectroscopy. In Figure 4 are shown the changes of the proportion of *trans*-formal with time. The result looks somewhat complicated at first glance but can be well interpreted in terms of the thermodynamic relations obtained on the diols. At the beginning of the reaction, a smaller proportion of *trans* isomer was observed at lower

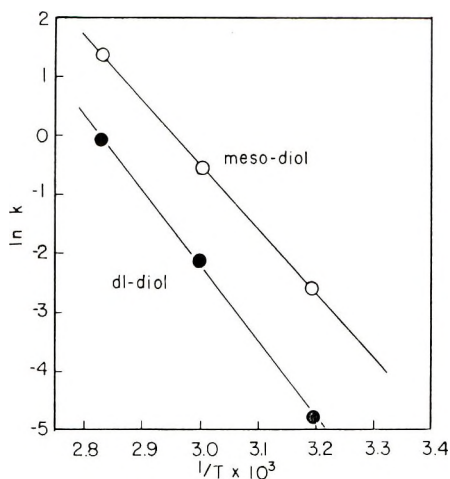


Fig. 2. Arrhenius plot of the rate constant  $k$  for formalization of pentane-2,4-diol. The concentration of HCl was 0.1  $N$ .

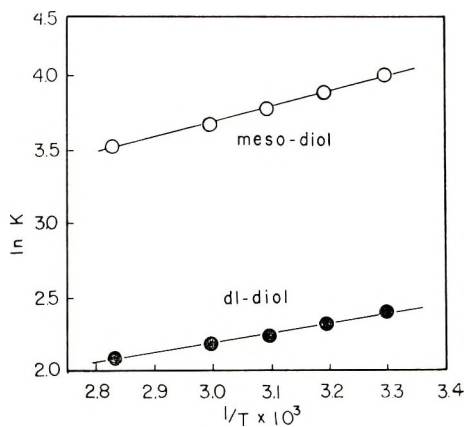


Fig. 3. Plots of  $d \ln K$  vs.  $1/T$  for formalization of pentane-2,4-diol.

temperatures. The proportions of *trans*-formal at zero time were estimated by extrapolation as 9.5% (40°C), 13% (60°C), and 17% (80°C), though an exact estimate was rather difficult to make due to the steep slope at higher temperatures. The initial *trans* content may also be estimated from the rates of formation of *cis*- and *trans*-formal from the diols provided the ring-forming step is rate-determining. In this case, the content may be expressed by a ratio,  $k_s/(k_i + k_s)$ . The ratio calculated from data of Table I is  $9.9 \times 10^{-2}$  at 40°C,  $15 \times 10^{-2}$  at 60°C, and  $18 \times 10^{-2}$  at 80°C. These values are in good agreement with the initial *trans* contents experimentally obtained for heterotactic triol.

The decrease of the *trans* content with time may be explained by an intramolecular migration of *trans*-formal to *cis* isomer. A similar type of migration is known to occur in reaction of glycerol with formaldehyde,

where the five-membered ring is formed predominantly at the beginning of the reaction but the six-membered ring becomes the main product when the reaction is continued for a long period.<sup>14</sup> The five-membered ring is the product of "kinetic control" and the six-membered ring is the product of "thermodynamic control" in this reaction. In the present case, formation of *cis*-formal is kinetically favored but is also thermodynamically favored to greater extent.

The *trans* content versus reaction time curves suggest that the equilibrium *trans* content decreases on raising temperature. This is consistent with that expected from an enthalpy difference between reactions of the

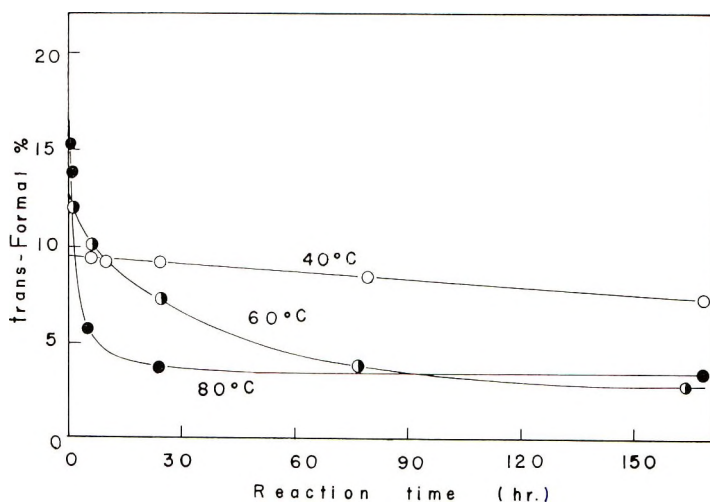


Fig. 4. Changes of the relative amount of *trans*-formal during formalization of heterotactic heptane-2,4,6-triol. Concentrations of HCl and the triol were 0.1 *N* and 10 wt-% respectively, and the equivalent formaldehyde to the triol was used in the reaction.

both diols with formaldehyde. In fact, as seen in Figure 4, the reaction was essentially at equilibrium at 60 and 80°C, and the equilibrium *trans* contents seem to be in good agreement with those obtained by the equilibrium hydrolysis experiment shown in Table I. On the other hand, equilibrium was not attained at 40°C because of insufficient reaction time.

The reaction of an equimolar mixture of isotactic and syndiotactic triols was compared with that of heterotactic triol as shown in Figure 5. In the mixed triols, the initial *trans* content was comparable to the reaction of heterotactic triol but the *trans* content showed an increase as the reaction proceeded in contrast with the case of heterotactic triol. This also indicates the presence of the *trans*-to-*cis* migration in the latter.

The ratio of *cis/trans* formals was also determined by the gas chromatography in the reaction of the triols. Figure 6 shows that both formals were clearly distinguished when dioctylsebacate was used as a liquid phase, as in

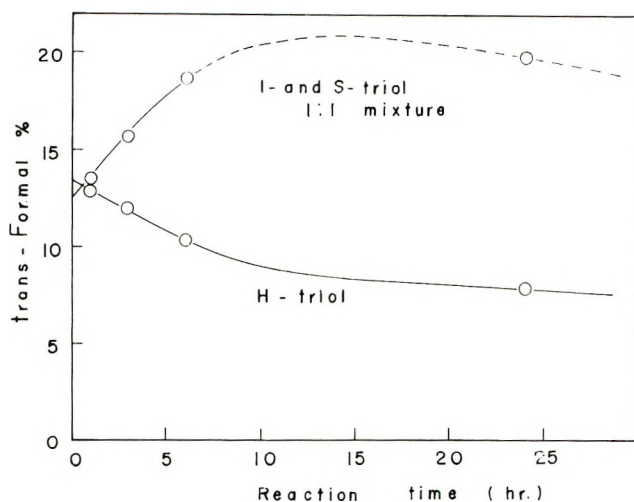


Fig. 5. Changes of the proportion of *trans*-formal during formalization of heterotactic triol and that of an equimolar mixture of isotactic and syndiotactic triols. Concentrations of HCl and the triol were 0.1 *N* and 10 wt-%, respectively, and the half-molar formaldehyde to the triol were used in the reaction. The reaction temperature was 60°C.

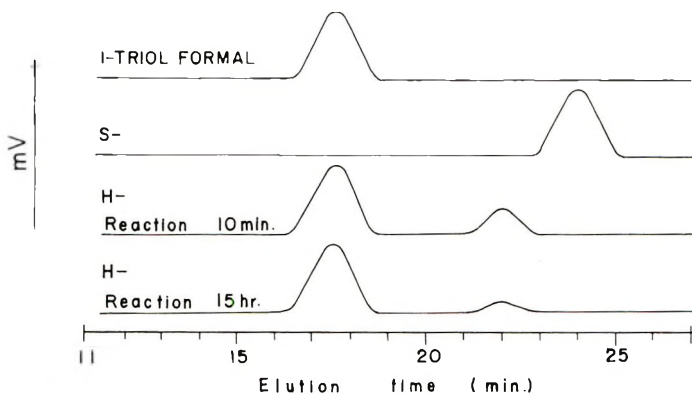


Fig. 6. Gas chromatograms of formalized triols. A dioctyl sebacate column (4 mm diameter, 3 m length) was used; a flow rate of helium gas, 70 ml/min, 165°C.

case of acetoacetals of the diols.<sup>3</sup> The *cis-trans* ratio estimated by the gas chromatography showed a good agreement with that determined by NMR spectroscopy.

The rates of hydrolysis of formals of the diols were compared with those of the triols. It was expected that a formal of a triol hydrolyzes faster than that of the corresponding diol because of the remaining hydroxyl group. Unexpectedly no such a difference was found, as shown in Table II. The rate of hydrolysis of the formal of triol is slightly lower than that of the corresponding diol.

TABLE II  
Rates of Hydrolysis of Model Formals

Original polyol	Rate of hydrolysis of formal $k' \times 10^3$ , kg/mole-hr
<i>meso</i> Pentane-2,4-diol	0.22 ± 0.05
Isotactic heptane-2,4,6-triol	0.16 ± 0.05
<i>dl</i> Pentane-2,4-diol	2.9 ± 0.2
Syndiotactic heptane-2,4,6-triol	2.7 ± 0.2

## DISCUSSION

As a result of rate measurements on model compounds having known stereostructures, it has been disclosed that the rate of formation of *cis*-formal was much faster than that of *trans*-formal, and that the ratio,  $k_i/k_s$ , increased as temperature was lowered; (e.g.,  $k_i/k_s = 4$  at 80°C,  $k_i/k_s = 9$  and 40°C). No such a definitive analysis had been made to the polymer reaction in relation to the steric structure of polymers.

The second important result attained in the present study is the elucidation of intramolecular migration of the formal ring during reaction of heterotactic triol with formaldehyde. This type of migration has to be taken into account in formalization of PVA also.

Thirdly, the present study gave an important suggestion on the reaction mechanism. It had been deduced from kinetic data that hemiacetal formation is a rate-determining step both in formation and hydrolysis of poly(vinyl acetal).<sup>7,15</sup> However, the present result seems to dispute this deduction, since it is rather unlikely that the polymer tacticity has such a large effect on the rate of hemiacetal formation. Microtacticity of methacrylate polymers has a profound effect on the rate of hydrolysis,<sup>16,17</sup> but in these polymers carboxyl groups formed by hydrolysis play an important role both in the electrostatic repulsion against the hydroxyl ion and in the functional interaction with neighboring ester groups.<sup>18</sup> However, such a stereochemical influence is much less important in hydrolysis of poly(vinyl acetate) and in esterification of PVA.<sup>19-21</sup> It is more probable that the ring-forming step is affected by the steric configuration of hydroxyl groups adjacent to a hemiacetal and this step is rate-determining. Evidence that the initial *trans* content in the reaction of heterotactic triol was in accord with that expected from the rates of reaction of the diols is also consistent with this view.

It is noteworthy that, in acetalization of PVA, one cannot find a rate-determining step from kinetic data alone. There are too many indefinite factors in this reaction from kinetic point of view. Formaldehyde does not exist in a simple chemical structure in a reaction mixture.<sup>12b</sup> The effect of the neighboring hydroxyl groups has not been fully understood and there have been two conflicting publications on this problem.<sup>7,22</sup> Furthermore, the dependence of the rate of reaction on the concentration of PVA (hydroxyl group concentration) does not provide a definitive answer

to the rate-determining problem because in this reaction the second step (ring formation) involves only two hydroxyl groups adjacent to a hemiacetal. Ogata et al.<sup>15</sup> deduced that hemiacetal formation was a rate-determining step from a kinetic scheme in which the reaction was first-order in respect to the PVA concentration. However, the same kinetic dependence may be observed even if the second step is rate-determining, and therefore the two steps are indistinguishable as a rate-determining step from the kinetic scheme alone.

Lastly it was found that the formal of the triol is not more reactive in hydrolysis than the formal of the corresponding diol. As in hydrolysis of poly(vinyl acetate),<sup>8,9</sup> the acetal of PVA is known to show a higher rate of hydrolysis with increasing hydroxyl content in the polymer.<sup>6,7</sup> The effect of hydroxyl groups directly adjacent to the functional groups have been suggested to account for the acceleration.<sup>7,9</sup> Recently detailed examinations on hydrolysis of poly(vinyl acetate) involving the use of various model compounds and polymer samples indicated that the rate increase by the adjacent hydroxyl group is not large enough to explain the acceleration during hydrolysis of the polymer; therefore some other effects have to be considered also.<sup>21</sup> The present findings suggests that the effect of the directly neighboring hydroxyl group is less important in hydrolysis of poly(vinyl formal) and some "polymeric effect" has to be considered to account for the acceleration.

The authors are greatly indebted to Dr. Y. Fujiwara for the NMR measurements, and to Drs. M. Matsumoto, J. Ukida, and Y. Oyanagi for their interest and encouragement during this work.

### References

1. K. Fujii, J. Ukida, and M. Matsumoto, *Makromol. Chem.*, **65**, 86 (1963).
2. K. Fujii, J. Ukida, and M. Matsumoto, *J. Polym. Sci. B*, **1**, 693 (1963).
3. M. Matsumoto and K. Fujii, *Kogyo Kagaku Zasshi*, **68**, 843 (1965).
4. K. Fujii, K. Shibatani, Y. Fujiwara, Y. Oyanagi, J. Ukida, and M. Matsumoto, *J. Polym. Sci. B*, **4**, 787 (1966).
5. K. Shibatani, K. Fujii, Y. Oyanagi, J. Ukida, and M. Matsumoto, *J. Polym. Sci. C*, **23**, 747 (1968).
6. N. Fujimoto, T. Osugi, and I. Sakurada, *Kobunshi Kagaku*, **7**, 14 (1950).
7. G. Smets and B. Petit, *Makromol. Chem.*, **33**, 41 (1959).
8. L. M. Minsk, W. J. Priest, and W. O. Kenyon, *J. Amer. Chem. Soc.*, **63**, 2715 (1941).
9. I. Sakurada et al., *Kogyo Kagaku Zasshi*, **45**, 1287, 1290, 1293 (1942).
10. E. Nagai, S. Kuribayashi, M. Shiraki, and M. Ukita, *J. Polym. Sci.*, **35**, 295 (1959).
11. K. Fujii, *J. Polym. Sci. B*, **3**, 375 (1965).
12. J. F. Walker, *Formaldehyde*, 3rd ed., Reinhold, New York 1966, (a) p. 508; (b) p. 52.
13. H. Kawase, O. Morimoto, and T. Mochizuki, paper presented at the 19th Annual Meeting of the Chemical Society of Japan, Tokyo, April 1966.
14. H. Hibbert and N. M. Carter, *J. Amer. Chem. Soc.*, **50**, 3120 (1928).
15. Y. Ogata, M. Okano, and T. Ganke, *J. Amer. Chem. Soc.*, **78**, 2962 (1956).
16. F. J. Glavis, *J. Polym. Sci.*, **36**, 547 (1959).

17. C. B. Chapman, *J. Polym. Sci.*, **45**, 238 (1960).
18. G. Smets and W. De Loecker, *J. Polym. Sci.*, **41**, 375 (1959).
19. K. Fujii, J. Ukida, and M. Matsumoto, *J. Polym. Sci. B*, **1**, 687 (1963).
20. K. Fujii, S. Brownstein, and A. M. Eastam, *J. Polym. Sci. A-1*, **6**, 2377 (1968).
21. K. Fujii, unpublished data.
22. I. Sakurada, Y. Sakaguchi, S. Yoshida, and Y. Osumi, *Kobunshi Kagaku*, **21**, 517 (1964).

Received September 9, 1969



## Radiation-Induced Solution Polymerization of Styrene in an Engineering Flow System

F. T. OSBORNE, S. OMI, V. STANNETT, and E. P. STAHEL,  
*Department of Chemical Engineering, North Carolina State University,  
Raleigh, North Carolina 27607*

### Synopsis

Radiation induced solution polymerization of styrene in methylene chloride in a small scale pilot plant utilizing a flow reactor is reported. Both conventional free radical and ionic polymerization have been achieved. With rigorous drying accomplished over molecular sieves the ionic mechanism predominates. Conclusive kinetic evidence as well as polymer properties substantiate radiation induced ionic polymerization for the first time in an engineering pilot plant. The validity of Williams' model is reinforced by this study and a survey of over 100 literature observations.

### INTRODUCTION

The  $\gamma$ -radiation-induced polymerization of styrene has been studied by numerous authors.<sup>1-30</sup> Early results, reviewed by Chapiro,<sup>4</sup> indicated that the polymerization proceeded via a free-radical mechanism. Results obtained within the last decade have shown the polymerization may also proceed via an ionic mechanism and with rigorous drying this ionic mechanism predominates.<sup>1,11,23-29</sup> All such polymerizations reported to date have been conducted as small batch reactions, either in solution<sup>1,2,5-10,12,13,18,19,21,22,25,27,30</sup> or in bulk.<sup>3,16,17,20,23,24,26,28,29,31</sup> This publication reports the radiation-induced solution polymerization of styrene in a small-scale pilot plant utilizing a flow reactor. Both conventional free-radical and ionic polymerization have been achieved.

### EXPERIMENTAL

A schematic diagram of the experimental apparatus is shown in Figure 1. Both final purification and polymerization are accomplished in this unit. The reactor system consists of a stirred vessel from which monomer solution is recirculated through a tubular reactor located in a high-intensity <sup>60</sup>Co irradiator. The reactor was contained in a 4-in. cylindrical canister through which a heat transfer medium was circulated. The eight Brookhaven Mark IV strips of <sup>60</sup>Co, each about 350 Ci, were uniformly positioned around the circumference of the cylindrical canister with an iris diaphragm arrangement. A detailed description of the equipment is provided elsewhere.<sup>15</sup>

The dose rate in the reactor was measured by using a slight modification of the procedure studied by Weiss.<sup>32</sup> Polyethylene tubes filled with Fricke solution were positioned in the tubular reactor which was filled with water prior to exposure in the irradiator. The average dose rate was 0.35 Mrad/hr, assuming  $G(\text{Fe}^{++} \rightarrow \text{Fe}^{+++}) = 15.5$ . The dose rate was quite uniform, varying by only 8% between the two reactor legs. End effects were of minor significance the dose rate in the nearest portions of the feed and return lines being less than 14% of the dose rate in the reactor.

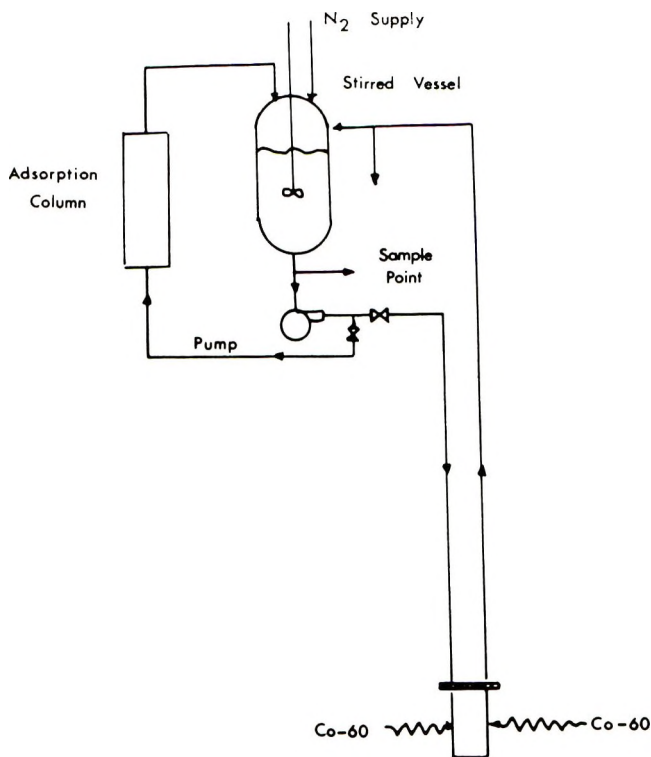


Fig. 1. Schematic diagram of experimental equipment.

In preparation for a polymerization run the equipment was first washed by recirculating methylene chloride solvent for about 2 hr. This procedure was repeated, followed by purging with nitrogen of ultra-high purity for 30 hr to remove absorbed moisture.

Both styrene monomer and methylene chloride solvent were prepurified by rectification on a Fisher Unitized Fractional Distillation Apparatus using a 1:1 reflux ratio in a 4-ft packed column. Technical grade methylene chloride was distilled at atmospheric pressure. A special sample of high purity styrene provided by Koopers Company was vacuum-distilled at 15 mm Hg. The first 200 ml of each 1-l. charge was discarded, and the next 500 ml was collected over a 6-hr period. The reagents were stored

under nitrogen at 35°F for no more than 5 days prior to use. Monomer solution was prepared by weighing 456 g of styrene into a 2-l. volumetric flask which was filled to volume with purified methylene chloride (2.18 mole/l. solution).

The monomer solution was charged to the stirred vessel under a nitrogen atmosphere. The solution was deoxygenated by repeated boiling under reduced pressure (18–20°C) with a nitrogen purge. For the ionic polymerization runs, the monomer mixture was dried by recirculation through a molecular sieve column for 24 hr. The temperature of the monomer solution was maintained near 0°C during drying. The method of operation capitalized on the more favorable moisture equilibrium at low temperature and minimizes polymerization during drying. Two types of molecular sieves were used. In one run, 1/16-in. pellets of Linde 4 Å sieves caused 86% polymerization during drying. Therefore, 4 × 8 mesh, low residual acid site, polymerization-resistant, type 362 3 Å Davison sieves were used. With these sieves, prepolymerization was reduced to less than 3.5%. As the rate of polymerization was determined from the time rate of change of conversion this low level of prepolymerization caused no difficulty.

After purification the monomer solution was recirculated through the tubular reactor located in a high intensity <sup>60</sup>Co irradiator. Samples were periodically withdrawn from the feed line below the stirred vessel. Each 5 ml sample was collected in a small tared bottle which was weighed on an analytical balance before inhibiting with a small amount of hydroquinone solution. After precipitation in 50 ml of methanol, the sample was filtered onto a sintered glass crucible. Conversion was calculated from the yield of dry polymer and the sample weight assuming a constant reactant density.

At the end of each run the reactant solution was displaced with nitrogen into a collecting vessel containing inhibitor. The polymer was recovered by precipitation into methanol. The filter cake was washed several times with methanol before drying overnight at 40°C. The intrinsic viscosity of this polymer was measured by use of a modified Ubbelohde viscometer. The polymer solutions were made in distilled benzene. Viscosity-average molecular weights  $\bar{M}_v$ , were calculated from the expression developed by Ewart and Tingey<sup>33</sup>

$$[\eta] = 0.97 \times 10^{-4} \bar{M}_v^{0.74} \quad (1)$$

The number-average molecular weight was estimated from the viscosity-average molecular weight:

$$\bar{M}_v = 1.85 \bar{M}_n \quad (2)$$

Molecular weight distributions were determined by Dr. R. F. Kratz and Dr. Dorothy J. Pollack of the Koppers Company by using a four-column gel-permeation chromatography assembly (10<sup>7</sup>, 10<sup>4</sup>, 10<sup>3</sup>, 10<sup>2.7</sup> Å). The calculations were corrected for dispersion by using a computer program.

## RESULTS

The data obtained were conversions at the exit of the stirred vessel as a function of time. Typical results from an experimental run are shown in Figure 2. Analysis of the dynamic behavior of the reactor system<sup>14</sup> shows that after an initial period the conversion is linear with time. The conversion rate in the reactor can be calculated from the slope of the linear portion of the conversion curve,

$$r_c = (\text{slope}) (V_T/V_P)$$

where  $r_c$  is total rate of conversion,  $V_T$  is the total volume of reaction mixture in the system, and  $V_P$  is the volume of the tubular reactor. The total polymerization rate  $R_P$  is the product of the conversion rate with the initial monomer concentration.

$$R_P = r_c[M]_0 \quad (3)$$

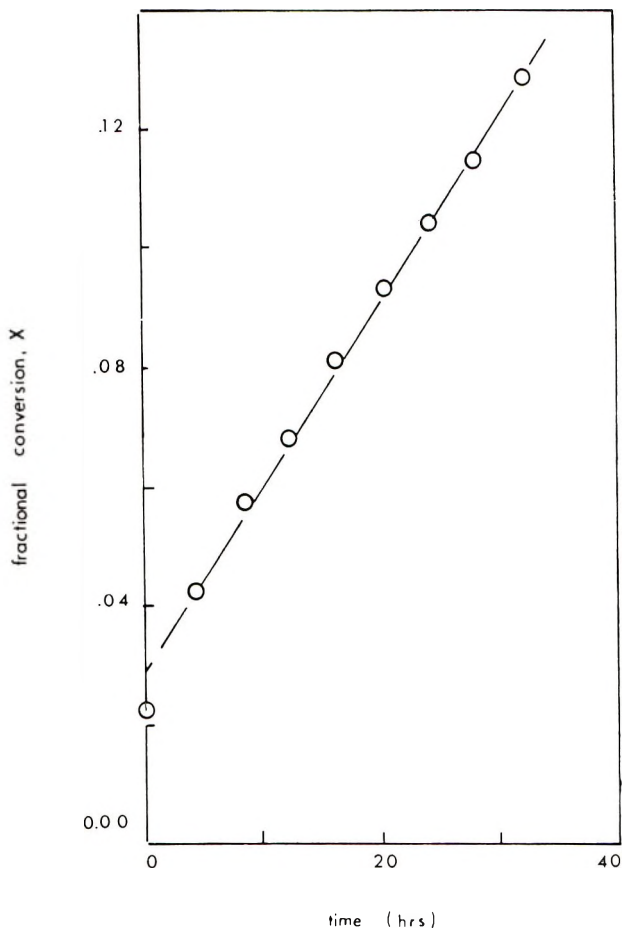


Fig. 2. Conversion history for typical run for styrene in methylene chloride, 11°C, dry.

TABLE I  
 Summary of Kinetic Results

Run no.	Environ- ment	Temp, °C	Total rate $\bar{r}_p$ $\times 10^5$ , mole/ l.-sec	Determined from viscosity			Determined from GPC		
				$\bar{M}_v$	$\bar{M}_n$	$\overline{DP}$	$\bar{M}_n$	$\bar{M}_w$	$\bar{M}_z$
5	Wet	30	1.01	10,850	5,860	56	6,820	22,020	114,600
7	Dry	30	4.92	31,540	17,050	164	19,790	55,500	102,900
8	Dry	15	4.84	49,980	27,020	260	25,850	68,080	115,400
9	Dry	0	6.09	65,390	35,350	340	32,970	84,440	147,000
10	Dry	-11	6.38	77,700	42,000	404	42,450	108,800	204,900

One polymerization was conducted under conditions selected to suppress any ionic polymerization and thus obtain a measure of the rate of free radical polymerization in methylene chloride solvent. For this run, a small amount of water (0.5 ml/l.) was added to the reaction mixture and the drying step was omitted. This free-radical or "wet" polymerization was conducted at 30°C. For all other polymerization runs the reaction mixture was dried by the procedure described earlier. Reaction temperature was varied from 30°C to -11°C. Polymerization rates calculated from the slope of a least squares line through the linear portion of the conversion histories are shown in Table I. Viscometry and gel-permeation chromatography results are also shown in Table I. Normalized molecular weight distributions are shown in Figure 3.

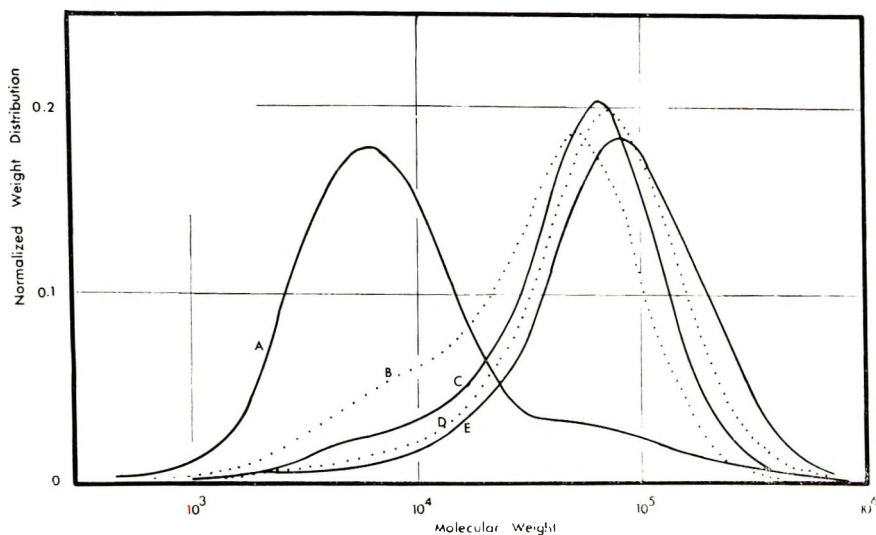


Fig. 3. Normalized molecular weight distributions from gel-permeation chromatography: (A) run 5; (B) run 7; (C) run 8; (D) run 9; (E) run 10. Experimental conditions shown in Table I.

## DISCUSSION

Under stringently dry conditions,  $\gamma$ -radiation induces both ionic and free-radical polymerization. As water is known to be a very effective inhibitor for the ionic mechanism, the rate of polymerization measured under wet conditions (Run 5, Table I) should correspond to the free-radical contribution. The rate of free-radical polymerization of styrene in methylene chloride is not well established. A good index for comparing free-radical polymerization rates is the relative reaction rate,

$$R_{pf}/R_{pf_0}$$

The most reliable source for  $R_{pf_0}$  is Chapiro,<sup>4</sup> who shows the bulk free-radical polymerization rate as a function of dose rate at 20°C. For other temperatures, the bulk rate was scaled by using the activation energy of 7.15 kcal/mole. The relative reaction rate is independent of temperature or dose rate and depends only upon concentration. Free-radical polymerization of styrene in chloroform and carbon tetrachloride has been systematically investigated.<sup>4</sup> Methylene chloride would be expected to demonstrate similar characteristics. For such solvents, the relative reaction rate is given as<sup>4</sup>

$$R_{pf}/R_{pf_0} = (1 + [S]/[M])^{1/2} \left[ \frac{1 + \phi_{rel} P_{rel} [S]/[M]}{1 + P_{rel} [S]/[M]} \right]^{1/2} \quad (4)$$

The relative reaction rate calculated from eq. (4) by using the values chloroform,  $P_{rel} = 10$ ,  $\phi_{rel} = 17$ , is compared with the experimental value measured in this study and values calculated from other observers in Table II. While neither the literature values nor the computed estimate for the relative reaction rate is strictly comparable, the value observed in this study is certainly near the expected value. The rate of polymerization observed under dry conditions is interpreted as the sum of a free-radical rate  $R_{pf}$  and an ionic rate  $R_{pi}$ .

$$R_p = R_{pf} + R_{pi} \quad (5)$$

The rate of free-radical polymerization at temperatures below 30°C was calculated from the rate measured under wet conditions at 30°C (run 5) by using an activation energy of 7.15 kcal/mol.<sup>4</sup> The rate of ionic polymeriza-

TABLE II  
Relative Rates of Free-Radical Polymerization

Temperature, °C	Dose rate, Mrad/hr	Monomer concentration, mole/l.	$R_{pf}/R_{pf_0}$	Reference
25	0.04	4.43	0.87	Charlesby <sup>7</sup>
20	0.02	2.3	1.23	Okamura <sup>12</sup>
30	0.35	2.18	0.71	Present work
—	—	2.18	0.59	Eq. (4)

tion was determined by difference. Polymerization rates calculated in this way are shown in Table III. When the ionic process was inhibited by the deliberate addition of water in run 5, a polymerization rate characteristic of the free-radical process was observed. The experimental evidences of an ionic contribution are: (1) drying the monomer solution produced an increase in the observed polymerization rate; (2) the polymerization rate increased with decreasing temperature; (3) the average molecular weight increased slightly with decreasing temperature.

TABLE III  
Calculated Polymerization Rates

Run no.	Temperature, °C	Total polymerization rate $R_p$ $\times 10^5$ , mole/l.-sec	Free-radical rate $\times 10^6$ , mole/l.-sec	Ionic rate $\times 10^5$ , mole/l.-sec
7	30	4.92	1.01 <sup>a</sup>	3.91
8	15	4.84	0.55	4.29
9	0	6.09	0.28	5.81
10	-11	6.38	0.16	6.22

<sup>a</sup> Results of run 5.

The effect of drying is most dramatic at the lowest temperature, where the observed polymerization rate was 40 times the free-radical rate calculated from the free-radical rate observed at 30°C.

The total polymerization rate of dried monomer exhibits distinctly non-Arrhenius temperature behavior having a minimum rate at 15°C. Exaggerated examples of this behavior have been observed by other authors working over a wider temperature range.<sup>5,10,19</sup> Interpreted as the sum of two processes, the ionic contribution is found to exhibit Arrhenius behavior as shown in Figure 4. The activation energy for the ionic contribution, calculated from the slope of the least squares line, is -1.9 kcal/mole. All authorities agree that the activation energy for free-radical polymerization is near +7 kcal/mole and the activation energy for ionic polymerization is small and negative. Activation energies from ionic rate measurements are shown in Table IV.

The average molecular weight of polymers produced in dry monomer solution increased with decreasing temperature. This in itself would be

TABLE IV  
Activation Energies for Ionic Polymerization

Temperature range, °C	Activation energy, kcal/mole	Reference
+21 to -80	+2.5	Metz <sup>11</sup>
-15 to -65	-1.2	Chen <sup>10</sup>
+30 to -11	-1.9	Present work

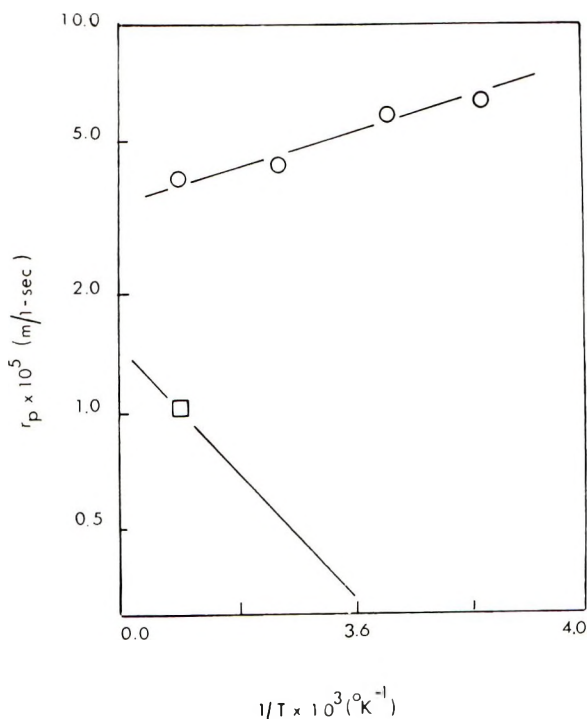


Fig. 4. Polymerization rates as a function of temperature: (○) ionic process; (□) free-radical process.

evidence of ionic polymerization if the experiment were carried out in bulk. Potter<sup>16</sup> has shown that for free-radical polymerization

$$d \ln \overline{DP}_i/dT = (\Delta E/R)(1/T^2) \quad (6)$$

All authorities agree that for bulk free radical polymerization  $\Delta E$  is positive and molecular weight increase with temperature. In solution, however, this behavior is reversed. Flory<sup>34</sup> has shown that if polymerization occurs in the presence of a chain transfer agent, such as solvent, the degree of polymerization is given by

$$\frac{1}{\overline{DP}} = \frac{k_i^{1/2} R_i^{1/2}}{k_p [M]_0} + \frac{k_{trm}}{k_p} + \frac{k_{trs} [S]}{k_p [M]} \quad (7)$$

where  $k_{trs}$  is the rate constant for chain transfer to solvent and  $k_{trm}$  is the rate constant for chain transfer to monomer. If termination is dominated by chain transfer to solvent, this becomes

$$1/\overline{DP} = k_{trs} [S]/[M] \quad (8)$$

The average molecular weight of 5860 observed from run 5 is much lower than the 50,000 observed in free-radical bulk polymerization at the same dose rate.<sup>4</sup> This supports the contention that the molecular weight is



TABLE V  
Results of Molecular Weight Calculations

Run no.	Temperature, °C	$\overline{DP}$	$\overline{DP}_f$	$\overline{DP}_i$
7	30	164	56 <sup>a</sup>	192
8	15	260	187	270
9	0	340	640	326
10	-11	404	1,870	366

<sup>a</sup> Observed in run 5.

controlled by chain transfer to solvent. The overall activation energy in this circumstance is

$$\Delta E = E_p - E_{trs} \quad (9)$$

which is  $-15$  kcal/mole for the styrene-ethylene dichloride system.<sup>35</sup> This behavior was observed by Chen and Stamm<sup>10</sup> for the free-radical polymerization of styrene in methylene chloride near room temperature. The apparent activation energy calculated from their data is  $-13.1$  kcal/mole; using the molecular weight from run 5 (Table II) to solve eq. (6) yields  $\overline{DP}_f$  as a function of temperature

$$\ln \overline{DP}_f = 6.61 (10/T)^3 - 17.77 \quad (10)$$

Since the polymers prepared under dry conditions were produced by both free-radical and ionic processes it seems reasonable to assume

$$R_{pf}\overline{DP}_f + R_{pi}\overline{DP}_i = R_p\overline{DP} \quad (11)$$

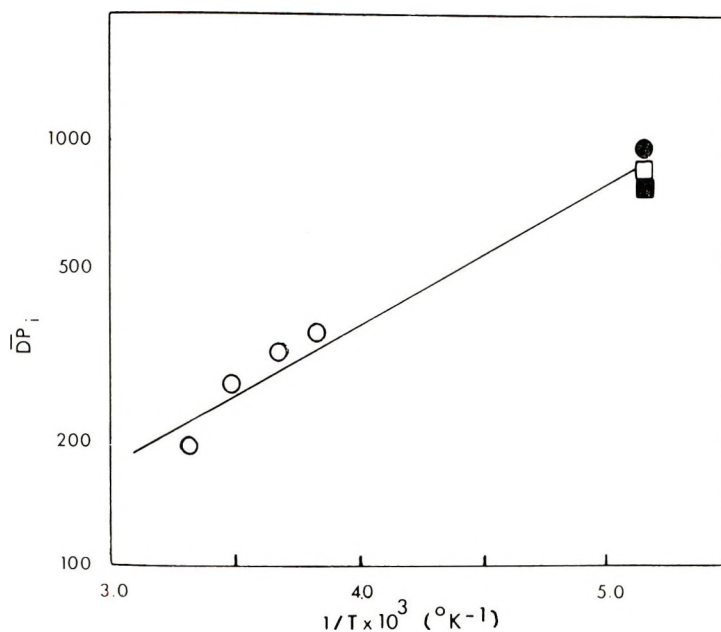


Fig. 5. Degree of ionic polymerization as a function of temperature: (●) data of Okamura et al.<sup>12</sup>; (□) data of Ueno et al.<sup>24</sup>; (■) data of Ueno et al.;<sup>26</sup> (○) present work.

TABLE VI  
Activation Energies from Molecular Weights

Temperature range, °C	Activation energy, kcal/mole	Reference
-20 to +40	-0.9 <sup>a</sup>	24
-65 to 0	-0.3	10
-78 to +30	-0.7	Present work

<sup>a</sup> Bulk styrene.

where  $R_{pf}$  and  $R_{pi}$  are known at various temperatures (Table III) and  $\overline{DP}_f$  can be calculated from eq. (10). The results of such calculations are shown in Table V. The  $\overline{DP}_f$  values calculated from eq. (2) seem too high at the lowest temperatures. It is doubtful that the large negative activation energy is constant over the entire temperature range. Because the free-radical rate is a small fraction of the total rate at the lowest temperatures this does not create any serious error.

Figure 5 is a plot of  $\log \overline{DP}_i$  as a function of reciprocal absolute temperature. Low-temperature data from other investigations are also shown. It is seen that the molecular weight of ionic polymer also increases with decreasing temperature but the magnitude of the activation energy is much smaller than for the free-radical process.

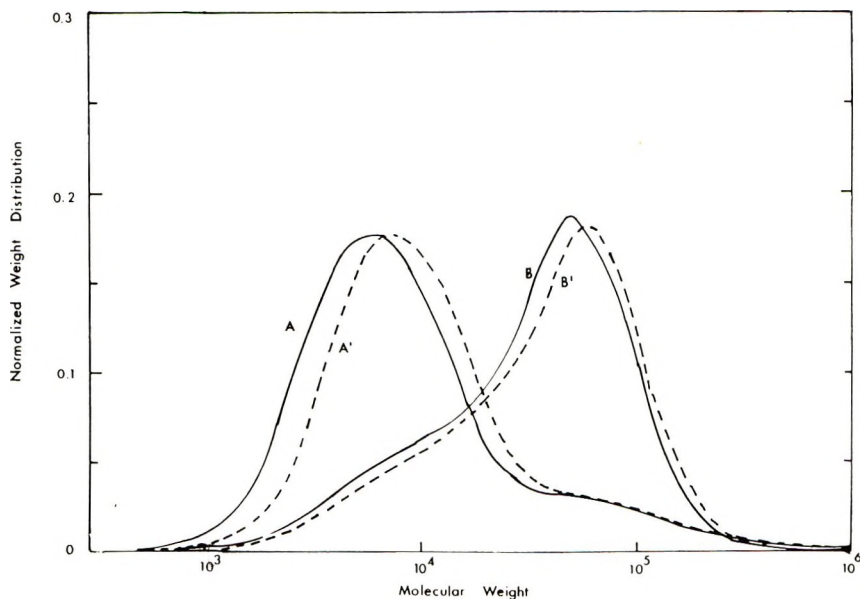


Fig. 6. Gel-permeation chromatograms of styrene on two different columns: (A) run 5, four-column assembly ( $10^{6.8}$ ,  $10^{5.9}$ ,  $10^3$ ,  $10^{2.7}$  Å); (B) run 7, four-column assembly; (A') run 5, five-column assembly ( $10^{6.8}$ ,  $10^{5.6}$ ,  $10^3$ ,  $10^{2.7}$ ,  $10^{1.6}$  Å); (B') run 7, five-column assembly. Solvent, tetrahydrofuran.

From the slope of Figure 5, the overall activation energy is found to be  $-0.7$  kcal/mole. Activation energies determined from molecular weight measurements by other observers are shown in Table VI. A low but negative overall activation energy from molecular weight measurements supports the presence of a dominant ionic contribution to the polymerization rate.

The gel permeation chromatograms further support the presence of both ionic and free radical polymerization mechanisms. Figure 3 shows clearly that drying, which enhances the ionic rate, shifts the molecular weight distributions upward. The samples prepared under dry conditions show a bimodal distribution. The smaller peak corresponding to the maximum in the free-radical distribution diminishes as the free radical contribution decreases with decreasing temperature. Surprisingly, the polymer prepared under wet conditions also shows a bimodal distribution with a minor peak corresponding to the maximum in the ionic distribution. This suggests that even the addition of water did not completely inhibit ionic polymerization.

A careful check was made to establish that these apparent bimodal distributions were not an artifact of the experimental method. Two of the samples (runs 5 and 7) were eluted through a five-column assembly ( $10^{6.8}$ ,  $10^{4.5}$ ,  $10^4$ ,  $10^{2.7}$ ,  $10^{1.6}$  Å) in an attempt to improve resolution. The results are nearly identical with the four-column results (Fig. 6). The lack of correction for dispersion probably accounts for the small differences.

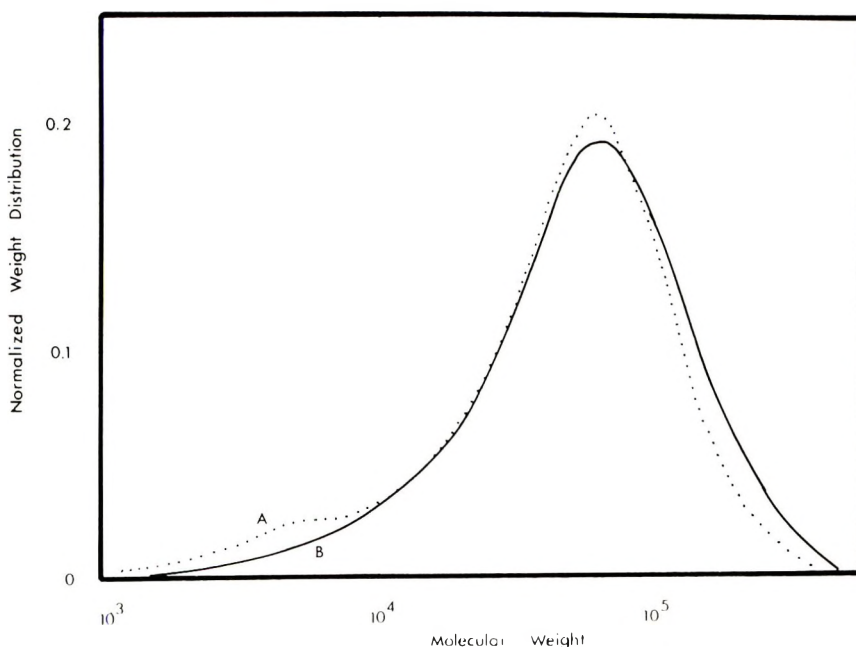


Fig. 7. Gel-permeation chromatogram for styrene in tetrahydrofuran on four-column assembly: (A) 2 ppm; (B)  $<0.5$  ppm.

Figure 7 presents two molecular weight distributions of polymers produced at 15°C at two different moisture levels. Except for the absence of the radical peak at low molecular weight, the distributions are almost identical. The sharp increase in rate associated with the drier polymerization precluded any appreciable polymer by the slower radical route.

Number-average molecular weights estimated from intrinsic viscosity are in good agreement with the GPC results. The viscosity-average molecular weights do not agree very well with the weight-average values, however. The molecular weight distributions are reasonably narrow; the  $\bar{M}_w/\bar{M}_n$  ratio ranges from 3.24 for the free-radical run to 2.56 for the ionic run at lowest temperature.

### COMPARISON WITH IONIC RATE EXPRESSION

The polymerization rate expression proposed by Williams et al.<sup>29</sup> will be used to compare the results of several ionic polymerization studies. This rate expression is

$$\begin{aligned} R_{pi} &= -d[M]/dt \\ &= k_p[M] R_i/(R_i k_t)^{1/2} + k_{tr}[X], \end{aligned} \quad (12)$$

where  $R_i = G_i I/100$  ( $I$  is in eV/g-sec).

The originators<sup>29</sup> have emphasized that eq. (12) is in accord with the experimentally observed fact that as the purity increases the exponent  $k$  in the expression  $R_p \propto I^k$  decreases from 1.0 to 0.5. If the impurity concentration  $[X]$  is relatively high, then

$$k_{tr}[X] \gg (R_i k_t)^{1/2} \quad (13)$$

and eq. (12) is given approximately as

$$R_p = k_p[M] R_i/k_{tr}[X] \quad (14)$$

This relation predicts that the polymerization rate is inversely proportional to the impurity concentration. Further, it predicts Arrhenius temperature behavior with an overall activation energy given by

$$E = E_p - E_{tr} \quad (15)$$

The logarithm of eq. (14) yields

$$\log R_p = \log [M] + \log (k_p R_i/k_{tr}[X])$$

A log-log plot of the polymerization rate as a function of monomer concentration should be linear with unit slope. The intercept at unit monomer concentration is  $(k_p R_i/k_{tr}[X])$ .

This rate expression satisfactorily correlates the bulk polymerization data obtained by Ueno et al.<sup>26</sup> It is of interest to apply this expression to available solution polymerization results. A large body of data is available spanning two decades of dose rate, 100°C of temperature, and a wide range

of concentrations. One factor limiting effective comparison to data has been the wide range of units employed. The results of over one hundred observations, reported for the ionic polymerization of styrene in methylene chloride, believed to contain all data, have been converted to common rate units. A few data from more recent bulk polymerization studies have also

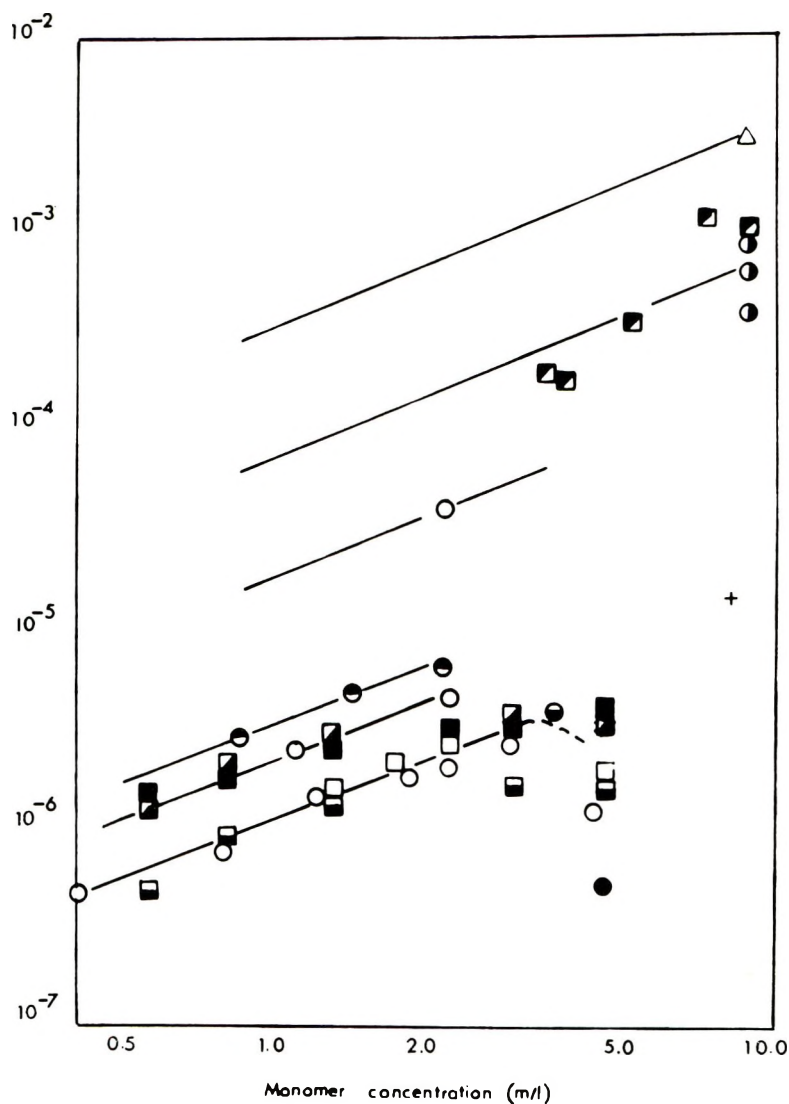


Fig. 8. Summary of 104 ionic polymerization rates normalized to 25°C and 0.35 Mrad/hr: (○) data of Okamura et al.; (●) data of Chen and Stamm;<sup>10</sup> (⊙) data of Okamura and Futami;<sup>12</sup> (⊖) data of Stannett et al.;<sup>21</sup> (⊕) data of Deno et al.;<sup>24</sup> (ϕ) data of Ueno et al.;<sup>27</sup> (□) data of Charlesby and Morris;<sup>7</sup> (◻) data of Charlesby and Morris;<sup>9</sup> (▣) data of Ueno et al.;<sup>25</sup> (Δ) data of Potter;<sup>16</sup> (■) silica, data of Charlesby and Morris;<sup>7</sup> (◼) silica, data of Charlesby and Morris;<sup>9</sup> (+) radical, data of Chapiro;<sup>4</sup> (⊖) present work.

been included. Because some data were taken from published figures, no more than two-digit precision is certain.

The data have been normalized to 25°C by using the activation energy of  $-1.9$  kcal/mole determined in this study. The results were normalized to a dose rate of 0.35 Mrad/hr by using the intensity components reported by the original authors. Where no intensity exponent was reported, it was taken to be unity. The calculations were executed on a digital computer.

Figure 8 shows the logarithm of the normalized rate as a function of  $\log [M]_0$ . When normalized, several observations plot a single point. The number of normalized data represented is shown adjacent to the symbol. According to the theory, the data should lie on lines of unit slope, each line intersecting unit monomer concentration at  $(k_p R_i / k_{tr} [X])$ . The data for each investigator are reasonably approximated by a line of unit slope up to 2.2 mole/l. where the rate exhibits a maximum. This behavior may be due to partial crystallization of the monomer solution. All data which show this maximum were measured at  $-78^\circ\text{C}$ . The freezing point-composition curve for the system is unknown, but Chen and Stamm<sup>10</sup> observed at 4.4 mole/l. solution to be partially crystalline at  $-78^\circ\text{C}$ . According to both Chen and Stamm<sup>10</sup> and Chapiro and Stannett,<sup>5</sup> the polymerization rate exhibits a maximum at the freezing point composition. Complete concentration data are lacking at higher temperatures and the data are badly scattered due to poor experimental reproducibility. The plot presents the rates in the anticipated order, the lower rates being observed by the earlier investigators who used the least stringent drying conditions.

Assigning an impurity level to one set of experiments permits estimating the rate constants. One of the lowest normalized rates was observed by Stannett et al.,<sup>21</sup> who deliberately added 5% water to a 3.48 mol/l. solution of styrene.

The solubility limit for water in styrene and in methylene chloride has been studied by Lane<sup>36</sup> and McGovern.<sup>37</sup> The solubility of water in styrene is negligible at  $-78^\circ\text{C}$ . The solubility in methylene chloride at  $-78^\circ\text{C}$  is 44 ppm. Assuming the solubility of water in the mixture  $S_M$  is given by

$$S_M = X_{St} S_{St} + X_{MCl} S_{MCl} \quad (16)$$

where  $X_{St}$  and  $X_{MCl}$  are the mole fractions of styrene and methylene chloride, respectively, and  $S_{St}$  and  $S_{MCl}$  are the solubilities in the pure components, the solubility of water in Stannett's mixture is estimated to be 32.2 ppm or  $[X] = 1.79 \times 10^{-3}$  mole/l. This agrees well with Ueno et al.<sup>25</sup> who observed that adding more than  $2 \times 10^{-3}$  mol/l. of water to a styrene-methylene chloride mixture did not further reduce the polymerization rate at  $-78^\circ\text{C}$ .

The magnitude of the rate constant  $k_{tr}$  can be calculated from the known polymerization rate and impurity level. The rate of initiation is calculated from the expression given by Williams et al.<sup>29</sup>

$$R_i = 1.66 \times 10^{-24} I \quad (17)$$

This assumes  $G_{(i_{ion})} = 0.1$  for all monomer concentrations and takes the density to be constant, 1000 g/l. By using Stannett's normalized rate of  $3.98 \times 10^{-6}$  mole/l.-sec, the ratio  $k_p/k_{tr}$  is calculated from the simplified rate expression

$$R_{pi} = k_p[M]_0 R_i / k_{tr}[X] \quad (18)$$

This gives  $k_p/k_{tr} = 0.205$ . Williams et al.<sup>29</sup> and Hayashi et al.<sup>31</sup> evaluated two rate constants from radiation-induced conductivity measurements. The values are

$$k_p = 5 \times 10^6 \text{ l./mole-sec}$$

$$k_t = 2 \times 10^{11} \text{ l./mole-sec}$$

Using their value of  $k_p$  to solve for  $k_{tr}$  yields

$$k_{tr} = 2.5 \times 10^7 \text{ l./mole-sec}$$

This value is smaller than the value  $1 \times 10^{10}$  used by Williams et al.<sup>29</sup> The value  $10^{10}$  was not an observation but was an upper limit chosen assuming the reaction with impurity was diffusion controlled. It has been shown that the efficiency of retardation parallels the proton affinity of the retarder for the series,<sup>26</sup>



Thus it is reasonable to expect the value of  $k_{tr}$  to be smaller for water retardation than for the trimethylamine retardation studied by Williams et al.<sup>29</sup> and Ueno et al.<sup>26</sup>

TABLE VII  
Impurity Levels Estimated from Data Shown in Figure 8  
Estimated impurity level,

Purification	mole/l.	Reference
CaH <sub>2</sub>	$1.8 \times 10^{-2}$	9, 10, 25
Na	$8.9 \times 10^{-4}$	7, 13
P <sub>2</sub> O <sub>5</sub>	$5.9 \times 10^{-4}$	12
Molecular sieves	$9.4 \times 10^{-5}$	Present work
Na/K, BaO	$2.8 \times 10^{-5}$	26, 27
Baked silica	$2.4 \times 10^{-4}$	16

Apparent impurity concentrations were calculated from the intercepts of each line with unit monomer concentration. At the highest purity level, the complete intercept expression,

$$\frac{k_p R_i}{(R_i k_t)^{1/2} + k_{tr}[X]}$$

must be used. A summary of the estimated impurity levels for each purification procedure is shown as Table VII.

The estimated water level for the present work is  $9.4 \times 10^{-5}$  mole/l. or 1.8 ppm. The highest purity,  $3.5 \times 10^{-6}$  mole/l. or 0.06 ppm, is one of the lower rates obtained by Potter.<sup>16</sup> The estimates agree well with the data of Ueno et al.,<sup>24</sup> who observed that  $6.8 \times 10^{-4}$  mole/l. of water was required to reduce the rate of bulk polymerization to the classical free radical rate.

Rates computed from Williams' model for these values for the rate constants and the impurity level agree well with experimentally observed values. For the present work, the computed value is  $4.5 \times 10^{-4}$  mole/l.-sec, the observed value,  $4.2 \times 10^{-5}$  mole/l.-sec. Potter's value<sup>16</sup> of  $3.2 \times 10^{-3}$  mole/l.-sec is computed precisely. This excellent agreement is somewhat fortuitous as the rate constants are not known this accurately.

In addition to correlating the observed rate data, the rate model can be used to check the intensity exponent. Potter<sup>16</sup> observed an intensity exponent of 0.87 over the range of  $4 \times 10^3$  rad/hr to  $6 \times 10^4$  rad/hr. The exponent calculated by using the rate model is 0.95.

Both bulk and homogeneous solution polymerization data are well correlated by the Williams' model. This strongly supports the adequacy of the proposed mechanistic development for homogeneous polymerization.

Heterogeneous polymerization experiments deviate from the model indicating a different mechanism may be operative. The experiments in which Charlesby and Morris<sup>7-9</sup> irradiated styrene solution in the presence of silica gel (denoted in Fig. 8 by "silica") give distinctly different behavior. They observed an intensity exponent of  $1/2$ , but the data are far below the maximum rates where the model predicts the intensity exponent approaches a limiting value of  $1/2$ . Clearly, these data must be attributed to a different process from the homogeneous ionic polymerization so well described by Williams' model.

## CONCLUSIONS

Radiation-induced ionic polymerization of styrene has been carried out in an engineering flow system. The all-steel 6-l. system, utilizing adsorption on molecular sieves as a drying procedure is capable of achieving "moderately" low moisture levels of approximately two ppm. At this moisture level both radical and ionic polymerization are observed. Conclusive kinetic evidence as well as the properties of the polymers formed substantiate radiation induced ionic polymerization for the first time in an engineering pilot plant. Complete specifications of the parameters in Williams' model was carried out enabling correlation of over one hundred literature observations for styrene in methylene chloride. The validity of this model is strongly reinforced.

This work was supported by the Division of Isotope Development of the U.S.A.E.C



## References

1. A. D. Abkin, A. P. Sheinker, and M. K. Yakovleva, *Vysokomol. Soedin.*, **3**, 1135 (1961).
2. A. D. Abkin, A. P. Sheinker, M. K. Yakovleva, and L. P. Mekhirova, *J. Polym. Sci.*, **53**, 39 (1961).
3. D. S. Ballantine, P. Colombo, A. Glines, and B. Manowitz. *Chem. Eng. Progr. Symp. Ser.*, **50**, No. 11, 267 (1954).
4. A. Chapiro, *Radiation Chemistry of Polymer Systems*. Interscience, New York, 1962.
5. A. Chapiro and V. Stannett, *J. Chim. Phys.*, **56**, 830 (1959).
6. A. Chapiro and Y. Tsuda, *J. Chim. Phys.*, **60**, 1021 (1963).
7. A. Charlesby and J. Morris, *Proc. Roy. Soc. (London)*, **A273**, 387 (1953).
8. A. Charlesby and J. Morris, in *Macromolecular Chemistry, Paris 1963*, (*J. Polym. Sci. C*, **4**), M. Magat, Ed., Interscience, New York, 1963, p. 1127.
9. A. Charlesby and J. Morris, *Proc. Roy. Soc. (London)*, **A281**, 392 (1964).
10. C. S. H. Chen and R. F. Stamm, *J. Polym. Sci.*, **58**, 369 (1962).
11. D. J. Metz and D. S. Ballantine, BNL 11344, Brookhaven National Laboratory, Upton, New York, 1967.
12. S. Okamura, and S. Futami, *Int. J. Appl. Rad. Isotopes*, **8**, 46 (1960).
13. S. Okamura, T. Higashimura, and S. Futami, *Isotop. Rad.*, **1**, 216.
14. F. T. Osborne, D. C. Martin, V. Stannett, and E. P. Stahel, paper presented at the 64th Annual A.I.Ch.E. Meeting, Cleveland, Ohio, May 1969.
15. F. T. Osborne, S. Omi, V. Stannett, and E. P. Stahel, to be published.
16. R. C. Potter, Ph.D. Thesis, Department of Chemical Engineering, Yale University, New Haven, Connecticut, 1966; University Microfilms, Inc., Ann Arbor, Michigan.
17. R. C. Potter, R. H. Bretton, and D. J. Metz, *J. Polym. Sci. A-1*, **4**, 2295 (1966).
18. A. P. Sheinker and A. D. Abkin, *Vysokomol. Soedin.*, **3**, 716 (1961).
19. A. P. Sheinker, M. K. Yakovleva, E. V. Kristal'nyi, and A. D. Abkin, *Dokl. Akad. Nauk SSSR*, **124**, 632 (1959).
20. S. Srivivansan, Ph.D. Thesis, Department of Nuclear Engineering, University of Maryland, College Park, Maryland, 1965; University Microfilms, Inc., Ann Arbor, Michigan.
21. V. Stannett, F. C. Bahstetter, Jr., A. Meyer, and M. Swarc, *Int. J. Appl. Rad. Isotopes*, **15**, 747 (1964).
22. Y. Tsuda, *J. Polym. Sci.*, **54**, 193 (1961).
23. K. Ueno, K. Hayashi, and S. Okamura, *J. Polym. Sci. B*, **3**, 363 (1965).
24. K. Ueno, K. Hayashi, and S. Okamura, *Polymer*, **7**, 431 (1966).
25. K. Ueno, K. Hayashi, and S. Okamura, *Polymer*, **7**, 451 (1966).
26. K. Ueno, F. Williams, K. Hayashi, and S. Okamura, *Trans. Faraday Soc.*, **63**, 1478 (1967).
27. K. Ueno, H. Yamaoka, K. Hayashi, and S. Okamura, *Int. J. Appl. Rad. Isotopes*, **17**, 513 (1966).
28. F. Williams, Atomic Energy Commission Document No. ORO-2968-21. North Carolina Science and Technology Research Center, Research Triangle Park, North Carolina, 1966.
29. F. Williams, K. Hayashi, K. Ueno, and S. Okamura, *Trans. Faraday Soc.*, **63**, 1501 (1967).
30. M. K. Yakovleva, A. P. Sheinker, and A. D. Abkin, *Vysokomol. Soedin.*, **3**, 828 (1960).
31. K. Hayashi, Y. Yamazawa, T. Takagaki, F. Williams, K. Hayashi, and S. Okamura, *Trans. Faraday Soc.*, **63**, 1489 (1967).
32. J. Weiss, *Nuclonics*, **10**, 28 (1952).
33. R. H. Ewart and H. C. Tingey, paper presented at the 111th Meeting of the American Chemical Society, Atlantic City, N. J., April 14-18, 1947.

34. P. J. Flory, *Principles of Polymer Chemistry*, Cornell Univ. Press, Ithaca, N. Y., 1953.
35. F. Mayo, *J. Amer. Chem. Soc.*, **65**, 2324 (1943).
36. W. H. Lane, *Ind. Eng. Chem. Anal. Ed.* **18**, 295 (1946).
37. E. W. McGovern, *Ind. Eng. Chem.* **35**, 1230 (1943).

Received September 9, 1969

## Copolymerization with Depropagation. IV. Computer Simulation of Copolymerization with Reversibility

M. IZU\* and K. F. O'DRISCOLL, *Department of Chemical Engineering, State University of New York at Buffalo, Buffalo, New York 14214*

### Synopsis

The results of Monte Carlo computer simulations of vinyl copolymerizations with complete reversibility are described for a variety of hypothetical systems using values of thermodynamic quantities typically found. Composition of copolymer, sequence distributions, relative chain lengths and equilibrium behavior have all been investigated. The existence of thermodynamic control of copolymerization behavior becomes more obvious as temperature is increased in some systems but may be masked by kinetic factors in others.

### INTRODUCTION

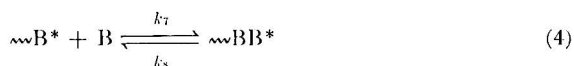
There have been a few attempts to derive the copolymer composition equation for copolymerization with reversibility. Most notable was that of Lowry<sup>1</sup> for one depropagating monomer. A first approach for complete reversibility was made by Durgariyan; but because of the complexity of the form of the solution, he applied the solution only to a very special case by making assumptions for simplification.<sup>2</sup> We have treated this complex type of copolymerization on the basis of probability considerations in the previous paper.<sup>3</sup> The analytical solution offered there is complemented by a completely numerical solution in this paper. Computer simulation by means of a Monte Carlo technique enables us to obtain a general idea of the behavior of the copolymerization. Price has previously applied the Monte Carlo method in order to visualize stereoregular polymers and pointed out that one of the merits of this technique is that we can see the simulated polymer chain,<sup>4</sup> thus providing an idea of the copolymerization behavior at a glance. Another merit is the simplicity of the logic in carrying out this computation. Owing to these merits, the Monte Carlo method is suitable to explore the general behavior of copolymerization with complete reversibility.

### APPLICATION OF MONTE CARLO METHOD

Assuming all four elementary steps in the conventional terminal model of the irreversible copolymerization to be reversible, the scheme of eqs.

\* On leave from Department of Hydrocarbon Chemistry, Kyoto University, Kyoto, Japan.

(1)–(4) is written with eight different rate constants:



Because the sequence in the terminal diad affects the fate of the next step, we term this model the "diad model." Analogously, a "triad model" with sixteen different rate constants is defined, assuming the forward reactions follow the penultimate model. Although we show here the application of Monte Carlo method to the diad model, there is no difficulty both in necessary logic and in programming to extend this to a triad model.

It is possible to regard a copolymerization as a stochastic process as is fully discussed in the previous paper.<sup>3</sup> Thus, considering the relation between the rates of competitive reactions and the probabilities of occurrences of the reactions, probabilities of occurrence of the events (addition of either monomer and detaching the chain end unit) assigned to four different terminal diads are expressed for example as

$$P_{\text{AA}(+\text{A})} = k_1[\text{A}]/(k_1[\text{A}] + k_2 + k_3[\text{B}]) \quad (5)$$

$$P_{\text{AA}(+\text{B})} = k_3[\text{B}]/(k_1[\text{A}] + k_2 + k_3[\text{B}]) \quad (6)$$

$$P_{\text{AA}(-\text{A})} = k_2/(k_1[\text{A}] + k_2 + k_3[\text{B}]) \quad (7)$$

Note that, in general,

$$P_{\text{BA}(-\text{A})} \neq P_{\text{AA}(-\text{A})} \quad (8)$$

It is seen that probabilities are expressed as simple functions of rate constants and monomer concentrations. The values of  $k_1, k_2, \dots, k_8$  must be determined experimentally or estimated theoretically. Here we suppose that  $r_1 (= k_1/k_3)$ ,  $r_2 (= k_7/k_4)$ ,  $s_1 (= k_1/k_5)$  and  $-\Delta G^\circ$  of all possible reactions are known. By using the equation:

$$-RT \ln K = \Delta G^\circ \quad (9)$$

where  $K$  is the rate constant of forward reaction/the rate constant of reverse reaction, ie. the equilibrium constant, we can calculate relative values of the rate constants from these inputs.

Knowing the values of the probabilities assigned to four different types of chain end, it is possible to carry out random experiments to construct a polymer chain by means of Monte Carlo method. The polymer chain

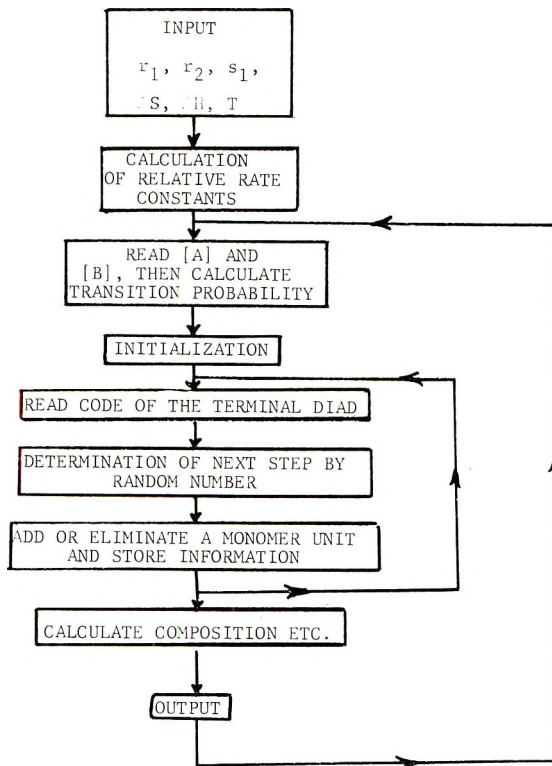


Fig. 1. Flow chart.

produced must be very similar to the actual polymer chain if the number of the random experiments is very large.

Random experiments were carried out on the CDC 6400 computer. The flow chart of the computation is shown in Figure 1. Binary code was

TABLE I  
Estimation of Relative Molecular Weight of the Polymer<sup>a</sup>

$[M_1]$	$[M_2]$	$P_1$	$N$	$\Sigma Ni$	$M$
0.9	0.1	0.916	500	516	490
0.8	0.2	0.838	500	568	400
0.7	0.3	0.782	500	628	360
0.6	0.4	0.742	500	702	260
0.5	0.5	0.686	500	884	220
0.4	0.6	0.630	500	1160	180
0.3	0.7	0.584	500	1470	180
0.2	0.8	0.510	500	2738	110
0.1	0.9	0.487	478	5000	58

<sup>a</sup> Input data and polymerization conditions:  $r_1 = 1.0$ ,  $r_2 = 1.0$ ,  $s_1 = 1.0$ ,  $-\Delta S_{11}^{\circ} = -\Delta S_{12}^{\circ} = -\Delta S_{21}^{\circ} = -\Delta S_{22}^{\circ} = 28.0$  cal/deg-mole,  $-\Delta H_{11}^{\circ} = 16$  kcal/mole;  $-\Delta H_{12}^{\circ} = -\Delta H_{21}^{\circ} = 13$  kcal/mole;  $\Delta H_{22}^{\circ} = 10$  kcal/mole; polymerization temperature = 400°K.

used to memorize polymer formed in the computer. Polymerization was started from the pentamer of the monomer having the higher ceiling temperature. Initialization was repeated up to five times when the initial polymer chain was decomposed. Random experiments were stopped either in the case that the number of monomer units polymerized exceeded 500 or in the case that the number of random experiments exceeded 5000.

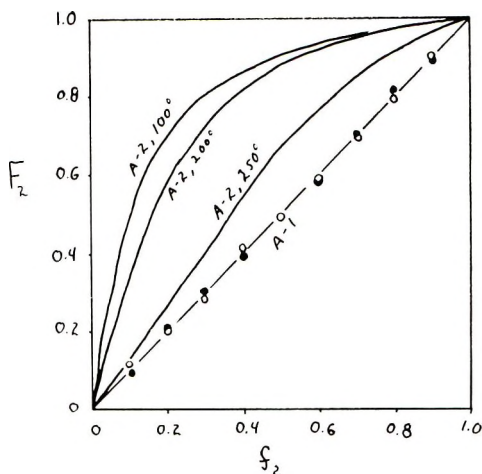


Fig. 2. Results of Monte-Carlo calculations of copolymer composition curves for case A-1 and A-2 of Table II; (O) A-1, 100°C; (●) A-2, 200°C.

The results shown in Figure 2 are typical. The deviation of some points on A-1 from a smooth curve, which looks like experimental error, will decrease with an increase in the number of the random experiments. The number of monomer units in the polymer chain  $N$  is equal to the number of random experiments  $\Sigma N_i$ , if no depropagation reaction occurs, but is less than the latter number when depropagation occurs, as shown in Table I.

The relative value of the time  $t$  which will be necessary to construct a copolymer can be approximated by the following equation.

$$t = \sum_{i=1}^{24} N_i/R_i \quad (10)$$

with  $N_i$  = the number of occurrences of an event  $i$  (there are three different events possible for each of 8 terminal diads, therefore  $i = 1, 2, \dots, 24$ );  $R_i$  = the rate of the occurrence of the event  $i$ .

Assuming that the life time of a propagating species is independent of the monomer-feed ratio, the relative magnitude of the molecular weight is simulated by the following

$$M = N/t \quad (11)$$

where  $M$  is the relative magnitude of the molecular weight and  $N$  is the number of monomer units in the polymer chain. The last column in Table I shows this estimated value.

Another possible application is to predict the equilibrium state in a closed system. For example, to predict equilibrium monomer concentration in the reversible copolymerization the decrease in the monomer concentration may be taken into account.

## RESULTS AND DISCUSSION

Every propagation step of a copolymerization should be treated as a reversible step, when monomers are copolymerized at a temperature near the ceiling temperature of the monomer having the higher ceiling temperature. Very few experimental data and theoretical predictions are now available on the copolymerization behavior of this type. Therefore, computer simulations of typical copolymerizations under these conditions were made on hypothetical cases in order to get a general idea of copolymerization with complete reversibility.

The composition-feed relationships for copolymerization of the monomer pairs having those hypothetical values of thermodynamic and kinetic quantities shown in Table II were simulated at various temperatures. It should be noted that the kinetic quantity is dependent on the polymerization mechanism whereas the thermodynamic quantity is independent of it.

Cases A-D correspond to copolymerizations with monomer pairs having the same ceiling temperatures.

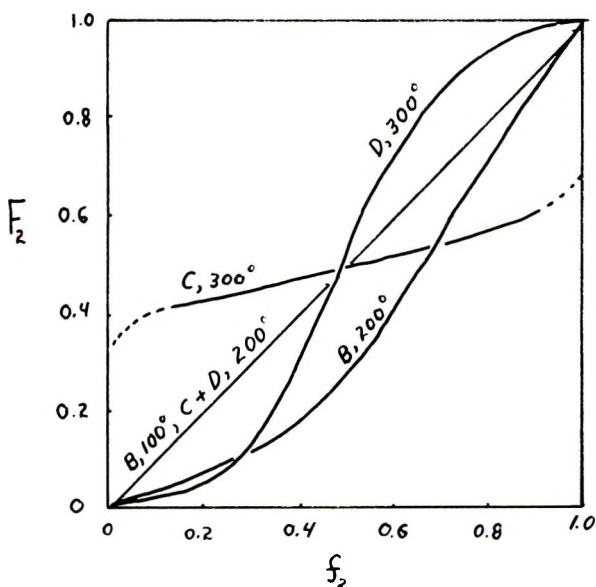


Fig. 3. Results of Monte-Carlo calculations of copolymer composition curves for cases B, C, and D of Table II.





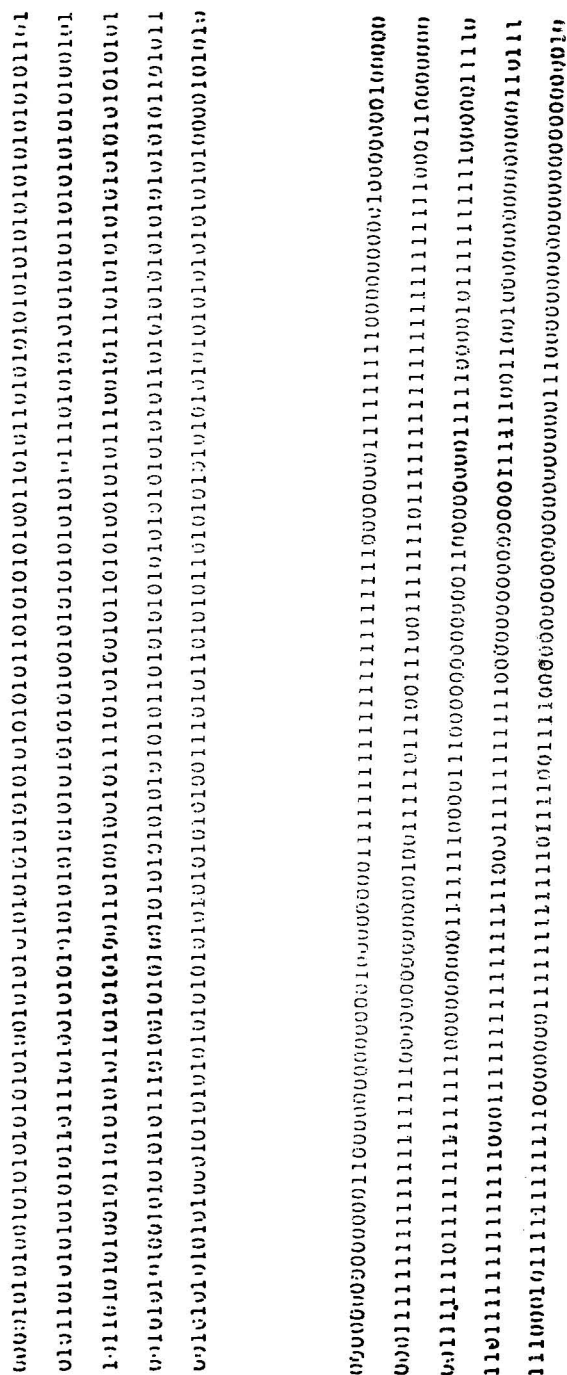


Fig. 4. Sequence distributions generated by Monte Carlo calculations: (A) the nearly alternating copolymer of case C, 300°C,  $f_2 = 0.5$ ,  $F_2 0.49$ ; (B) the block-type copolymer of case D, 300°C,  $f_2 = 0.5$ ,  $f_2 = 0.51$ . The binary code uses a 0 to identify monomer A (or  $M_1$ ) and a 1 to identify monomer B (or  $M_2$ ).

In cases A-1 and A-2 we assume that all the elementary steps have the same thermodynamic quantities and that the values of  $r_1$  and  $r_2$  are different. The results for case A-1 in Figure 2 show the polymer composition is identical to that of the feed at 100°C and 200°C, as is expected. We

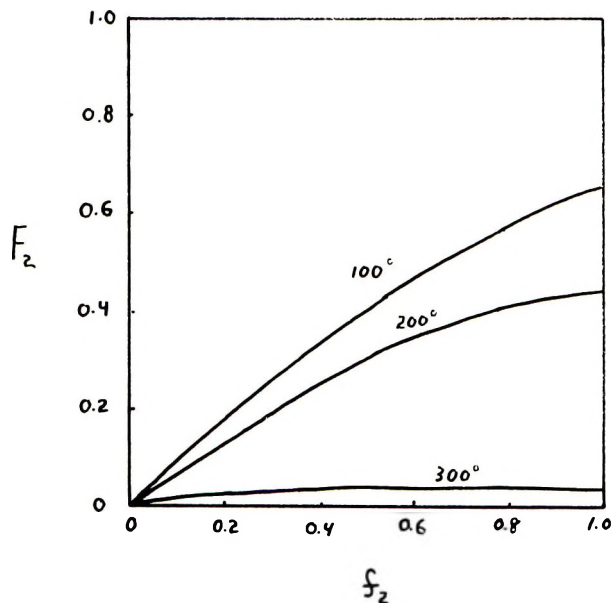


Fig. 5. Results of Monte-Carlo calculations of copolymer composition for Case E-1.

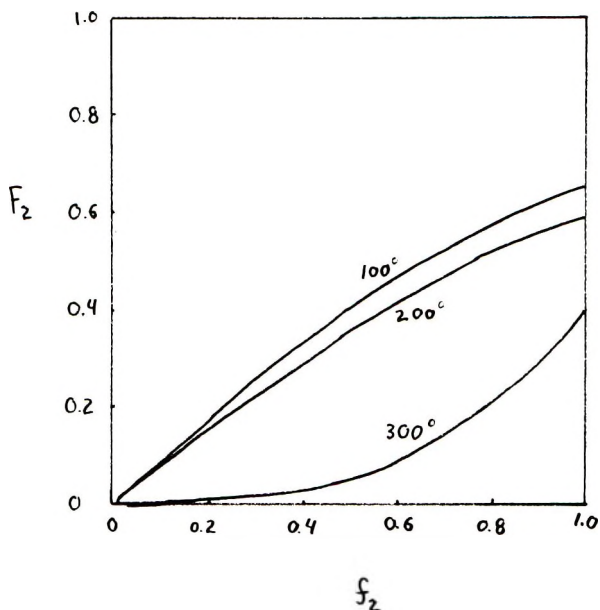


Fig. 6. Results of Monte-Carlo calculations of copolymer compositions for case E-2.

could not get polymer at 300°C. It is possible to determine, by the computation, the condition above which it is impossible to convert the monomer into the polymer.

The curve at 100°C in Figure 2 for case A-2 is similar to that obtained by plotting the Mayo-Lewis equation with the same  $r_1$  and  $r_2$  because very few depropagation reactions occurred. As the temperature rises, it becomes similar to the case A-1, which shows that thermodynamic control dominates the kinetic control. The case B shown in Figure 3 is different from case A-1 only in the values of  $-\Delta H_{12}^\circ$  and  $-\Delta H_{21}^\circ$ ; the sum of them is 30 kcal/mole in both cases. In Figure 3, it can be seen that this did not make case B different from A-1 at the lower temperature (100°C).

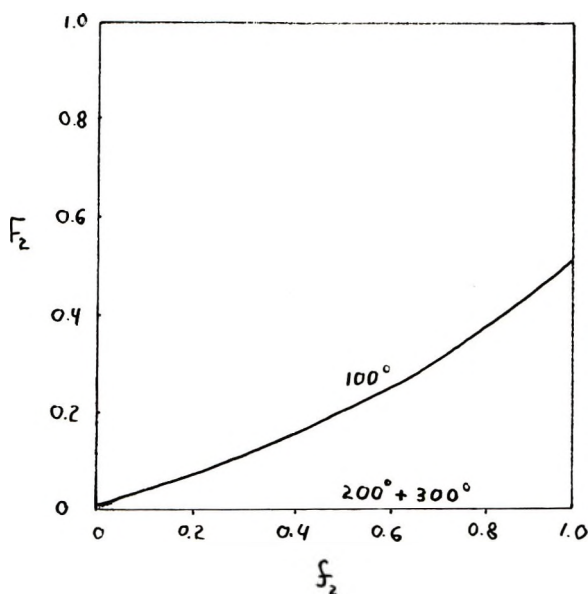


Fig. 7. Results of Monte-Carlo calculations of copolymer compositions for case E-3.

But, the curve at the higher temperature (200°C) appears similar to a curve with  $r_1 < 1.0$  and  $r_2 > 1.0$  in the Mayo-Lewis equation. This again shows that thermodynamic factors controlled the reaction at the higher temperature. When both of  $-\Delta H_{12}$  and  $-\Delta H_{21}$  are less than the heat of homopolymerization (case D, Fig. 3), the curve approaches one which corresponds to the case that both  $r_1$  and  $r_2$  are larger than unity in the Mayo-Lewis equation; the copolymer formed under this condition is similar to a block copolymer, as is seen in the generated polymer chain in Figure 4. When both  $-\Delta H_{12}$  and  $-\Delta H_{21}$  are larger than the heat of homopolymerization (case C, Fig. 3), the curve resembles one obeying the Mayo-Lewis equation with  $r_1$  and  $r_2$  having values smaller than unity; the predicted sequence distribution is essentially that of an alternating copolymer.

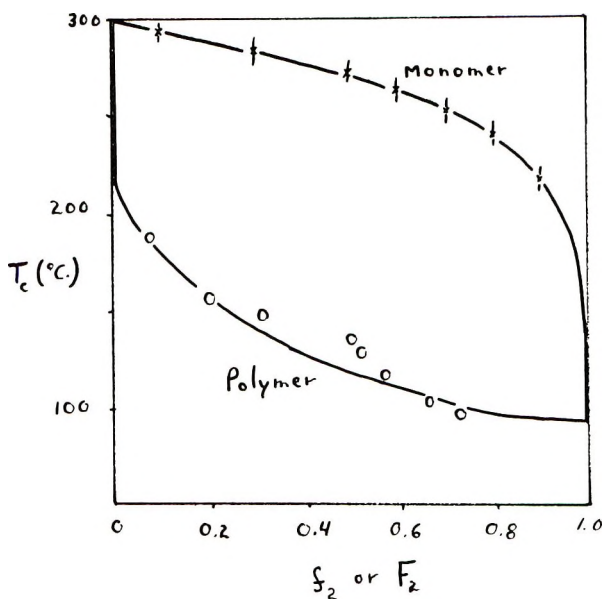


Fig. 8. A pseudo phase diagram for a system having the following values:  $r_1 = r_2 = s_1 = 1.0$ ;  $-\Delta S_{ij}^\circ = \text{cal/deg/mole}$ ;  $-\Delta H_{11}^\circ = 16.0 \text{ kcal/mole}$ ;  $-\Delta H_{12}^\circ = -\Delta H_{21}^\circ = 13.0 \text{ kcal/mole}$ ;  $-\Delta H_{22}^\circ = 10.0 \text{ kcal/mole}$ . The error in calculating the monomer curve is indicated by the vertical bars. Errors in the polymer curve are large due to the extrapolation necessary.

The deviations from the Mayo-Lewis equation at the higher temperature due to the occurrence of the depropagation reaction are apparent in Figures 2 and 3. However, it will often be found that the thermodynamic control is not obvious in the free-radical copolymerizations of a monomer pair having the similar thermodynamic quantities. The reason is that, due to a relationship between the rate constants and the heats of cross propagations in the copolymerization, the thermodynamics will often cause effects on the composition-feed curve which are analogous to the kinetic effects.

The series of cases E-1-E-3 (Figs. 5-7) correspond to copolymerizations of two monomer which have a relatively large difference in their ceiling temperatures. The copolymerization of methyl methacrylate and  $\alpha$ -methylstyrene, which will be discussed in the next paper belongs to this case. The effect of the change in the relative magnitude of  $-\Delta H_{12}$  and  $-\Delta H_{21}$  was specifically examined in this series; all other factors, including the sum of  $-\Delta H_{12}$  and  $-\Delta H_{21}$ , are fixed in this series.

The general trend of the behavior of the composition-feed curve is that the shape of the curves becomes flatter with increasing temperature; that is, the copolymer formed at the higher temperature is nearly a homopolymer of the monomer having a higher ceiling temperature, even under the condition of a large excess of another monomer in the feed. Besides the general trend, Figures 5-7 show that the composition-feed curve is af-

ected by the relative magnitude of the heats of cross propagations at the intermediate temperature.

Therefore, it may be possible by a composition study to estimate the relative magnitude of  $-\Delta H_{12}$  and  $-\Delta H_{21}$ . These quantities are unmeasurable by thermodynamic experiments such as the measurements of the heat of copolymerization and of the heat of formation of the copolymer. Orr<sup>5</sup> has pointed out that the sum of  $-\Delta H_{12}$  and  $-\Delta H_{21}$  is the measurable quantity.

As mentioned above, the critical point of the copolymerization above which it is impossible to convert the monomer mixture into the polymer can be determined directly by this simulation. The value of this critical temperature may be termed the ceiling temperature of the comonomer mixture. We computed this temperature in a typical case and plotted it against the composition of the monomer mixture in Figure 8. Polymerization will never occur in the system whose conditions correspond to a point above this line. In Figure 8 is plotted also the copolymer composition obtained by extrapolating the copolymer composition at various temperatures to the critical monomer feed: practically, this means the horizontal extrapolation of composition curves to  $f_2$  values of unity at various temperature. From Figure 8, it is possible to imagine what will occur when we gradually cool the monomer mixture above the critical point. When the temperature of the monomer mixture reaches the critical point, the polymer having the composition expressed by the polymer line will be formed; in this special case, homopolymer of  $M_1$  will be formed mostly. Thus, this graph is analogous (but not identical) to a liquid-vapor phase diagram for a binary mixture. More detailed discussions on this point will be presented in a subsequent paper of this series treating the thermodynamics of the copolymerization of this type.<sup>6</sup>

Support of this work by the National Science Foundation, Grant GK-1878 is gratefully acknowledged. The Computing Center at SUNY, Buffalo, whose facilities were so useful in this work, is partially supported by NIH Grant FR-00126 and NSF Grant GP-7318.

### References

1. G. G. Lowry, *J. Polym. Sci.* **42**, 463 (1960).
2. A. A. Durgaryan, *Vysokomol. Soedin.*, **8**, 790 (1966).
3. J. Howell, M. Izu, and K. O'Driscoll, *J. Polym. Sci. A-1*, **8**, 699 (1970).
4. F. R. Price, *J. Polym. Sci. C*, **25**, J. B. Kinsinger, Ed., Interscience, New York, 1967, p. 3.
5. R. J. Orr, *Polymer*, **2**, 74 (1961).
6. M. Izu and K. O'Driscoll, *Polym. J.*, **1**, 27 (1970).

Received September 17, 1969

## **Copolymerization with Depropagation. V. Copolymerization of $\alpha$ -Methylstyrene and Methyl Methacrylate between Their Ceiling Temperatures**

M. IZU\* and K. F. O'DRISCOLL, *Chemical Engineering Department,  
State University of New York, Buffalo, New York 14214*

### **Synopsis**

The variation of copolymer composition with monomer feed has been studied for the system  $\alpha$ -methylstyrene-methyl methacrylate at 60, 114, and 147°C. The compositions predicted by the diad model of Part III of this series accurately describe the data.

### **INTRODUCTION**

As has been generally discussed in the previous paper<sup>1</sup> of this series, the reaction temperature has a marked influence on copolymerization where reversibility of the propagation reaction must be considered. In this paper we report the effect of reaction temperature on the copolymer composition curve in the free-radical copolymerization of  $\alpha$ -methylstyrene and methyl methacrylate which have relatively low ceiling temperatures (61 and 164°C, respectively).<sup>3</sup> The temperature effect is well interpreted by the kinetics described in the previous papers of this series.<sup>1,2</sup>

### **EXPERIMENTAL**

#### **Materials**

Commercial methyl methacrylate (MMA) was washed with an aqueous solution of 5% NaOH and 20% of NaCl, washed with water, dried, and distilled at 99°C under a nitrogen atmosphere. Commercial  $\alpha$ -methylstyrene ( $\alpha$ -MST) was distilled at 66°C under a pressure of 18 mm. 2,2'-Azobisisobutyronitrile was recrystallized from the acetone solution. Di-*tert*-butyl peroxide (Lucidol) was used without purification.

#### **Polymerization Procedure**

Copolymerizations of various mixtures of MMA and  $\alpha$ -MST were carried out in glass ampoules (30 ml capacity) under vacuum and stopped at

\* On leave from Department of Hydrocarbon Chemistry, Kyoto University, Kyoto, Japan.

conversions of less than 5%. 2,2'-Azobisisobutyronitrile and di-*tert*-butyl peroxide were used as initiators at 60 and 114°C, respectively; the copolymerizations at 147°C were carried out without initiator. Polymer was precipitated from the reaction mixture in methanol, separated by filtration, dried *in vacuo*, and purified by reprecipitation from chloroform solution.

### Characterization of the Polymer

The  $\alpha$ -MST content of the copolymer was determined by the ultraviolet absorption at 262 m $\mu$  which was assignable to the phenyl group. The ultraviolet spectrum of 1 g/l. chloroform solution of the polymer was measured with a Perkin-Elmer Model 202 spectrometer. The relation between the  $\alpha$ -MST content and the absorbance was calibrated by both elementary analyses and NMR measurements.

### RESULTS AND DISCUSSION

Figure 1 shows the relation between the ultraviolet absorbance at 262 m $\mu$  for a 1 g/l. chloroform solution of the copolymer and the composition determined either by the elementary analyses, or by the NMR measurement. By using this calibration graph, the copolymer compositions at 60, 114, and 147°C were determined from the ultraviolet measurements and are

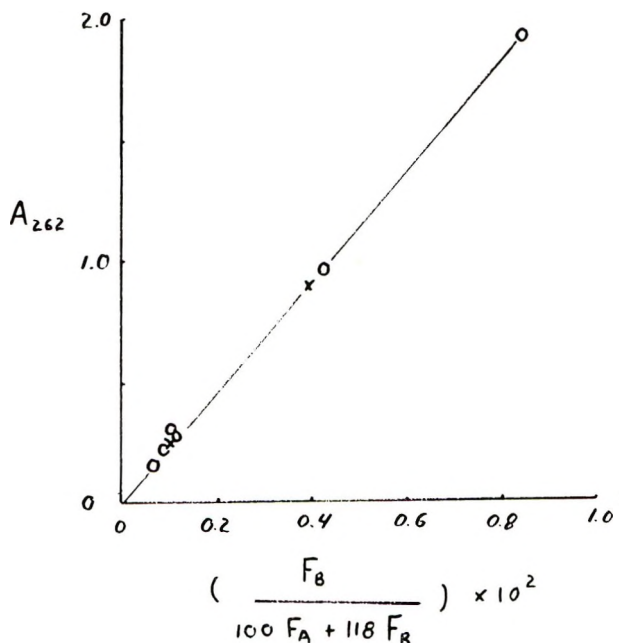


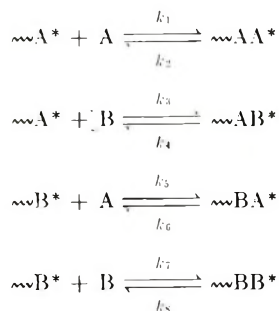
Fig. 1. Absorbance at 262 m $\mu$  of a 1 g/l. solution in CHCl<sub>3</sub> of a copolymer of MMA (monomer A) and  $\alpha$ -MSt (monomer B): (O) calibration by elementary analysis; (X) calibration by NMR.

plotted in Figure 2. These results show that the reaction temperature had a marked effect on the copolymer composition for a given feed.

The data at 60°C may be analyzed by using the Mayo-Lewis equation. A Fineman-Ross plot of the data gave approximate values of  $r_1 = 0.40$  and  $r_2 = 0.15$  (cf. literature<sup>3</sup> values of  $r_1 = 0.50$ ,  $r_2 = 0.14$ ). These values are not so different from the values of  $r_1 = 0.41$  and  $r_2 = 0.16$  estimated by applying the  $Q-e$  scheme.

However, a straightforward application of the Mayo-Lewis equation to our data at the higher temperatures of 114 and 147°C gave negative values of  $r_2$ . Doak had previously reported a negative value for  $r_2$  at 99°C.<sup>4</sup> Clearly, a negative value of reactivity ratio has no physical meaning. This result shows that the assumption used in the derivation of the Mayo-Lewis equation is invalid at higher temperatures. Considering the relatively low ceiling temperatures of both monomers, it is suggested that the invalidity arises from the assumption of irreversibility for the elementary reactions of the copolymerization.

We therefore adopt, as a simple explanation, the following diad model for this copolymerization:



In order to describe the copolymer composition using the theoretical treatment of this model developed previously<sup>1,2</sup> it is necessary, as a minimum, to estimate the relative values of the eight rate constants.

The relative values of the eight rate constants above are estimated by the seven constants below:

$$\begin{aligned} K_1 &= k_1/k_2 \\ K_2 &= k_3/k_1 \\ K_3 &= k_5/k_6 \\ K_4 &= k_7/k_8 \\ r_1 &= k_1/k_3 \\ r_2 &= k_7/k_5 \\ s_1 &= k_1/k_5 \end{aligned}$$

The values of  $K_1$  and  $K_4$  are available from the thermodynamic data of homopolymerization by using the relation:

$$-RT \ln K_i = \Delta G_i^\circ = \Delta H_i^\circ - T\Delta S_i^\circ \quad (1)$$



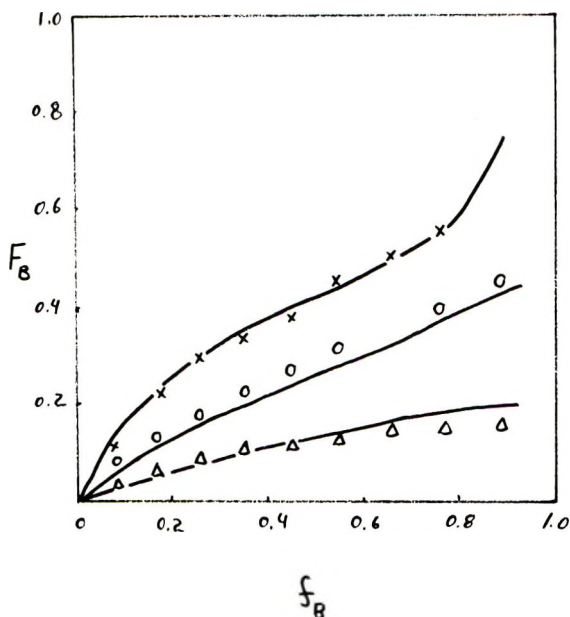


Fig. 2. Influence of temperature and feed composition ( $f$ ) on the copolymer composition ( $F$ ) in the case of MMA (monomer A) and  $\alpha$ -MS (monomer B) copolymerized by free-radical initiation: ( $\times$ ) 60°C; ( $\circ$ ) 114°C; ( $\Delta$ ) 147°C; (—) theoretical prediction, calculated as described in text.

Since no data are available on  $K_2$  and  $K_3$  we assume here:

$$\Delta G_2^\circ = \Delta G_3^\circ = 1/2(\Delta G_1^\circ + \Delta G_4^\circ) \quad (2)$$

Values of  $r_1$ ,  $r_2$ , and  $s_1$  were estimated by the  $Q$ - $e$  scheme:  $Q$  values used were 0.74 for MMA and 0.98 for  $\alpha$ -MST;  $e$  values were 0.40 for MMA and  $-1.27$  for  $\alpha$ -MST;<sup>3</sup>  $P$  values were  $5.8 \times 10^2$  for MMA and  $5.6 \times 10^1$  for  $\alpha$ -MST.<sup>5</sup> Table I summarizes the values used in this paper.

TABLE I  
Input to Calculate the Relative Magnitudes of the Rate Constants

	At 60°C	At 114°C	At 147°C
$\Delta G_1^\circ$ , kcal/mole <sup>a</sup>	-3.08	-1.48	-0.51
$\Delta G_2^\circ$ , kcal/mole	-1.26	0.31	1.27
$\Delta G_3^\circ$ , kcal/mole	-1.26	0.31	1.27
$\Delta G_4^\circ$ , kcal/mole <sup>b</sup>	0.55	2.11	3.06
$r_1$	0.41	0.41	0.41
$r_2$	0.16	0.16	0.16
$s_1$	5.6	5.6	5.6

<sup>a</sup> Estimated by using the values,<sup>6</sup>  $\Delta H_{ss}^\circ = -12.9$  kcal/mole,  $\Delta S_{ss}^\circ = -29.5$  cal/mole-deg.

<sup>b</sup> Estimated by using the values,<sup>7</sup>  $\Delta H_{ss}^\circ = -8.02$  kcal/mole,  $\Delta S_{ss}^\circ = -28.75$  cal/mole-deg. These values were measured at  $-20^\circ\text{C}$ . Therefore,  $\Delta H_{ss}^\circ$  (at about  $100^\circ\text{C}$ ) was estimated to be  $-9.02$  kcal/mole assuming  $\Delta C_p = -10$  cal/mole-deg.

Applying the theory presented in the previous paper of this series,<sup>2</sup> the copolymerization behavior of this model is theoretically predictable. The compositions of the polymer is expressed by eq. (3) as a function of parameters  $\eta$  and  $\epsilon$ .

$$F_A/F_B = (1 - \eta)/(1 - \epsilon) \quad (3)$$

where  $F_A$  and  $F_B$  are the mole fractions of monomer A and B in the copolymer,  $\eta$  is the probability of the occurrence of a B monomer unit in a chain given that the adjacent position is occupied by a B unit, and  $\epsilon$  is the probability of the occurrence of an A monomer unit, given that the adjacent position is occupied by an A unit.

The values of  $\eta$  and  $\epsilon$  are determined by solving simultaneously eqs. (18), (31), (33), and (34) in Part IV, of this series.<sup>1</sup> Since these equations are nonlinear, we solved them by a numerical method. The solid lines in Figure 2 show the theoretical prediction obtained by this procedure. The theoretical curves fit well to the experimental points. Since the temperature range and its effect is quite large, the diad model appears to be quite adequate for accurately describing the reversible copolymerization of this monomer pair.

Support of this work by the National Science Foundation, Grant GK-1878 is gratefully acknowledged. The Computing Center at SUNY, Buffalo, whose facilities were so useful in this work, is partially supported by NIH Grant FR-00126 and NSF Grant GP-7318.

NMR data were obtained through the kindness of Professor H. J. Harwood of the University of Akron.

### References

1. M. Izu and K. F. O'Driscoll, *J. Polym. Sci. A-1*, this issue.
2. J. A. Howell, M. Izu, and K. F. O'Driscoll, *J. Polym. Sci. A-1*, **8**, 699 (1970).
3. *Polymer Handbook*, J. Brandrup and E. Immergut, Eds., Interscience, New York, 1966.
4. Doak.
5. S. Okamura, K. Katagiri, and T. Yonezawa, *J. Polym. Sci.*, **42**, 535 (1960).
6. S. Bywater, *Trans. Faraday Soc.*, **51**, 1272 (1955).
7. S. Bywater, *J. Polym. Sci.*, **26**, 299 (1957).

Received September 17, 1969

## High-Resolution Proton Magnetic Resonance and Infrared Spectra of Poly(vinyl Formal) and Its Model Compounds

KYOICHIRO SHIBATANI, YUZURU FUJIWARA,  
and KIYOSHI FUJII, *Central Research Laboratories,  
Kurashiki Rayon Company, Sakazu, Kurashiki, Okayama, Japan*

### Synopsis

High-resolution proton magnetic resonance and infrared spectra of poly(vinyl formal) were studied in comparison with those of the model formals obtained from stereoisomers of pentane-2,4-diol and heptane-2,4,6-triol in order to learn spectral changes due to differences of the steric structures of the polymer. In the NMR spectrum of *trans*-formal obtained from *dl* diol or *dl,dl* (syndiotactic) triol, all proton signals were well interpreted by assuming a rapid chair-chair inversion of the formal ring. On the other hand, no such inversion was observed spectroscopically in *cis*-formal obtained from the *meso* diol or *meso,meso* (isotactic) triol, and the *cis*-formal ring was supposed to take a diequatorial form preferentially. Consequently, dioxymethylene protons gave a single peak (equivalent) in *trans*-formal and an AB quartet (nonequivalent) in *cis*-formal. In the spectra of poly(vinyl formal), the dioxymethylene signal was an overlap of the singlet and quartet in dimethylsulfoxide solution. Observations of the spectra of various poly(vinyl formals) obtained from poly(vinyl alcohols) of different tacticities and study of temperature dependence of the signal have shown that the singlet and quartet are attributed to *trans*- and *cis*-formals, respectively, in the polymer spectrum also. In the infrared spectra of poly(vinyl formals), the 800 and 785  $\text{cm}^{-1}$  bands were found to be related to *cis*- and *trans*-formal rings respectively. A linear relationship was confirmed between  $D_{785}/D_{800}$  and *trans/cis* ratios determined from the peak intensities of the dioxymethylene proton signals.

### INTRODUCTION

The reaction of poly(vinyl alcohol) (PVA) with aldehyde gives two types of acetal rings that are sterically isomeric. The acetal ring obtained from the isotactic (*meso*) diol portion may be assumed as a *cis*-4,6-derivative of 1,3-dioxane and that from the syndiotactic (*dl*) portion as a *trans* derivative.<sup>1</sup> The *cis*-acetal is much more stable against hydrolysis than the *trans*-acetal, and this difference of reactivity has been studied from various points of view.<sup>2-5</sup> These configurational differences may be an interesting subject from the spectroscopic point of view, but not much study has been made on this point. In a previous communication,<sup>6</sup> it was shown that the dioxymethylene proton signal was useful in distinguishing *cis*- and *trans*-formals in the high-resolution nuclear magnetic resonance (NMR) spec-

trum of poly(vinyl formal). No NMR spectroscopic studies had been reported for poly(vinyl formal). The infrared spectrum of poly(vinyl formal) was first studied by Beachel et al.,<sup>7</sup> who studied oxidative degradation of the polymer. Some absorption bands were assigned by Tadokoro et al.,<sup>8</sup> during their study of the  $1141\text{-cm}^{-1}$  crystallization-sensitive band of PVA, but the spectrum has not attracted any attention from the stereochemical point of view. The vibrational change due to different steric structures was first noted in poly(vinyl acetoacetals) obtained from PVA samples of different tacticities.<sup>5</sup>

In the present investigation, the vibrational change was studied together with the NMR spectra of various poly(vinyl formal) samples and model formals in order to ascertain the effect of structural changes of the polymer on the spectra. Since NMR spectroscopy can provide quantitative information on the steric structure of the formal rings, this enabled us to study the vibrational change of the polymer with better knowledge on the polymer structures than before. Details of the NMR spectra of various poly(vinyl formals) and of model formals will also be presented.

## EXPERIMENTAL

### Preparation of Samples

The model compounds of poly(vinyl formal) were prepared by reaction of formaldehyde with stereoisomers of pentane-2,4-diol<sup>9</sup> and heptane-2,4,6-triol.<sup>10</sup> The reaction was carried out in a 10% aqueous solution of the polyol in the presence of 0.1 *N* hydrochloric acid with equimolar formaldehyde at 60°C. The formals formed were purified by vacuum distillation after neutralizing the acid with sodium carbonate. No formation of hemiformal was observed in the reaction.

The highly formalized PVA samples were prepared as follows. In a flask with a glass stopper were placed 1 g of PVA, 0.7 g of paraformaldehyde, 36 ml of dioxane, and 1 ml of hydrochloric acid (reagent grade, 35%). The reaction mixture was kept at 60°C for 3 days and then poured into water containing a small amount of sodium carbonate. The polymer was purified by repeated precipitations from a dioxane solution into water. The degree of formalization was 86–87%.

The polymer samples of different degrees of formalization were prepared from the conventional PVA, which was obtained from vinyl acetate, by reacting with various amounts of formaldehyde in the dioxane–water mixed solvents in the presence of sulfuric acid.

Various PVA samples of different tacticities were obtained from polymers of vinyl formate, *tert*-butyl ether, or trimethylsilyl ether. The equivalent polymer samples have been investigated in previous work and their preparative conditions have been published elsewhere.<sup>2,11,12</sup> Their tacticities summarized in Table I were estimated from the relative intensities of three acetoxy proton signals of poly(vinyl acetate) derived from them.

TABLE I  
Tacticities of Poly(vinyl Alcohol) Samples

Sample	DP	Tacticity		
		<i>I</i>	<i>H</i>	<i>S</i>
A (isotactic-rich)	1000	0.59	0.30	0.11
B ( " )	690	0.71	0.20	0.09
C (syndiotactic-rich)	970	0.16	0.46	0.38
D ( " )	310	0.19	0.31	0.50
E (conventional)	1700	0.23	0.47	0.30

### NMR Spectra

A Varian HA-100 spectrometer operating at 100 Mcps was employed, together with a Varian variable temperature probe. The spectrum was obtained on solutions containing 10% (w/v) formals in dimethyl sulfoxide with tetramethylsilane as an internal reference. The model compounds and the polymer samples were run at 30 and 120°C, respectively.

### Infrared Spectra

The spectra were measured by using a Hitachi-EPI-G2 grating infrared spectrometer at 23°C. Poly(vinyl formal) was cast in films 4–8  $\mu$  thick from dioxane or dioxane–water solution. The model formal was sandwiched between rock salt plates.

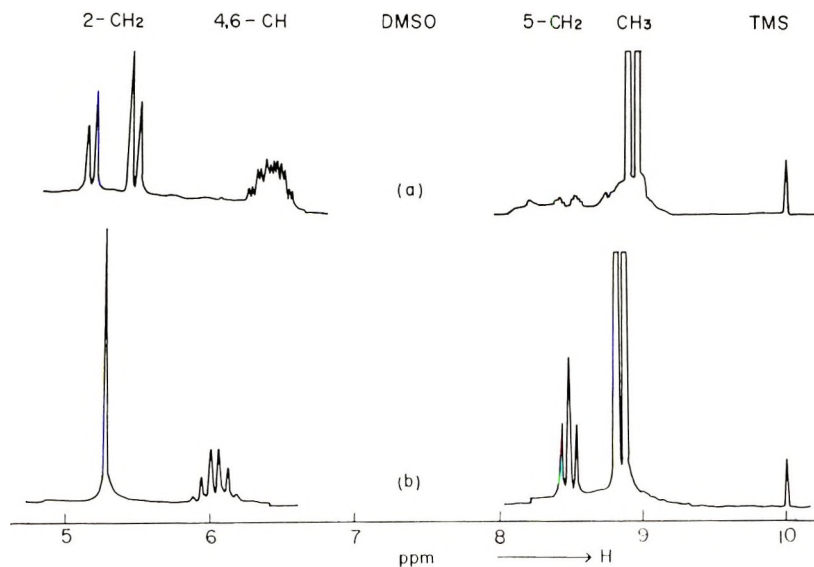


Fig. 1. NMR spectra of (a) *cis* and (b) *trans* 4,6-dimethyl-1,3-dioxane in dimethyl sulfoxide at 30°C.

## RESULTS AND DISCUSSION

## NMR Spectra of Model Formals

The NMR spectra of *cis*- and *trans*-4,6-dimethyl-1,3-dioxane (formals of *meso* and *dl* pentane-2,4-diol) are shown in Figure 1. There are four groups of proton signals which are centered at 8.9, 8.5, 6.1, and 5.3  $\tau$ . From the chemical shifts and signal intensities, they were assigned to the C<sub>4</sub> and C<sub>6</sub> methyl, C<sub>5</sub> methylene, C<sub>4</sub> or C<sub>6</sub> methine, and C<sub>2</sub> dioxymethylene protons, respectively (see Fig. 2).

A striking difference was observed in the 2-C dioxymethylene signal between the two isomers. The difference can be well interpreted in terms of an inversion of the two chair forms of 1,3-dioxane. The *cis* isomer may take the diequatorial conformation preferentially, and therefore the two C<sub>2</sub> protons may be observed as nonequivalent, giving rise an AB quartet. On the other hand, in the *trans* isomer, they can be observed as equivalent because of a rapid inversion between equatorial-axial and axial-equatorial forms that are energetically equivalent. It is noteworthy that the C<sub>2</sub>

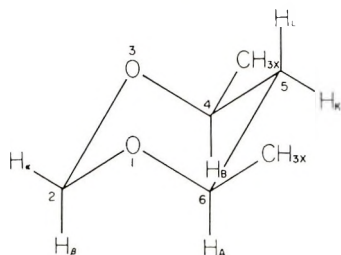


Fig. 2.

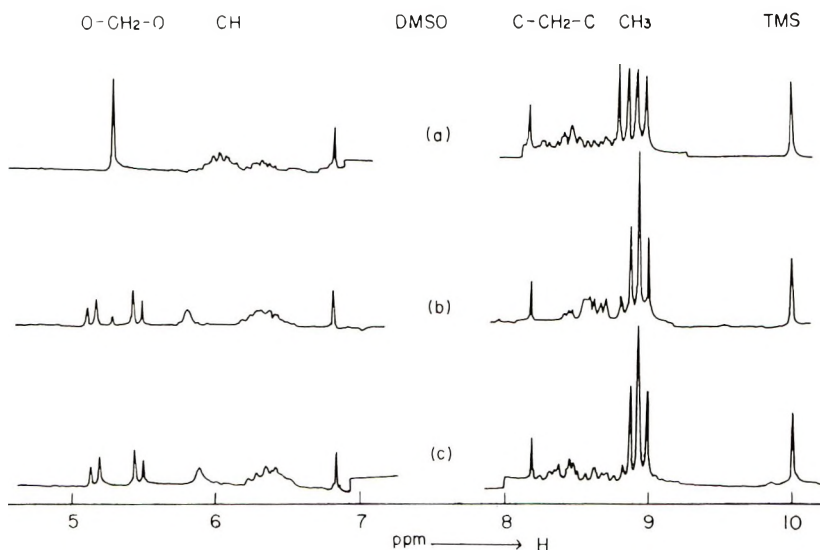


Fig. 3. NMR spectra of formals from (a) syndiotactic (b) heterotactic, and (c) isotactic heptane-2,4,6-triol in dimethyl sulfoxide at 30°C.

methylene protons were observed as equivalent even in the *trans* formal of syndiotactic (*dl-l* or *l-d*) trimer where 4- and 6-substituents are asymmetrical. This strongly suggested that the signal may be useful in distinguishing *cis* and *trans* formals in poly(vinyl formal). In fact, an overlap of a singlet and a quartet was observed in the C<sub>2</sub> proton signal of formal of heterotactic (*dl-meso*) triol, which was supposed to give a mixture of *cis*- and *trans*-formals, depending on the diol portion involved in the reaction. As shown in Figure 3, the singlet is much weaker than the quartet. This is consistent with the conformational law that the *ae* or *ea* configuration is less stable than the *ee* configuration.

### NMR Spectra of Poly(vinyl Formal)

The dioxymethylene proton signals of poly(vinyl formals) prepared from three PVA samples of different tacticities are illustrated in Figure 4. As seen in the model spectrum, an overlap of a singlet and a quartet was observed in the polymer spectra, and chemical shifts of the two signals were essentially identical both in the models and polymers. In spite of high molecular weights of the polymer samples, the signals were quite sharp and were clearly distinguishable.

Before determining the steric configuration of poly(vinyl formal) from relative intensities of these two signals, it must be ascertained that the rate of inversion of all-*trans* formal is rapid enough so as the two C<sub>2</sub> protons are observed as equivalent in the polymer spectra too. If a stereoregular PVA of a 100% syndiotacticity is available as a starting polymer, this can be confirmed as clearly as in the models. However this was not the case, and, instead, the temperature dependence of the relative intensities of the two

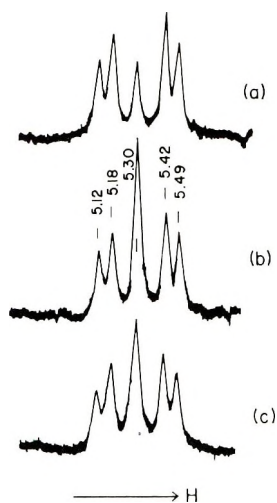


Fig. 4. Dioxymethylene proton signals of poly(vinyl formals) in dimethylsulfoxide at 120°C: (a) from isotactic-rich A, (b) from syndiotactic-rich C, (c) from conventional E poly(vinyl alcohol).

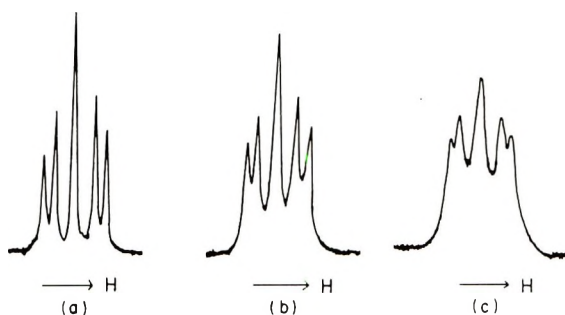


Fig. 5. Effect of temperature on dioxymethylene signals of poly(vinyl formal) from atactic poly(vinyl alcohol)-E: (a) 170°C; (b) 130°C; (c) 90°C.

signals was examined on poly(vinyl formal) derived from the ordinary PVA. As shown in Figure 5, the signals became sharper on raising the temperature from 90 to 170°C, but the intensity ratio of the two signals was not affected. Hence there must be no *trans*-formals which have the incipient temperature in this region.

Of course this does not completely exclude the possibility that there are small amounts of *trans*-formals in which one chair form (*ea* or *ae*) is highly favored over the other (*ae* or *ea*) because of the steric hindrance by the neighboring polymer chain. However, there is at least one methylene linkage between two acetal rings along the polymer chain, and this should give some freedom for staggering of the polymer chain. Therefore the presence of such a steric hindrance is rather unlikely. Thus all experimental findings showed that the *cis/trans* ratio of formal rings in the polymer can be determined from the intensity ratio of the two signals.

In Table II are shown the proportions of *cis* and *trans* formals formed during reaction of the conventional PVA with formaldehyde. Evidently the isotactic diol portion is reacting much faster than the syndiotactic portion. Since the details of the stereochemical analysis of this type of polymer reaction have been published previously,<sup>13</sup> they will not be further discussed in this paper.

TABLE II  
Configuration of Formal Rings in Partially Formalized  
Poly(vinyl Alcohol), Sample E

Run	Degree of formalization, mol %		
	Total	<i>cis</i> -Formal	<i>trans</i> -Formal
1	23.0	22.3	0.7
2	36.7	33.4	3.3
3	44.8	40.0	4.8
4	63.1	51.8	11.3
5	83.0	56.2	26.8
6	87.0	59.0	28.0



### NMR Spectra of Formal

In the *cis*-formal, one of the C<sub>2</sub> methylene protons takes the equatorial position preferentially and the other the axial position. From the line positions of the spin spin coupled quartet, the coupling constant  $J_{\alpha\beta}$  and chemical shift difference  $\delta_{\alpha\beta}$  were obtained as 6.2 cps and 0.31 ppm, respectively. These values are in fair agreement with those reported for 4-methyl- and other 1,3-dioxane derivatives by Crabb and Cookson.<sup>14</sup> In the AB quartet the relative heights in each pair of peaks agree with those of the theoretical spectrum where  $J_{\alpha\beta}/\delta_{\alpha\beta} = 0.20$ . Generally the axial proton signal is known to appear at higher field and to be broader than the equatorial proton signal except in some cyclohexanone derivatives,<sup>15,16</sup> but in the present case the half-width of a pair of peaks at high field was 0.8 cps and that at low field was 1.8 cps in a slow sweep experiment on *cis*-4,6-dimethyl-1,3-dioxane.

There are three possible causes for this type of line broadening: different relaxation times, exchange, and different long-range couplings. It is unlikely that the equatorial proton is subjected to a substantially faster relaxation than the axial proton, and this is incompatible with the power saturation behavior which showed the essentially same  $T_1$  for both protons. The exchange mechanism may be excluded on the basis of the findings that the difference of the line width was independent of temperature and that this compound does not undergo chair-chair inversion as discussed above. Therefore, the long-range coupling has to be taken into account; this was confirmed by decoupling experiments on the C<sub>2</sub> protons from C<sub>3</sub> protons and vice versa. It was shown that the C<sub>2</sub> equatorial proton

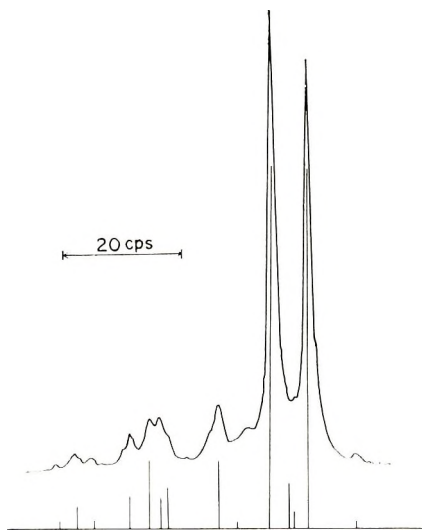


Fig. 6. Observed and calculated spectra of C<sub>2</sub> methylene protons of *cis*-4,6-dimethyl-1,3-dioxane at 100 Mcps.

TABLE III  
NMR Parameters of C<sub>5</sub> Methylene Protons of  
2,4-Dimethyl-1,3-Dioxane

Isomer	Solvent	Coupling constant, cps					Chemical shift, ppm Kl.
		$J_{AK}$	$J_{AL}$	$J_{BK}$	$J_{BL}$	$J_{KL}$	
<i>cis</i>	CS <sub>2</sub>			(by analysis)			
		11.1	2.5	11.1	2.5	12.9	24.1
<i>trans</i>	CS <sub>2</sub>			(by decoupling)			
		10.8	2.8	10.8	2.8	13.1	20.8
		5.4	5.4	5.4	5.4	(12.9)	0

has spin-spin coupling with the C<sub>5</sub> equatorial proton and the coupling constant,  $J_{25}$ , was 0.6 cps. A similar type of long-range coupling has been found recently for various 4-substituted 1,3-dioxanes.<sup>17,18</sup>

The effect of the different rate of inversion was also observed on the C<sub>5</sub> methylene proton signals of the two diol formals. Two C<sub>5</sub> methylene protons are distinguishable only in *cis*-formal as the C<sub>2</sub> methylene protons. The spectra and NMR parameters are shown in Figure 6 and Table III, respectively. A similar difference can be seen in the methyl signal also. In case of acetoacetal of the *dl* diol, 4- and 6-methyl protons were clearly distinguished,<sup>5</sup> but in the present study only one methyl signal (a doublet) was observed both in *cis*- and *trans*-formals.

### Infrared Spectra of Poly(vinyl Formal) and Model Formals

The infrared spectrum of PVA showed some interesting change when reacted with formaldehyde. On formalization, the O-H stretching vibration bands at 3500–3400 cm<sup>-1</sup> weakened and shifted towards higher frequencies due to cleavage of polymeric hydrogen bond chain. The C-H stretching bands characteristic of formal<sup>7,8</sup> appeared at 2975, 2850, 2760, and 2660 cm<sup>-1</sup>. In the region of C-H bending vibration,<sup>19</sup> new bands appeared at 1470, 1428, 1400, 1390, and 1360 cm<sup>-1</sup>. The bands at 1180, 1135, 1070, and 1020 cm<sup>-1</sup> seem to relate to C–O–C–O–C stretching vibrations.<sup>20</sup> The most interesting change appeared in the region of the skeletal vibrations.

In formalization of the conventional atactic PVA, a new band appeared initially at 800 cm<sup>-1</sup> and another band started to appear at 785 cm<sup>-1</sup> when conversion exceeded 40% (Fig. 7). Since the NMR analysis indicates that most formal rings formed have *cis* structure up to 40% formalization, the 800 and 785 cm<sup>-1</sup> bands appear to be related to *cis*- and *trans*-formals, respectively. The *trans/cis* ratios were determined by NMR analysis for various poly(vinyl formal) samples and compared with the absorbance ratios,  $D_{785}/D_{800}$ . A linear relationship was confirmed, as shown in Figure 8; this shows that  $D_{785}/D_{800}$  may be used as a measure of *trans/cis* formals in the polymer. This assignment was also supported by

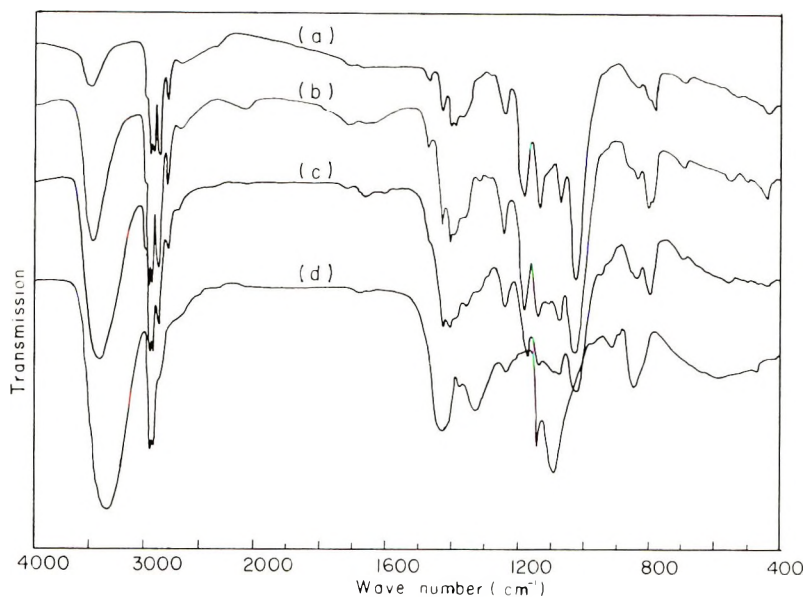


Fig. 7. Infrared spectral changes of poly(vinyl alcohol) on formalization: (a) 83.0% formalized; (b) 63.1% formalized; (c) 37.1% formalized; (d) original atactic poly(vinyl alcohol) E.

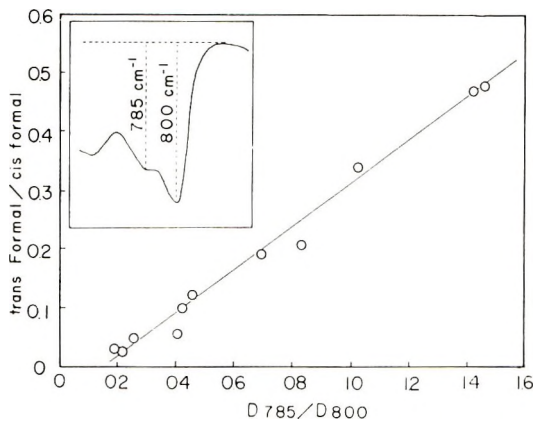


Fig. 8. Plots of  $D_{785}/D_{800}$  vs. *trans/cis* formal ratio.

evidence that the  $800\text{ cm}^{-1}$  band is stronger in a sample derived from PVA of higher isotacticity than in a sample from PVA of higher syndiotacticity, as shown in Figure 9. Interestingly, similar spectral differences were observed in the model formals. Figure 9 shows that formal of syndiotactic triol has a band at  $790\text{ cm}^{-1}$  while formal of isotactic triol absorbs at higher frequencies ( $808\text{--}803\text{ cm}^{-1}$ ). Similar differences were also observed in formals of the diols, but the spectra were more complex in the lower molecular weight models.

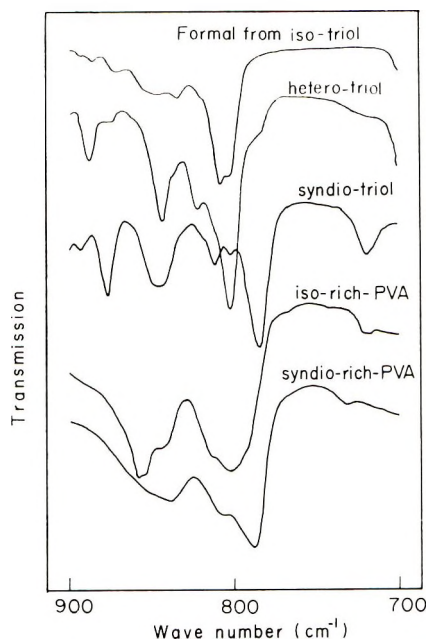


Fig. 9. Infrared spectra of formaldehyde of isotactic-rich B and syndiotactic-rich D poly-(vinyl alcohols), and of stereo-isomeric heptane-2,4,6-triols. (Degree of formalization of the polymer is 87%.)

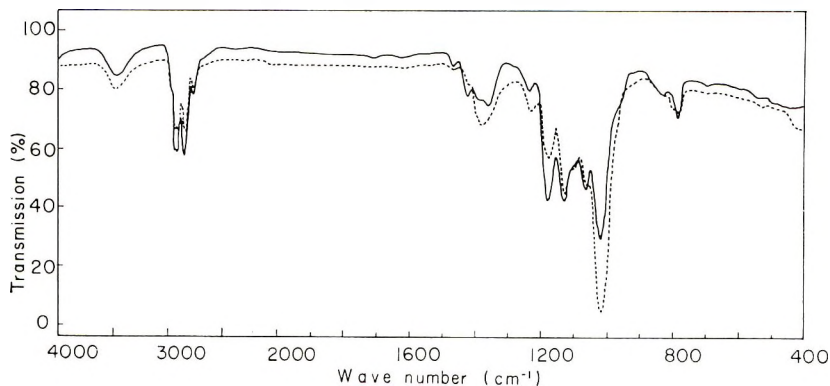


Fig. 10. Infrared spectra of oriented poly(vinyl formal) observed with polarized radiation: (—) *E* vector perpendicular to fiber axis; (---) *E* vector parallel to fiber axis.

In formalization of the atactic PVA, the 800 and 785  $\text{cm}^{-1}$  bands were almost equal in intensity at 70% formalization, and the latter became predominant at higher conversions. This may be a reason why the presence of the 800  $\text{cm}^{-1}$  band has never been noted. The 785  $\text{cm}^{-1}$  band was reported by Tadokoro et al.,<sup>8</sup> and a relation to the skeletal vibration was suggested. The 800  $\text{cm}^{-1}$  band also seems to be related to the skeletal vibrations. As shown in Figure 10, the 785  $\text{cm}^{-1}$  band showed perpendicu-

lar dichroism in contrast to the parallel dichroism of the  $800\text{ cm}^{-1}$ . This seems to suggest different chain orientations of *cis*- and *trans*-formal in the stretched polymer samples.

The authors are greatly indebted to Drs. M. Matsumoto, J. Ukida, and Y. Oyanagi of Kurashiki Rayon Company and to Professor S. Fujiwara of Tokyo University for their interest and encouragement during this work.

### References

1. M. Matsumoto, *Poly(vinyl Alcohol)* I. Sakurada, Ed., Society of Polymer Science, Japan 1955, p. 448.
2. K. Fujii, J. Ukida, and M. Matsumoto, *Makromol. Chem.*, **65**, 86 (1963).
3. K. Fujii, J. Ukida, and M. Matsumoto, *J. Polym. Sci. B*, **1**, 693 (1963).
4. I. Sakurada, Y. Sakaguchi, and Z. Shiiki, *Kobunshi Kagaku*, **21**, 289 (1964).
5. M. Matsumoto and K. Fujii, *Kogyo Kagaku Zasshi*, **68**, 843 (1965).
6. K. Fujii, K. Shibatani, Y. Fujiwara, Y. Oyanagi, J. Ukida, and M. Matsumoto, *J. Polym. Sci. B*, **4**, 787 (1966).
7. H. C. Beachell, P. Fotis, and J. Hucks, *J. Polym. Sci.*, **52**, 353 (1952).
8. H. Tadokoro, S. Seki, and I. Nitta, *Nippon Kagaku Zasshi*, **78**, 1070 (1957).
9. E. Nagai, S. Kuribayashi, M. Shiraki, and M. Ukita, *J. Polym. Sci.*, **35**, 295 (1959).
10. K. Fujii, *J. Polym. Sci. B*, **3**, 375 (1965).
11. S. Murahashi, S. Nozakura, and M. Sumi, *J. Polym. Sci. B*, **3**, 245 (1965).
12. K. Fujii, S. Brownstein, and A. M. Eastham, *J. Polym. Sci. A-1*, **6**, 2387 (1968).
13. K. Shibatani, K. Fujii, Y. Oyanagi, J. Ukida, and M. Matsumoto, *J. Polym. Sci. C*, **23**, 647 (1968).
14. T. A. Crabb and R. C. Cookson, *Tetrahedron Letters*, **12**, 679 (1964).
15. K. L. Williamson and W. S. Johnson, *J. Amer. Chem. Soc.*, **83**, 4623 (1961).
16. M. Wellman and F. G. Bordwell, *Tetrahedron Letters*, **25**, 1703 (1963).
17. K. C. Ramey and J. Messick, *Tetrahedron Letters*, **49**, 4423 (1965).
18. J. Delman and J. Duplan, *Tetrahedron Letters*, **6**, 559 (1966).
19. N. Nagai and N. Sagane, *Kobunshi Kagaku*, **12**, 195 (1955).
20. K. -D. Ledwoch, *Z. Anal. Chem.*, **197**, 323 (1963).

Received September 9, 1969

Revised September 19, 1969

## Effect of High Pressures on the Cyclopolymerization of Acrylic Anhydride

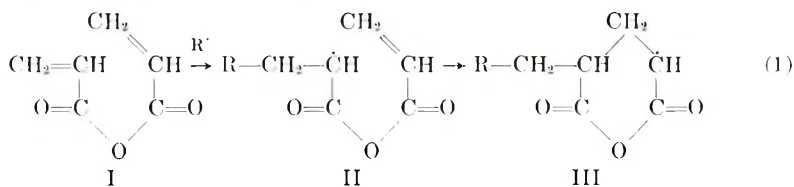
J. P. J. HIGGINS\* and K. E. WEALE, *Department of Chemical Engineering and Chemical Technology, Imperial College of Science and Technology, London England*

### Synopsis

The effect of pressures up to 4000 atm on the free-radical cyclopolymerization of acrylic anhydride in solution has been investigated. Both the molecular weight and degree of cyclization of the polymer are increased by pressure. The rate of polymerization at first decreases with increasing pressure, but above 2500 atm a normal acceleration occurs.

### INTRODUCTION

The free radical cyclopolymerization of the symmetrical 1,6-diene, acrylic anhydride (I), has been extensively studied<sup>1-4</sup> and the major reaction may be represented as shown in eq. (1).



The soluble cyclopolymers obtained contain hexaatomic glutaric anhydride rings due to the cyclization reaction and also some residual unsaturation due to the addition of monomer to the uncyclized radical (II). Recent investigations<sup>5</sup> have indicated that, in the cyclopolymerization of many nonconjugated dienes, the application of high pressure usually increases both the rate of polymerization and the degree of cyclization. This paper describes some anomalous effects of high pressures on the free-radical cyclopolymerization of acrylic anhydride.

### EXPERIMENTAL

The acrylic anhydride monomer was obtained commercially and was triple-distilled before use (bp 55°C/5 mm Hg). The *N,N*-dimethylformamide (DMF) solvent was first dried for 1 hr over phosphorus pentoxide to

\* Present address: Research Department, Imperial Oil Enterprises Ltd., Sarnia, Ontario, Canada.

avoid traces of acid and water, and then distilled from  $P_2O_5$ . The azobisisobutyronitrile initiator (AIBN) was recrystallized from a dry ether solution.

Polymerization experiments were carried out using standard commercially available high pressure equipment. The design and operation of such high-pressure equipment has been described by many authors,<sup>6-8</sup> so only a brief outline will be given here. The high-pressure vessel used was capable of containing pressures of up to 4000 atm and the pressure-transmitting medium was liquid paraffin B.P. A schematic diagram of the system used is given in Figure 1.

The pressure transmitting oil is contained in a reservoir in the top of the hand-operated pump (P) and enters the system through a nonreturn valve (V). Pump pressure is read on a gauge (G). The pressure delivered by the pump is increased to high pressure in the pressure vessel (C) by means of an intensifier (I). Low pressure is applied to a large-diameter piston of area  $A$  which in turn drives a smaller diameter high-pressure piston of area  $a$ . Thus, if friction is neglected, the low pressure is intensified by a factor  $A/a$ . For the vessel used, this ratio is approximately 5. The high-pressure piston, topped by a Poulter packing advances into a 0.6-in. diameter tube (clearance 0.001 in.) in a Vibrac V45 cylinder above the intensifier. Pressure is transmitted from this cylinder to the pressure vessel which consists of two cylinders of Vibrac V45 steel, shrunk together and is sealed with a Poulter packing held in place by a threaded steel plug. The reaction chamber is about 0.75 in. in diameter.

Samples of up to 10 ml were inserted in a Teflon container in a steel case and inserted in the reaction chamber. The pressure vessel is immersed in

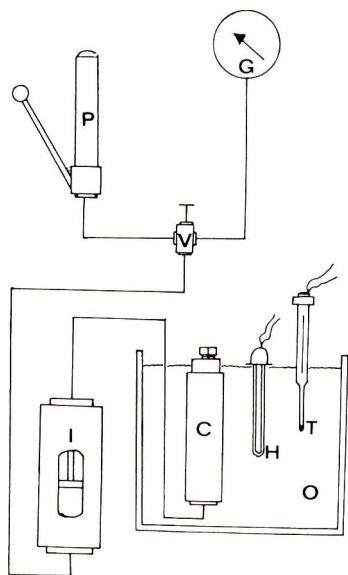


Fig. 1. Schematic diagram of high-pressure equipment.

a stirred thermostatted oil bath (O) which is heated by a 1 kW electric immersion heater (H). The temperature of the oil bath is controlled within  $\pm 0.1^\circ\text{C}$  by a Sunvic on-off relay switch operating a contact thermometer (T).

Polymerizations took place at constant temperature over periods of 30–60 min. At the end of the reaction period the sample was removed from the pressure vessel. The polymer was precipitated in dry ether, filtered and dried *in vacuo*. The rate of polymerization was determined gravimetrically. The amount of residual unsaturation was obtained by bromometry in a method similar to that outlined by Siggia.<sup>9</sup>

Intrinsic viscosities were determined in 2*N* NaOH solution at 30°C with an Ubbelohde viscometer. Molecular weights were calculated from the viscosities using a form of the Mark-Houwink-Sakurada equation given by Crawshaw and Butler.<sup>1</sup>

$$[\eta] = 4.27 \times 10^{-3}(\overline{DP})^{0.69}$$

It was assumed that in strong NaOH solution, poly(acrylic anhydride) is completely hydrolyzed to poly(acrylic acid).

## RESULTS

Acrylic anhydride was polymerized in DMF solution at 50°C with 0.1% AIBN initiator. It was found that above a precipitation threshold of 1.8 mole/l., a rapid "popcorn"-type polymerization developed,<sup>5</sup> and a monomer concentration of 1.7 mole/l. was selected for the rate measurements. The variation in the rate of polymerization with pressure at this concentration is given in Table I.

TABLE I  
Rates of Polymerization of Acrylic Anhydride in DMF at 50°C<sup>a</sup>

No.	Pressure, atm	$10^3 R_p$ , mole/l./sec
1	1	1.74
2	1	1.78
3	1000	1.66
4	1500	1.60
5	2000	1.52
6	2000	1.47
7	2500	1.90
8	3000	2.87
9	4000	5.75

<sup>a</sup> [M] = 1.7 mol/l.; initiator, 0.1% AIBN.

Figure 2 illustrates these results.

The rates of radical addition polymerization usually increase continuously with pressure,<sup>5</sup> but up to about 2500 atm the rate of polymerization of acrylic anhydride decreases slightly with pressure. A plot of  $\ln R_p$  versus pressure is linear in this range, and from the equation  $\partial \ln R_p / \partial P =$



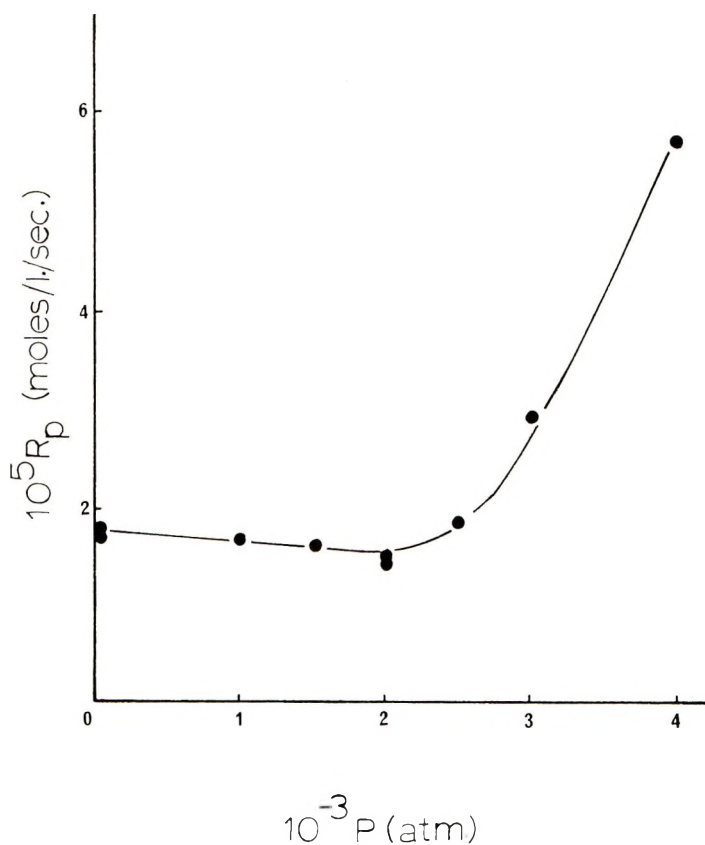


Fig. 2. Rate of polymerization of acrylic anhydride in DMF solution at 50°C.

$-\Delta V_{T^*}/RT$ , the overall volume of activation  $\Delta V_{T^*}$  is calculated to be about +1.5 cc/mole. Above 2500 atm, the rate exhibits the more usual increase with pressure and  $\Delta V_{T^*}$  is found to be -14cc/mole.

Table II shows the variations of molecular weight and degree of cyclization  $f_c$  with pressure.

TABLE II  
Effects of Polymerization Pressure on Cyclopolymers of Acrylic Anhydride<sup>a</sup>

No.	Pressure, atm	$[\eta]$	$10^{-3} \bar{M}_n$	$f_c$
2	1	0.74	210	0.49
3	1000	0.99	327	0.79
4	1500	—	—	0.91
5	2000	1.24	469	—
6	2000	1.34	515	0.90
7	2500	—	—	0.93
8	3000	1.41	570	0.95
9	4000	1.44	605	—

<sup>a</sup> For polymers produced at  $[M] = 1.7$  mole/l.; 0.1% AIBN; 50°C.

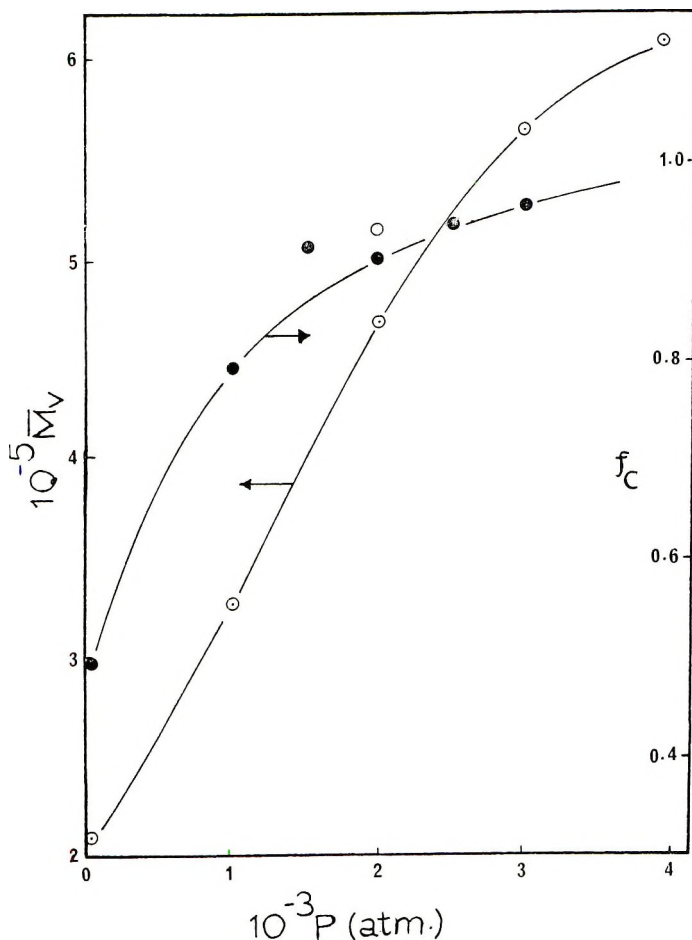


Fig. 3. Plots of ( $\odot$ ) molecular weight and ( $\bullet$ ) degree of cyclization of acrylic anhydride polymers formed at various pressures.

The results given in Table II are illustrated in Figure 3.

The molecular weight more than doubles between 1 and 2000 atm, and the degree of cyclization increases very markedly in the same range. Above about 2000 atm the changes in both properties are much less pronounced, but it is in this region of higher pressures that substantial pressure acceleration of the reaction occurs.

### DISCUSSION

Mercier and Smets<sup>10</sup> investigated the free-radical cyclopolymerization of acrylic anhydride at atmospheric pressure and found that the "homogeneous" polymerization of this monomer is, in many ways, similar to the heterogeneous bulk polymerization of acrylonitrile. The exponent of the catalyst concentration in the overall rate equation was determined to be 0.67

in bulk, 0.75–0.83 (depending on monomer concentration) in cyclohexanone solution, and 1.0 in DMF solution (at  $[M] = 1.8$  mole/l.). In cyclohexanone solution, the rate of polymerization was found to be independent of monomer concentration below 4.3 mole/l. Above this concentration, the rate increased linearly with monomer concentration. Mercier and Smets also noted that in cyclohexanone solution (at 4.0 mole/l.) the turbidity of the medium had increased by a factor of 240 at 1.6% conversion. They concluded that this was due to the presence of microgel particles suspended in the apparently homogeneous solution. Electron spin resonance measurements indicated a large amount of radical entrapment in the growing microgel particles, and the trapped radical concentration increased with both percent conversion and temperature.

Although no experimental study of this point has been made, it seems likely that the presence of microgel particles may similarly be responsible for the unusual effect of pressure on the rate of cyclopolymerization of acrylic anhydride in DMF solution. The interpretation suggested is that in DMF solution at 1.7 mole/l., microgel particles are quickly formed but are sufficiently dispersed throughout the polymerization medium to preclude either gelation or precipitation. Once the particles have formed, the rate of polymerization is largely governed by the rates of diffusion of monomer molecules into and within them. It is known<sup>4,5,10</sup> from residual unsaturation measurements, that the polymer molecules and radicals have reactive acrylyl groups pendant on the chains; and reactions involving these pendant groups would lead to some crosslinking and occlusion in the microgel particles.

With increasing pressure, an acceleration of the reactions involving pendant acrylyl groups in the microgel particles would increase the amount of chain branching and crosslinking in them, and so decrease the "penetrability" of the particles by monomer molecules. This would lead to an initial decrease in the rate of polymerization and, if sufficient crosslinking occurred, a simultaneous increase in molecular weight as the pressure increased.

However, at higher pressures, the degree of cyclization also increases and this introduces an opposing effect. Cyclization is favored either by an increase in pressure<sup>5</sup> or by a decrease in the monomer concentration.<sup>3,4</sup> At intermediate pressures the degree of cyclization will be enhanced by the relatively lower monomer concentration near the growing chain ends, which results from increased occlusion in the microgel particles. As the pressure, and thus the rate of cyclization, is increased, the relative amount of occlusion in the microgel particles will decrease; and when the pressure is sufficiently high for the cyclization reaction to predominate the microgel particles will be largely free of crosslinks and readily permeable to monomer molecules. The rate of chain growth should then be independent of diffusion processes and should increase normally with pressure. The reduced amount of occlusion in this region would also be expected to cause the increase in molecular weight with pressure to tend to level off, as is observed.

### References

1. A. Crawshaw and G. B. Butler, *J. Amer. Chem. Soc.*, **80**, 5464 (1958).
2. J. F. Jones, *J. Polym. Sci.*, **33**, 15 (1958).
3. G. Smets, P. Hous, and N. Deval, *J. Polym. Sci. A-1*, **2**, 4825 (1964).
4. J. C. Hwa, W. A. Fleming, and L. Miller, *J. Polym. Sci., A-1*, **2**, 2385 (1964).
5. J. P. J. Higgins, Ph.D. Thesis, Univ. of London, 1969.
6. K. W. Weale, *Chemical Reactions at High Pressures*, Spon, London, 1967, p. 78.
7. P. W. Bridgman, *The Physics of High Pressure*, Bell, London, 1949.
8. E. W. Comings, *High Pressure Technology*, McGraw-Hill, New York-London, 1956.
9. S. Siggia, *Quantitative Organic Analysis via Functional Groups*, Wiley, New York-London, 1963, p. 34.
10. J. Mercier and G. Smets, *J. Polym. Sci.*, **57**, 763 (1962).

Received September 25, 1969

## Polyelectrolyte Behavior and Macromolecular Properties of Sodium Amylopectin Xanthate in Dilute Solution

A. G. PRAMANIK and P. K. CHOUDHURY, *Department of Applied Chemistry, Calcutta University, Calcutta, India*

### Synopsis

Sodium amylopectin xanthate was prepared by xanthation of potato amylopectin in alkaline medium. The pure product was characterized by I<sub>2</sub> solution and ultraviolet spectra of the xanthate groups. The polyelectrolyte behavior of Na amylopectin xanthate in aqueous and salt solutions was investigated by viscometry and light scattering. Its polyelectrolyte behavior in aqueous solution as studied viscometrically was completely different from that of Na amylose xanthate, which is characteristic of linear polyelectrolyte molecules. This difference in behavior could be partly due to the branched structure of amylopectin molecule. A dissymmetry study of Na amylopectin xanthate in aqueous and salt solutions, however, showed that Na amylopectin xanthate molecule underwent expansion in water by about 1.3 times its linear dimension in 0.5M NaCl (unperturbed value). Light-scattering measurements confirmed that the Na amylopectin xanthate molecule had a polydisperse random-coil chain configuration in 0.25M NaCl. Its molecular weight, end-to-end length, and other parameters in salt and alkali solutions were also determined, and the data were then compared with those of Na amylose xanthate in the same media. The solution behavior of Na amylopectin xanthate in 1M NaOH was further investigated and linear expansion factor  $\alpha$ , excluded volume factor  $A_2\bar{M}_w/[\eta]$ , and Flory's hydrodynamic constant  $\phi$  were evaluated.

Our investigations on sodium amylose xanthate in dilute solution have already been reported.<sup>1,2</sup> In this communication, we shall present some data obtained from viscometry and light scattering on polyelectrolyte behavior and macromolecular properties of sodium amylopectin xanthate in aqueous and salt solutions. As amylopectin is a branched molecule, a study of this nature and a comparison of its properties with linear sodium amylose xanthate will be useful.

Since the reduced viscosity of polyelectrolytes depends upon factors such as normal conformation of the polymer chains, density of attached ions, structural limitations to deformation and the concentration of the polymer in solution, for a fair comparison of linear and branched polyelectrolytes of comparable molecular weights at the same concentration level, the spacings of the charges and a knowledge of the polymer structures are of fundamental importance. If it is assumed that the different spatial distribution of charges on linear and branched polyelectrolytes does not change the inter-

ionic repulsions, then any difference in the viscosity between branched and linear polyelectrolytes, after the above factors have been taken into consideration, may be attributed to the structure and to the structural limitations to extension. Such studies of the influence of structure upon the viscous behavior of carboxymethyl amylose and carboxymethyl amylopectin have been reported by Winter and Beckmann.<sup>3</sup> Similarly, Pasika and Cragg<sup>4</sup> studied the polyelectrolyte behavior of both linear and branched dextran sulfates in aqueous and salt solutions. Although useful data on solution properties of amylose derivatives such as amylose triacetate,<sup>5,6</sup> amylose tricarbanilate,<sup>7,8</sup> and carboxymethyl amylose<sup>9</sup> are available, the only analogous study of an amylopectin derivative is that of hydroxyethyl amylopectin by Cerny et al.<sup>10</sup>

In the present study, the polyelectrolyte behavior of sodium amylopectin xanthate in aqueous and salt solutions and its macromolecular properties in salt and alkali solutions have been investigated.

## EXPERIMENTAL

### Preparation and Characteristics of Amylopectin Sample

Amylopectin was obtained from the aqueous dispersion of potato starch after separation of amylose as the amylose–butanol complex<sup>1</sup> following the method of Schoch.<sup>11</sup> It was dehydrated with fresh methanol, filtered and dried in vacuum. The iodine absorption value of amylopectin was negligible. The intrinsic viscosity  $[\eta]$  in water was 0.75 dl/g, and the molecular weight  $\bar{M}_w$  by light scattering in aqueous solution was  $4.1 \times 10^7$ . The magnitude of molecular weight of potato amylopectin was in good agreement with molecular weight data reported by others.<sup>12</sup>

### Preparation and Isolation of Pure Na Amylopectin Xanthate (NaA<sub>p</sub>X)

Xanthation of amylopectin and its purification were carried out in the same way as that for amylose.<sup>1</sup>

### Determination of Content of Xanthate Sulfur

Xanthate sulfur (percentage) in Na amylopectin xanthate was determined iodometrically and was found to be higher than that in Na amylose xanthate prepared under identical conditions. Since the frequency of branching of amylopectin molecule in our sample was not known, we have not converted the percentage xanthate sulfur to degree of substitution.

### Ultraviolet Spectra of the Xanthate Group

The optical density (OD) of pure Na amylopectin xanthate in double distilled water was measured from 2100 Å to 4000 Å (Fig. 1) in a Beckman DU spectrophotometer and was found to be  $\lambda_{\max} = 3020 \text{ Å}$ , which is characteristic of the xanthate anion ( $\sim \text{CSS}^-$ ).<sup>13</sup>

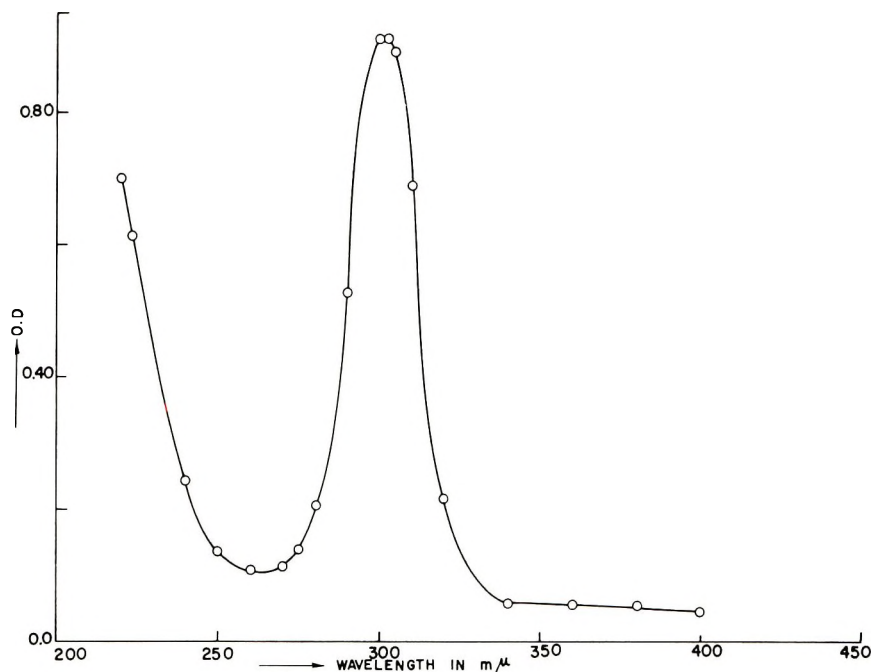


Fig. 1. Ultraviolet spectrum of Na amylopectin xanthate in water.

### Viscosity Measurements

Viscosity measurements for both aqueous and salt solutions were carried out with a standard Ostwald viscometer having a flow time of 106.5 sec for water at  $30 \pm 0.1^\circ\text{C}$ . For the study of polyelectrolyte behavior of Na amylopectin xanthate in aqueous medium, solutions were clarified through a grade-4 sintered glass filter, and dilution was made with the respective sol-

TABLE I  
Viscosity of Na Amylopectin Xanthate in Aqueous Solution

No.	Concn $c$ , g./dl	$\eta_{sp}/c$
1	0.7868	6.639
2	0.4721	4.963
3	0.3777	4.613
4	0.3022	4.258
5	0.2418	4.028
6	0.1934	3.849
7	0.1547	3.775
8	0.1238	3.644
9	0.0990	3.550
10	0.0790	3.501
11	0.0475	3.383
12	0.0285	3.132
13	0.0171	2.856
14	0.0102	2.837

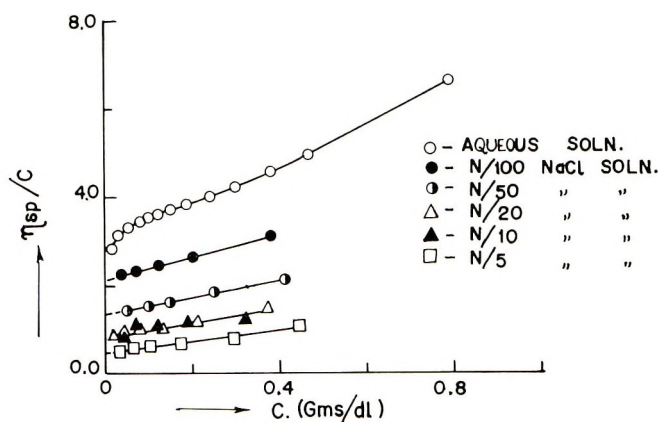


Fig. 2. Viscosity of Na amylopectin xanthate in water and salt solutions.

vent in the same viscometer down to a polymer concentration of 0.005 g/dl. No kinetic energy correction was made as it was negligible. Viscosity data are presented in Table I and in Figure 2.

### Light-Scattering Measurements

Light-scattering measurements were made in a Brice-Phoenix Universal 1999-10 series light-scattering photometer calibrated against an opal reference standard. The Rayleigh ratio  $R_{\theta}$  was calculated from the relation given by Cowie.<sup>14</sup> In the determination of molecular weight of Na amylopectin xanthate in salt solutions by the dissymmetry method, turbidity was calculated from  $90^{\circ}$  scattering.<sup>15</sup> Depolarization and absorption corrections were neglected being small. All scattering measurements were performed at  $5460 \text{ \AA}$ . Values of refractive index increments  $dn/dc$  were also determined at  $5460 \text{ \AA}$  for each solution by using the Brice-Phoenix differential refractometer. Solutions were prepared and clarified following the same procedure described earlier.<sup>1,2</sup> The molecular weight and other parameters of Na amylopectin xanthate in alkali solution were obtained by treating the light-scattering data according to the method of Zimm.<sup>16</sup>

## RESULTS AND DISCUSSION

### Polyelectrolyte Behavior of Na Amylopectin Xanthate in Aqueous and Salt Solutions

Data for  $\eta_{sp}/c$  against  $c$  for Na amylopectin xanthate in aqueous solution have been presented in Table I and the corresponding plots of  $\eta_{sp}/c$  versus  $c$  for both aqueous and salt solutions are shown in Figure 2. From these data it may be noted that plot of  $\eta_{sp}/c$  versus  $c$  for Na amylopectin xanthate in aqueous solution is very different from that of Na amylose xanthate in water,<sup>1</sup> which is typical for the viscosity behavior of linear polyelectrolytes. In the case of Na amylopectin xanthate, a continuous decrease in the re-



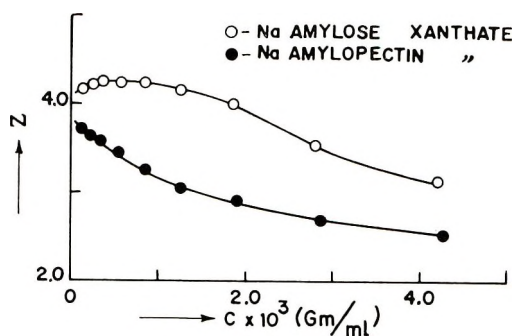


Fig. 3. Dissymmetry  $Z$  vs.  $c$  of Na amylose xanthate and Na amylopectin xanthate in water.

duced viscosity  $\eta_{sp}/c$  has been observed with dilution, even up to a polymer concentration of 0.005 g/dl. Such a linear relationship, although somewhat strange, has been observed for very high molecular weight Na carboxymethyl dextran in aqueous solution.<sup>17</sup>

The anomalous behavior of Na amylopectin xanthate in aqueous solution can be explained on the basis of the branched structure of the amylopectin molecule. In the case of linear Na amylose xanthate, the axial ratio is very large. This ratio further increases with dilution due to repulsion of the charged xanthate groups. This high degree of extension is reflected in the increase of  $\eta_{sp}/c$  with dilution.<sup>1</sup> While the resultant extension of the branched Na amylopectin xanthate molecule will be much less and as the unit chains will be pointing towards many directions, this will result in a comparatively small change in axial ratio. On dilution, the contribution of the overall extension towards increase in viscosity will be negligible, and hence  $\eta_{sp}/c$  decreases with dilution as observed for Na amylopectin xanthate in water and this is more or less similar as that for uncharged polymers.

The dissymmetry of scattering, calculated as the ratio of intensity of scattered light at  $45^\circ$  to that at  $135^\circ$  was measured for both Na amylose xanthate and Na amylopectin xanthate in water with continuous dilution and is shown in Figure 3. It is noted from Figure 3 that the dissymmetry at infinite dilution, i.e., intrinsic dissymmetry  $[Z]$ , of both Na amylose xanthate and Na amylopectin xanthate in aqueous solution has been found to be 4.25 and 3.8, respectively. The corresponding values of NaAX in 0.25M NaCl (a  $\theta$  solvent for NaAX<sup>1</sup>) and of NaA<sub>p</sub>X in 0.5M NaCl (a  $\theta$  solvent for NaA<sub>p</sub>X, Fig. 6) are 3.5 and 3.35, respectively. Assuming coiled configurations for Na amylose xanthate and Na amylopectin xanthate in aqueous and salt solutions, the linear dimension of Na amylose xanthate in water is found to be 5546 Å and in 0.25M NaCl 3068 Å (unperturbed dimension), respectively, while the corresponding values for those of Na amylopectin xanthate in water and 0.50M NaCl are 3489 and 2859 Å, respectively (the latter being the unperturbed value). Thus Na amylose xan-

that in water expands 1.8 times the linear dimension in the unperturbed state while Na amylopectin xanthate is expanded in water by 1.3 times only unperturbed linear dimension.

### Macromolecular Shape of Na Amylopectin Xanthate as Determined by Light Scattering

Though Na amylose xanthate has the polydispersed random-coil chain configuration in salt solution,<sup>1</sup> the presence of branched sites along the backbone chain of Na amylopectin xanthate molecule may evoke some doubt regarding the exact nature of its macromolecular configuration in salt solution. As an exact knowledge of the macromolecular shape in solution is

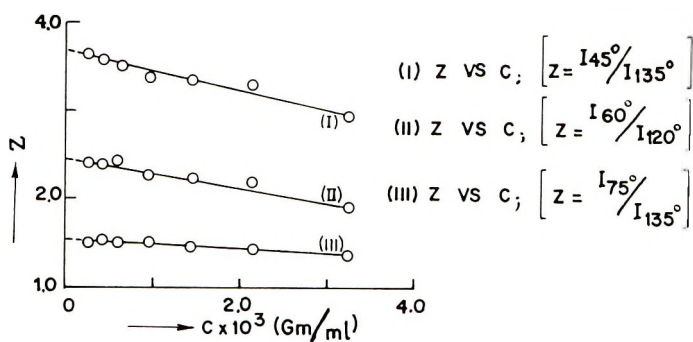


Fig. 4. Dissymmetry  $Z$  vs.  $c$  for Na amylopectin xanthate in  $0.25M$  NaCl at three different pairs of dissymmetry angles.

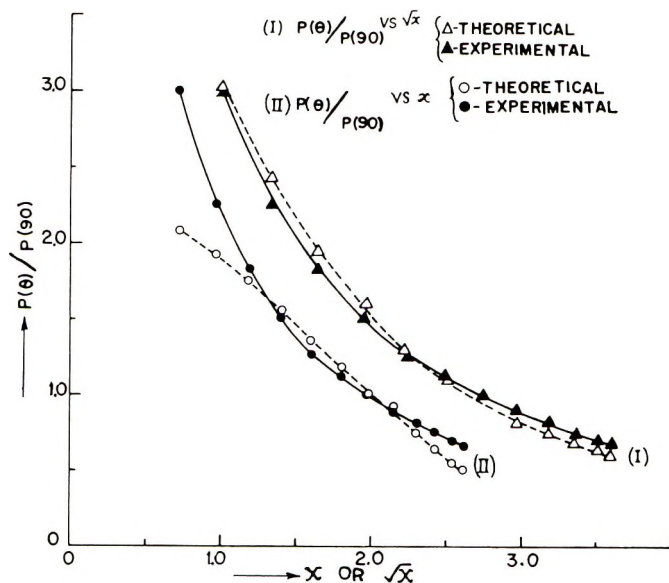


Fig. 5. Determination of shape of Na amylopectin xanthate in  $0.25M$  NaCl: (I) assuming polydispersed random coil; (II) assuming spherical shape.

required for the determination of the actual molecular weight of polymer molecules in solution by the dissymmetry method, we have estimated the shape of Na amylopectin xanthate in 0.25*M* NaCl from light-scattering data (Figs. 4 and 5). A detailed description of these two methods has already been given.<sup>1</sup> From the above plots it could be easily inferred that Na amylopectin xanthate molecule in 0.25*M* NaCl conforms to a polydispersed random-coil configuration rather than that of a sphere. This is also supported by the work of Oene and Cragg<sup>18</sup> on dextran, which in aqueous solution assumes the configuration of a compact "shaggy" helical coil with the main chain wound in a helix and the branches attached to it and directed outwards from it. In the light of the close similarity between the structure and macromolecular configuration of dextran and amylopectin, it is reasonable to conceive that the polydispersed random-coil configuration of Na amylopectin xanthate in 0.25*M* NaCl is quite justified.

### Molecular Weights, end-to-end Lengths and Other Parameters of Na Amylopectin Xanthate in Salt and Alkali Solutions

The light-scattering data on Na amylopectin xanthate in salt solutions were treated by the dissymmetry method i.e., by plotting separately  $Hc/\tau$  versus  $c$  and dissymmetry  $Z$  versus  $c$  and shown in Figures 6 and 7, respectively, while the corresponding data of Na amylopectin xanthate in 1*M* NaOH were treated according to the method of Zimm<sup>16</sup> and shown in Figure 8. The refractive index increments, molecular weights, and other molecular parameters of Na amylopectin xanthate in salt and alkali solutions are presented in Table II.

From these data it can be noted that the behavior of Na amylopectin xanthate in salt solutions is somewhat different from that of Na amylose xanthate.<sup>1</sup> In contrast to the behavior of Na amylose xanthate in salt solutions, Na amylopectin xanthate exhibits decidedly positive second virial coefficient in a 0.25*M* NaCl ( $0.3 \times 10^{-5}$ ) which falls almost to zero in

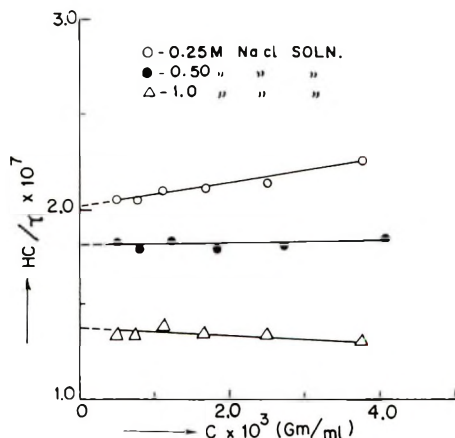


Fig. 6.  $Hc/\tau$  vs  $c$  for Na amylopectin xanthate in NaCl solution.

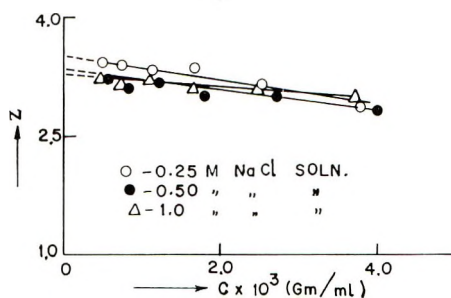


Fig. 7. Dissymmetry  $Z$  vs.  $c$  for Na amylopectin xanthate in NaCl solution.

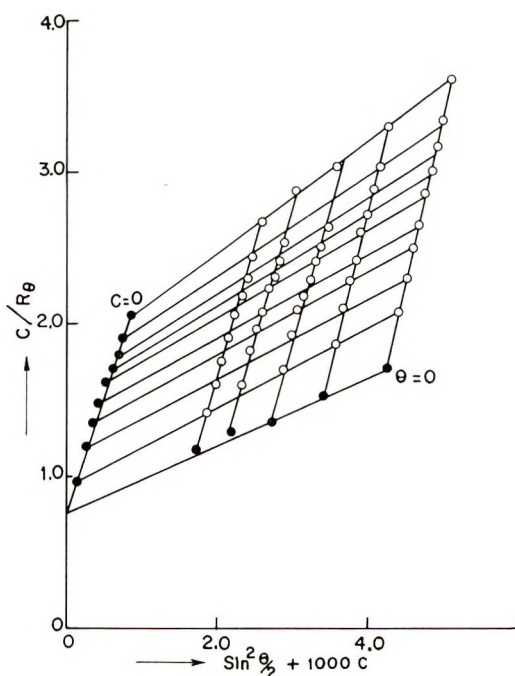


Fig. 8. Zimm plot for Na amylopectin xanthate in 1M NaOH.

0.5M NaCl (a thermodynamically ideal solvent in which end-to-end length of  $\text{NaA}_p\text{X}$  is in the unperturbed state) and then becomes negative ( $-0.2 \times 10^{-5}$ ) in 1.0M NaCl. This gradual change in the value of the slope from positive to negative is a clear indication of the transition from the preference of solute-solvent interaction in dilute salt solution to the solute-solute interaction in more concentrated salt solutions. The plots of  $Hc/\tau$  versus  $c$  for Na amylopectin xanthate in salt solutions have also an opposite trend to that of Na amylose xanthate in the same media in that the  $(Hc/\tau)_{c \rightarrow 0}$  values gradually decrease, resulting in the slight increase of apparent molecular weights with an increase in salt concentrations. This can be explained by considering the systems to be three-component ones<sup>19</sup> and assum-

TABLE II  
Molecular Weight, Dissymmetry, End-to-End Length of  
Na Amylopectin Xanthate in Salt and Alkali Solutions

No.	Solvent	$dn/dc$ , ml/g	$\bar{M}_w \times 10^{-7}$	$[Z]$	$A_2 \times 10^5$ , ml-mole/g <sup>2</sup>	$(\bar{R}^2)^{1/2}$ , Å <sup>a</sup>
1	0.25M NaCl	0.1875	2.302	3.500	0.300	3068
2	0.50M NaCl	0.1528	2.333	3.350	0	2859
3	1.0M NaCl	1.1375	2.935	3.300	-0.200	2845
4	1.0M NaOH	0.1600	0.7843 <sup>b</sup>	—	2.120	2247

<sup>a</sup> End-to-end lengths calculated on the basis of polydispersed random coils.

<sup>b</sup> Molecular weight determined from Zimm plot.

ing that in these solvents  $\text{NaA}_p\text{X}$  molecules show a preference for the water molecules and so the optical properties in the immediate neighborhood of the solute molecules are not representative of the medium as a whole. However, the slight lowering of  $[Z]$  in salt solutions of increasing salt concentration might be due to decrease in the size of the polycoid as the chain becomes more compact in structure with increase in salt concentration. It is also interesting to note that the change in the refractive index increment,  $dn/dc$  values of Na amylopectin xanthate calculated in salt solutions tends to decrease with increasing in salt concentration, in contrast to Na amylose xanthate for which the  $dn/dc$  values increase from 0.1460 in 0.11M NaCl to 0.1741 in 1.0M NaCl.<sup>1</sup> As in other polyelectrolyte systems,<sup>20</sup> the small decrease in the refractive index increment values with increasing salt concentration may indicate that the polarizability of the polyelectrolyte molecules decreases slightly with decreasing ionization.

Thus, the molecular weight of Na amylopectin xanthate calculated in salt solutions has been found to increase from  $2.3 \times 10^7$  in 0.25M NaCl to  $2.9 \times 10^7$  in 1.0M NaCl. The same Na amylopectin xanthate has a molecular weight of  $7.84 \times 10^6$  and an end-to-end length of 2247 Å in 1M NaOH. This decrease in the molecular weight of the xanthate in alkali medium might be the result of better solvent action of alkali which is evidenced by the higher value of the second virial coefficient  $A_2$  ( $2.12 \times 10^{-5}$ ). The possibility of some degradation of xanthate molecules in the alkali medium has been kept at a minimum by storing the alkali solution of Na amylopectin xanthate at about  $-5.0^\circ\text{C}$  until light-scattering measurements were actually undertaken. Further, great care was taken when actual light-scattering measurements were carried out on the solution to minimize the effect of degradation.

The Na amylopectin xanthate in salt or alkali solutions gave somewhat lower molecular weight than that of original amylopectin in aqueous solution. Since the linkages at branch points are more sensitive to degradation,<sup>21</sup> it is highly probable that during xanthation of amylopectin in an alkaline medium, some degradation of branch units took place. On the other hand, as pure water is a very poor solvent for amylopectin, the increased solute-solute interaction in such medium might have resulted in an

apparent increase of molecular weight of amylopectin in this system, while aqueous salt or alkali solutions being better solvents for Na amylopectin xanthate due to greater degree of solute-solvent interaction might have resulted in the decrease in molecular weight of Na amylopectin xanthate in such media. Such phenomenon have also been observed by Hyde and Wippler<sup>22</sup> in case of polystyrene in two different solvents, benzene and methyl ethyl ketone.

### Solution Behavior of Na Amylopectin Xanthate in 1M NaOH

**Expansion Factor  $\alpha$ .** Due to the tendency of Na amylopectin xanthate molecules to aggregate in salt solutions, light-scattering data in alkaline solution of Na amylopectin xanthate have further been analyzed to evaluate the nature of solute-solvent interaction prevailing in such medium. For this purpose, the expansion factor  $\alpha$  was evaluated by utilizing the well-known equation of Flory and Orofino:<sup>23</sup>

$$A_2 = (16\pi/3^{3/2})(N\langle\bar{s}^2\rangle^{3/2}/M^2) \ln [1 + \pi^{1/2}/2)(\alpha^2 - 1)] \dots \quad (1)$$

where  $A_2$  is the second virial coefficient;  $N$  is Avogadro's number;  $\langle\bar{s}^2\rangle^{1/2}$  is the root-mean-square radius of gyration of the polycoil, and  $M$  is the molecular weight of the polymer. The value of  $\alpha$  calculated from the above equation was 1.42 for Na amylopectin xanthate of molecular weight  $7.84 \times 10^6$  in 1M NaOH solution. Cerny et al.,<sup>10</sup> however, reported some what higher value of  $\alpha$  (1.82) for hydroxyethyl amylopectin of molecular weight  $1.92 \times 10^6$  in aqueous solution. Expansion factors of similar magnitude have also been reported for cellulose derivatives<sup>24,25</sup> such as hydroxyethyl cellulose (HEC) and Na carboxymethyl cellulose (NaCMC) in water, salt solution and cadoxen.

**Excluded Volume Factors.** The excluded volume of polymer molecule has been included in at least two empirical relationships.<sup>23,26</sup> Since the excluded volume would be proportional to  $\langle\bar{S}^2\rangle^{3/2}$ , one such factor for polymers of high molecular weight in thermodynamically good solvents can be expressed by  $A_2 \bar{M}_w / \langle\bar{S}_w^2\rangle^{3/2} = x_1$  where  $x_1$  is a constant. Since  $\bar{M}_w / \langle\bar{S}_w^2\rangle^{3/2} \propto 1/[\eta]$ ,  $A_2 \bar{M}_w / [\eta] = x_2$ , where  $x_2$  is another constant. By combining Zimm's single-contact theory with Flory's viscosity theory, Krigbaum<sup>27</sup> has shown that for linear macromolecules the above two parameters  $x_1$  and  $x_2$  should have the value of  $4.4 \times 10^{24}$  and 160, respectively. For some synthetic polymers in good solvents<sup>28,29</sup> such conclusions have been confirmed. However, for the system under investigation, these two parameters have the values of  $3.77 \times 10^{24}$  and 181, respectively. These data signify the good solvent effect of 1M NaOH for Na amylopectin xanthate and actually represent the higher limits attainable for these constants as in other polymer-solvent systems.<sup>28,29</sup> Recently, Granath<sup>30</sup> reported

values of the factor  $x_2$  which range from 110 to 200 for branched polymers such as dextran in aqueous solution.

**Flory's Hydrodynamic Constant.** The hydrodynamic behavior of coiled macromolecules in solution with moderate molecular extension can be described according to Flory and Fox<sup>31</sup> by the expression:

$$\Phi = q[\eta]\bar{M}_w/(\bar{R}_z^2)^{3/2} \quad (2)$$

where  $(\bar{R}_z^2)^{1/2}$  is the Z-average end-to-end length,  $\Phi$  is Flory's universal constant, and  $q$  is a function of polydispersity expressed by  $q = (\bar{M}_w/\bar{M}_n)^\delta$ . The exponent  $\delta$  is probably much nearer to unity for a Gaussian distribution of molecular weights, while that derived from the Lansing-Kramer distribution is 13/8. Assuming  $\bar{M}_w/\bar{M}_n = 2$ , which is approximately correct as observed from the nature of Zimm plot (Fig. 8), the value of  $\Phi$  for Na amylopectin xanthate in 1M NaOH was  $0.78 \times 10^{21}$  and  $1.17 \times 10^{21}$  for the two types of distributions as discussed above. Such magnitudes of  $\Phi$  have also been reported for several other polymer-solvent systems.<sup>32,33</sup> However, the corresponding value of  $\Phi$ , for branched dextran in aqueous solution as reported by Bovey,<sup>34</sup> was about  $2.2 \times 10^{21}$  in the range of molecular wts. of 8.1–14.6  $\times 10^7$ .

## CONCLUSIONS

Viscometric study of the polyelectrolyte behavior of Na amylopectin xanthate in aqueous solution reveals that, unlike linear polyelectrolytes, e.g., Na amylose xanthate in aqueous solution, there is a continuous decrease in the value of the reduced viscosity,  $\eta_{sp}/c$  with dilution. This may be partly due to the branched structure of amylopectin molecule. However, dissymmetry studies of aqueous and salt solutions of Na amylopectin xanthate confirm that the polyelectrolyte molecule undergoes expansion in water by about 1.3 times its linear dimension in 0.5M NaCl (unperturbed value).

Light-scattering measurements indicate that Na amylopectin xanthate molecule has essentially the polydispersed random-coil chain configuration in 0.25M NaCl.

Molecular weight, end-to-end length, and other parameters of Na amylopectin xanthate in salt and alkali solutions as determined by light scattering indicate that the Na amylopectin xanthate molecule has the tendency to aggregate in salt solutions.

The values of  $\alpha$ ,  $A_2\bar{M}_w/[\eta]$ ,  $A_2\bar{M}_w^2/(\bar{S}^2)^{3/2}$ , and  $\Phi$  of NaApX in 1M NaOH have been determined, and the data show that alkali is a better solvent for Na amylopectin xanthate than salt solutions.

The authors express their gratitude to the University Grants Commission, New Delhi for the award of a research fellowship to one of them (A. G. P.).

## References

1. A. G. Pramanik and P. K. Choudhury, *J. Polym. Sci. A-1*, **6**, 1121 (1968).
2. A. G. Pramanik and P. K. Choudhury, *J. Polym. Sci., A-1*, **7**, 1055 (1969).
3. S. S. Winter and C. O. Beckmann, *J. Phys. Chem.*, **60**, 883 (1956).
4. W. M. Pasika and L. H. Cragg, *J. Polym. Sci.*, **57**, 301 (1962).
5. J. M. G. Cowie, *J. Polym. Sci.*, **49**, 455 (1961).
6. R. S. Patel and R. D. Patel, *J. Polym. Sci. A*, **3**, 2123 (1965).
7. W. Burchard and E. Husemann, *Makromol. Chem.*, **44**, 358 (1961).
8. W. Burchard, *Abhandl. Deut. Akad. Wiss. Berlin Kl. Med.*, **6**, 81 (1964).
9. J. R. Patel, C. K. Patel, and R. D. Patel, *Stärke*, **19**, 330 (1967).
10. L. C. Cerny, R. C. Graham, and H. James, *J. Appl. Polym. Sci.*, **11**, 1941 (1967).
11. T. J. Schoch, *Advan. Carbohydrate Chem.*, **1**, 247 (1945).
12. L. P. Witnauer, F. R. Senti, and M. D. Stern, *J. Chem. Phys.*, **20**, 1978 (1952); *J. Polym. Sci.*, **16**, 1 (1955).
13. E. Klein, J. K. Bosarge, and I. Norman, *J. Phys. Chem.*, **64**, 1666 (1960).
14. J. M. G. Cowie, *Makromol. Chem.*, **42**, 230 (1961).
15. *The New Brice-Phoenix Universal 1000 Series Light Scattering Photometer*, Operation Manual OM-1000, Phoenix Precision Instrument Company, 3803-05 North Fifth Street, Philadelphia, Pennsylvania.
16. B. H. Zimm, *J. Chem. Phys.*, **16**, 1093, 1099 (1948).
17. R. A. Wall and S. S. Winter, *J. Polym. Sci.*, **26**, 245 (1957).
18. H. V. Oene and L. H. Cragg, *J. Polym. Sci.*, **57**, 175 (1962).
19. R. H. Ewart, C. P. Roe, P. Debye, and J. R. McCarthey, *J. Chem. Phys.*, **14**, 687 (1946).
20. V. P. Strauss, E. H. Smith, and P. L. Wineman, *J. Am. Chem. Soc.*, **75**, 3935 (1953).
21. *Polysaccharides in Biology, Transactions of the Third Conference, May 1957*, The Josiah Macy Jr. Foundation, p. 138.
22. A. J. Hyde and C. Wippler, *Research (London)*, **10**, 209 (1957).
23. P. J. Flory and T. A. Orofino, *J. Chem. Phys.*, **26**, 1067 (1957).
24. W. Brown, D. Henley, and J. Ohman, *Makromol. Chem.*, **64**, 49 (1963).
25. P. J. Flory, O. K. Spurr, Jr., and D. K. Carpenter, *J. Polym. Sci.*, **27**, 231 (1958).
26. A. R. Schultz, *J. Am. Chem. Soc.*, **76**, 3422 (1954).
27. W. R. Krigbaum, *J. Polym. Sci.*, **18**, 315 (1955).
28. E. W. Gouinlock, P. J. Flory, and H. A. Scheraga, *J. Polym. Sci.*, **16**, 386 (1955).
29. G. Levy and H. P. Frank, *J. Polym. Sci.*, **17**, 247 (1955).
30. K. A. Granath, *J. Colloid. Sci.*, **13**, 308 (1958).
31. T. G. Fox and P. J. Flory, *J. Amer. Chem. Soc.*, **73**, 1904, 1909 (1951).
32. P. Doty, N. S. Schneider, and A. Holtzer, *J. Amer. Chem. Soc.*, **75**, 754 (1953).
33. R. St. J. Manley, *Arkiv Kemi*, **9**, 519 (1956).
34. F. A. Bovey, *J. Polym. Sci.*, **35**, 167 (1959).

Received December 27, 1968

Revised October 15, 1969



## Synthetic Thermally Reversible Gel Systems. V

HOWARD C. HAAS, MONIS J. MANNING, and MARTIN H. MACH, *Research Laboratories, Polaroid Corporation, Cambridge, Massachusetts, 02139*

### Synopsis

Differential thermal analysis has been used to study the fusion of aqueous thermally reversible gels of gelatin and polyacrylylglycinamide (PAG). In the case of gelatin gels, endotherms close to the melting point are readily observed and these are sometimes preceded by a small exothermic heat of gel reorganization. Calculations are presented to show that breaking of the gelatin gel network requires only a small fraction of the observed endothermic heat of fusion and that most of the heat is required for melting larger crystallites within gelatin aggregates and for perhaps a helix  $\rightarrow$  coil transition. Failure to observe endotherms by DTA over the known temperature range of fusion of PAG gels is consistent with prior measurements and conclusions. The noncrystallinity of PAG gels and soluble aggregates together with a heat of crosslinking of only  $-5$  to  $-10$  kcal/mole of crosslinks places the heat of fusion of PAG gels outside the lower limits of DTA sensitivity.

This paper describes the use of differential thermal analysis (DTA) to study the thermal behavior of aqueous thermally reversible gels. Surprisingly, no literature references could be found in which DTA was used for this purpose.

Previous papers in this series<sup>1-4</sup> were mainly concerned with the synthesis<sup>1</sup> of acrylyl (AG) and methacrylylglycinamide (MG), the polymerization kinetics of AG<sup>4</sup> and the properties of polyacrylylglycinamide (PAG), its solutions and its thermally reversible aqueous gels.<sup>2,3</sup> The third paper<sup>3</sup> dealt primarily with the nature of the thermally reversible crosslinks in aqueous PAG and gelatin gels. A thermodynamic approach was used which was based on equilibrium swelling measurements to determine the molecular weight between crosslinks  $\bar{M}_c$  and moduli measurements to obtain the fraction of groups per chain involved in crosslinking.

The results with PAG were remarkably simple. The  $\bar{M}_c$  from swelling corresponded almost exactly to the value obtained by dividing the known  $\bar{M}_n$  of the PAG used by the number of groups per chain minus one involved in crosslinking. The necessary conclusion was that a thermally reversible crosslink in an aqueous PAG gel involves one group from each of two chains. By using the thermodynamic approach of Eldridge and Ferry,<sup>5</sup> the heat of crosslinking  $\Delta H_c$  of aqueous PAG gels was measured and found to range from  $-5$  to  $-11$  kcal/mole of crosslinks. Assuming that in PAG gels

the thermally reversible crosslinks are of the hydrogen bond type with a heat of formation of  $-5$  kcal/mole of hydrogen bonds, the expected  $\Delta H_c$  for PAG gels would be  $-5$  to  $-10$  kcal/mole of crosslinks, depending on whether the pendent group is acting in a monofunctional or difunctional hydrogen-bonding capacity. A further implication of these results is that crystallite formation plays no part in crosslink formation or in the formation of aggregated species in solution.

The results with gelatin were not so straightforward. Firstly, the value of  $\bar{M}_c$  from equilibrium swelling was twice that of  $\bar{M}_n$ . It was obvious therefore that the number-average molecular weight of the gelatin is not important but rather the  $\bar{M}_n$  of the gelatin aggregate at the point of incipient gelation. The exact aggregate molecular weight is not required as long as it is sufficiently large. If it was assumed that the peptide groups per chain involved in crosslinking were randomly distributed throughout the aggregate, the  $\bar{M}_c$  value was much smaller than that obtained from equilibrium swelling. To rationalize these results, we concluded that the peptide groups involved in crosslinking were distributed non randomly but rather existed in randomly distributed packets containing between 21 and 38 groups per packet. A crosslink consists of a pack from each of two aggregate chains. Again if the individual bonds within a crosslink are of the H bond type,  $\Delta H_c$  values that fall within the experimental<sup>5</sup>  $-50$  to  $-220$  kcal/mole of crosslinks range for gelatin gels are obtained.

## EXPERIMENTAL

A DuPont Model 900 differential thermal analyzer was used for the measurements. The samples of gel were contained in small sealed aluminum cups. Rates of heating ranged from 5 to 20°C/min. Sample weights were between 14 and 21 mg. Numerous determinations were made.

The gelatin gel was prepared from photographically inert Rousselot limed ossein gelatin. The gelatin was dissolved in distilled water and held at 60°C for 1 hr. It was allowed to gel and was then stored at 3°C for several weeks. The final preparation contained 18.4% gelatin by weight (volume fraction,  $\nu_2 = 0.141$ ) and also a small amount of bactericide.

The heat of crosslinking  $\Delta H_c$  for gelatin gels prepared from this same gelatin and conditioned at 0 and 15°C for 18 hr after preparation were determined by the method of Eldridge and Ferry.<sup>5</sup>

The PAG gel was formed by allowing a dry film to undergo equilibrium swelling in water at 25°C. The original PAG had an  $[\eta]$  in 2 *M* NaCNS at 25°C of 0.64, corresponding to a  $\bar{M}_n$  of  $200 \times 10^3$ ; this was the same sample studied in detail previously.<sup>3</sup>

The gel contained 19.65% PAG by weight ( $\nu_2 = 0.151$ ). By using a Fisher-Johns apparatus, the approximate melting range of this gel was found to be 80–90°C.

## RESULTS

At a heating rate of 20°C/min, four stages were noted in the DTA thermogram of the gelatin gel: a stable baseline below 15°C, an occasional premelt exotherm from 15 to 25°C, fusion of the gel from 30 to 35°C, and a steady baseline above 45°C. These temperatures are not equilibrium values and will vary somewhat with heating rate. Average data for the heat of fusion  $\Delta H_f$ , the premelt exotherm  $\Delta H_r$ , and the heat capacities before and after melting are given in Table I on a calories per gram of gel basis; a typical thermogram is presented in Figure 1.

TABLE I  
Average Thermal Data for Gelatin Gel

Temperature interval, °C	$C_p$ , cal/g °C	$\Delta H_f$ , cal/g	$\Delta H_r$ , cal/g <sup>a</sup>
<15	1.04 ± 0.08	—	—
15-25	Changing exotherm	—	-0.11
30-37	Changing endotherm	1.18 ± 0.04	—
>45	0.99 ± 0.09	—	—

<sup>a</sup>  $\Delta H_r$  is an exothermic heat of gel reorganization.

The melting points and the calculated heats of crosslinking  $\Delta H_c$  for gelatin gels conditioned at 0 and 15°C are given in Table II.

Many thermograms were run on the PAG gel at various heating rates, and no consistent results could be obtained over the temperature range in which the gel is known to melt. Occasionally very small deviations occurred from the baseline in the 80-90°C range, but they occurred inconsistently among different samples and were not reproducible on the same sample. The conclusion is that the thermal effects involved in the

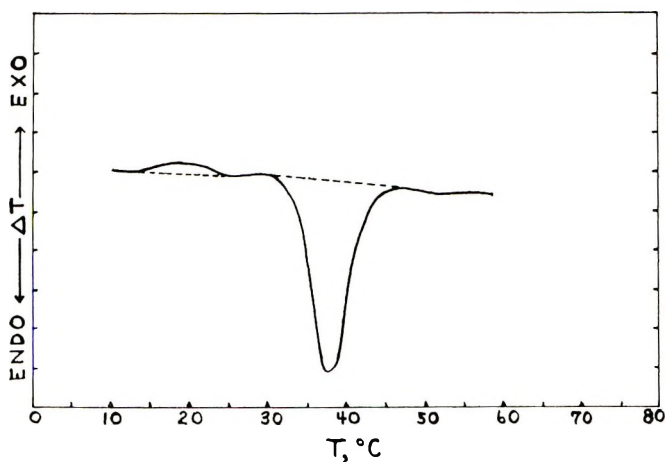


Fig. 1. DTA thermogram of 18.4% gelatin gel.

TABLE II  
Melting Points and  $\Delta H_c$  Values for Gelatin Gels

Gelatin concn, g/l.	Melting point, °C		$\Delta H_c$ , kcal/mole	
	0° gel	15° gel	0° gel	15° gel
42.7	30.3	30.8	70.9	82.6
64.5	30.8	31.1		
86.6	31.6	31.7		
108.8	32.3	32.3		
131.4	32.6	32.7		

fusion of PAG gels are outside of the limits of sensitivity of the DTA instrument.

### DISCUSSION

Gelatin systems are very sensitive to past thermal history. Pehelin<sup>6</sup> has shown that the moduli of gelatin films vary considerably depending on whether the gelatin solution is dried at 5 or 50°C. This is probably the result of different film structures since gelatin molecules undergo a reversible conformation helix  $\rightleftharpoons$  coil change in this temperature range. Below 10°C, gelatin molecules are helical, and above 30°C they acquire the conformation of a statistical coil. Similarly, the properties of gelatin gels depend on the conditions under which they are formed. If a gelatin solution is rapidly quenched to 0°C, the crosslinks of the gel are haphazardly formed and are of lower order and stability than in gels formed at 15°C. The latter are closer to equilibrium (minimum free energy) and have higher melting points and higher heats of crosslinking than those formed at lower temperatures.<sup>5</sup> In the case of our gelatin (Table II) this is also true, but we do not find as large a difference in  $\Delta H_c$  values as is usually observed.

The premelt exotherm occasionally observed in the DTA thermograms of gelatin gels deserves comment. We have no knowledge of the relative amounts of helix and coil conformations within the gel but since the helix  $\rightarrow$  coil transition is endothermic, the premelt exotherm cannot be related to a conformational change. On the other hand, as the temperature of a gel is raised, weaker bonds start to break and more stable crosslinks are formed at their expense. This annealing process just below the melting range allows the formation of stronger and more ordered crosslinks and larger crystallites within gelatin aggregates and is necessarily exothermic. It represents the same phenomenon as the difference between gels formed at different temperatures.

Of interest is to compare the magnitude of the melting endotherm with the endotherm expected from measured heats of crosslinking. Many workers<sup>7</sup> have shown that the modulus of a gelatin gel is proportional to the concentration squared of gelatin up to at least 6 g/100 ml and may deviate somewhat from the square dependence at higher concentrations.

This result is interpreted as follows. The modulus is proportional to the concentration of useful intermolecular crosslinks, which in turn is proportional to the square of the polymer concentration. In a more recent paper,<sup>8</sup> the square dependence of rigidity on concentration was again verified and information is presented which shows a linear dependence of  $\rho$ , the fraction of amino acid residues per gelatin chain involved in crosslinking, on gelatin concentration. The calculation which follows will be to establish an order of magnitude only. For this calculation we will assume the following: The modulus of a gelatin gel of a given concentration at a given temperature has been shown to be independent of  $\overline{DP}$  (except for low  $\overline{DP}$  material) but to vary somewhat with the type of gelatin. We will assume that this variation is not sufficiently large to influence our conclusion. We also believe it is reasonably legitimate to extrapolate the linear  $\rho$  versus  $c$  plot (Fig. 4 of ref. 8) to higher concentrations. Cumper and Alexander,<sup>9</sup> for example, report that only at a gelatin concentration above 20 g/100 ml does the rigidity increase appreciably more rapidly than that predicted by the square law. The gels of Szczeniak and MacAllister<sup>8</sup> were set at 10°C for 18 hr, whereas ours were conditioned at 3°C; this might introduce a small error which is not relevant to our argument.

Our gelatin gel contains approximately 19.3 g of gelatin per 100 ml of gel. Extrapolation of Figure 4 of reference 8 to this gelatin concentration yields for a value of  $\rho$ ,  $41.5 \times 10^{-3}$ . We will choose for an arbitrary number-average molecular weight of a gelatin aggregate in water at the point of incipient gelation a value of  $3 \times 10^6$ . The assigned magnitude is of no importance, as long as it is a reasonably large multiple of the  $\overline{M}_n$  of the molecularly dispersed polymer. Boedtger and Doty<sup>10</sup> have shown that the molecular weights of gelatin aggregates in water are in the millions. The degree of polymerization of a gelatin aggregate chain of this molecular weight will be  $3.24 \times 10^4$ , employing a base backbone molecular weight of 92.4. The number of groups per aggregate chain involved in crosslinking is  $\overline{DP} \times \rho$  ( $3.24 \times 10^4 \times 41.5 \times 10^{-3}$ ) = 1345, and if one group per chain constitutes a crosslink, since two chains must be involved, there will be 673 crosslinks per chain. The heat of crosslinking  $\Delta H_c$  (Table II) for a gel aged at 0°C is 71 kcal/mole of crosslinks and if it is assumed the crosslinks are hydrogen bonds at 5/kcal/mole, each crosslink must consist of approximately 14 hydrogen bonds or 14 amino acid residues per crosslink per chain. The assumption that the crosslinks are hydrogen bonded structures is not at all necessary since it has been shown independently<sup>3</sup> from swelling and modulus measurements that 14 residues per crosslink from each of two chains is a very realistic number for a gel formed haphazardly at a low temperature. Using the value of 14, we have for our gel 48 effective crosslinks per aggregate chain.

One gram of our gel contains 0.184 g of gelatin and  $0.184/3 \times 10^6$  or  $6.1 \times 10^{-8}$  moles of aggregate chains. It follows therefore that one gram of gelatin gel contains  $48 \times 6.1 \times 10^{-8}$  or  $2.93 \times 10^{-6}$  moles of crosslinks.

Using the value of  $7.1 \times 10^4$  cal/mole of crosslinks, the endothermic heat required to melt the network gel should be 0.21 cal/g.

The calculated heat of 0.21 cal/g to melt the gel network is only a small fraction of the 1.18 cal/g endotherm observed with our gelatin gel over the 30–35°C temperature range. This is not at all unreasonable. It has been shown by x-ray techniques<sup>10</sup> that gelatin gels yield crystalline diffraction patterns and that even after melting these patterns persist for a short time. This is consistent with the idea that fusion of a gelatin gel consists firstly of melting the network structure followed by the melting of the large crystallites within the now soluble gelatin aggregates. Since primarily the same types of bonds must exist both within the crosslinks and within the larger crystallites, both melting phenomena occur within the same temperature range. Although melting of the larger crystallites probably accounts in our gel for over 80% of the observed endotherm, there may be some contribution to this 80% figure by a helix-coil transition. Recent results of Pudenko and Levi<sup>11</sup> show two breaks in plots of specific conductance versus temperature for gelatin gels and solutions. The first occurs at the melting point of the gel and the second at about 32°C. These authors interpret these changes in conductance as being the result of network breakup followed by the helix-coil transition at 32°C.

The negative results obtained with the PAG gels are quite consistent with our thinking. From equilibrium swelling and modulus data, we concluded<sup>3</sup> that a thermally reversible crosslink in a PAG gel consists of perhaps one group from each of two chains and that crystallization plays no part in either crosslinking or aggregate formation. If this is true, the only contribution to a DTA endotherm at the temperature of fusion of a PAG gel would be that due to crosslinking. Since the heat of crosslinking of PAG is about  $-5$  to  $-10$  kcal/mole or only 7 to 10% of that of gelatin, we would be looking for at most approximately 0.03 cal/g. The fact that we observe no appreciable or reproducible endotherms with the PAG gel supports our prior conclusion concerning the structure of PAG gels and the heat involved in PAG gel melting is below the limits of DTA instrument sensitivity.

### References

1. H. C. Haas and N. W. Schuler, *J. Polym. Sci. B*, **2**, 1095 (1964).
2. H. C. Haas, R. D. Moreau, and N. W. Schuler, *J. Polym. Sci. A-1*, **5**, 915 (1967).
3. H. C. Haas, C. K. Chiklis, and R. D. Moreau, in press.
4. H. C. Haas, R. L. MacDonald, and A. N. Schuler, in press.
5. J. E. Eldridge and J. D. Ferry, *J. Phys. Chem.*, **58**, 992 (1954).
6. V. A. Pehelin, *Dokl. Akad. Nauk, SSSR*, **180**, 402 (1968).
7. J. D. Ferry, *J. Amer. Chem. Soc.*, **70**, 2244 (1948).
8. A. S. Szczesniak and R. V. MacAllister, *J. Appl. Polym. Sci.*, **8**, 1391 (1964).
9. C. W. N. Cumper and A. E. Alexander, *Austral. J. Sci. Res. Ser. A*, **5**, 153 (1952).
10. H. Boedtker and P. M. Doty, *J. Phys. Chem.*, **58**, 968 (1954).
11. S. V. Pudenko and S. M. Levi, *Vysokomol. Soedin. A*, **10**, 647 (1968).

Received October 31, 1969

## Carrier Mobility and Long-Range Order in Disordered Systems. II

F. GUTMANN, *Department of Physical Chemistry, The University of  
Sydney, N.S.W. 2006, Australia*

### Synopsis

Recent comments by Fleming on a previous paper dealing with long-range order in disordered systems are answered. Discrepancies between the results given therein and those obtained by Fleming are discussed and ascribed to different normalization procedures. Experimental evidence for the existence of such order is adduced.

Recently, Fleming<sup>1</sup> has published an alternative treatment of the problem of residual long-range order discussed by the present writer.<sup>2</sup> Fleming fails to find any evidence for such order to be generated by the accumulation of small random disturbances. This communication is intended to answer Fleming's comments.

He queries, first of all, the significance of, as well as why the normalization factor of 1.582 obtained in eq. (7) of the original paper has been dropped in eq. (1):

$$s = (1 + \delta) \tag{1}$$

where  $s$  is the lattice spacing resulting from disturbing the original spacing by a small, random, positive disturbance  $\delta$ . The problem is considered in one dimension only.

Equation (1), by definition, holds irrespective of normalization and has, indeed, been used by other prior workers<sup>3</sup> in this field. Normalization is introduced later, in eq. (7) and thus cannot be said to have been dropped from eq. (1).

The normalization factor has been derived from the requirement that the sum of all the probabilities  $\gamma$  that any given random deviation does occur, must add up to unity, assuming these probabilities to obey a (truncated) Poisson distribution. The factor has been allowed for in the computer program and anyhow, enters in merely as a scale factor.

Fleming then questions the justification for this summation, in eqs (2) and (3) [eqs. (6) and (9) of the original paper], to begin with zero:

$$K \int_0^1 e^{-\epsilon} d\epsilon = 1 \tag{2}$$

$$\sum_0^n \epsilon_n e^{-\epsilon n} = I \quad (3)$$

where  $\epsilon$  is defined as a random number so that

$$0 < \epsilon \leq 1 \quad (4)$$

$k$  here is the normalizing factor, and  $n$  stands for a certain finite number of terms after which the original lattice spacing will reappear in that a "molecule" will be found at its proper (unidimensional) lattice position.

The value zero might have been allowed for  $\epsilon$  in eq. (4), although it could be argued that the error in the resulting normalization coefficient can be made arbitrarily small by allowing  $\epsilon$  to approach 0 infinitely closely; the contribution to it by the  $\epsilon$ 's with values between 0 and an infinitely small and entirely arbitrary nonzero lower limit would be negligible. The zero limit means there is no disturbance and thus  $s = a$ , which is surely an allowable possibility.

Fleming points out that the residual sort of long-range order resulting from the present writer's treatment<sup>2</sup> is a rather peculiar one. This may well be the case, though to which extent this type of arrangement may be called long-range order is perhaps mainly a question of semantics and of definition.

Fleming<sup>1</sup> attacks the same problem in a manner which is independent of the distance between consecutive  $n$ th points, using the method developed by Chandrasekhar.<sup>5</sup> It is not quite clear whether or not Fleming implicitly applies Liapunov's Theorem<sup>5</sup> that

$$f(\delta) = \sum_0^n \delta \quad (5)$$

becomes a normal distribution for  $n \rightarrow \infty$ . If so, then Fleming's treatment should be expected to yield conclusions similar to those obtained by Moorjani and Feldman.<sup>3</sup> These authors find that the long range order disappears if the root-mean-square value of the disturbance exceeds the lattice constant since then the "molecule" becomes smeared out over a region greater than the lattice distance. However, Moorjani and Feldman<sup>3</sup> normalize the root-mean-square value of the disturbance so that

$$\delta^2 = I \quad (6)$$

and impose no other restrictions on  $\delta$ , either in sign or in magnitude, cf. eq. (4).

Fleming computes the number of lattice points occupied within a given positional uncertainty and finds that these probabilities approximate very closely to twice the positional uncertainty. In a way, this is the converse of the original treatment which seeks the number of lattice spacings from the origin at which, within a given positional uncertainty, a "molecule" might



be found. One should expect both approaches to yield a closely similar result.

However, it appears to the writer that the disagreement might be due to the absence of a normalization condition in Fleming's treatment. The original discussion<sup>2</sup> always required that the total number of populations within given regions of positional uncertainty should add up to a constant, viz. 10.000, though the computer calculations for the sharper cut-off functions, with their very long tails (very slow decay) were unfortunately not carried out far enough for this to be evident in the published table. From Fleming's Table I it is seen that the total populations do not add up to a constant, for  $e^{-2}$  their sum  $\gg 10.000$  even up to  $n = 64$ . In fact, the population density within any one given uncertainty region remains substantially the same, constant, and independent of distance.

Finally, Fleming points out what appears to be, at first sight, a very puzzling feature of the writer's treatment.<sup>2</sup> "... it is difficult to understand why, for  $n = 40$ , the entry under cut-off function  $e^{-3}$  should be larger than that under cut-off function  $e^{-3}$ . If an atom is positioned within an uncertainty  $e^{-3}$  of a lattice point, it must also be considered as positioned within an uncertainty  $e^{-3}$  of that same site. A similar anomalous entry appears for  $n = 8$ ." It should be pointed out that the axiom that any subset of a given set  $\leq$  set holds only for any one given set. The choice of a different cut-off function, or positional uncertainty, means that each generates its own set which is different from those sets generated from different cut-off functions. Thus, with the sharper cut-off functions a far greater portion, or even the bulk, of the total population is located in regions remote from the origin, while in the case of the wider positional uncertainties most of the population is sited close to the origin. This, of course, implies that the total population is being kept constant—a requirement which has been obeyed in the original discussion<sup>2</sup> but obviously not in Fleming's treatment. To which extent this requirement, or its absence, is related to physical reality is not clear at this juncture.

It will be interesting to see the results of Dr. Fleming's further work in this field which is to be concerned with a sequence of disturbances obeying the distribution

$$\delta = K\epsilon \exp\left\{-\epsilon/\lambda\right\} \quad 0 < \epsilon < 1 \quad (7)$$

where  $k$  is a normalization constant and  $\lambda$  is the cut-off function.

It might be apposite, in the context of this paper, to check for other, especially experimental, evidence for the existence of long range order in disordered systems; for a recent review of order in polymers, the reader is referred to a paper<sup>6</sup> given at a recent conference the proceedings of which, unfortunately, are not accessible to the present writer.

Perhaps the most convincing experimental evidence for the existence of a type of long range order in amorphous solids may be found in (a) studies of

ferromagnetic amorphous solid films,<sup>7</sup> (b) in the local order observed in glassy polymers<sup>8</sup> and (c) in the transfer of electronic excitation in sensitized phosphorescent and fluorescent, noncrystalline systems.<sup>9</sup>

Duwez and associates<sup>7</sup> have produced glassy, amorphous films of Fe-P-C alloys by very rapid cooling from the liquid. These films exhibit strong ferromagnetism though having an amorphous, liquidlike structure. It is hard to see how a long-range interaction of the kind involved in ferromagnetism could occur without the presence of at least some rudimentary, or perhaps transient, form of long-range order. This is further supported by the findings of Richter,<sup>10</sup> who assigns a higher degree of order to amorphous films than to liquids.

Differential thermal analysis of samples of amorphous poly(ethylene terephthalate) have shown the existence of a kind of local order corresponding to an equivalent degree of crystallinity of approximately 1%, about the same order of magnitude as that given in the original paper.<sup>2</sup> Poly(vinyl chloride) behaves in a like manner.<sup>8</sup>

The classic work of Foerster and his school<sup>11-13</sup> on the transfer mechanism of electronic excitation involved in fluorescence and phosphorescence yields for the time  $\tau$  required for such transfer from an excited sensitizer molecule to an acceptor molecule, assumed to be in its ground state and separated a distance  $R$ ,

$$\frac{1}{\tau} = \frac{1}{\tau_0} \left[ \frac{R_0}{R} \right]^6 \quad (8)$$

where  $\tau_0$  is the (spontaneous) decay constant and  $R_0$  the mean distance between those two molecules for which the transfer rate equals the emission rate. A typical value for this quantity is of the order of 50–100 Å in the case of organic scintillators, indicating quite a long-range interaction which must involve at least a transient kind of long-range ordering.

A computer study, using a Monte Carlo procedure, of flexible branched macromolecules<sup>14</sup> also yields evidence for the existence of a (residual? FG) long range interaction. However, the problem discussed in this work is somewhat different from, though related to, the subject of the present discussion.

There is at present only rather indirect and tenuous confirmation of eq. (17), viz., the expectation that the extent of residual long-range order should be, *ceteris paribus*, proportional to the (molecular weight  $M$ )<sup>1/2</sup>; the electric charge carrier concentration, as well as the catalytic activity of polymers which is related to it, have been found<sup>15,16</sup> to increase with  $M$ . In fact, amorphous polymers of high  $M$  are often better conductors than crystalline polymers.<sup>17-20</sup>

The writer wishes to thank Dr. Fleming and the Editor of the *Journal of Polymer Science* for the opportunity to study Fleming's MS prior to publication and for this opportunity to reply.

## References

1. R. J. Fleming, *J. Polym. Sci.*, in press.
2. F. Gutmann, in *Electrical Conduction Properties of Polymers (J. Polym. Sci. C, 17)*, A. Rembaum and R. F. Laudel, Eds., Interscience, New York, 1967, p. 41.
3. K. Moorjani and C. Feldman, *Revs. Mod. Phys.*, **36**, 1042 (1964).
4. S. Chandrasekhar, *Revs. Mod. Phys.*, **15**, 1 (1943).
5. H. Cramer, *Mathematical Methods of Statistics*, Princeton Univ. Press, Princeton, N. J., 1946.
6. S. H. Maron and F. Filisko, *Anal. Calorimetry, Proc. Amer. Chem. Soc. Symp. 155th*, **1968**, 153.
7. P. Duwez, *Progr. Solid State Chem.*, **3**, 377 (1967); *Amer. Soc. Metals Trans. Quart.*, **60**, 606 (1967); U. S. Pat. 3,297,436 (1967).
8. M. I. Kashmiri and R. P. Sheldon, *J. Polym. Sci. B*, **7**, 55 (1969).
9. F. Gutmann and L. E. Lyons, *Organic Semiconductors*, Wiley, New York, 1967.
10. H. Richter, paper delivered to the Internatl. Conf. on Thin Films, Boston, Mass. April 1969; see also *Physics Today*, **22**, 94 (1969).
11. T. Foerster and K. Kasper, *Z. Physik. Chem. (Frankfurt)*, **1**, 275 (1964); *Z. Elektrochem.*, **59**, 976 (1955); *ibid.*, **64**, 157 (1960).
12. T. Foerster, *Fluoreszenz Organischer Verbindungen*, Van den Hoeck and Ruprecht, Goettingen, 1951.
13. F. Foerster, *Disc. Faraday Soc.*, **27**, 7 (1959).
14. C. V. Gallacher and S. Windwer, *J. Chem. Phys.*, **44**, 1139 (1966).
15. R. M. Vlasova et al. *Dokl. Akad. Nauk Fiz. Khim.*, **171**, 132 (1966).
16. O. V. Kargina et al. *Dokl. Akad. Nauk Fiz. Khim.*, **170**, 1130 (1966).
17. V. I. Kasatochkin et al. *Izv. Akad. Nauk SSSR, Ser. Khim.*, **1963**, 1766.
18. A. A. Dulov et al., *Izv. Akad. Nauk. SSSR, Ser. Khim.*, **1963**, 1910.
19. B. E. Davydov et al., *Dokl. Akad. Nauk SSSR*, **160**, 650 (1965).
20. F. Gutmann, *J. Res. Inst. Catalysis Hokkaido Univ.*, **17**, 96 (1969).

Received November 5, 1969

## Influence of Torsional Stiffness upon Temperature Response of a Polymeric Chain

JOHN N. MAJERUS, *Rohm and Haas Company, Redstone Research Laboratories, Huntsville, Alabama 35807*

### Synopsis

The influence of torsional stiffness upon the temperature dependence of the mean square end-to-end polymer chain distance  $\langle r_0^2 \rangle$  was studied parametrically for six different polymer chain models. The equations for  $\langle r_0^2 \rangle$ , expressed in terms of the torsional potential energy, were differentiated with respect to temperature and the resulting equations were evaluated numerically. The magnitudes and locations of the secondary barrier heights, angular location and magnitudes of the energy minima, angular location of the maximum barrier  $U_0$ , spacing of the extrema, and the number of extrema were all found to play a significant role in the value of the predicted thermal expansion coefficients. The coefficients were also found to critically depend upon the relative energy ratio and were usually a highly nonlinear function of this ratio. Transitions between positive and negative values of the thermal expansion coefficients were found to exist and to depend upon the torsional potential shape, energy ratio, and the polymer chain model.

### INTRODUCTION

Polymer chemists have long been searching for insights into the features of the microstructure which govern certain types of binder properties. Important characteristics of a binder are its linear coefficient of thermal expansion and its stiffness and extensibility as a function of temperature. Therefore, one would like to know how the microstructure influences these various characteristics. For a three-dimensional network of polymer chains chemically crosslinked together, the thermal response depends upon the temperature behavior of the subchains between crosslink junctions. Although a complete statistical analysis of the three-dimensional network would be quite involved,<sup>1-3</sup> a first approximation for studying the influence of microstructure would be an investigation of the response of a single polymer chain, e.g., the network kinetic theory of elasticity.<sup>4-6</sup>

A representative microstructural variable of a polymer chain is its unperturbed mean square end-to-end vector distance  $\langle r_0^2 \rangle$ .<sup>3,7a</sup> Based upon the assumptions of the network kinetic theory of elasticity, the thermal expansion coefficient ( $T \partial \ln \langle r_0^2 \rangle / \partial T$ ) equals the relative internal energy change  $f_e$  for uniaxial deformation.<sup>4-6</sup> For elastic materials the magnitude of  $f_e$  can range from zero for a "rubbery" type response (purely entropy) to 100% for a "glassy" type response (purely internal energy). Conse-

quently, the thermal expansion coefficient should provide considerable information concerning the type of mechanical response for a specific temperature. Also, since  $\langle r_0^2 \rangle$  plays a significant role in the theories of intrinsic viscosity,<sup>8-11</sup> the temperature dependence of  $\langle r_0^2 \rangle$  should indicate the temperature dependency of the intrinsic viscosity. Therefore, the thermal expansion coefficient should provide considerable information concerning the thermal dependence of both viscosity and solid-state response and has received considerable attention in recent years.<sup>12-15</sup>

Although it has been shown<sup>7</sup> that the isomeric approach (which depends only on the energy difference  $\Delta E$  between the *trans* and *gauche* torsional energy states) yields accurate results for the value of  $\langle r_0^2 \rangle$ , one would suspect that the entire torsional potential energy plays an important role in the temperature dependence of  $\langle r_0^2 \rangle$ . This investigation is concerned with the qualitative influence of the torsional potential energy upon the thermal expansion coefficient of various type polymer chains. The potentials investigated ranged from simple unimodal to extremely complex shapes. To facilitate this study, a generalized potential energy equation was introduced so that the torsional potential energy could be readily varied. Assuming various forms of the torsional potential, the equations for the temperature derivative of various polymer chain models were numerically evaluated. The influence of both angular distribution of energy and the relative thermal energy ( $U_{\max}/kT$ ) was parametrically studied and the valence bond angle was varied for the case of "nearest-neighbor" correlation.

## MODELS OF POLYMER CHAINS

Since a polymer chain model is used to calculate the mean square end-to-end distance  $\langle r_0^2 \rangle$  of an actual chain molecule, the model will depend upon the chemical constitution and configuration of the molecule being represented. In general there are two main categories for the torsional potentials—symmetrical and unsymmetrical. These categories depend upon whether or not the molecules possess stereoisomeric centers.<sup>16,17</sup> Many polymers, e.g., polyethylene, polyisobutylene, polytetrafluoroethylene, have no stereoisomeric centers, and the torsional potentials of these polymers are characterized by the symmetry conditions

$$U(\phi_i) = U(-\phi_i) \quad (1)$$

and

$$U(\phi_i, \phi_{i+1}) = U(-\phi_i, -\phi_{i+1}) \quad (2)$$

with similar conditions for higher-order correlations.

In this study, three models were selected for polymers with no stereoisomeric centers. The uncorrelated equation of Debye, Taylor, Kuhn, and Benoit (the DTKB model) was used for chains of the type  $(-\text{CRR}-\text{CR}_1\text{R}_1-)_n$ . Volkenstein's uncorrelated equation<sup>7a</sup> was used for chains of

the type  $(-\text{CRR}-\text{CR}_1\text{R}_1-\text{O}-)_n$  where essentially two different torsional potentials,  $U_1(\phi_i)$  and  $U_2(\phi_i)$ , are associated with the monomer unit. The last model (the PSV model) of this group uses the Ptitsyn and Sharonov<sup>18</sup> and Volkenstein<sup>19</sup> equation for pair correlation of bulky side group interactions of neighboring backbone units. The three models associated with polymers with no stereoisomeric centers will be referred to as group A. The relevant equations of group A are given below.

### Group A (No Stereoisomeric Centers)

DTKB Model:

$$\langle r_0^2 \rangle = Nl^2 \frac{1 + \cos \theta}{1 - \cos \theta} \frac{(1 + \eta)}{(1 - \eta)} \quad (3)$$

$$\frac{\partial}{\partial T} [\ln \langle r_0^2 \rangle] = \frac{2}{(1 - \eta^2)} \frac{\partial \eta}{\partial T} \quad (4)$$

Volkenstein Model:

$$\langle r_0^2 \rangle = Nl^2 \frac{1 + \cos \theta}{1 - \cos \theta} \frac{1 - \eta_1 \eta_2}{(1 - \eta_1)(1 - \eta_2)} \quad (5)$$

$$\frac{\partial}{\partial T} [\ln \langle r_0^2 \rangle] = \frac{1}{(1 - \eta_1 \eta_2)(1 - \eta_2)(1 - \eta_1)} \left[ (1 - \eta_2)^2 \frac{\partial \eta_1}{\partial T} + (1 - \eta_1)^2 \frac{\partial \eta_2}{\partial T} \right] \quad (6)$$

PSV Model:

$$\langle r_0^2 \rangle = Nl^2 \frac{1 + \cos \theta}{1 - \cos \theta} \left[ \frac{1 - \eta^2 + \cos \theta (\eta^2 - \eta_c) + \epsilon_c}{(1 - \eta)^2} \right] \quad (7)$$

$$\frac{\partial}{\partial T} [\ln \langle r_0^2 \rangle] = \frac{1}{K} \left\{ \frac{2}{1 - \eta} [(1 - \eta) + (\eta - \eta_c) \cos \theta + \epsilon_c] \frac{\partial \eta}{\partial T} - \frac{\partial \eta_c}{\partial T} \cos \theta + \frac{\partial \epsilon_c}{\partial T} \right\} \quad (8)$$

where

$$K = [1 - \eta^2 + (\eta^2 - \eta_c) \cos \theta + \epsilon_c]$$

In these equations

$$\eta = \frac{\int_0^{2\pi} \Phi(\phi) \cos \phi d\phi}{\int_0^{2\pi} \Phi(\phi) d\phi} \quad (9)$$

$$\epsilon = \frac{\int_0^{2\pi} \Phi(\phi) \sin \phi d\phi}{\int_0^{2\pi} \Phi(\phi) d\phi} \quad (10)$$

$$\eta_c = \frac{\int_0^{2\pi} \int_0^{2\pi} \Phi(\phi_l, \phi_{l+1}) \cos \phi_l \cos \phi_{l+1} d\phi_l d\phi_{l+1}}{\int_0^{2\pi} \int_0^{2\pi} \Phi(\phi_l, \phi_{l+1}) d\phi_l d\phi_{l+1}} \quad (11)$$

$$\epsilon_c = \frac{\int_0^{2\pi} \int_0^{2\pi} \Phi(\phi_l, \phi_{l+1}) \sin \phi_l \sin \phi_{l+1} d\phi_l d\phi_{l+1}}{\int_0^{2\pi} \int_0^{2\pi} \Phi(\phi_l, \phi_{l+1}) d\phi_l d\phi_{l+1}} \quad (12)$$

$$\Phi = \exp [-\beta \mathbf{U}(\phi)] \quad (13)$$

$$\beta = 1/kT$$

and  $k$  is Boltzman's constant,  $T$  is absolute temperature,  $\phi$  is the angle of rotation about chain backbone bond and is defined as zero for the *trans* state configuration of three successive bonds,  $\phi_l$  is the angle of rotation about an  $l$  bond,  $\phi_{l+1}$  is the angle of rotation about an  $l + 1$  bond,  $\theta$  is the supplement of the valence bond angle, and  $\eta_1, \eta_2$  are cosine average functions for potentials  $\mathbf{U}_1$  and  $\mathbf{U}_2$ .

The majority of polymer chains possess stereoisomeric centers, and their torsional potentials are not restricted by the above symmetry conditions. Owing to the complexity of the equations for the stereoisomeric polymer chain models including the "nearest-neighbor" correlations, only models without correlations will be used in this study. The two equations for isotactic and syndiotactic chains were those derived simultaneously by Birshtein and Ptitsyn,<sup>20</sup> Lifson,<sup>21</sup> and Volkenstein.<sup>22</sup> The Birshtein and Ptitsyn<sup>7b</sup> interpolation equation was used for an ideal atactic chain (probability of head-to-head and head-to-tail sequences are equal). The three equations for polymers exhibiting tacticity will be referred to as group B.

### Group B (Stereoisomeric Centers)

Isotactic Model:

$$\langle r_0^2 \rangle = Nl^2 \frac{1 + \cos \theta}{1 - \cos \theta} \left[ \frac{1 - (\eta^2 + \epsilon^2)}{(1 - \eta)^2 + \epsilon^2} \right] \quad (14)$$

$$\frac{\partial}{\partial T} [\ln \langle r_0^2 \rangle] = \frac{2}{[(1 - \eta)^2 + \epsilon^2][1 - (\eta^2 + \epsilon^2)]} \left\{ [(1 - \eta)^2 - \epsilon^2] \frac{\partial \eta}{\partial T} - 2(1 - \eta)\epsilon \frac{\partial \epsilon}{\partial T} \right\} \quad (15)$$

Syndiotactic Model:

$$\langle r_0^2 \rangle = Nl^2 \frac{1 + \cos \theta}{1 - \cos \theta} \left\{ \frac{1 - (\eta^2 + \epsilon^2)^2}{(1 - \eta)^2 + [\eta - (\eta^2 + \epsilon^2)]^2} \right\} \quad (16)$$

$$\begin{aligned} \frac{\partial}{\partial T} [\ln \langle r_0^2 \rangle] &= \frac{2}{[1 - (\eta^2 + \epsilon^2)] \{ (1 - \eta)^2 + [\eta - (\eta^2 + \epsilon^2)]^2 \}} \\ &\times \left[ 2\epsilon \{ \eta [1 + (\eta^2 + \epsilon^2)^2] - 2(\eta^2 + \epsilon^2)(1 - \eta + \eta^2) \} \frac{\partial \epsilon}{\partial T} \right. \\ &+ \{ (1 + \eta^2)^2 (1 - \eta)^2 + \epsilon^2 [1 - \epsilon^2 (1 + \epsilon^2)] + \eta \epsilon^2 [\eta (2 - \epsilon^2 + \eta^2) \\ &\quad \left. - 2(2 - \epsilon^2)] \} \frac{\partial \eta}{\partial T} \right] \quad (17) \end{aligned}$$

Atactic Model:

$$\langle r_0^2 \rangle = Nl^2 \frac{1 + \cos \theta}{1 - \cos \theta} \left[ \frac{1 - (\eta^2 + \epsilon^2)}{(1 - \eta)^2} \right] \quad (18)$$

$$\begin{aligned} \frac{\partial}{\partial T} [\ln \langle r_0^2 \rangle] &= \frac{2}{[1 - (\eta^2 + \epsilon^2)](1 - \eta)} \\ &\times \left\{ (1 - \eta - \epsilon^2) \frac{\partial \eta}{\partial T} - \epsilon (1 - \eta) \frac{\partial \epsilon}{\partial T} \right\} \quad (19) \end{aligned}$$

The logarithm of  $\langle r_0^2 \rangle$  was used in the previous equations, since this quantity has been determined by various experimental techniques. The derivative term is independent of chain length (excluding extremely short chains which invalidate the statistics of the model equations) and the valence angle appears explicitly only in the case of a correlated potential. The only other chain parameters which appear are those which are implicit in the torsional potential. These torsional potentials depend upon the backbone bond lengths and saturation, valence angles and side group size and polarity. Therefore, the potentials must be assumed, or they must be numerically or experimentally determined to evaluate the above equations.

### TORSIONAL POTENTIALS

The form of the torsional potential for small molecules has been extensively studied in the past,<sup>7a</sup> and a variety of shapes can be obtained, depending upon the molecular symmetry. Kuhn,<sup>23</sup> Taylor,<sup>24</sup> and Pitzer and Gwinn<sup>25</sup> introduced a trimodal potential (symmetrical with respect to  $\phi = 180^\circ$ ) which has the same form as exhibited by ethylene. Any such trimodal potential used in this investigation (see Fig. 1) will be referred to as the PGKT (Pitzer, Gwinn, Kuhn and Taylor) potential.

While a Fourier cosine series has been used to represent more complicated potentials associated with small molecules, the series is difficult to manipulate for representing other potentials. Consequently a mathematical expression, which can be readily adapted to any chosen potential is desirable.



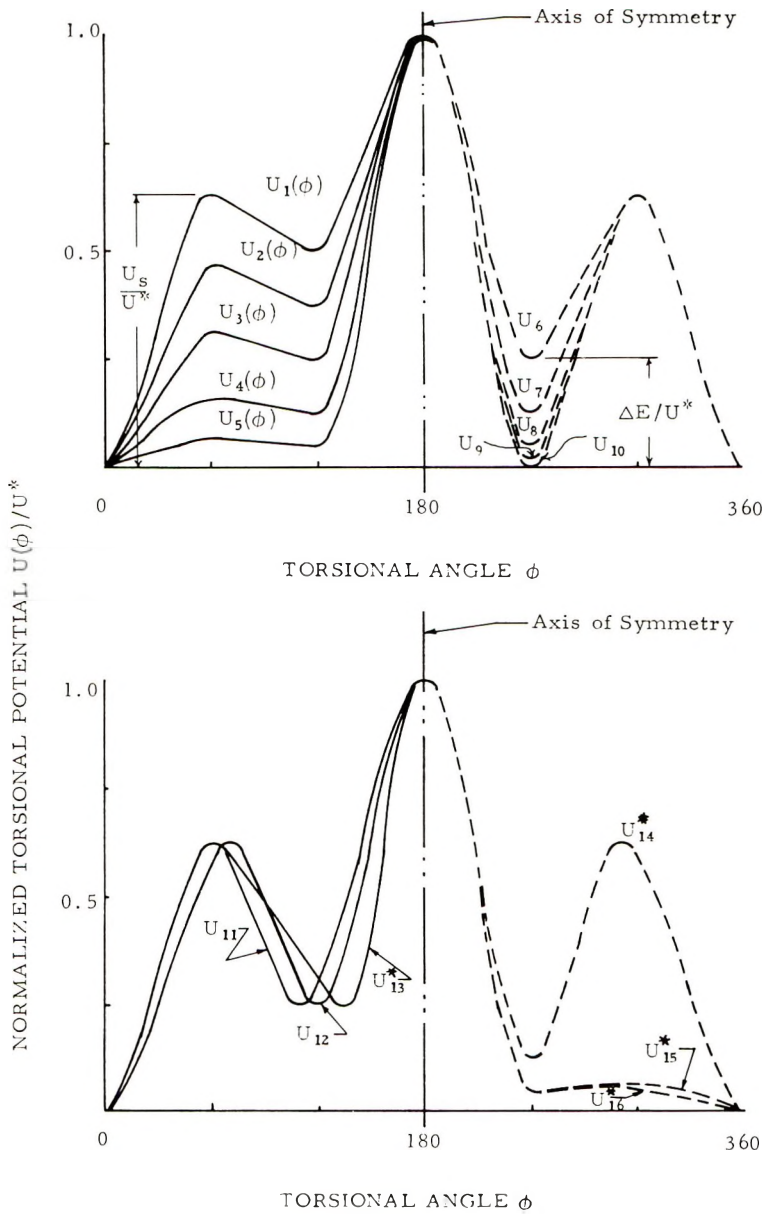


Fig. 1. Normalized symmetrical trimodal torsional potentials used in parametric study.

Such a generalized potential function can be written in terms of the Heaviside function  $H(\phi - \phi_i)$  as

$$U(\phi) = \sum_{i=1}^N [U_j - 1/2(U_j - \Delta E_k)(1 + \cos \alpha_i)][H(\phi - \phi_i) - H(\phi - \phi_{i+1})] \quad (20a)$$

or

$$U(\phi_i) = \sum_{i=1}^N [U_k - 1/2(U_k - \Delta E_j)(1 + \cos \alpha_i^*)] [H(\phi - \phi_i) - H(\phi - \phi_{i+1})] \quad (20b)$$

where

$$\begin{aligned} j &= 1/4[2i + 1 - (-1)^i] \\ k &= 1/4[2i + 3 + (-1)^i] \\ \alpha_i &= 180^\circ \left[ \frac{(\phi_{i+1} - \phi)}{(\phi_{i+1} - \phi_i)} + i \right] \end{aligned}$$

and  $\phi_i$  is the location of the  $i$ th extremum,  $\phi$  is the torsional angle,  $0 \leq \phi \leq 360^\circ$ ;  $U_j$  is the  $j$ th maximum,  $\Delta E_k$  is the  $k$ th minimum,  $N$  is twice the number of potential folds,

$$\begin{aligned} H(\phi - \phi_i) &= \begin{cases} 0 & \text{when } \phi < \phi_i \\ 1 & \text{when } \phi \geq \phi_i \end{cases} \\ \alpha_i^* &= 180^\circ \left[ \frac{(\phi_{i+1} - \phi)}{(\phi_{i+1} - \phi_i)} + (i - 1) \right] \end{aligned}$$

Equation (20a) refers to a potential which possesses a trough (energy minimum) at the  $\phi \equiv 0$  orientation while eq. (20b) refers to a potential possessing an energy barrier at the  $\phi = 0$  location. While  $U(\phi_i)$  cannot be directly used in determining values of  $U$ ,  $\Delta E$ , and  $\phi_i$  from experimental data, it is extremely useful for a parametric study since a potential curve can be immediately generated once the magnitudes and the locations of the extremi are chosen. However, eq. (20) is restricted to uncorrelated torsional motion, and a pair correlation potential must be introduced for usage in eqs. (11) and (12). Since energy is an extensive quantity, the pair correlation potential  $U(\phi_i, \phi_{i+1})$  may be expanded in terms of zero, first, and higher order correlation terms, i.e.

$$U(\phi_l, \phi_{l+1}) = U(\phi_l) + U(\phi_{l+1}) + \bar{U}(\phi_l) + \bar{U}(\phi_{l+1}) + \Theta(\phi) \quad (21)$$

where  $U(\phi_l)$  is the potential about the  $l$  bond when all other molecular chain bonds are in the extended position,  $U(\phi_{l+1})$  is the potential about the  $l + 1$  bond when all other molecular chain bonds are in the extended position,  $\bar{U}(\phi_l)$  is the first order correlation to  $U(\phi_{l+1})$ , i.e., an increase in  $U(\phi_{l+1})$  due to rotation about the  $l$ th bond,  $\bar{U}(\phi_{l+1})$  is the first-order correlation to  $U(\phi_l)$ , i.e., an increase in  $U(\phi_l)$  due to rotation about the  $(l + 1)$ th bond, and  $\Theta(\phi)$  represents higher-order correlations which involve coupling of the angles  $\phi_l$  and  $\phi_{l+1}$ .

This study will only include the first four terms of eq. (21), and since the equation will be used in group A equations, the potentials  $U(\phi_l)$  and  $U(\phi_{l+1})$  will be the same. Also, the first-order correlation potentials

should be the same and they will be assumed to be symmetrical. The individual potentials in eq. (21) will be generated by using eq. (20) and the following equation,

$$\bar{U}(\phi_i) = \bar{U}(\phi_{i+1}) = \sum_{j=1}^M [\bar{U}_j - 1/2(\bar{U}_j - \Delta\bar{E}_k)(1 + \cos \bar{\alpha}_i)] \times [H(\phi - \bar{\phi}_i) - H(\phi - \bar{\phi}_{i+1})] \quad (22)$$

where  $\{\bar{U}_j, \Delta\bar{E}_k\}$  is the set of chosen extrema,  $M$  is twice the number of potential folds, and  $\bar{\phi}_i$  is the location of the  $i$ th extremum.

Due to the above conditions of symmetry and the form of  $U(\phi_i, \phi_{i+1})$ ,  $\epsilon_c$  of eqs. (8) and (12) and the temperature derivative of  $\epsilon_c$  will be identically zero. Therefore, eqs. (8), and (11) can be rewritten as,

$$\frac{\partial}{\partial T} \ln \langle r_0^2 \rangle = \frac{1}{K} \left\{ \frac{2}{(1-\eta)} [(1-\eta) + (\eta - \eta_c) \cos \theta] \frac{\partial \eta}{\partial T} - \frac{\partial \eta_c}{\partial T} \cos \theta \right\} \quad (23)$$

and

$$\eta_c = \frac{\left[ \int_0^{2\pi} \exp \{-\beta U_c(\phi)\} \cos \phi d\phi \right]^2}{\left[ \int_0^{2\pi} \exp \{-\beta U_c(\phi)\} d\phi \right]^2} \quad (24)$$

where the correlation potential  $U_c$  is now defined as

$$U_c(\phi) = U(\phi) + \bar{U}(\phi)$$

By using the above relationships,  $\eta_c$  reduces to  $\eta^2$  where there are no correlations, i.e.,  $U(\phi)$  is zero. This is consistent with the fact that eq. (23) should reduce to eq. (4) when correlations are not considered.

The above integrals cannot be evaluated in closed form even for the simple unimodal potential. Therefore, a numerical scheme must be used to evaluate the integrals. This can be readily accomplished by means of Gaussian quadrature<sup>26</sup> and a computer program was developed to evaluate both the integrals and the algebraic equations [Eqs. (4), (6), (15), (17), (19) and (23)].

### Discussion of Results

The purpose of this study was to investigate what features, if any, of the torsional potential predominately affect the magnitude, sign, and temperature dependency of the mean free end-to-end distance  $\langle r_0^2 \rangle$  for different polymer chain models. The variable in this investigation was the relative energy ratio  $\beta U^*$ , where  $U^*$  is the maximum potential barrier and  $\beta$  is the reciprocal thermal energy, and the parameters were those associated with the torsional potentials. It should be noted that  $\beta$  is approximately 1.7 mole/kcal for ambient temperatures and the range of  $U^*$  is from about

3–30 kcal/mole. Consequently the range of the energy ratio was usually chosen to be 0 to 60 as being representative of all possible  $\beta U^*$  values. The thermal expansion coefficients were usually generated using potentials which possess an absolute minimum at the *trans* ( $\phi \equiv 0$ ) state. If the potential curve is shifted  $180^\circ$  along the  $\phi$  axis so that the absolute minimum occurs at the “*cis*” ( $\phi \equiv 180^\circ$ ) state, the predicted coefficients merely change their sign in relation to the corresponding *trans* state. Consequently, only the predicted behavior for the *trans* state will be shown for these potentials.

### Group A Chain Models

#### *Trimodal Behavior of the DTKB Model*

An important question associated with the PGKT-type potential (trimodal with the minimum occurring for either the *trans*  $\phi \equiv 0^\circ$  or *cis*  $\phi \equiv 180^\circ$  state) is which factors have the greatest influence on the predicted thermal expansion coefficients. Consequently, the trimodal torsional potentials shown in Figure 1 were arbitrarily chosen for use in the Group A models so that various factors could be studied. Since the potentials are symmetrical about  $\phi \equiv 180^\circ$ , for clarity some are sketched only in the range  $0$ – $180^\circ$  while others are shown only in the range  $180$ – $360^\circ$ .

**Influence of the Maximum Barrier Height  $U^*$ .** Since the torsional potential is normalized by the value of the maximum potential barrier  $U^*$ , the influence of its relative size was studied using potentials  $U_1(\phi)$  through  $U_5(\phi)$ . Prior to normalization, these five potentials were exactly the same in the region  $-120^\circ < \phi < 120^\circ$  and different in the region  $120^\circ \leq \phi \leq 240^\circ$  due to a larger maximum barrier  $U^*$ , i.e.,  $U_5^* = 10U_1^*$ ,  $U_4^* = 4U_1^*$ ,  $U_3^* = 2U_1^*$  and  $U_2^* = 4/3U_1^*$ . The predicted coefficients for the DTKB model are shown in Figure 2. These curves illustrate that as the relative size of  $U^*$  increases, the location of the minimum shifts to higher values of  $\beta U^*$  and its magnitude decreases somewhat. Consequently, it first appears that the actual value of  $U^*$  is extremely important. However, since the thermal expansion coefficient depends upon the value of  $\beta U^*$ , increasing the value of  $U^*$  shifts the relative energy ratio (for a fixed temperature) to higher values. Therefore, different relative energy ratios must be used to compare the predicted coefficient for the various  $U_1$  through  $U_5$  potentials. Consequently, arbitrarily picking a value, one finds that the five predicted coefficients (for a fixed value of  $\beta$ ) differ at most by about 15%. Therefore, it can be concluded that the predicted temperature coefficient does not depend critically upon the absolute size of the maximum potential barrier. This fact is extremely important because the potential functions generated from nuclear models<sup>27</sup> do not include the maximum barrier height and therefore the value assigned to it is not critical.

**Influence of the Secondary Barrier Height  $U_s$ .** Another factor associated with the PGKT-type potential which may be important is the secondary barrier height  $U_s$  (Fig. 1). Prior to normalization, the potentials

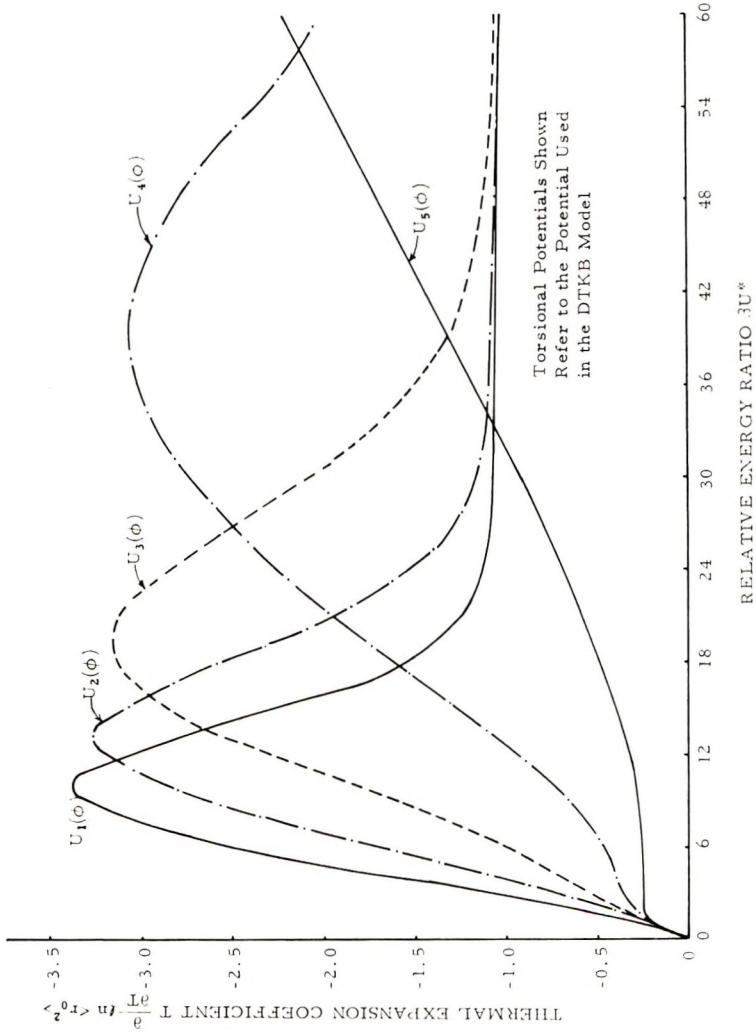


Fig. 2. Predicted DTKB thermal expansion coefficients for five different torsional potentials.

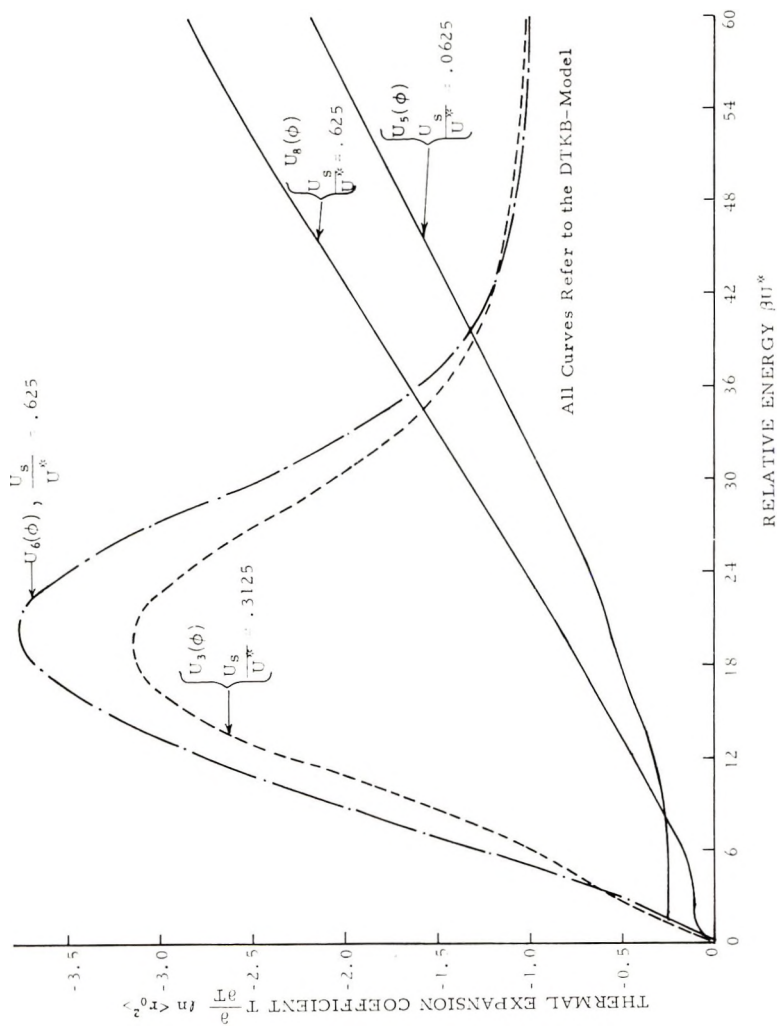


Fig. 3. Influence of secondary barrier height upon predicted thermal expansion coefficients  $\beta U^*$ .

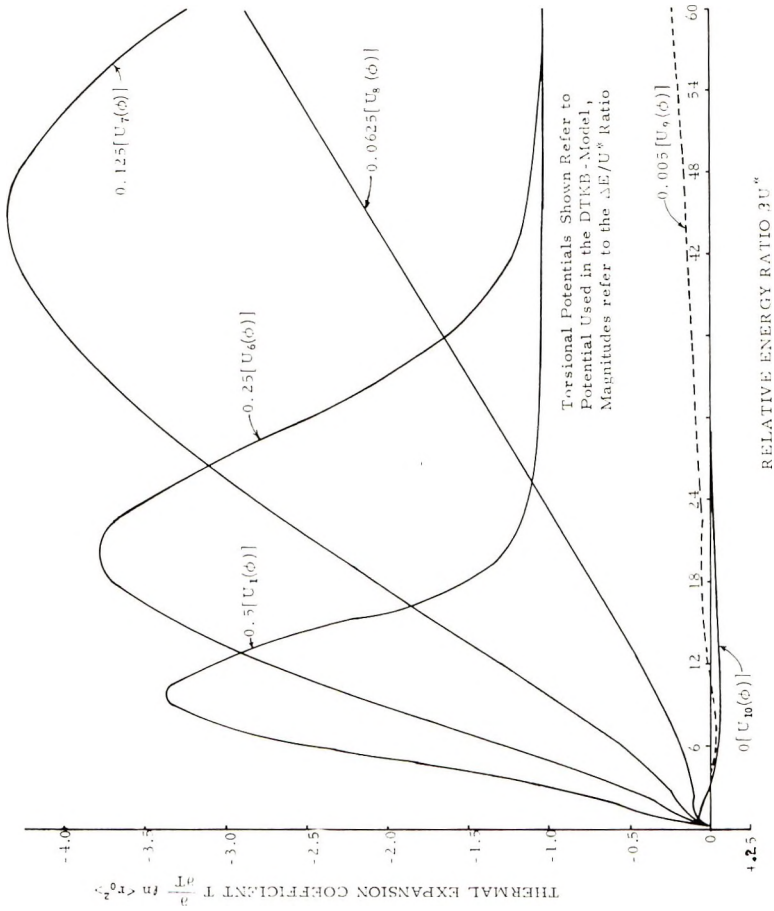


Fig. 4. Influence of the magnitude of the energy minimum upon predicted thermal expansion coefficients.

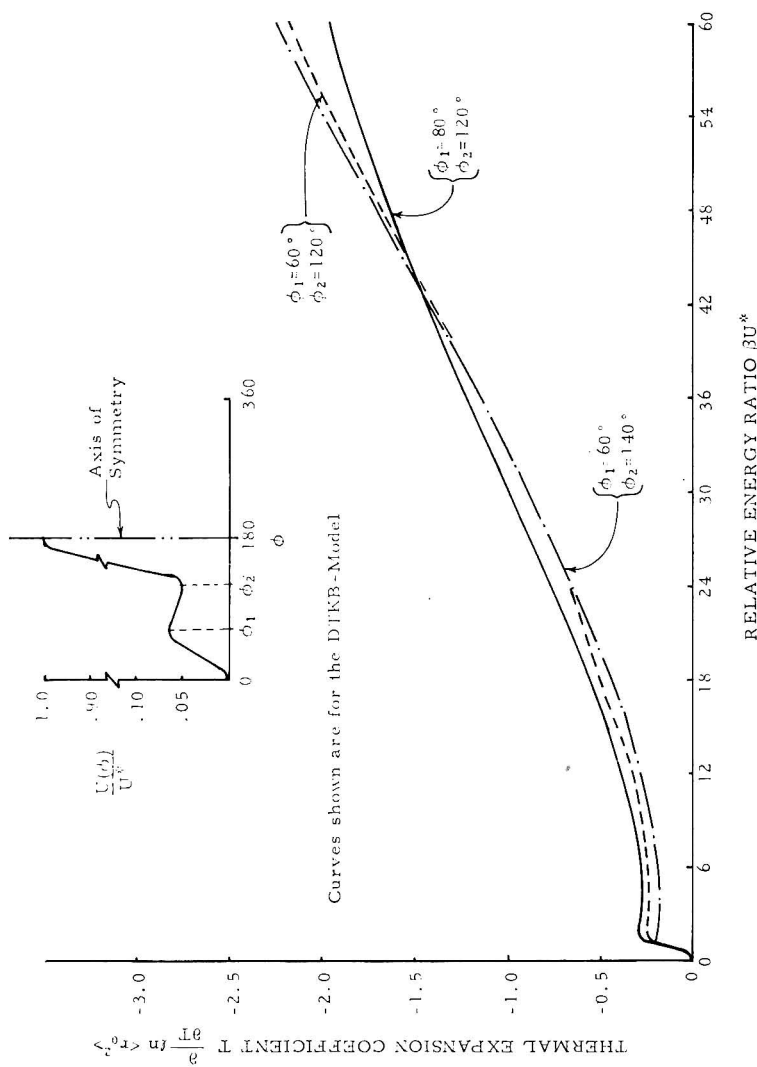


Fig. 5. Influence of trough and secondary barrier width upon predicted thermal expansion coefficients.



$U_6(\phi)$  and  $U_8(\phi)$  were the same as potentials  $U_3(\phi)$  and  $U_5(\phi)$ , respectively, except that the value of  $U_s$  was different. The predicted coefficients are shown in Figure 3, and significant differences are found to exist between the corresponding predicted results which is contrary to the isomeric assumption. Other than for small values of  $\beta U^*$  (less than about 5), the predicted coefficients for the potentials with the larger  $U_6$  are always greater than the coefficients associated with the smaller  $U_5$ . Therefore, it is readily apparent that the secondary potential barriers play an important role and should be known in order to predict *a priori* a thermal expansion coefficient.

**Influence in the Energy Difference  $\Delta E$  Between the Two Energy Minima.** The only factor of the PGKT-type potentials which appears in the isomeric approach is the energy difference denoted by  $\Delta E$ . Prior to normalization potentials  $U_1(\phi)$  and  $U_6(\phi)$  through  $U_{10}(\phi)$  were identical in the  $-60^\circ < \phi < 60^\circ$  region and differed in the  $60^\circ \leq \phi \leq 300^\circ$  region only due to the value of  $\Delta E$ , which was 0.5, 0.25, 0.125, 0.0625, 0.005, and 0.0, respectively (see Fig. 1). The corresponding thermal expansion coefficients are shown in Figure 4 and the influence of the  $\Delta E$  magnitude is immediately obvious. This influence is definitely greater than the influence of the secondary barrier height. Overall, it appears that decreasing the magnitude of  $\Delta E$  causes the minimum (maximum for corresponding *cis* state) thermal expansion coefficient to first increase and then decrease. It should be noted that the predicted coefficient for the  $U_{10}(\phi)$  potential is not zero (as normally presumed) and exhibits a transition at low  $\beta U^*$  values. Also, the predicted coefficient is positive over most of the  $\beta U^*$  range while the coefficients for larger  $\Delta E$  values are negative over most, or, all of the  $\beta U^*$  range. Another important aspect of the predicted coefficients for potentials  $U_9(\phi)$  and  $U_{10}(\phi)$  is that the predicted magnitudes are well within the range of experimental values. This implies that the actual energy difference  $\Delta E$  associated with polymeric torsional potentials of the PGKT type may be quite small.

**Influence of the Angular Location of the  $\Delta E$  Energy Minima and the Secondary Barrier Height  $U_s$ .** Two other factors which may be important in a *cis* or *trans* trimodal type of torsional potential is the angular location  $\phi_1$  of the secondary barrier height  $U_s$  and the angular location  $\phi_2$  of the energy minimum  $\Delta E$ . Figure 5 illustrates the influence of these angular locations upon the predicted thermal expansion coefficients. It appears that the location of the secondary barrier height  $U_s$  is more critical than the exact location of the energy minimum  $\Delta E$  (for the *cis* or *trans* type potential) but neither location is as important as the magnitudes of  $U_s$  and  $\Delta E$ .

#### *Trimodal Behavior of the PSV Model*

Now that the various torsional potential factors have been investigated for the DTKB model, the difference between the various models can be studied. Figures 6 through 10 illustrate the predicted DTKB, Volken-

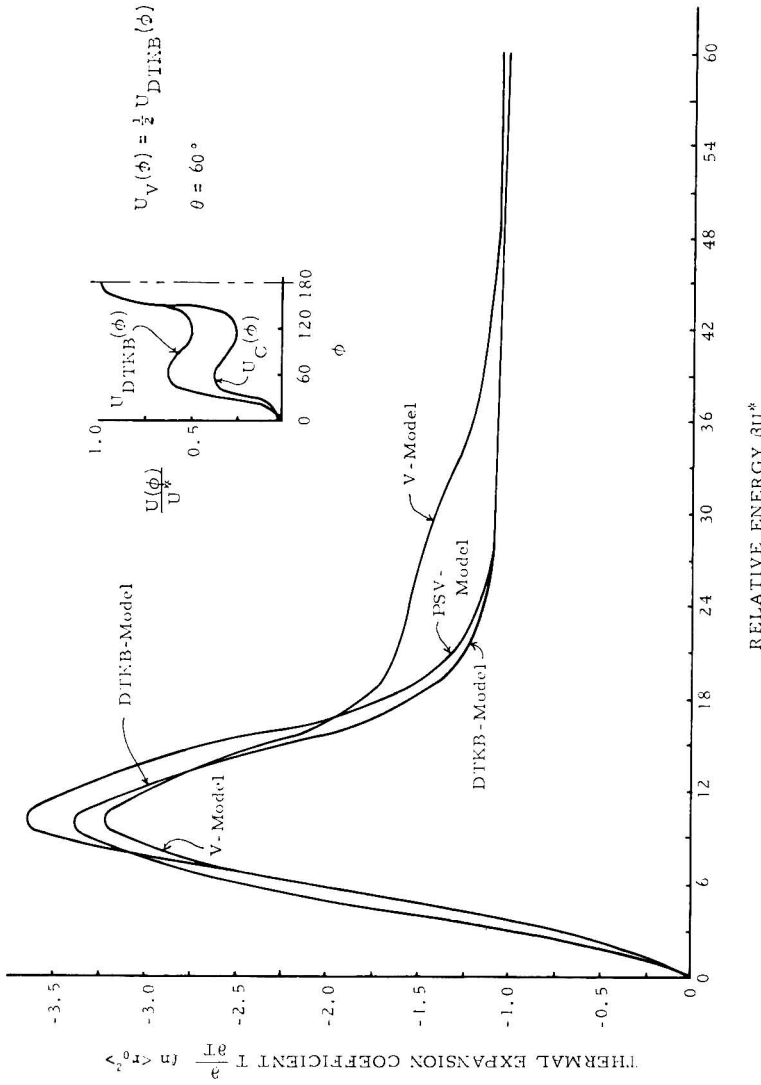


Fig. 6. Predicted thermal expansion coefficients for PSV, DTKB, and V models.

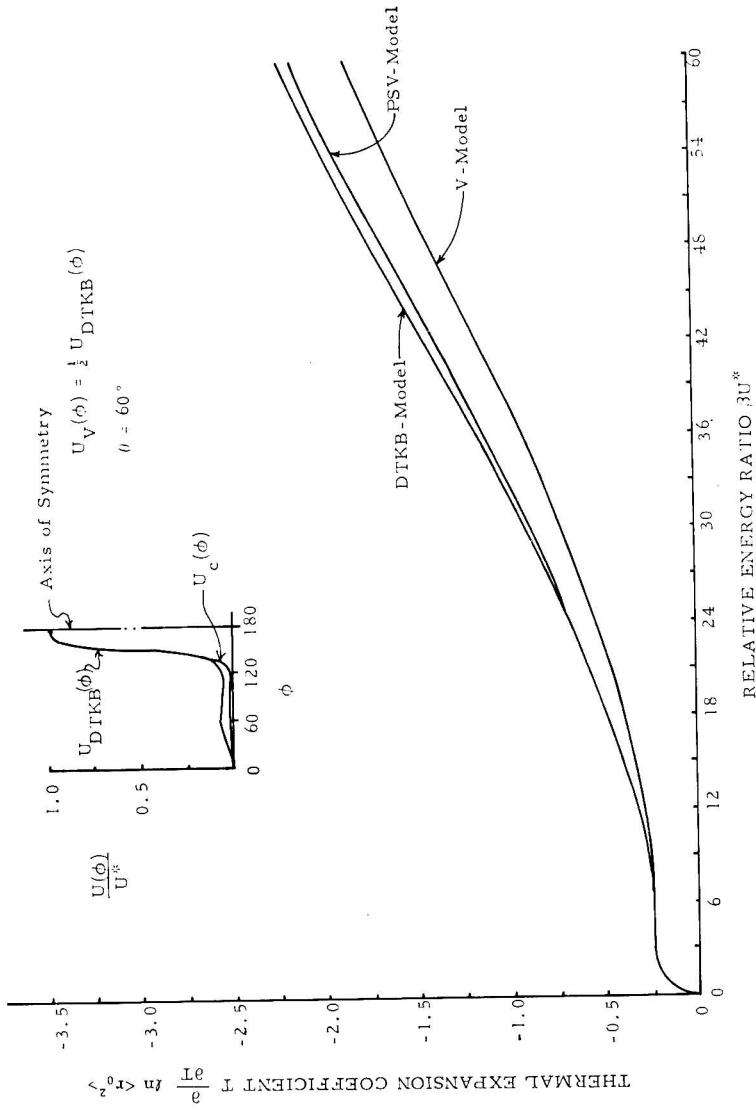


Fig. 7. Predicted thermal expansion coefficients for PSV, DTKB, and V models.

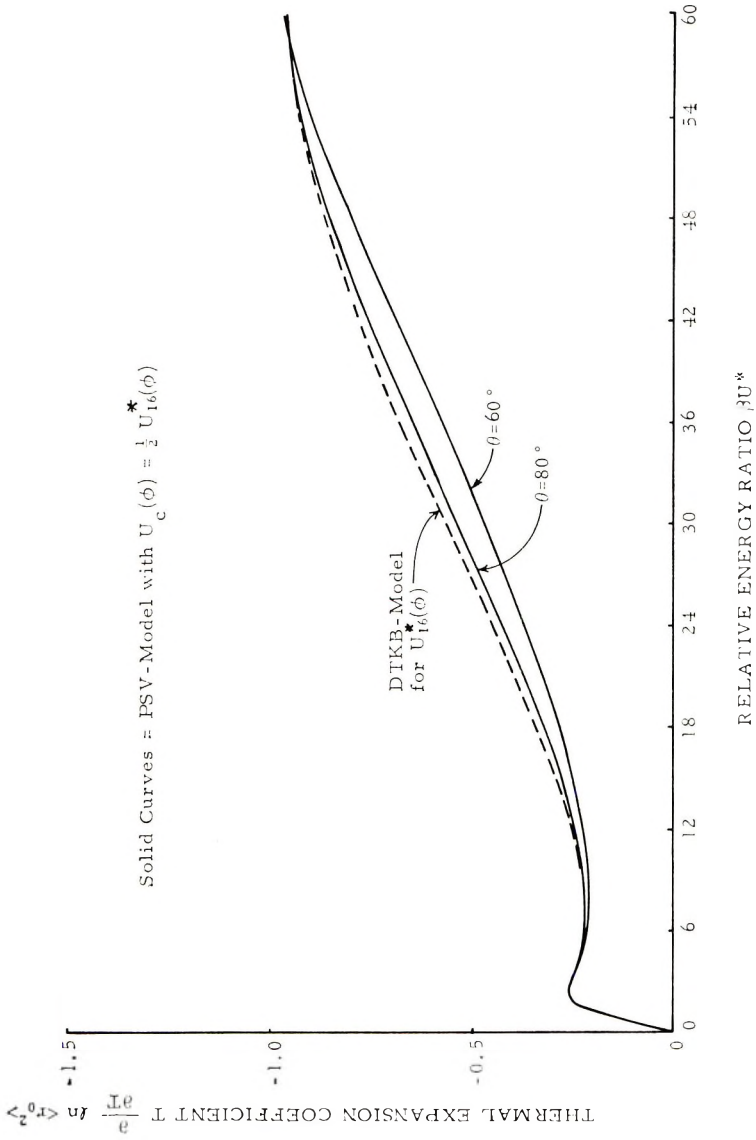


Fig. 8. Influence of valence angle ( $180-\theta^\circ$ ) upon predicted thermal expansion coefficients.

stein, and PSV coefficients for different type potentials and indicate that significant differences can exist between the various model predictions.

Since the PSV model involves the correlation of nearest neighbors, the values of  $U_c(\phi)$  will represent the assumed correlation potential and is shown in each of the corresponding figures. When  $U_c(\phi)$  is zero, the predicted coefficients for the PSV and DTKB models will be equal. Therefore as  $U_c(\phi)$  gets larger the difference between the DTKB and PSV models should increase. The angle  $\theta$  listed in Figures 6 through 8 and Figure 11 refers to the complement of the valence angle associated with the backbone bonds. The curves in Figures 6 and 7 illustrate that, depending upon the relative energy ratio, the PSV predictions can be higher or lower than the DTKB predictions. Also, the amount of difference between the predictions for the correlated and uncorrelated potentials depends upon the size and shape of both  $U_{\text{DTKB}}(\phi)$  and  $U_c(\phi)$ .

It appears that the first-order correlation (of the assumed type) will increase the predicted thermal expansion coefficient only if the uncorrelated potential possesses large secondary barriers and  $\Delta E$  values and the extrema are spaced at equal intervals of the torsional angle  $\phi$ . Probably few torsional potentials can be approximated by this shape and therefore the usual influence of correlations will be to decrease the size of the predicted thermal expansion coefficient. This decrease is predicted by the correlated isomeric models.<sup>7,28</sup>

One remaining factor which enters into the explicit equation of the correlated model [eq. (23)] is the complement  $\theta$  of the valence angle. The influence of changing this angle from  $60^\circ$  to  $80^\circ$  is illustrated in Figure 8. The  $80^\circ$  correlated coefficients were closer to the uncorrelated coefficients and there was only a slight difference (8%) between the  $60^\circ$  and  $80^\circ$  predictions. Consequently, it appears that although the bond angle plays an important role in the mean end-to-end vector distance and the shape and magnitude of the torsional potential, its explicit influence on  $T\partial \ln \langle r_0^2 \rangle / \partial T$  is small unless the correlation potential is large.

#### *Trimodal Behavior of the Volkenstein Model*

The Volkenstein model is somewhat analogous to a copolymer in which different torsional potentials are associated with each of the monomer units in the backbone chain. The value of  $U_v(\phi)$  can be considered to be the torsional potential of the second monomer while  $U_{\text{DTKB}}(\phi)$  refers to the first monomer of the backbone unit. When  $U_v(\phi)$  equal  $U_{\text{DTKB}}(\phi)$  the two backbone monomers are the same and the predicted values of the DTKB and V coefficients are the same. The predicted coefficients for different potentials are shown in Figures 9 and 10. The behavior of the V model is somewhat similar to that of the previously discussed PSV model, in that the coefficients may be smaller or larger than the corresponding DTKB coefficient depending upon the potentials and the relative energy ratio. However, the difference between the DTKB and V coefficients can be considerably larger than in the DTKB versus PSV case. In general,

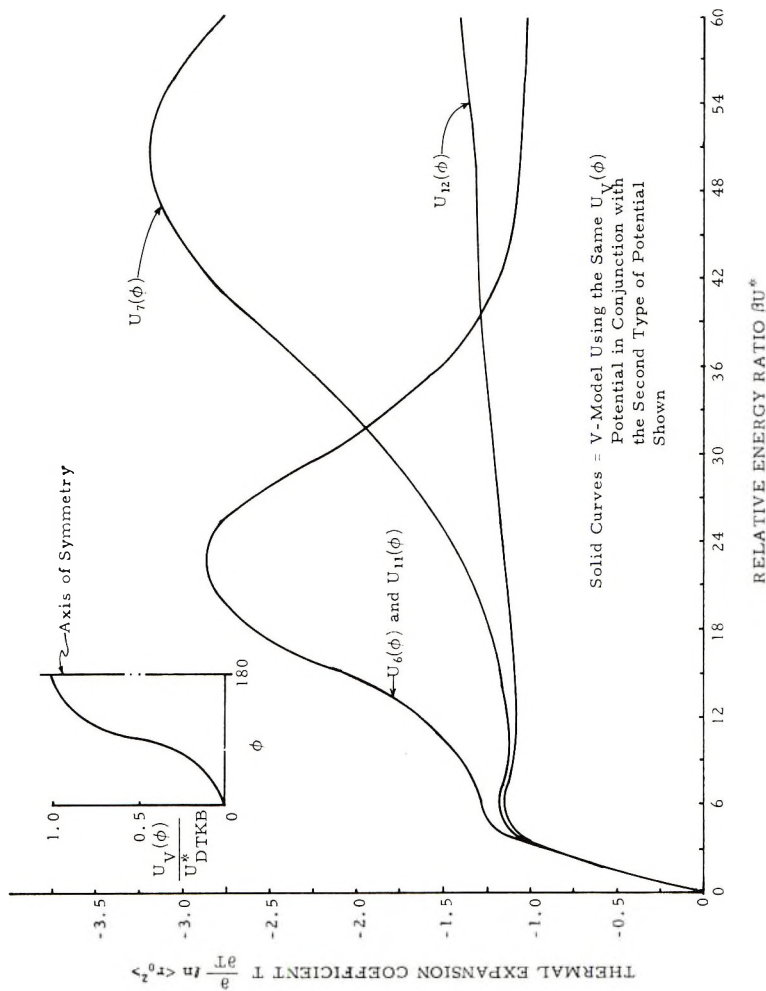


Fig. 9. Influence of a *trans* torsional potential associated with the V model upon the predicted thermal expansion coefficients.

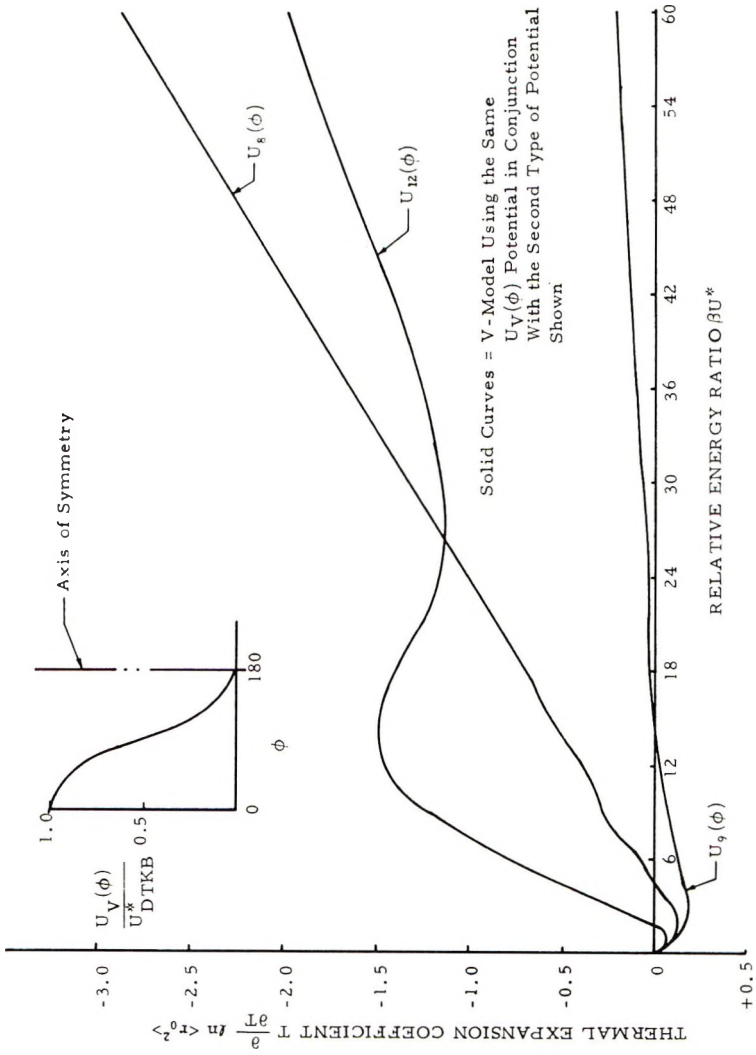
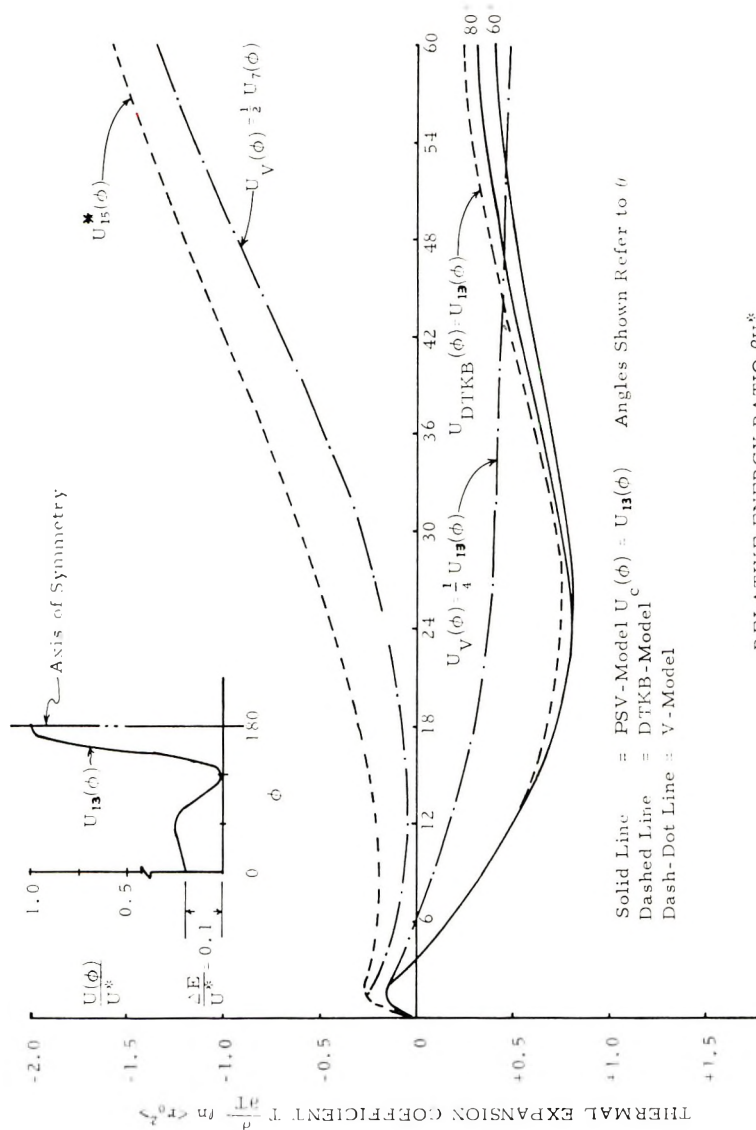


Fig. 10. Influence of a *cis* torsional potential associated with the V model upon the predicted thermal expansion coefficients.



RELATIVE ENERGY RATIO  $\beta U^*$

Fig. 11. Influence of the location of the absolute minimum upon the predicted thermal expansion coefficients of the PSV, DTKB, and V models.



it appears that the thermal expansion coefficients for a copolymer type chain will differ appreciably from the corresponding coefficient for a polymer with only one of the monomer units in the backbone.

#### *Multimodal Behavior of All Three Models*

Before discussing the predicted coefficients for polymer chains possessing tacticity, the influence of potentials other than the PGKT type will be briefly considered. Although enumerable variations could exist, the importance of overall potential shape is readily demonstrated by a few variations. The chosen torsional potentials and the predicted temperature coefficients are shown in Figures 11 and 12.

The torsional potential  $U_{13}(\phi)$  (Fig. 11) is the same as the  $U_5(\phi)$  type potential (see Fig. 1), except that the location of  $\Delta E$  and the absolute minimum have been interchanged. The absolute minimum now occurs at the *gauche* rather than the *trans* position. The most immediate difference between the behavior of the DTKB model for  $U_{13}(\phi)$  and for  $U_5(\phi)$  is the occurrence of a transition at small value of  $\beta U^*$ . The DTKB coefficient reaches a maximum (at  $\beta U^* = 24$ ) and then decreases in the same  $\beta U^*$  region where the magnitude of the DTKB coefficients for  $U_5(\phi)$  increases. Also, in the  $\beta U^*$  range of 6 to 30, the DTKB coefficients for  $U_{13}(\phi)$  are larger in magnitude than the DTKB coefficients of  $U_5(\phi)$ . For higher relative energies, the  $U_5(\phi)$  predicted coefficients become increasingly larger in magnitude than the corresponding  $U_{13}(\phi)$  coefficients. These differences illustrate the extreme importance of the angular location of the absolute minimum.

The predicted coefficients for the correlated PSV and the Volkenstein models are also shown in Figure 11. For the  $U_{13}(\phi)$  potential, the correlated coefficients are larger than the uncorrelated ones. This is contrary to what was generally observed previously when the torsional potentials yielded negative coefficients. It appears that correlations (of the assumed type) usually make a positive contribution to the predicted temperature coefficient. Therefore, if the uncorrelated coefficient is negative, correlations will make the predicted coefficient smaller while positive coefficients will become larger. It is interesting to note that all the predicted temperature coefficients involving a  $U_{DTKB}(\phi)$  of type  $U_{13}(\phi)$  are within the range of observed experimental magnitudes.

The influence of the actual torsional shape versus the unimodal approximation is shown in Figure 12. The unimodal can be considered as approximating either a PGKT, a 5 mode or a 7 mode type torsional potentials. Also, the PGKT type could be considered as approximating the 5 and 7 mode potentials. However, the predicted DTKB coefficients in Figure 23 indicate that neither approximation is very good. The unimodal potential approximates the 7 mode  $U_{13}(\phi)$  predictions best (50% max. difference) for low  $\beta U^*$  values (less than 18) and the difference increases as the value of  $\beta U^*$  increases. However, the PGKT and 5 mode  $U_A(\phi)$  type predictions approach the unimodal coefficients for the large relative energy ratios.

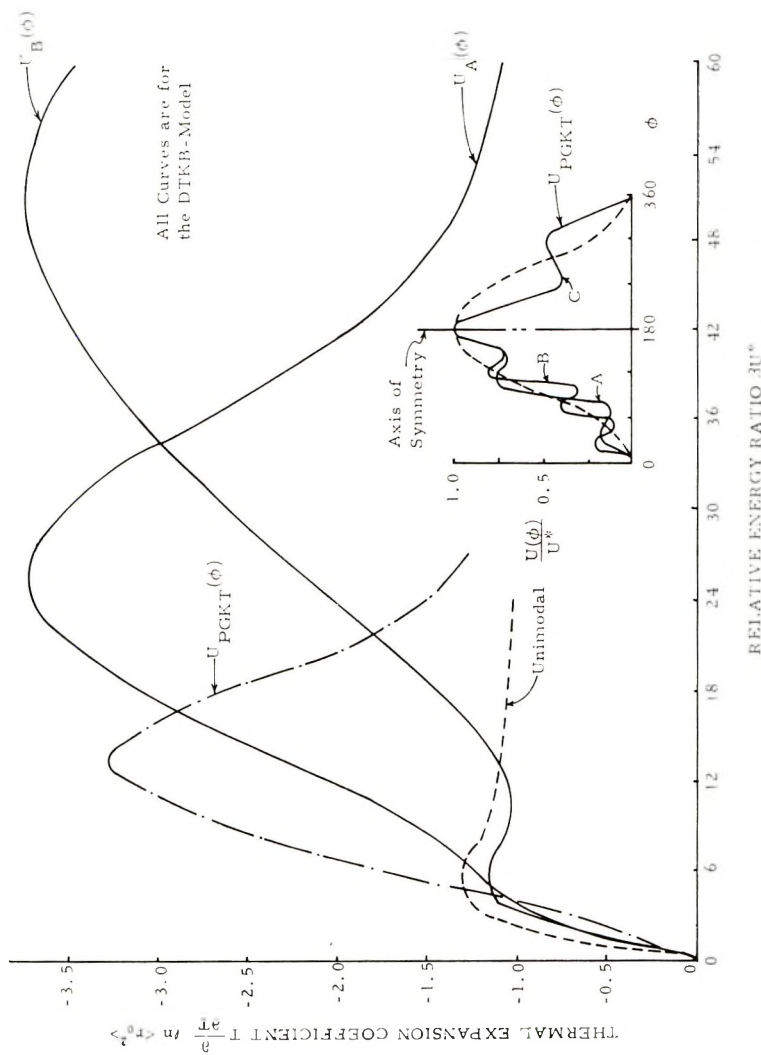


Fig. 12. Predicted thermal expansion coefficients for various multimodal torsional potentials.

For small relative energies the unimodal coefficients are larger than the multimodal predictions while over the remainder of the  $\beta U^*$  range the unimodal coefficients are less than the corresponding multimodal ones.

### Group B Type Chain Models

The predicted thermal expansion coefficients for the group B type chains are shown in Figures 13 through 20 for various types of assumed torsional potentials. The notation, I model, refers to the predictions of the isotactic model, S model refers to the syndiotactic model, while A model indicates the atactic model.

Obviously, the predicted coefficients for the isotactic, syndiotactic and atactic models will depend upon the same factors as previously discussed for the group A type polymer chain models. Therefore, only a few of these factors will be explicitly studied to see whether certain influences are greater or less in the case of chains exhibiting tacticity.

#### *Trimodal Behavior of All Three Models*

In Figure 13, a comparison is made between the predicted coefficients for the three models. The isotactic predictions are considerably lower than either the atactic or syndiotactic predictions. However, the maximum difference between the atactic and syndiotactic predictions is only 13%, the atactic coefficients being less than the syndiotactic. The magnitudes of these coefficients are within the range of experimental values and the predictions qualitatively agree with experimental data<sup>13,29,30</sup> where the syndiotactic coefficients were found to be larger than the atactic coefficients which, in turn, are larger than the isotactic coefficients.

**Influence of the Angular Location of the Energy Minima and the Secondary Barrier Heights  $U_{s1}$  and  $U_{s2}$ .** Other influences upon the predicted thermal expansion coefficients are the location of the energy minima  $\Delta E_1$  and  $\Delta E_2$ , the secondary barrier heights  $U_{s1}$  and  $U_{s2}$  and the absolute minimum (defined to be zero). Figures 14 through 17 illustrate the influence of these various locations. The  $U_{15}(\phi)$  torsional potential of Figure 14 is exactly the same as the  $U_{14}(\phi)$  potential of Figure 13, except that the angular locations of the absolute minimum and  $\Delta E_1$  have been interchanged, i.e.,  $U_{15}(\phi)$  refers to a *gauche* type potential. This *gauche* potential causes all the class B type models to predict a positive-negative transition of the thermal expansion coefficient. The isotactic model undergoes the transition at the smallest value of  $\beta U^*$  (about 8) while the transition associated with the syndiotactic model occurs at a relative energy ratio of about 12. These transitional  $\beta U^*$  values are considerably larger than the transitional values predicted for the class A type models with a similar *gauche* potential (see Fig. 11) and the coefficients for the  $U_{15}(\phi)$  do not exhibit a maximum. Also, contrary to what was generally predicted for other type potentials (see Figs. 13 and 16), the  $U_{15}(\phi)$  potential predicts positive isotactic coefficients which are considerably larger than both the atactic and syndiotactic values. Over most of the relative energy range

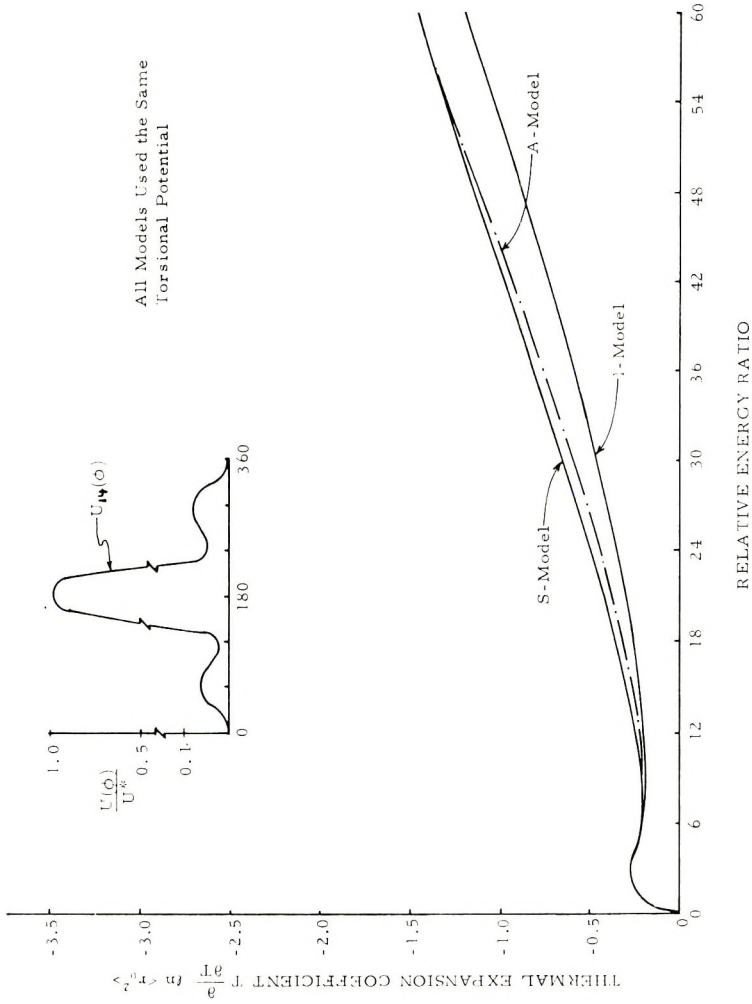


Fig. 13. Predicted thermal expansion coefficients for the A, S, and I models employing a *trans* trimodal torsional potential.

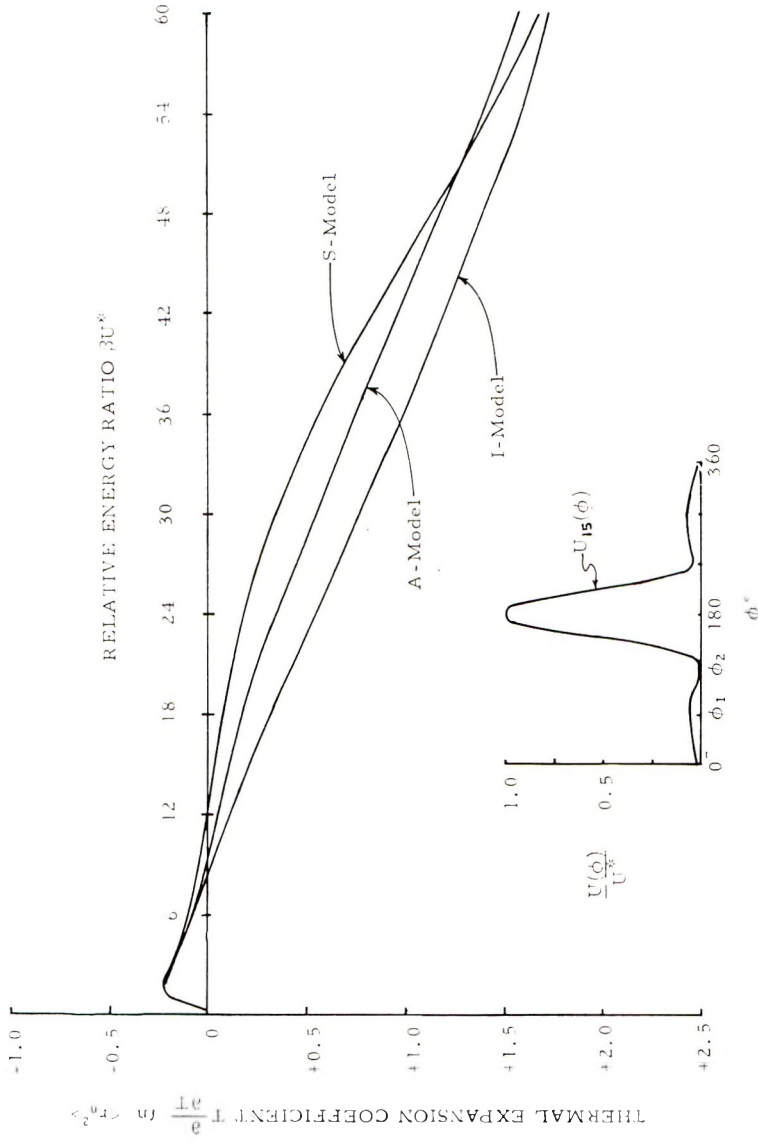


Fig. 14. Predicted thermal expansion coefficients for the A, S, and I models employing a *gauche* trimodal torsional potential.

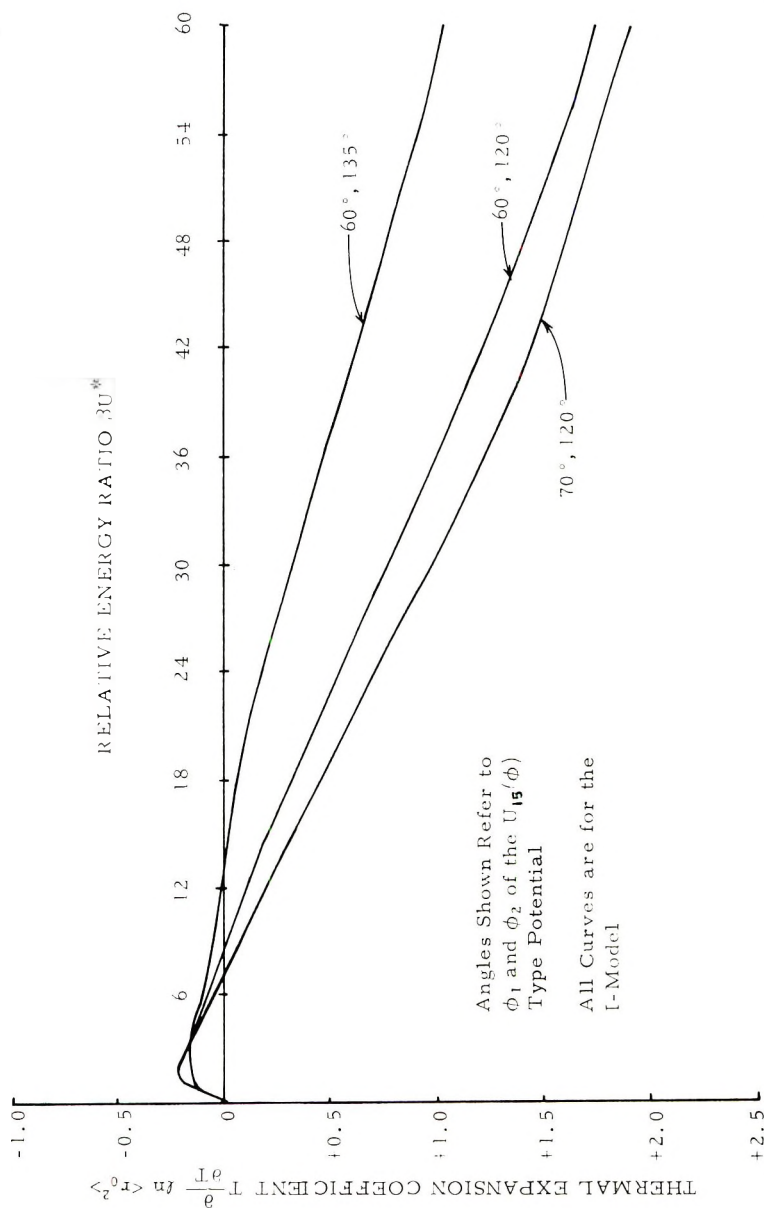


Fig. 15. Influence of the symmetrical location of the secondary barriers  $U_{1s}$  and  $U_{2s}$  and the energy minima  $\Delta E_1$  and  $\Delta E_2$  of a *gauche* type potential upon the predicted thermal expansion coefficients.

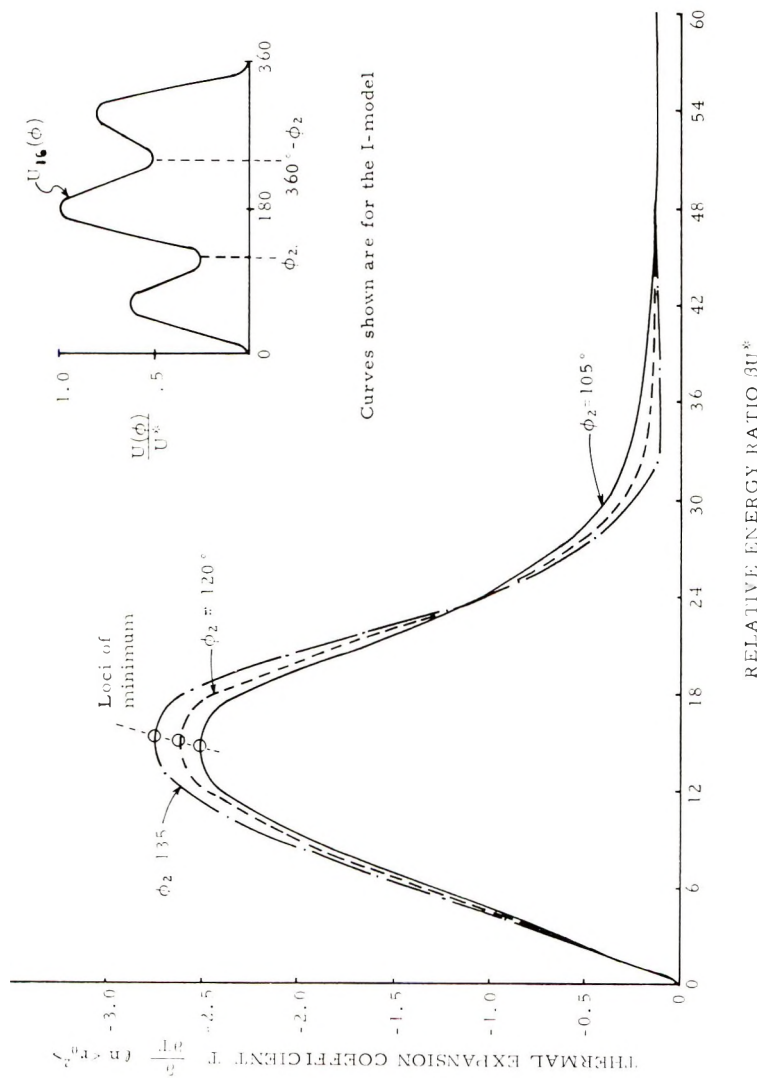
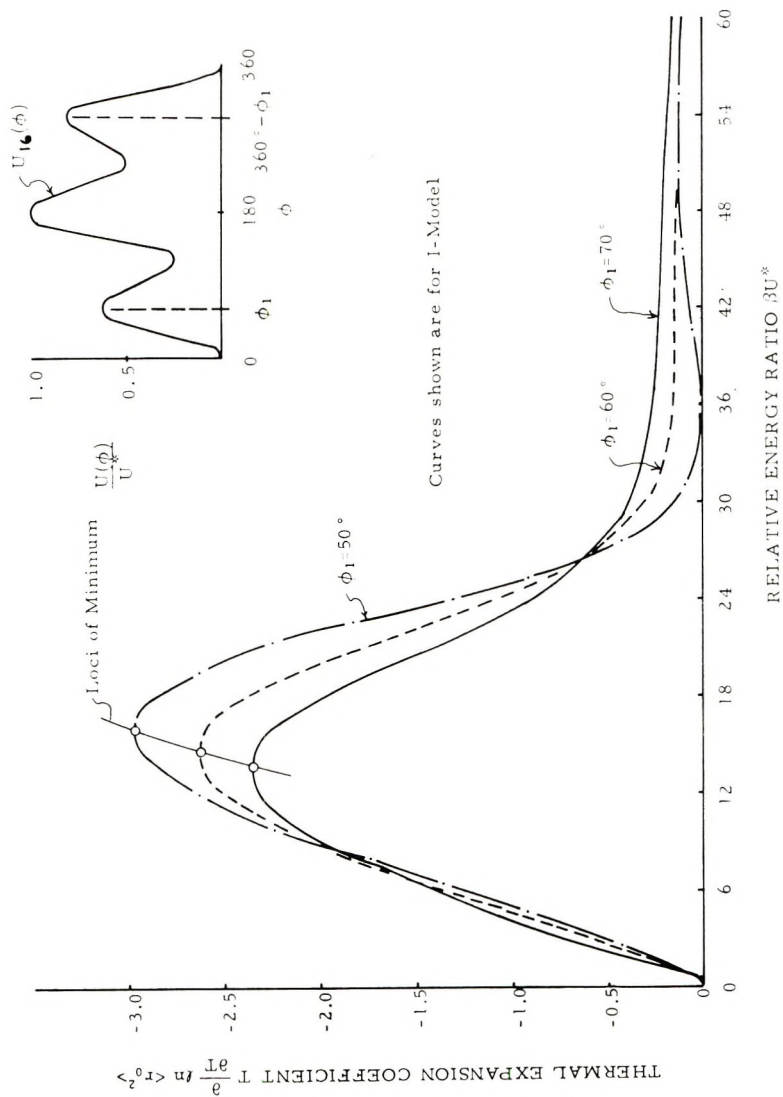


Fig. 16. Influence of the symmetrical location of the secondary barriers  $U_{1s}$  and  $U_{2s}$  of a *trans* type potential upon the predicted thermal expansion coefficients.



Curves shown are for I-Model

Fig. 17. Influence of the symmetrical location of the energy minima  $\Delta E_1$  and  $\Delta E_2$  upon the predicted thermal expansion coefficients.



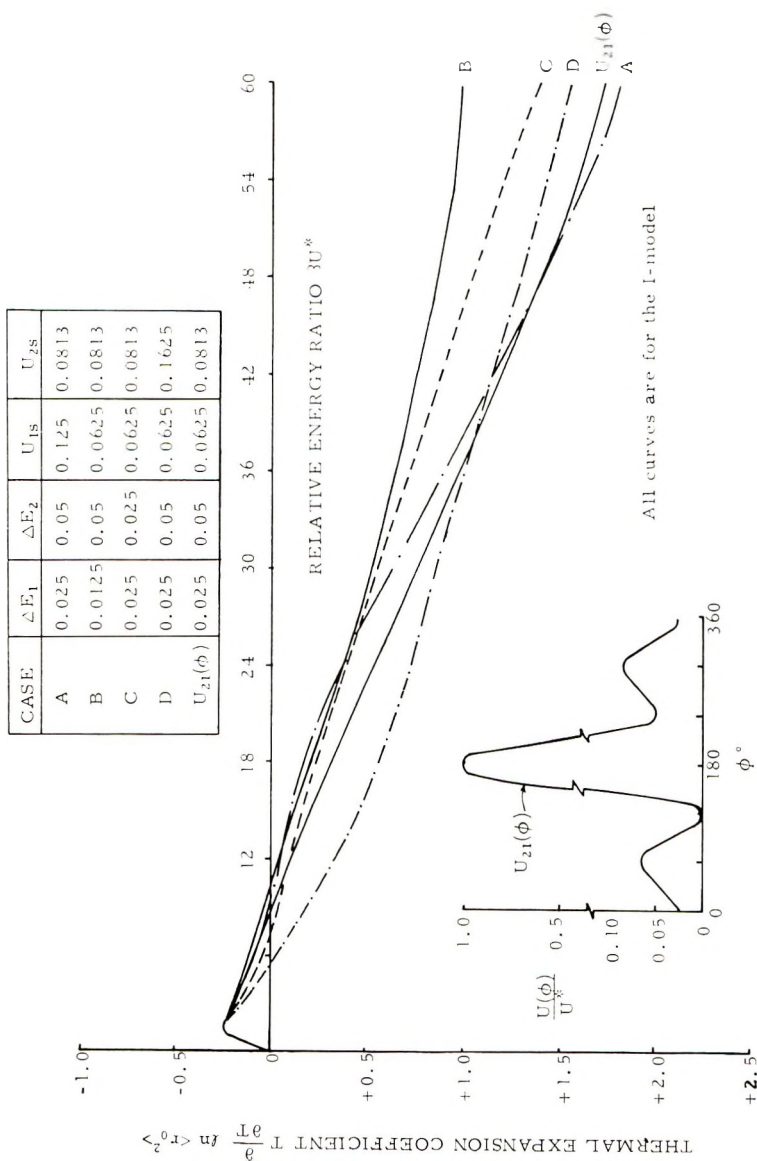


Fig. 18. Influence of the magnitudes of the potential barriers and minima of a *gauche* type potential upon the predicted thermal expansion coefficients.

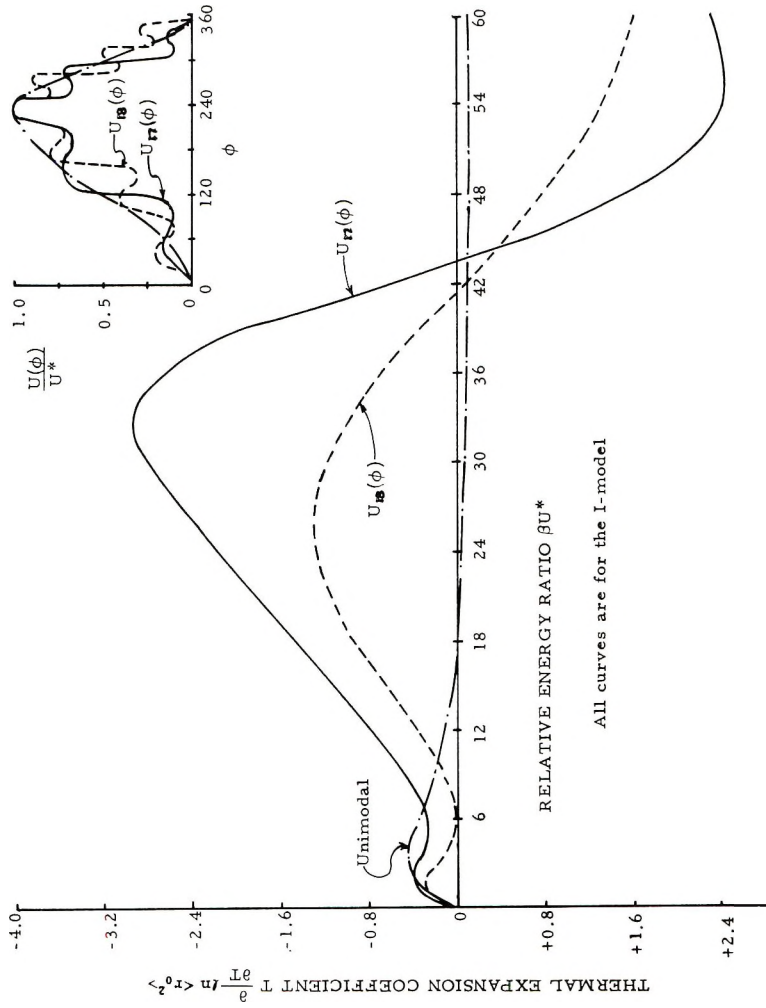


Fig. 19. Predicted thermal expansion coefficients for various multimodal torsional potentials.

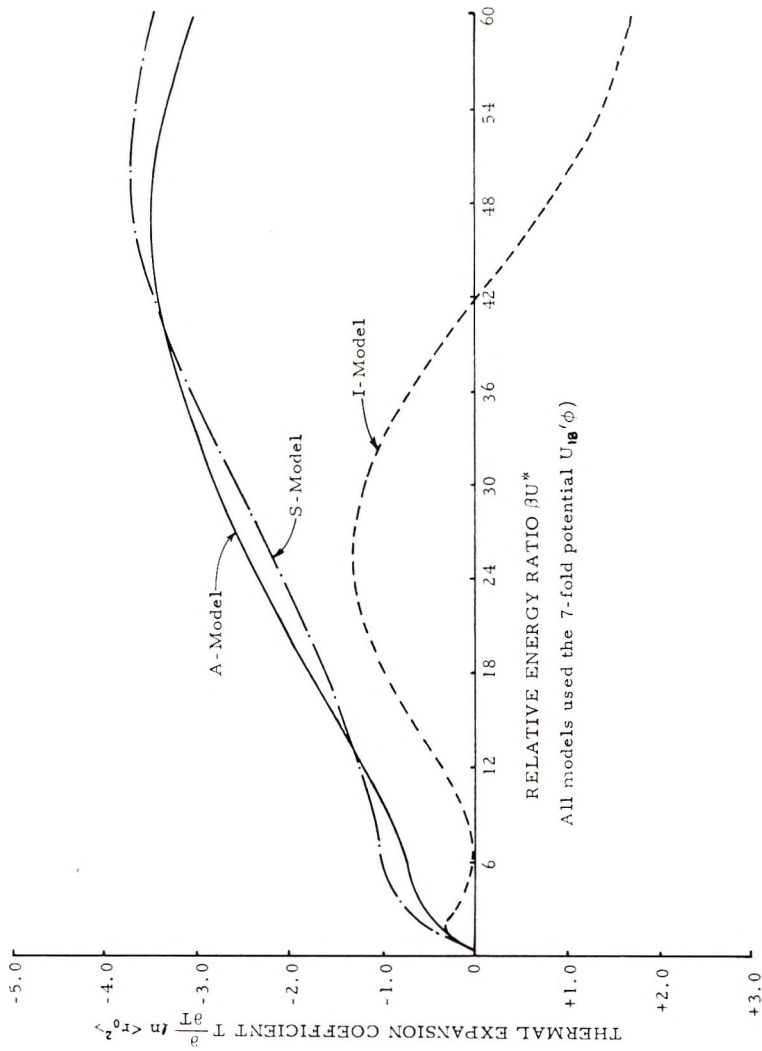


Fig. 20. Comparison of the predicted thermal expansion coefficients for the A, S, and I models employing a 7-fold torsional potential.

both the atactic and isotactic coefficients can be approximated as a linear function of  $\beta U^*$ . It should be noted that for a *cis* (minimum at  $180^\circ$ )  $U_{20}(\phi)$  type potential, the predicted isotactic, syndiotactic, and atactic coefficients are positive and the isotactic values are less than the corresponding syndiotactic and atactic values. Therefore, it appears that the isotactic coefficients will be larger than the syndiotactic ones only if the torsional potential possesses its absolute minimum in the *gauche* position. Furthermore, while the assumed atactic model's predicted coefficients have previously been quite close to the syndiotactic coefficients (see Figs. 13 and 16), the *gauche* potential yields A-model coefficients almost midway between the isotactic and syndiotactic coefficients. Hence, it appears that the relative sizes of the thermal expansion coefficient for an atactic, isotactic and syndiotactic chain critically depends upon the location of the absolute energy minimum.

The influence of small changes in the actual location  $\phi$  of absolute minimum is illustrated in Figure 15, where the I model coefficients are shown for a  $U_{15}(\phi)$  type potential with the value of  $\phi_2$  increased from  $120^\circ$  to  $135^\circ$ . The most noticeable change is the shift in the positive-negative transition to a larger value of  $\beta U^*$  (around 12). The corresponding transition for the syndiotactic model occurred at a  $\beta U^*$  value of about 18. It might be possible to experimentally observe such transitions if the maximum barrier height was around 10 kcal/mole (the corresponding  $\Delta E_1$  would be about 250 cal/mole). Increasing the angular location of the absolute energy minimum also caused a substantial reduction (a factor of two) in the magnitude of the positive coefficients as compared to the  $\phi_2 = 120^\circ$  predictions. Therefore, it appears that the angular location of the absolute energy minimum should be known fairly accurately ( $\pm$  a few degrees).

The angular location  $\phi_1$  of the secondary barrier heights  $U_{1s}$  and  $U_{2s}$  may also be important and Figure 15 indicates the influence of  $\phi_1$  of the  $U_{15}(\phi)$  type potential upon the predicted coefficients for the I model. Increasing the angular location of  $U_{1s}$  (and subsequently decreasing the angular location of  $U_{2s}$ ) by  $10^\circ$  caused the positive-negative transition to shift to smaller values of  $\beta U^*$  and increased the size of the positive coefficient.

In Figure 16 the isotactic model predictions are shown for a  $U_{16}(\phi)$  potential where the angular location  $\phi_1$  of the secondary barriers are varied. In the case where the angular location of  $U_{1s}$  is increased by  $10^\circ$  ( $U_{2s}$  is correspondingly decreased by  $10^\circ$ ) the predicted coefficients initially increase, then decrease, and finally increase over the last half (30–60) of the relative energy range (see solid curve in Fig. 16). Decreasing  $\phi_1$  by  $10^\circ$  (see dash-dot curve in Fig. 16) causes almost the converse change in the predicted thermal expansion coefficients.

The torsional potential in Figure 17 is exactly the same as the  $U_{16}(\phi)$  potential (Fig. 16), except that the angular location of the  $\Delta E_1(\phi_2)$  and  $\Delta E_2(360^\circ - \phi_2)$  minima were varied. Decreasing the location by  $15^\circ$  ( $\Delta E_1 = 105^\circ$ ) caused a considerable change in the predicted coefficients. Increasing the angular location by  $15^\circ$  ( $\phi_2 = 135^\circ$ ) caused the predicted

coefficients to change in the exact opposite as to what was observed for the  $\phi_2 = 105^\circ$  predictions. It appears that a symmetrical change (increased or decreased by the same amount) in the  $\Delta E_1$  and  $\Delta E_2$  locations causes a converse change in the predicted coefficients.

**Influence of the Magnitudes of the Energy Minima and the Secondary Barrier Heights  $U_{s1}$  and  $U_{s2}$ .** The predicted isotactic thermal expansion coefficients in Figure 18 illustrate the influence of the various extremum ( $\Delta E_1$ ,  $\Delta E_2$ ,  $U_{1s}$ , and  $U_{2s}$ ) associated with the  $U_{15}(\phi)$  type potential. Other than the change in one extremum magnitude, the potential shape remained the same for each of the cases shown in Figure 18. Case B corresponds to decreasing the  $\Delta E_1$  minimum by a factor of two and, over the entire range of positive coefficients, this produced an isotactic coefficient which was considerably less than the corresponding  $U_{21}(\phi)$  coefficient. The secondary minimum  $\Delta E_2$  was decreased by a factor of two in case C and this again reduced the magnitude of the predicted temperature coefficient over most of the  $\beta U^*$  range. However, the reduction in this case was not as great as in case B. Increasing the  $U_{1s}$  potential barrier by a factor of two (case A) decreased the coefficient over part of the  $\beta U^*$  range and slightly increased the values for the extremely high relative energies. Lastly, the  $U_{1s}$  barrier was increased by a factor of two (case D) and this caused a significant increase in the predicted coefficients for  $\beta U^*$  values between 9 and 27. At high relative energies, the predicted coefficients for case D were slightly less than the corresponding values for the  $U_{21}(\phi)$  potential. Consequently, it appears that for a  $U_{21}(\phi)$  type (*gauche*) potential the secondary barrier heights are critical for relative energies in the lower half of the range while the energy minima are more important in the upper relative energy range.

#### *Multimodal Behavior of All Three Models*

Another important factor is the number of extrema that actually exist in the torsional potential. Figure 19 illustrates the isotactic thermal expansion coefficients for unimodal, 5 mode [ $U_{17}(\phi)$ ] and 7 mode [ $U_{18}(\phi)$ ] type potentials. Although the unimodal potential could be considered as approximating the other potentials, the predicted coefficients are extremely different. The unimodal potential predicts a positive-negative transition at 18 while the higher mode potentials predict a transition around 42. The isotactic coefficients predicted for  $U_{17}(\phi)$  and  $U_{18}(\phi)$  can be less than or greater than the corresponding unimodal predictions depending upon the relative energy. Even the predicted coefficients between  $U_{17}(\phi)$  and  $U_{18}(\phi)$  are considerably different over most of the relative energy range.

The predicted coefficients for the isotactic, syndiotactic and atactic models are shown in Figure 20 for the sevenfold  $U_{18}(\phi)$  type potential. It should be noted that the higher mode potentials were found to predict atactic and syndiotactic coefficients which are always larger than the coefficients for a corresponding unimodal potential. The syndiotactic coefficients appear to be either greater than or less than the corresponding atactic coefficient depending upon the value of the relative energy ratio.

## CONCLUSIONS AND IMPLICATIONS OF THE PARAMETRIC STUDY

Contrary to the assumptions of the isomeric theory, numerous factors associated with the torsional potential, other than the energy minimum  $\Delta E_{\min}$  have a significant influence on the predicted thermal expansion coefficients. The magnitudes and locations of the secondary barrier heights, angular locations of the  $\Delta E$  energy minima and the maximum barrier  $U^*$ , spacing of the extrema intervals, and the number of extrema were all found to play a significant role in the predicted coefficient. Furthermore, some of these factors may be more significant than the magnitude of  $\Delta E_{\min}$ .

The magnitude of  $U^*$  was found to be of secondary importance for the group A-type chains, while  $U^*$  needs to be more closely estimated for chains exhibiting tacticity. However, this barrier height need only be known to within a factor of about two and once the general magnitude is known, the torsional potential can be normalized and the  $\beta U^*$  value determined for any specific temperature. Also, it was found that increasing the magnitude of the secondary barrier heights causes a substantial increase in the magnitude of the thermal expansion coefficients. For the assumed type of secondary correlations, the valence angle (although extremely important in generating the torsional potential and in calculating  $\langle r_0^2 \rangle$ ) had less influence than most of the other factors upon the predicted temperature coefficient. The effect of the second-order type correlations was usually to decrease the size of the predicted temperature coefficient. However, this depends upon both the relative energy ratio and the type of torsional potential. For the *gauche* type potentials, the effect of correlations was to increase the size of the predicted coefficient over almost the entire  $\beta U^*$  range. It was found that decreasing the valence angle from  $120^\circ$  to  $100^\circ$  caused the correlated coefficients to become closer to the uncorrelated ones.

The predicted coefficients also depend critically upon the relative energy ratio  $\beta U^*$  associated with the temperature and maximum barrier height. As a function of temperature, the predicted thermal expansion coefficient may be either almost constant, highly nonlinear, or, even undergo a transition from negative to positive (or vice versa) values, depending upon the model and torsional potential. When two different torsional potentials are associated with the chain backbone, e.g., a copolymer, large differences can exist in the coefficient behavior as compared to a monomeric type chain. It appears that introducing a *trans* or *cis* unsaturated backbone in one of the monomers within the copolymer may cause the thermal expansion coefficient to undergo a positive-negative transition. In the case of a *gauche* type potential (absolute minimum energy occurs near  $120^\circ$ ), small changes in the magnitude of the secondary barrier was more important than small changes in the  $\Delta E$  value for small (less than 30)  $\beta U^*$  value. However, the converse was true for the large (greater than 30) relative energy ratios.

The magnitude of the predicted thermal expansion coefficients were found to be within the range of experimental values (which range from zero to  $\pm 1.5$  depending upon the type of polymer and the experimental technique) only when the maximum barrier height was at least 10 times larger than the energy minimum  $\Delta E_{\min}$ . The  $\Delta E_{\min}$  magnitude appears to be the most predominant factor for chains which do not possess stereoisomeric centers, whose torsional potential was 3-fold and possessed an absolute energy minimum in either the "cis" or "trans" state. In this case it was found that decreasing the  $\Delta E_{\min}$  magnitude decreases the magnitude of the thermal expansion coefficients. However, even when the  $\Delta E_{\min}$  energy was zero, the predicted coefficients were not zero unless the torsional potential also exhibited equal potential barriers and equal spacing of the extremum.

Other significant factors of the three-fold PGKT type torsional potentials were the width of the trough associated with the absolute energy minimum and the width of the secondary barrier  $U_s$ . Widening the trough (increasing the angular location of the secondary barriers) was found to cause a progressive increase, decrease, and then increase in the value of the thermal expansion coefficient as a function of  $\beta U^*$ . Also, widening the trough significantly increased the magnitude of the largest value of the predicted coefficient and shifted the associated relative energy to lower values of  $\beta U^*$  (lower temperatures). Narrowing the width of the secondary barriers (decreasing the angular location of the  $\Delta E_{\min}$  energy) were found to have the same effect as widening the trough. In general, the predicted coefficients indicate that the width of the trough is more important than the width of the secondary barrier.

One of the most important factors was the location of the absolute energy minimum. When this minimum occurred near a *gauche* value of  $120^\circ$ , the predicted thermal expansion coefficients for all the investigated models were found to be initially negative and then undergo a transition to positive values as the relative energy was increased. The magnitude of the relative energy at which the transition took place depended upon the model and the torsional potential. In general for chains possessing tacticity (class B type) the predicted transition occurred at much higher values of  $\beta U^*$  (lower temperatures) than did the class A type polymer chains.

For *cis* or *trans* type torsional potentials, the isotactic chain was predicted to possess the smallest thermal expansion coefficient over the entire range (1 to 60) of relative energy ratios. However, when the absolute energy minimum corresponded to the *gauche* ( $\phi \approx 120^\circ$ ) position, the predicted isotactic coefficients were considerably larger than the corresponding coefficients for either the syndiotactic or atactic type chain.

The isotactic chain was found to predict positive-negative transitions which appear to depend mainly on the symmetry of the associated torsional potential. The predicted atactic transitions always occur at higher relative energy values than the corresponding isotactic transitions. The syndiotactic chains were found to predict no transitions except for the *gauche* type

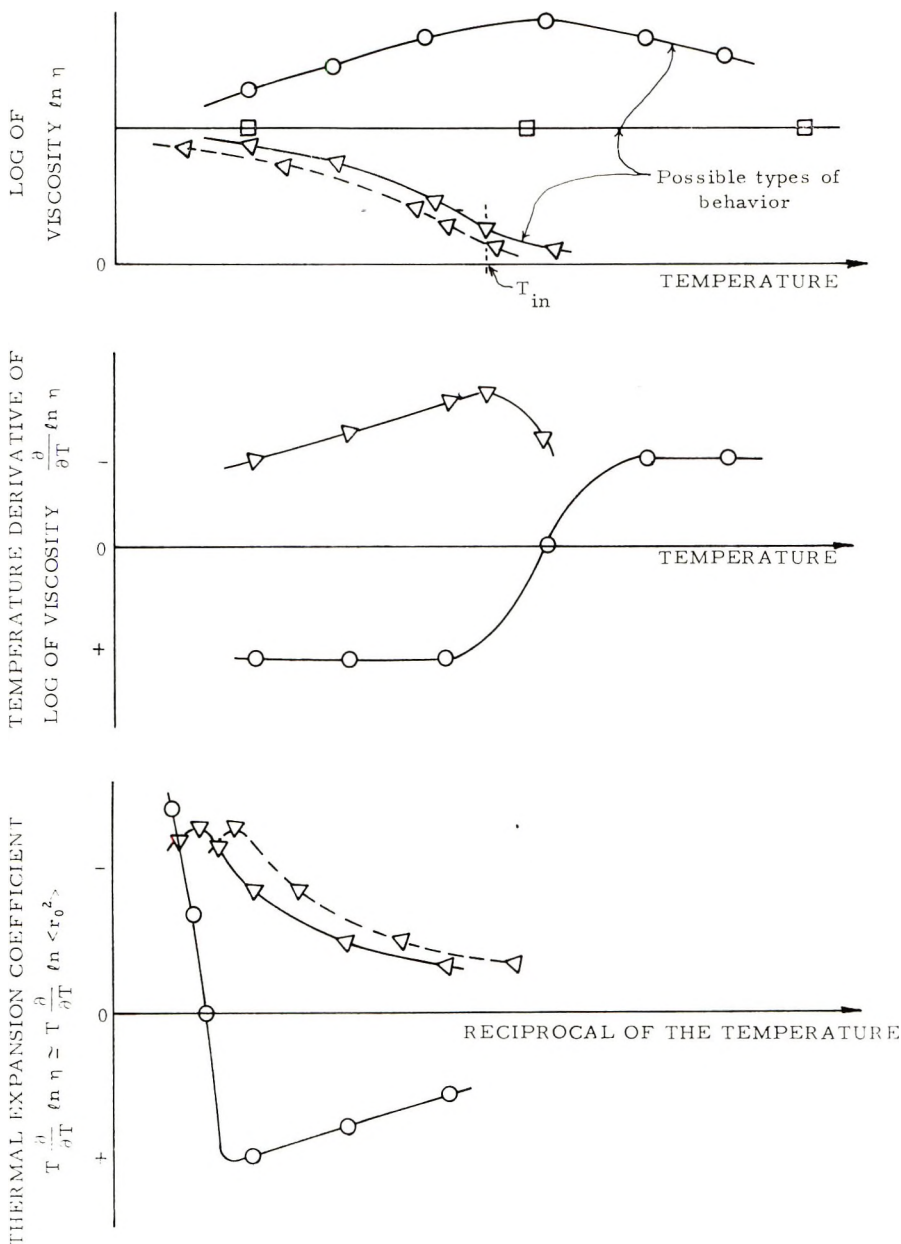


Fig. 21. Implications of the thermal expansion coefficient's behavior concerning the corresponding viscosity behavior.

potentials. The magnitudes of the atactic coefficients were usually close to the syndiotactic coefficients but for certain torsional potentials were closer to the isotactic values.

The actual number of modes which a torsional potential possessed was found to have a large influence upon the predicted coefficients of both the



class A and class B type polymer chains. In general the unimodal or trimodal approximations yielded predicted coefficients which were considerably different from the corresponding 5- or 7-mode potentials. The actual difference may be greater, or less, than the higher mode predictions depending upon the type of potential, the chain model, and the relative energy ratio.

Since the torsional potentials were merely assumed and the corresponding chain models were fairly simple, the predicted coefficients and their behavior can be considered only as qualitative. However, the above mentioned qualitative trends have two important physical implications. These implications are concerned with polymeric fluid viscosity and the thermoelastic response of a polymeric solid.

As is well known from both a theoretical and an empirical viewpoint, the viscosity of a polymeric fluid depends directly upon the size of the polymer molecule ( $\langle r_0^2 \rangle$ ) raised to some power  $\alpha$  greater than one. If one assumes that the coefficient of proportionality  $\Phi$  and power  $\alpha$  of the viscosity equation are independent of temperature, then the temperature derivative of the logarithm of the viscosity equation yields the product of  $\partial \ln \langle r_0^2 \rangle / \partial T$  and some constant. Therefore,  $\partial \ln \langle r_0^2 \rangle / \partial T$  can be considered to be an indication of the temperature dependency of the viscosity (Fig. 21). With the appropriate modifications and holding  $U^*/k$  constant, one sees that the negative-positive transition that was found for certain chains with a *trans* or *gauche* type torsional potential corresponds to a maxima in the viscosity-temperature behavior (see circular points in Fig. 21). The corresponding positive-negative transition associated with a *cis* type torsional potential corresponds to a minimum in the viscosity-temperature behavior. It should be noted that maxima have been observed<sup>11</sup> in experimental intrinsic viscosity versus temperature behavior. Figure 21 also illustrates that the steepness of the negative-positive transition indicates the curvature in the vicinity of the maximum viscosity as a function of temperature, i.e., smoothly varying versus a "cusp" type change.

An extremum in the predicted thermal expansion coefficient corresponds to an inflection point in the viscosity-temperature behavior (see triangular points in Fig. 21). For a specific type of polymer chain, this inflection point corresponds to a certain temperature  $T_{in}$ . Increasing the temperature beyond  $T_{in}$  causes the viscosity to approach some limiting value. If the thermal expansion coefficient is negative, the viscosity approaches some minimum value while for a positive thermal expansion coefficient the corresponding viscosity approaches some maximum value. In either case,  $T_{in}$  could be considered as an indication of the highest temperature with regards to some limiting viscosity for any given type polymer chain. Therefore, if the shape of the thermal expansion curve is kept constant, shifting the minimum value of thermal expansion coefficient to higher value of  $\beta U^*$  corresponds to shifting the viscosity inflection temperature to lower temperatures. This shifts the entire viscosity curve parallel to the original curve (see dashed curves in Fig. 21) and therefore lowers the viscosity over

a certain temperature range. Similarly, shifting the maximum value of thermal expansion coefficient to lower values of  $\beta U^*$  lowers the viscosity over a certain temperature range.

Lastly, the thermal expansion coefficient has certain implications on the thermoelastic response of a polymeric solid. For an incompressible polymeric solid consisting of crosslinked network of chains, the thermal expansion coefficient is equal to the change in internal energy due to a uniaxial, isothermal extension.<sup>4,5</sup> By definition a "rubbery response" is one whose corresponding force of retraction is due entirely to entropic changes, i.e., the internal energy change is zero. Conversely, the retractive force of a crystalline lattice is due almost entirely to internal energy changes. Hence, the predicted coefficients indicate that the internal energy contribution to the deformational response depends critically upon the type of polymer chain, torsional potential and the relative thermal energy  $U^*/kT$ . Furthermore, since a zero coefficient refers to an "ideal" rubber, a negative-positive transition indicates that the polymer chain is undergoing a transition from a "rubbery" entropic response to a "solid-state" energetic response. This intramolecular transition is analogous to the so-called glass transition and should play an important role in the overall macroscopic response (which depends upon both inter- and intramolecular interactions<sup>1-3</sup>) of a polymeric solid.

This work was carried out under Army Ordnance Contracts No. DAAH01-68-C-0632 and DAAH01-69-C-0772.

### References

1. J. H. Gibbs and E. A. DiMarzio, *J. Chem. Phys.*, **28**, 807 (1958).
2. W. R. Krigbaum and M. Kaneko, *J. Chem. Phys.*, **36**, 99 (1962).
3. J. N. Majerus, *Proc. 7th ICRPG Meet. Working Group Mech. Behavior*, (CPIA Pub. No. 177), 267 (1968).
4. P. J. Flory, C. A. J. Hoeve, and A. Ciferri, *J. Polym. Sci.*, **34**, 337 (1959).
5. A. Ciferri, *Trans. Faraday Soc.*, **57**, 846 (1961).
6. P. J. Flory, A. Ciferri, and C. A. J. Hoeve, *J. Polym. Sci.*, **45**, 235 (1960).
7. M. V. Volkenstein, *Configurational Statistics of Polymer Chains*, Interscience, New York, 1963, (a) Chaps. 2, 4, 6; (b) p. 191.
8. P. J. Flory, *Makromol. Chem.*, **98**, 128 (1966).
9. H. Inagaki, H. Susuki, M. Fujii, and T. Matsuo, *J. Phys. Chem.*, **70**, 1718 (1966).
10. H. Yamakawa, *J. Chem. Phys.*, **45**, 2606 (1966).
11. G. Delmas and D. Patterson, *Polymer*, **7**, 513 (1966).
12. J. E. Mark and G. B. Thomas, *J. Phys. Chem.*, **70**, 3588 (1966).
13. H. Inagaki, T. Miyamoto, and S. Ohta, *J. Phys. Chem.*, **70**, 3420 (1966).
14. G. Allegra, U. Flisi, and G. Grespi, *Makromol. Chem.*, **75**, 189 (1964).
15. A. Opschoor, *Makromol. Chem.*, **85**, 249 (1965).
16. P. Corraadini, *Rubber Chem. Technol.*, **39**, 14 (1966).
17. F. Danusso, *Polymer*, **8**, 281 (1967).
18. O. B. Ptitsyn and Y. A. Sharonov, *Zh. Tech. Fiz.*, **27**, 2744 (1957).
19. M. V. Volkenstein, *J. Polym. Sci.*, **29**, 441 (1958).
20. T. M. Birshtein and O. B. Ptitsyn, *Zh. Fiz. Khim.*, **28**, 213 (1954).
21. S. Lifson, *J. Chem. Phys.*, **29**, 80 (1958).
22. M. V. Volkenstein, *Dokl. Akad. Nauk SSSR*, **78**, 879 (1951).

23. H. Kuhn, *J. Chem. Phys.*, **15**, 843 (1947).
24. W. J. Taylor, *J. Chem. Phys.*, **15**, 412 (1947).
25. K. S. Pitzer and W. D. Gwinn, *J. Chem. Phys.*, **2**, 485 (1941).
26. A. H. Stroud and D. Secrest, *Gaussian Quadrature Formulas*, Prentice-Hall, Englewood Cliffs, N.J., 1966.
27. P. DeSantis, E. Giglio, A. M. Liquori, and A. Ripamonti, *J. Polym. Sci. A*, **1**, 1383 (1963).
28. T. M. Birshtein and O. B. Ptitsyn, *Conformations of Macromolecules*, Interscience, New York, 1966, Chap. 6.
29. A. Nakajima and K. Kato, *Makromol. Chem.*, **95**, 52 (1966).
30. I. Sakurada, A. Nakajima, O. Yoshizaki, and K. Nakamae, *Kolloid-Z*, **186**, 41 (1962).

Received November 10, 1969

## Substituent Effects in Free Radical Copolymerization of Substituted Styrenes with Acrylates and Methacrylates

JAN W. H. FABER and W. F. FOWLER, JR., *Research Laboratories,  
Eastman Kodak Company, Rochester, New York 14650*

### Synopsis

Relative reactivity ratios have been determined for *o*-chlorostyrene with five lower acrylates and methacrylates, respectively, and for methyl acrylate with a number of substituted styrenes in free-radical copolymerization. Analysis of the data shows that: (a) acrylates are less reactive than methacrylates with *o*-chlorostyrene; (b) length of the side chain has little or no effect in methacrylates, but its effect is pronounced in acrylates with respect to their reactivity ratios; (c) chlorine substitution in the side chain of either acrylates or methacrylates has a significant influence on the reactivity ratio; (d) relative reactivity ratio data for methyl acrylate with substituted styrenes fail to show the expected relationship between monomer structure and resonance theory, inductive effect and, consequently, the Hammett  $\sigma$  values.

### INTRODUCTION

Since Walling et al.<sup>1</sup> published their work on the effect of *meta* and *para* substituents on the relative reactivity of the styrene double bond in copolymerization, a number of publications have appeared in which substituent effect either could or could not be correlated with Hammett's  $\sigma$  values.

Other authors<sup>2-4</sup> have attempted to give a theoretical basis to the well-known  $Q$  and  $e$  scheme, even though its originators<sup>5</sup> cautioned that this was strictly an empirical formula. Indeed, in many cases calculated  $Q$  and  $e$  values do not agree with literature data, or, conversely, relative reactivity ratios calculated from published  $Q$  and  $e$  values do not agree with experi-

TABLE I  
Calculated versus Experimental Reactivity Ratio Data,  
 $M_1 = o$ -Chlorostyrene

Acrylate $M_2$	$Q_1^a$	$e_1^a$	$Q_2^a$	$e_2^a$	$r_1$		$r_2$	
					Calcd	Found	Calcd	Found
Methyl	1.28	-0.36	0.42	0.60	2.16	6	0.184	0
Ethyl	1.28	-0.36	0.52	0.22	2.00	3.89	0.358	0
<i>n</i> -Butyl	1.28	-0.36	0.50	1.06	1.535	2.19	0.087	0.17
2-Ethylhexyl	1.28	-0.36	0.41	0.39	2.38	2.77	0.239	0.21

<sup>a</sup> From Young's Tables.<sup>10</sup>

mental data (Table I). In short, no complete explanation has been offered for substituent effects in binary, free-radical copolymerization; therefore, one cannot predict with reasonable certainty the course of polymerization or the structure of the final product. In this paper we report experimental relative reactivity ratios involving monosubstituted styrenes as one of the two comonomers and conclusions that can be drawn from them. In a future publication we hope to discuss the substituent effect on a more theoretical basis as more data become available.

## EXPERIMENTAL

### Copolymerization of *o*-Chlorostyrene with Five Lower Acrylates and Methacrylates

**Monomers.** The monomers were commercially available materials. The monomers used and the sources are listed in Table II. The suppliers listed are not necessarily the sole distributors. Purification was by washing and distillation; pure monomers were stored in crown-capped bottles under nitrogen in a deep freeze. Monomer purity was checked by gas chromatography, refractive index, and infrared spectroscopy.

TABLE II

Monomer	Source
<i>o</i> -Methylstyrene	Columbia Organic Chemical Co.
<i>m</i> -Methylstyrene	Columbia Organic Chemical Co.
<i>p</i> -Methylstyrene	Monomer Polymer Laboratory
<i>p</i> -Methoxystyrene	Monomer Polymer Laboratory
<i>o</i> -Chlorostyrene	Dow Chemical Company
<i>m</i> -Chlorostyrene	Monomer Polymer Laboratory
<i>p</i> -Chlorostyrene	Monomer Polymer Laboratory
<i>o</i> -Bromostyrene	Columbia Organic Chemical Co.
<i>p</i> -Bromostyrene	Monomer Polymer Laboratory
<i>o</i> -Fluorostyrene	Chemical Procurement Laboratory
<i>p</i> -Fluorostyrene	Chemical Procurement Laboratory
Methyl acrylate	Rohm and Haas Company
Ethyl acrylate	Rohm and Haas Company
<i>n</i> -Butyl acrylate	Rohm and Haas Company
2-Ethylhexyl acrylate	Rohm and Haas Company
2-Chloroethyl acrylate	Monomer Polymer Laboratory
Methyl methacrylate	Rohm and Haas Company
Ethyl methacrylate	Rohm and Haas Company
<i>n</i> -Butyl methacrylate	Rohm and Haas Company
2-Ethylhexyl methacrylate	Monomer Polymer Laboratory
2-Chloroethyl methacrylate	Monomer Polymer Laboratory

**Polymerization.** *o*-Chlorostyrene was copolymerized by standard polymerization technique in mass, solvent, and emulsion systems. Comonomer feed compositions were changed in 10 mol-% increments, resulting in nine comonomer feed compositions containing 10–90 mole-% *o*-chlorostyrene

for each system studied. Copolymerizations were allowed to proceed to 4% conversions.

The relative reactivity ratios are listed in Tables III and IV. Typical polymerizations are given below.

**Bulk Polymerization of 40 mole-% *o*-Chlorostyrene and 60 Mole-% Methyl Acrylate.** In a 100-cc polymerization tube were placed 25 g of a solution of 55.4 g (40 mole-%) of *o*-chlorostyrene and 51.6 g (60 mole-%) of methyl acrylate with 0.0025 g of benzoyl peroxide. The tube was flushed with nitrogen for 30 sec, sealed, and placed in a constant-temperature bath at 60°C. The onset of polymerization was determined by shaking the tube and observing the viscosity as indicated by the speed of the rising

TABLE III  
Reactivity Ratios for *o*-Chlorostyrene ( $M_1$ ) with Acrylates ( $M_2$ ),  $T = 40^\circ\text{C}$

$M_2$	Mass		Solution		Emulsion	
	$r_1$	$r_2$	$r_1$	$r_2$	$r_1$	$r_2$
Methyl acrylate	5.9 ± 0.27	0.059 ± 0.04	5.94 ± 0.37	0 ± 0.03	6 ± 0.43	0 ± 0.03
Ethyl acrylate	3.73 ± 0.035	0 ± 0.06	3.94 ± 0.035	0 ± 0.06	4.01 ± 0.43	0.048 ± 0.05
<i>n</i> -Butyl acrylate	2.10 ± 0.15	0.16 ± 0.03	2.13 ± 0.04	0.16 ± 0.005	2.25 ± 0.20	0.2 ± 0.05
2-Ethylhexyl acrylate	2.77 ± 0.15	0.24 ± 0.08	2.77 ± 0.03	0.21 ± 0.08	2.65 ± 0.23	0.17 ± 0.10
2-Chloroethyl acrylate	—	—	—	—	1.71 ± 0.08	0.533 ± 0.015

gas bubbles. As soon as any increase in viscosity was noted, the tube was opened and the contents poured into methanol. The precipitated polymer was redissolved in chloroform, precipitated three times, and dried to constant weight. If the yield of polymer indicated more than 4% conversion, the experiment was repeated until yields of 4% or less were obtained.

**Solvent Polymerizations.** These were run in benzene with a monomer:solvent ratio of 1:3. Polymerization progress estimation and purification were the same as in the bulk polymerization.

**Emulsion Polymerization of 40 mole-% *o*-Chlorostyrene and 60 mole-% Methyl Acrylate.** In a 100-ml beverage bottle were placed 20 g of a mixture of 55.4 g (40 mole-%) of *o*-chlorostyrene and 51.6 g (60 mole-%) of methyl acrylate with 80 ml distilled water, 1 g (5 wt %) Duponol Me (polymerization grade), 0.1 g  $\text{K}_2\text{S}_2\text{O}_8$ , and 0.05 g  $\text{K}_2\text{S}_2\text{O}_5$ . The bottle was flushed with nitrogen, capped, and tumbled in a 40°C constant-temperature bath. Within 15 min, polymerization started, as indicated by the appearance of a bluish tint and the disappearance of foam. The bottle was opened and the contents were poured into methanol. Purification was the same as described above.

TABLE IV  
 Reactivity Ratios for *o*-Chlorostyrene ( $M_1$ ) with Methacrylates ( $M_2$ ),  $T = 40^\circ\text{C}$

$M_2$	Mass		Solution		Emulsion	
	$r_1$	$r_2$	$r_1$	$r_2$	$r_1$	$r_2$
Methyl methacrylate <sup>a</sup>	1.29 $\pm 0.165$	0.413 $\pm 0.15$	1.31 $\pm 0.01$	0.53 $\pm 0.075$	1.34 $\pm 0.01$	0.46 $\pm 0.075$
Ethyl methacrylate	1.40 $\pm 0.035$	0.457 $\pm 0.05$	1.31 $\pm 0.017$	0.475 $\pm 0.0325$	1.34 $\pm 0.032$	0.45 $\pm 0.03$
<i>n</i> -Butyl methacrylate	1.30 $\pm 0.33$	0.352 $\pm 0.12$	1.25 $\pm 0.33$	0.335 $\pm 0.11$	1.24 $\pm 0.33$	0.324 $\pm 0.11$
2-Ethylhexyl methacrylate	2.8 $\pm 0.23$	0.425 $\pm 0.08$	2.74 $\pm 0.04$	0.394 $\pm 0.09$	2.74 $\pm 0.04$	0.394 $\pm 0.09$
2-Chloroethyl methacrylate	—	—	—	—	0.909 $\pm 0.005$	0.885 $\pm 0.107$

<sup>a</sup> Literature:<sup>1</sup>  $r_1 = 1.37 \pm 0.1$ ;  $r_2 = 0.50 \pm 0.03$  at  $60^\circ\text{C}$ .

Water solubilities of the various monomers were measured (Tables V and VI). No correlation exists between reactivity ratio data and the water solubility, an observation supported by the fact that relative reactivity ratios for a given pair of monomers are practically identical for mass, solvent, and emulsion polymerization.

The only instance where water solubility exerts an effect is in the reaction rate. Systems having a high content of relatively water-soluble monomer polymerize faster than those having a low content in an emulsion system as indicated by the exotherm (Fig. 1). Exotherms were measured internally in the polymerization media with a thermocouple connected to a recorder.

TABLE V  
Water Solubility of Acrylates at 40°C

Monomer	Solubility, g/100 ml
<i>o</i> -Chlorostyrene	0.0046
Methyl acrylate	5.09
Ethyl acrylate	1.60
<i>n</i> -Butyl acrylate	0.151
2-Ethylhexyl acrylate	0.014

TABLE VI  
Water Solubility of Methacrylates at 40°C

Monomer	Solubility, g/100 ml
<i>o</i> -Chlorostyrene	0.0046
Methyl methacrylate	0.468
Ethyl methacrylate	0.118
<i>n</i> -Butyl methacrylate	0.016
2-Ethylhexyl methacrylate	0.017

Although the heat of polymerization of methyl acrylate (18.8 kcal/mole) is 2.7 kcal/mole more than that of *o*-chlorostyrene (16.08 kcal/mole), we do not believe that the exotherm can be attributed solely to this energy difference; therefore water solubility, i.e., the rate of diffusion, plays a major role.

**Reactivity Ratio Determinations.** For the determination of the *o*-chlorostyrene content of the copolymers, a calibration curve was plotted for the intensity of ultraviolet absorption of various concentrations of poly-*o*-chlorostyrene in the copolymers. A family of absorption curves is shown in Figure 2. From the calculated curve it was then possible, at a known concentration (0.1500 g/250 ml of chloroform) of copolymer, to ascertain the percentage of *o*-chlorostyrene in the unknown.<sup>6,7</sup>

Data were then tabulated in the manner of the Fineman-Ross plotting form,<sup>8</sup> the slope and intercept of the curves being determined by a least-squares analysis of the data.



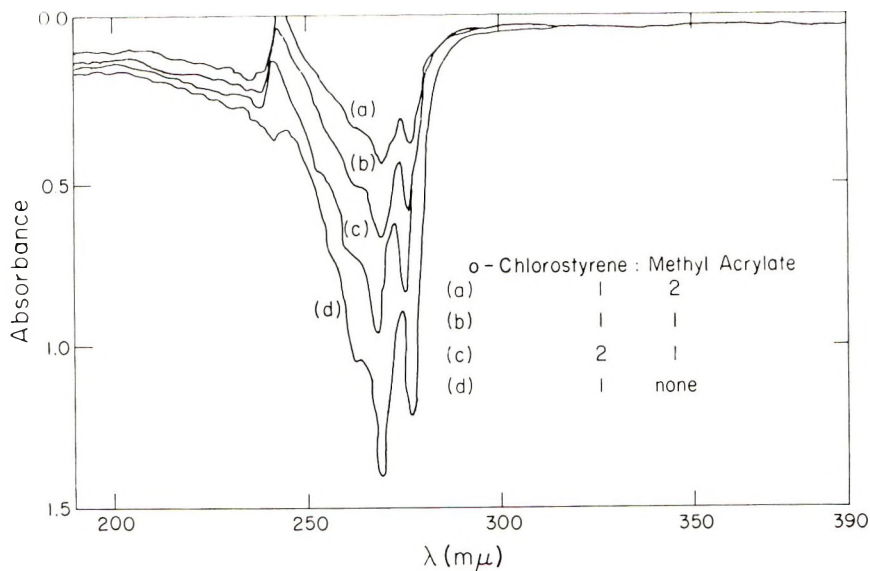
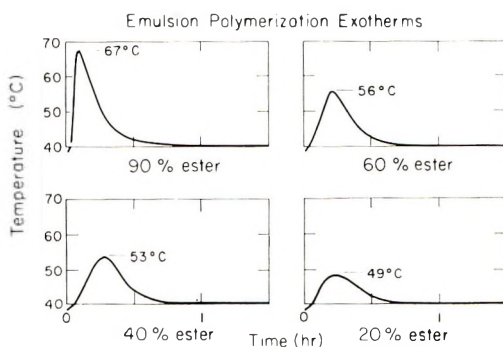
Fig. 1. *o*-Chlorostyrene absorbance curves.

Fig. 2. Emulsion polymerization exotherms.

### Copolymerization of Methyl Acrylate with Substituted Styrenes

All monomers are commercially available except *o*-methoxystyrene, which was prepared as described elsewhere.<sup>9</sup>

The purity of the monomers was checked by gas chromatography, refractive index, and infrared spectroscopy.

Polymerization technique and relative reactivity ratio determinations are identical with those given above. In Table VII are given the relative reactivities, where  $M_1$  is substituted styrene and  $M_2$  is methyl acrylate.

TABLE VII  
Relative Reactivity Ratios of Substituted Styrene  
and Methyl Acrylate ( $M_2$ )

Substituent on styrene ( $M_1$ )	$r_1$	$r_2$
—	0.75	0.2
<i>o</i> -Me	0.98	0.27
<i>p</i> -Me	1.65	0.14
<i>p</i> -Me	1.54	0.17
<i>o</i> -MeO	2.6	0.04
<i>p</i> -MeO	2.0	0.07
<i>o</i> -I <sup>a</sup>	3.8	0.01
<i>p</i> -F	2.6	0.04
<i>o</i> -Cl	6	0.002
<i>p</i> -Cl	4.8	0.002
<i>p</i> -Cl	3.9	0.01
<i>o</i> -Br	6.9	0
<i>p</i> -Br	6	0.01
<i>r</i> -C=N <sup>a</sup>	9.5	0

<sup>a</sup> Measured only on three points on the curve.

## DISCUSSION

Observation of the data in Tables I and III shows the apparent effect of hyperconjugation of the methyl group in the methacrylate unit upon the double bond; the length of the side chain seems to have little influence. In the series in which the acrylate esters are copolymerized with *o*-chloro-styrene, the side-chain length has a pronounced effect on the relative reactivity ratio. We are at a loss to explain this, but it does show how minor structural differences in a monomer and/or radical can profoundly change its behavior in copolymerization. This is also observed in both 2-chloro-ethyl esters. It is improbable that the effect of the chlorine is transmitted solely through the chain and we believe that a rather strong field effect is responsible for the enhanced reactivity of these esters. Further studies of this phenomenon are in progress.

From Table VII we can draw the following conclusions, which to us were rather startling.

(1) No matter what the substituent is, it increases the relative reactivity of the styrene moiety.

(2) The closer the substituent is to the vinyl double bond of the styrene derivative the greater the influence it exerts (except for *o*-methyl).

(3) The change in reactivity in halogen-substituted styrenes is the reverse of what one would expect from electronegativity data.

(4) The number of unshared electron pairs in a substituent is more important than the size of the substituent.

In short, the effect of a substituent on styrene in free-radical copolymerization with methyl acrylate depends, at least in part, on: (a) the dis-

tance of the substituent to the vinyl double bond; (b) the size of the substituent; and (c) the number of unshared electron pairs in the substituent.

Literature data<sup>10</sup> show that the same effects operate in the free radical copolymerization of substituted styrenes with methyl methacrylate.

The failure of these data to conform with existing resonance and inductive effect theory (and consequently Hammett's  $\sigma$  values) points up the risk inherent in attempting to apply concepts, theories and mechanisms from the field of ionic chemistry to free-radical copolymerization theory.

### References

1. C. Walling, E. R. Briggs, K. Wolfstern, and F. R. Mayo, *J. Amer. Chem. Soc.*, **70**, 1537 (1948).
2. T. C. Schwan and C. C. Price, *J. Polym. Sci.*, **40**, 457 (1959).
3. M. Chorton and A. J. Capata, *J. Polym. Sci. A*, **2**, 1321 (1964).
4. M. C. Shen, *J. Polym. Sci. B*, **1**, 11, (1963).
5. T. Alfrey, Jr., and C. C. Price, *J. Polym. Sci.*, **2**, 101 (1947).
6. H. A. Cartinen, F. A. Miller, and T. D. Parks, *J. Amer. Chem. Soc.*, **69**, 2707 (1947).
7. E. J. Meehan, *J. Polym. Sci.*, **1**, 175 (1946).
8. M. Fineman and S. D. Ross, *J. Polym. Sci.*, **5**, 259 (1950).
9. C. S. Marvel and D. Hein, *J. Amer. Chem. Soc.*, **70**, 1895 (1948).
10. G. E. Ham, *Copolymerization*, Interscience, New York, 1964.

Received November 13, 1969

## Molecular Weight Distribution in Polyacrylamide Prepared by a Photochemical Method

K. VENKATARAO\* and M. SANTAPPA, *Department of Physical  
Chemistry, University of Madras, Madras, 25, India*

### Synopsis

The molecular weight distribution of polyacrylamide, prepared by uranyl ion-photo-sensitized polymerization of acrylamide in visible light of wavelength  $436\text{ m}\mu$ , was studied in detail. The polymer was fractionated and the experimental integral and differential distribution curves were drawn. The theoretical distribution function was derived from the kinetics of photopolymerization, assuming the rate constants calculated from previous studies. The theoretical and experimental molecular weight distributions were compared. The results support the mechanism proposed for the photopolymerization reaction.

### INTRODUCTION

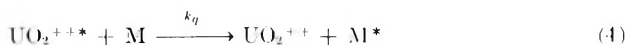
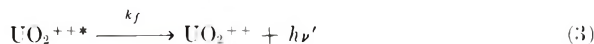
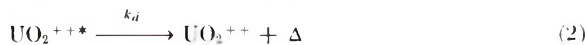
The molecular weight distribution in a polydisperse polymer depends on the kinetics of polymerization. A comparison of the theoretical distribution of molecular weights (from kinetics) with the distribution curve obtained from molecular weights determined experimentally, is usually good evidence for the correctness of the kinetic scheme proposed. Baxendale and co-workers<sup>1</sup> have compared the theoretical and experimental distribution for poly(methyl methacrylate) initiated by  $\text{Fe}^{++}-\text{H}_2\text{O}_2$  system and got good agreement. We have studied<sup>2,3</sup> the kinetics of polymerization of acrylamide photosensitized by uranyl ions. Our studies on the molecular weight distribution for polyacrylamide indicate good agreement between the theoretical and experimental distribution curves, thus confirming the correctness of the kinetic mechanism proposed earlier.<sup>3</sup>

### DERIVATION OF THE DISTRIBUTION FUNCTION

It has been shown by our recent studies<sup>3</sup> that the initiation of polymerization of acrylamide, photosensitized by uranyl ions, takes place through energy transfer from excited uranyl ion to the monomer and the subsequent reaction of the excited monomer molecule with an unexcited monomer molecule to produce two free radicals. These radicals initiate the growth of polymer radical chains, whose chain lengths are determined by the ter-

\* Present address: Department of Chemistry, Madurai University, Madurai 2, India.

mination mechanism. The kinetic scheme proposed for the polymerization of acrylamide photosensitized by uranyl ions in aqueous acid solutions in visible light is shown in eqs. (1)–(9).



Here  $\text{R}_r$  represents the growing polymer radical with  $r$  monomer units and  $\text{P}_r$  represents the dead polymer with chain length  $r$ . The rate constants  $k_p$  and  $k_t$  and hence  $k_p/k_t^{1/2}$  are assumed to be independent of chain length, as has been proved by experiment.

The steady-state expressions for  $\text{UO}_2^{++*}$ ,  $\text{M}^*$  and  $\text{R}_r$  are:

$$k_i I = k_q[\text{M}][\text{UO}_2^{++*}], k_q[\text{M}] \gg (k_d + k_f) \quad (10)$$

$$k_q[\text{M}][\text{UO}_2^{++*}] = k_i[\text{M}^*][\text{M}] + k_d'[\text{M}^*] \quad (11)$$

From equations (10) and (11)

$$[\text{M}^*] = k_i I / (k_d' + k_i[\text{M}]) \quad (12)$$

$$2k_i[\text{M}^*][\text{M}] = k_p[\text{M}][\text{R}_1] + k_t[\text{R}_1] \sum_1^{\infty} [\text{R}_n] \quad (13)$$

Substituting for  $[\text{M}^*]$  from eq. (12) we get,

$$2k_i/k_i I[\text{M}] / (k_d' + k_i[\text{M}]) = [\text{R}_1] \left( k_p[\text{M}] + k_t \sum_1^{\infty} [\text{R}_n] \right) \quad (14)$$

$$k_p[\text{R}_1][\text{M}] = [\text{R}_2] \left( k_p[\text{M}] + k_t \sum_1^{\infty} [\text{R}_n] \right) \quad (15)$$

$$k_p[\text{R}_{r-1}][\text{M}] = [\text{R}_r] \left( k_p[\text{M}] + k_t \sum_1^{\infty} [\text{R}_n] \right) \quad (15r)$$

where  $[\text{M}]$  is the monomer concentration at time  $t$ . The values of light absorption fraction  $k_i$  and light intensity  $I$  are not affected during the course of polymerization. Adding eqs. (14), (15), . . . , (r) to infinity yields:

$$2k_i k_i I[\text{M}] / (k_d' + k_i[\text{M}]) = k_i \left( \sum_1^{\infty} [\text{R}_n] \right)^2$$

and

$$\sum_1^{\infty} [R_n] = \left[ \frac{2k_i k_e I [M]}{k_t (k_d' + k_i [M])} \right]^{1/2} \quad (16)$$

By multiplying together eqs. (14) to (15r), we get a value for  $[R_r]$ :

$$\left( \frac{2k_i k_e I [M]}{k_d' + k_i [M]} \right) (k_p [M]^{r-1}) = [R_r] \left( k_p [M] + k_i \sum_1^{\infty} [R_n] \right)^{+r}$$

$$[R_r] = \left( \frac{2k_i k_e I}{k_p (k_d' + k_i [M])} \right) \left( 1 + \frac{k_i \sum_1^{\infty} [R_n]}{k_p [M]} \right)^{-r} \quad (17)$$

The rate of production of polymer of chain length  $r$ , by disproportionation of two polymer radicals (Step 9) is given by

$$d[P_r]/dt = k_t \sum_1^{\infty} [R_n] [R_r] \quad (18)$$

$$-d[M]/dt = k_p \sum_1^{\infty} [R_n] [M] \quad (19)$$

Dividing eq. (18) by eq. (19) yields:

$$-d[P_r]/d[M] = k_t [R_r] / k_p [M] \quad (20)$$

Substituting for  $[R_r]$  from eq. (17) into eq. (20) yields:

$$\frac{-d[P_r]}{d[M]} = \left( \frac{k_t}{k_p [M]} \right) \left\{ \frac{2k_i k_e I}{k_p (k_d' + k_i [M])} \right\} \times \left\{ 1 + \frac{\sqrt{2k_i^{1/2} k_e^{1/2} k_t^{1/2} I^{1/2}}}{k_p [M]^{1/2} (k_d' + k_i [M])^{1/2}} \right\}^{-r} \quad (21)$$

writing  $k_p/k_i^{1/2} = \beta$  and  $k_d'/k_i = \alpha$  yields

$$\frac{-d[P_r]}{d[M]} = \left[ \frac{2k_e I}{\beta^2 [M] (\alpha + [M])} \right] \left[ 1 + \frac{\sqrt{2k_e^{1/2} I^{1/2}}}{\beta [M]^{1/2} (\alpha + [M])^{1/2}} \right]^{-r} \quad (22)$$

Now the concentration of polymer of chain length  $r$ ,  $[P_r]$ , may be expressed as a function of  $\gamma$  ( $= [M]/[M_0]$ ), the fraction of unpolymerized monomer, at any value of  $r$ :

$$[P_r] = \int_{\gamma=0.1}^{\gamma=1.0} \left[ \frac{2k_e I}{\beta^2 \gamma (\alpha + [M_0] \gamma)} \right] \left[ 1 + \frac{\sqrt{2k_e^{1/2} I^{1/2}}}{\beta [M_0]^{1/2} \gamma^{1/2} (\alpha + [M_0] \gamma)^{1/2}} \right]^{-r} d\gamma \quad (23)$$

Equation (23) was solved for various values of  $r$ , by a computer program in an IBM 1300 computer. The values  $\alpha = 2.46$  and  $\beta = 2.098$  obtained from our earlier kinetic studies<sup>3</sup> and  $k_e = 0.282$  and  $I = 1.38 \times 10^{-6}$   $Nh\nu/1$ -sec, were used for calculation of  $[P_r]$ . Since the kinetics may not be obeyed beyond  $\sim 90\%$  conversion, the reaction was stopped at 90% con-

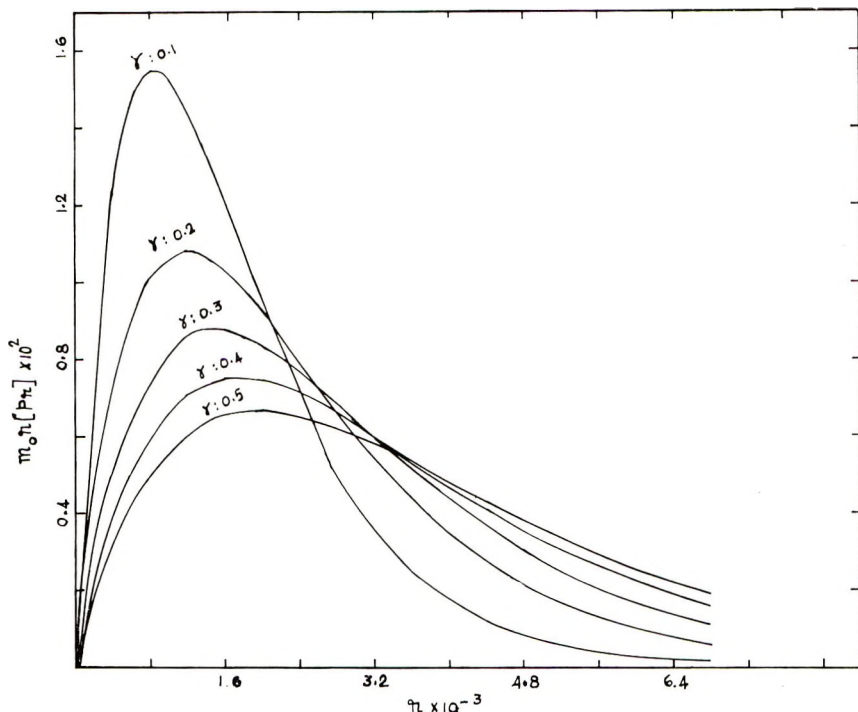


Fig. 1. Theoretical variation of distribution during polymerization.

version, i.e.,  $\gamma = 0.1$  to make the comparison between the theory and experiment valid. The  $[P_r]$  values, which give the concentration of polymer with chain length  $r$  in moles/l., are multiplied by  $m_0$  (molecular weight of the monomer = 71) and  $r$ , the chain length, to get the weight of polymer with chain length  $r$  per liter.  $m_0 r [P_r]$  values for  $\gamma = 0.1-0.5$  were plotted against  $r$  (Fig. 1), and it was observed that the maxima of the curves shifted to lower chain lengths as the  $\gamma$  decreased, i.e., the reaction neared completion. This is as expected from the kinetics, since with increasing conversion (i.e., decreasing  $\gamma$ ), the monomer concentration goes down and hence the proportion of high molecular weight species decreases.

### EXPERIMENTAL

The polyacrylamide was prepared by irradiation at  $436 \text{ m}\mu$  of a deaerated solution containing  $0.5M$  acrylamide,  $0.005M$  uranyl perchlorate,  $0.1M$  perchloric acid, and sufficient sodium perchlorate to get an ionic strength  $\mu = 1.25 M$ . The photochemical equipment was described earlier.<sup>2</sup> The reaction was allowed to proceed to 90% conversion of the monomer, after which the polymer was precipitated by pouring the reaction mixture into isopropanol. The precipitated polymer was purified by reprecipitating from water two or three times, by isopropanol, and then dried under vacuum at about  $50^\circ\text{C}$ . The polymer was then dissolved in water to get

~1% solution and this solution was subjected to fractional precipitation at a constant temperature, by successive addition of isopropanol, heating to dissolve the precipitated polymer and then slowly cooling the solution. The precipitated polymer was separated after being allowed to stand at least for 12 hr in a constant temperature bath. About 3.5 g of the polymer was separated into eighteen fractions, each fraction weighing 0.3 g or less. The chain lengths of the polymer fractions (0.1% polymer solutions in 1.0*M* aqueous sodium nitrate) were determined viscometrically in an Ubbelohde-type viscometer at  $30 \pm 0.01^\circ\text{C}$  by using the Mark-Houwink relation due to Dainton and co-workers:<sup>4</sup>

$$[\eta] = 6.8 \times 10^{-4}(\bar{M}_n)^{0.65} \quad (24)$$

### CONSTRUCTION OF DISTRIBUTION CURVES

The procedure followed was essentially that formulated by Baxendale and co-workers.<sup>1</sup>  $d[P_r]$ , the number of molecules in the heterodisperse polymer having chain lengths between  $r$  and  $r + dr$ , may be expressed as a function of  $r$ ,

$$d[P_r] = Cf(r)dr \quad (25)$$

where  $C$  is a constant, depending on the total number of polymer molecules. The weight of polymer,  $dW_r$ , between the limits of chain length  $r$  and  $r + dr$  is

$$m_0 r d[P_r] = m_0 C r f(r) dr \quad (26)$$

Since the molecular weights are spread over a range even in a fractionated polymer, eq. (16) may not be used to construct the differential distribution curve directly from the experimental data. But if the fractions are reason-

TABLE I  
Fractionation Data for Polyacrylamide\*

Frac- tion no.	Actual weight of the fraction, g	Chain length, $r$	Integral weight fraction $F(r)$ up to $r$	Frac- tion no.	Actual weight of the fraction, g	Chain length, $r$	Integral weight fraction $F(r)$ up to $r$
1	0.0474	259	0.0070	10	0.2052	2418	0.4837
2	0.0816	387	0.0259	11	0.2561	2746	0.5510
3	0.1314	518	0.0572	12	0.2414	2992	0.6242
4	0.1454	707	0.0979	13	0.1819	3232	0.6865
5	0.1904	967	0.1772	14	0.1098	3696	0.7295
6	0.2724	1332	0.2152	15	0.2182	4137	0.7776
7	0.2172	1589	0.2872	16	0.1647	4662	0.8338
8	0.1765	1819	0.3450	17	0.2092	5479	0.8887
9	0.2800	2055	0.4120	18	0.2737	8104	0.9596

\*  $[M] = 0.5$  mole/l.,  $k_t = 0.282$ ,  $I = 1.38 \times 10^{-6}$   $Nh\nu$ /l.-sec,  $[\text{HClO}_4] = 0.1$  mole/l.,  $\lambda = 436$   $m\mu$ ,  $\mu = 1.25$  mole/l.,  $t = 35^\circ\text{C}$ .



ably sharp, then the integral weight,  $W_r$ , may be calculated from the eq. (26):

$$W_r = m_0 C \int_1^r r f(r) dr \quad (27)$$

The integral distribution curve may be constructed by plotting the weight of polymer below a chain length  $r$  divided by total weight of polymer,  $F(r) = W_r/\text{total weight of polymer}$ , against  $r$ .  $dF(r)/dr$  versus  $r$  gives the differential curve. In constructing the integral weight fraction,  $F(r)$ , versus  $r$  curve, it was assumed (a) that only the fraction to which the weight is summed contains polymer of chain length above that of mean and (b) that the distribution of chain lengths in each fraction is symmetrical about the measured mean chain length. Thus to obtain a point ( $W_r, r$ ) on the curve, the weight of fractions up to and including the fraction of measured chain length  $r$  are summed and assuming (a) and (b), one half of the weight of the last fraction is subtracted. Then the integral weight fraction  $F(r)$  was obtained by dividing  $W_r$  by the total amount of polymer. The fractionation data along with the integral weight fractions are given in Table I. The theoretical integral weight distribution was calculated from a plot of  $m_0[P_r]$  versus  $r$ , with  $[P_r]$  from eq. (23), and is given in Table II. The comparison of theoretical and experimental integral weight distributions are given in Figure 2. The differential distribution curves calculated from Figure 2 are given in Figure 3.

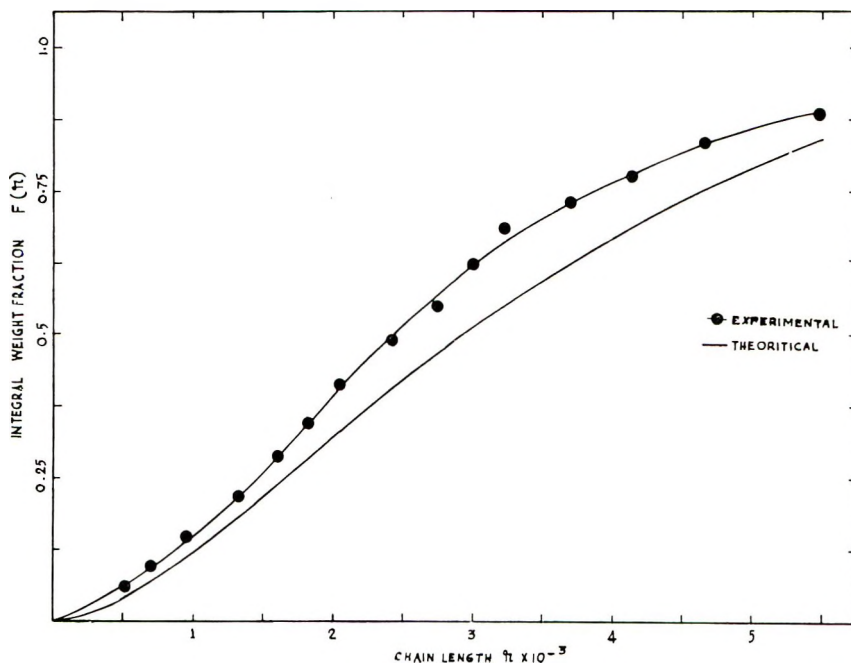


Fig. 2. Comparison of theoretical and experimental integral weight distributions.

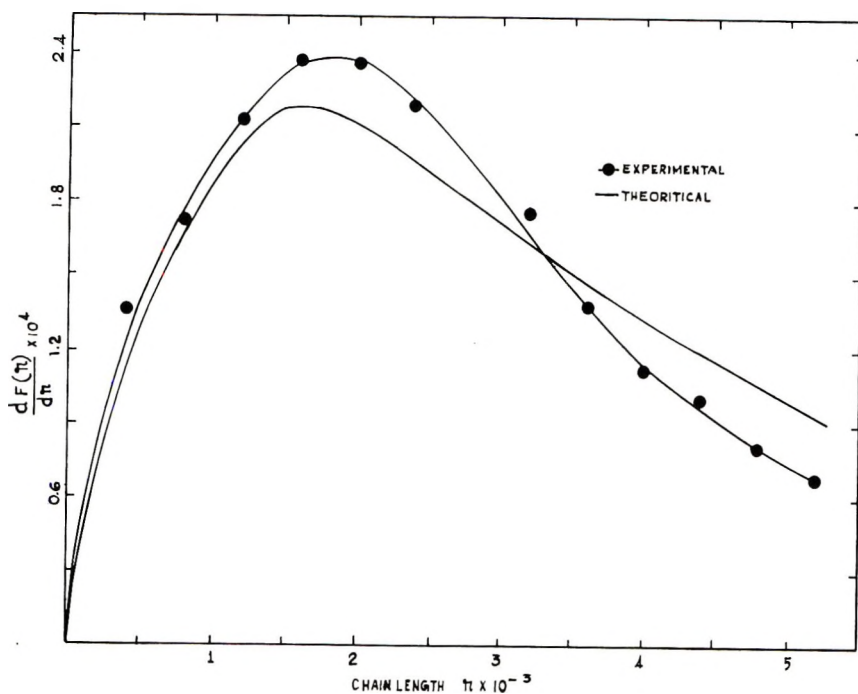


Fig. 3. Comparison of theoretical and experimental differential distributions

TABLE II  
Theoretical Integral Weight Distribution

No.	Chain length, $r$	Integral weight fraction $F(r)$ up to $r$	No.	Chain length, $r$	Integral weight fraction $F(r)$ up to $r$
1	400	0.0235	11	4400	0.7211
2	800	0.0807	12	4800	0.7686
3	1200	0.1555	13	5200	0.8104
4	1600	0.2371	14	5600	0.8480
5	2000	0.3200	15	6000	0.8812
6	2400	0.4003	16	6400	0.9111
7	2800	0.4760	17	6800	0.9374
8	3200	0.5466	18	7200	0.9610
9	3600	0.6102	19	7600	0.9819
10	4000	0.6682			

## DISCUSSION

The integral and differential distribution curves show the comparison between the theory and experiments. It can be seen that the proportion of high molecular weight species in the experimental curve is lower than is predicted by theory. However, the general pattern of the curves and the

maxima of the differential curves agree very well. The deviations may be due to inefficient fractionation and the consequent inaccuracy in the assumptions used in the construction of the experimental curves. Further, there may be some chain transfer to the monomer, which has not been detected by kinetics due to the complexity of the mechanism. But the overall agreement between the experimental and theoretical curves along with the close maxima in both the curves indicates that the mechanism proposed for the reaction was substantially correct. The nature of mutual termination (whether it is combination or disproportionation) cannot be predicted conclusively by kinetics alone. But, the fact that the molecular weight distribution from theory for termination by mutual combination deviates very much from the experimental distribution proves that the termination may very well be disproportionation.

Grateful thanks are due to C.S.I.R., New Delhi, for giving a Senior Fellowship to one of us (K. V. R.) and also to the C. A. S. in Biophysics and Crystallography, University of Madras, for giving computer facilities.

### References

1. J. H. Baxendale, S. Bywater, and M. G. Evans, *Trans. Faraday Soc.*, **42**, 65 (1946).
2. K. Venkatarao and M. Santappa, *J. Polym. Sci. A-1*, **5**, 637 (1967).
3. K. Venkatarao and M. Santappa, *J. Polym. Sci. A-1*, in press.
4. F. S. Dainton and M. Tordoff, *Trans. Faraday Soc.*, **53**, 499 (1957).

Received September 9, 1969

Revised November 18, 1969

## Helix Formation and Formaldehyde Crosslinking in Gelatin Solutions

I. H. COOPES, *Research Laboratory, Kodak (Australasia) Pty. Ltd., Coburg, Victoria, Australia*

### Synopsis

Optical rotation measurements on 5% gelatin solutions containing 0, 2, and 5% formaldehyde (w/w gelatin) are carried out at a series of temperatures between 20°C and 50°C. The solutions without formaldehyde show a diminished growth in rotation with rising temperatures, but even at 50°C there is still a steady rise in rotation with time. The addition of formaldehyde diminishes the optical rotation growth, and at 40°C and above solutions with 5% formaldehyde show no change in rotation at all. The specific rotation and time figures are fitted to a series of third-degree polynomial equations. It is shown that the data do not conform to any pattern of simple reaction kinetics. The mechanism of the formaldehyde-gelatin interaction is discussed.

### INTRODUCTION

The complex process of gelatin gel formation has been widely studied. Ferry and Eldridge<sup>1</sup> suggested that two processes were involved, an intramolecular rearrangement reflected by changes in optical activity, and an intermolecular crosslinking process associated with changes in rigidity.

The mechanism of helix formation was investigated by Von Hippel and Harrington,<sup>2</sup> who suggested that a rapid intramolecular transition establishing a *trans-trans'* configuration at the proline-hydroxyproline bond took place, followed by a slow assumption of the helix in the vicinity of these bonds. A different view was taken by Flory and Weaver<sup>3</sup> who postulated a rate-determining step involving the rearrangement of a single random coil molecule followed by the rapid formation of the triple-strand compound helix. It has been established<sup>4,5</sup> that the helix is stabilized by interchain association, and that the rate of helix formation is much higher with  $\gamma$ -gelatins (three chain molecules) than with  $\alpha$ - and  $\beta$ -gelatins (one and two chain molecules respectively).<sup>6</sup> Veis and Schnell<sup>7</sup> have suggested that the first step in the gelation process involves the interaction of chain segments via hydrogen bonding to form aggregates, followed by collagen-fold formation within the aggregates.

The evidence available at present tends to support the theory that single-strand helices cannot exist as stable entities, but require interaction with other chain segments, which may be from either the same or different molecules. It is probable that two chain helices predominate, owing to the

low probability of three chains becoming correctly aligned, except in the case of  $\gamma$ -molecules, in which the chains are already held in alignment by the interchain covalent bonds.

Other investigations<sup>8-11</sup> have established relationships between melting temperature, concentration, rigidity, aggregate size, and collagen-fold growth.

The research work described above reveals a fairly clear pattern for the molecular processes taking place during gelation, although some questions remain to be answered. The first stage of gelation involves the formation of weak intermolecular crosslinks formed by neighboring hydrogen bonds. The second stage involves the formation of the collagen-fold. It has been demonstrated by Yaron and Berger<sup>12</sup> that poly-L-proline required at least six residues to form a stable helix, and in view of the close similarity between the poly-L-proline II helical structure and the collagen fold<sup>13</sup> it may be assumed that a similar requirement exists for gelatin chains. From a thermodynamic analysis Pouradier<sup>14</sup> has concluded that crosslinks in a gelatin gel contain from one to about twelve hydrogen bonds. It seems likely therefore that the more stable crosslinks consist of lengths of chain in the collagen-fold conformation stabilized by interchain hydrogen bonds. As the gel matures the helical structure grows along the chain, resulting in greater rigidity in the gel.

For many practical purposes gelatin must be treated with crosslinking reagents to promote insolubility and dimensional stability. Such treatment further complicates the molecular processes associated with gelation. The most widely studied crosslinking agent is formaldehyde. Fraenkel-Conrat and Oleott<sup>15</sup> considered that formaldehyde hardening took place between amino and primary amide or guanidyl groups. Davis and Tabor<sup>16</sup> made a study of the kinetics of crosslinking by formaldehyde and glyoxal, using viscosity as the criterion of the degree of crosslinking. They found that the reaction rate was influenced by gelatin concentration, formaldehyde concentration and pH. Robinson<sup>17</sup> measured the rate of crosslinking by means of a gelation timing device and found that the rate increased with temperature.

Davis and Tabor<sup>16</sup> suggested that the crosslinking reaction took place between the side-chain amino group of one gelatin molecule and a group containing an active hydrogen, probably hydroxyl, on a second gelatin molecule, leading to the formation of methylene ether bridges, which might subsequently be reorganized to become more stable methylene bridges. The amino groups of the polypeptide backbone are not involved in these reactions, which probably involve only lysine, hydroxylysine, arginine, asparagine, and glutamine residues.<sup>18,19</sup>

In a previous investigation of the behavior of gelatin films<sup>20</sup> it was found that the rotation of the films having more than 1% formaldehyde (by dry weight of gelatin) was considerably lower than that of unhardened films, and the rotation fell in proportion to the amount of formaldehyde present. This result has important implications for the study of the molecular be-

havior of gelatin. Clearly, covalent crosslinks above a certain concentration seriously hinder the assumption of the collagen fold. In an unhardened gel the intermolecular crosslinks are formed initially by hydrogen bonds. Where the conditions are favorable, that is where there is a sufficiently high proline-hydroxyproline content, formation of the collagen fold takes place, thus stabilizing the crosslinks. Where conditions are unfavorable, the crosslinks will remain weak and easily broken, enabling rearrangement to more favorable positions to take place. However, when hardener has been added to a gelatin solution it will form stable crosslinks between chain segments which may not be suitably aligned for collagen-fold formation. While the number of such crosslinks is small there will be little effect on the growth of collagen fold, but as the number increases there will be greater restrictions on the freedom of movement of the polypeptide chains, impairing their ability to form the collagen fold.

This phenomenon deserves further study, since it is so closely related to the degree of order attained by gelatin gels, a factor of great importance in determining the physical properties of gelatin films.<sup>21,22</sup> For the present study solutions rather than films were chosen, as they are simpler systems. The experiments described study optical rotation changes over periods of up to 4 days. In no case does the reaction go to completion, since that would require a period of impracticable duration. The work is an attempt to discover more about the mechanism of the formaldehyde hardening process, and in particular to obtain a better knowledge of the way in which hardening influences the growth of ordered structure in the gel.

## EXPERIMENTAL

### Materials

The gelatin used in most of this work was a lime process calfskin gelatin, pH 5.7, referred to subsequently as gelatin 1. Another gelatin, gelatin 2, consisting of a blend of 16% lime process calfskin and 84% lime process ossein, pH 6.3, was used in a small number of experiments, where indicated. Previous experience indicates that the two gelatins behave in a similar manner, and it is assumed that the results from the one are broadly applicable to the other.

### Procedure

The optical rotation measurements were made by using a Bellingham and Stanley Model A Polarimeter with sodium lamp source. The light passed through a filter before entering the polariser. The polarimeter readings were reproducible to within  $\pm 0.01^\circ$ . The measurements were made with the samples in water-jacketed observation tubes which were kept at temperatures constant to within  $\pm 0.1^\circ\text{C}$ .

Viscosity measurements were made with Ostwald viscometers temperature controlled to within  $\pm 0.1^\circ\text{C}$ .

TABLE I  
Optical Rotation of 5% Solutions of Gelatin 1 as a Function  
of Time, Temperature, and Formaldehyde Concentration

Sample no.	Temperature, °C	Formaldehyde concn, %	Time, min	Specific levorotation, degrees			
1	20	0	15	174.3			
			45	193.6			
			135	202.9			
			165	205.2			
			195	206.7			
			225	207.8			
			255	209.2			
			285	209.8			
			315	211.1			
			1335	222.5			
			2	20	2.0	15	171.7
45	188.2						
75	193.8						
105	197.4						
135	199.2						
165	201.3						
255	205.0						
285	206.3						
315	207.5						
375	208.9						
405	209.0						
3	20	5.0	15	164.1			
			45	183.0			
			75	190.3			
			105	192.9			
			135	194.9			
			225	198.8			
			255	200.1			
			285	200.9			
			315	201.7			
			345	202.0			
			375	202.4			
4	25	0	15	147.3			
			45	153.0			
			75	156.0			
			165	161.3			
			225	163.3			
			285	165.4			
			315	165.4			
			345	164.6			
			1365	178.3			
			5	25	2.0	15	147.3
						45	151.3
75	153.9						
165	158.5						

TABLE I (continued)

Sample no.	Temperature, °C	Formaldehyde concn, %	Time, min	Specific levorotation, degrees
			195	159.8
			225	160.7
			285	162.3
			315	162.8
			345	163.6
			1335	171.9
6	25	5.0	25	146.5
			45	148.9
			75	151.2
			105	153.2
			135	154.0
			225	156.2
			255	157.1
			280	157.8
			345	158.4
			375	158.9
			1395	168.1
7	30	0	35	138.4
			60	139.0
			90	139.1
			130	139.4
			155	139.3
			210	139.4
			240	139.5
			270	139.8
			300	139.7
			330	139.7
			360	140.0
			390	140.2
			420	140.4
8	30	2.0	15	135.4
			45	136.9
			75	136.9
			135	137.0
			165	137.0
			195	137.3
			225	137.1
			255	137.4
			285	137.4
			315	137.3
			345	137.4
			1305	137.9
			1335	137.6
9	30	5.0	15	136.9
			45	137.4
			75	137.6
			150	138.3
			180	138.4

(continued)



TABLE I (continued)

Sample no.	Temperature, °C	Formaldehyde concn, %	Time, min	Specific levorotation, degrees
			210	138.1
			240	138.4
			270	138.1
			300	138.2
			330	138.5
			360	138.2
			1320	138.6
10	35	0	15	134.5
			45	134.6
			75	134.9
			135	134.9
			165	135.1
			195	135.5
			225	135.7
			255	135.3
			285	135.6
			315	136.2
			1355	137.9
			1395	138.1
11	35	2.0	15	134.4
			45	134.3
			75	134.1
			135	134.0
			165	133.9
			195	134.0
			255	133.9
			285	133.9
			315	133.6
			1335	134.5
			1395	134.3
12	35	5.0	15	133.2
			45	134.8
			75	135.0
			135	134.9
			165	135.0
			195	134.9
			255	134.8
			285	134.9
			315	134.8
13	40	0	15	134.8
			45	134.9
			75	134.9
			165	134.8
			195	135.2
			225	135.2
			285	135.5
			315	136.0
			345	135.9
			1365	139.2
			1425	139.3

TABLE I (continued)

Sample no.	Temperature, °C	Formaldehyde concn, %	Time, min	Specific levorotation, degrees			
14	40	2.0	15	133.1			
			45	132.9			
			75	132.8			
			135	132.9			
			180	133.3			
			210	133.3			
			270	133.5			
			300	133.6			
			330	133.8			
			1350	137.0			
			1410	137.0			
			15	40	5.0	15	131.5
						45	131.4
75	131.6						
135	131.6						
165	131.4						
195	131.2						
225	131.7						
255	131.6						
285	131.8						
315	131.5						
1335	131.6						
16	45	0	15	130.5			
			45	130.5			
			75	130.9			
			105	130.9			
			135	131.1			
			165	131.4			
			255	131.9			
			285	132.2			
			315	132.7			
			345	134.2			
			375	135.2			
			405	136.4			
			435	133.4			
1425	135.0						
17	45	2.0	15	132.1			
			45	132.4			
			75	132.3			
			105	132.3			
			135	132.3			
			165	132.6			
			225	132.4			
			285	132.5			
			315	132.4			
			345	132.5			
			375	132.7			
			405	132.7			
			435	132.7			
1395	132.8						

(continued)

TABLE I (continued)

Sample no.	Temperature, °C	Formaldehyde concn, %	Time, min	Specific levorotation, degrees
18	45	5.0	15	130.9
			45	130.8
			75	130.8
			105	130.9
			135	130.8
			165	130.8
			255	130.9
			285	130.9
			315	130.9
			345	130.8
			375	130.9
			405	130.7
			435	130.9
			19	50
45	130.5			
75	130.5			
105	130.5			
135	130.7			
165	130.8			
1140	135.5			
1170	135.8			
1215	136.1			
1245	136.2			
1275	136.4			
1305	136.4			
1425	137.3			
1455	137.3			
1485	137.4			
1545	137.4			
1605	137.5			
2580	140.9			
2610	141.0			
2640	141.2			
2700	141.2			
2760	141.2			
2850	141.4			
2955	141.8			
2985	142.0			
3045	142.3			
4020	145.5			
4050	145.5			
4110	145.6			
4170	145.6			
4200	145.7			
4290	145.7			
4335	145.7			
4395	145.9			
4425	146.0			

TABLE I (continued)

Sample no.	Temperature, °C	Formaldehyde concn, %	Time, min	Specific levorotation, degrees
			4485	145.9
			5460	147.8
			5520	147.9
			5550	147.9
			5580	148.1
20	50	2.0	15	129.9
			45	130.3
			75	130.3
			165	129.9
			195	129.5
			225	129.5
			285	129.1
			315	129.1
			345	129.1
			1335	130.7
			1365	131.1
			1425	131.5
			1485	131.5
			1575	131.5
			1605	131.5
			1635	131.9
			1665	131.9
			1725	131.9
			1755	131.9
			2760	133.5
			2790	133.5
			2850	133.5
			2895	133.9
			2955	133.9
			3045	133.1
			3075	133.1
			3105	133.1
			3165	133.1
			3195	133.5
			3225	133.5
			4200	135.1
			4230	134.7
			4290	134.7
			4335	135.1
			4365	135.1
			4485	135.1
			4515	135.1
			4545	135.1
			4605	135.1
			4635	135.5
			5640	136.7
			5670	136.3

(continued)

TABLE I (continued)

Sample no.	Temperature, °C	Formaldehyde concn, %	Time, min	Specific levorotation, degrees
			5730	136.3
			5775	136.3
			5865	136.7
			5895	136.3
			5985	137.1
21	50	5.0	15	127.9
			45	127.9
			75	128.3
			165	128.7
			195	128.3
			225	128.3
			285	128.3
			315	128.3
			1335	127.1
			1365	127.1
			1425	127.1
			1455	127.5
			1485	127.5
			1515	127.5
			1605	127.5
			1635	127.5
			1665	127.5
			1725	127.5
			1785	127.5
			2760	126.7
			2790	126.7
			2850	127.1
			2895	126.7
			2925	126.7
			2955	126.7
			3105	127.5
			3165	127.1
			4200	126.7
			4230	126.7
			4290	126.7
			4335	126.7
			4395	127.1
			4485	127.1
			4515	127.1
			4554	127.5
			5605	127.5
			4665	127.1
			5670	127.1
			5700	127.1
			5730	127.1
			5865	127.1
			5895	127.1
			5925	127.1

The gelatin samples were soaked in distilled water for at least 2 hr and dissolved by heating to 50°C. The appropriate amounts of formaldehyde were then added. The solutions were placed in the observation tubes and left to equilibrate for 15 min before the first readings were made.

## RESULTS

Optical rotation measurements were made on 5% solutions of gelatin 1 containing 0, 2, and 5% formaldehyde (based on the oven-dried weight of gelatin) at temperatures of 20, 25, 30, 35, 40, 45, and 50°C. Measurements were made at various intervals over a period of 24 hr, zero time being taken as the moment the samples were placed in the observation tube (Table I). At 50°C the measurements were extended to 4 days, because of the slow rate of change at this temperature.

An experiment was carried out to examine the reversibility of the growth of optical rotation. 5% of solutions of gelatin 2 containing 0, 1, 2, and 5% formaldehyde were prepared as described above and held at 20°C for 24 hr, the optical rotation being read at intervals. The temperature was raised to 50°C for 30 min; at the end of that period the rotation was read, and the temperature dropped back to 20°C. After a further 15 min the readings were begun again, and continued for another 24 hr. The results are shown in Fig. 1, except for the  $[\alpha]_D$  values measured at 50°C, which are shown in Table II. The results obtained with 1% formaldehyde are not shown, as they were indistinguishable from those from the unhardened sample.

TABLE II  
Optical Rotation of 5% Gelatin 2 held at 50°C for 30 Min  
after 24 hr at 20°C as a Function of Formaldehyde Content

Formaldehyde concn, %	Specific levorotation, degrees
0	131
1	132
2	133
5	133

The effect of potassium thiocyanate on the optical rotation was also investigated. Optical rotation measurements were carried out on 5% gelatin 2 in water and 0.1M potassium thiocyanate solution, without formaldehyde (Fig. 2). Viscosity measurements were made on 5% gelatin 2 in water and 0.1M potassium thiocyanate containing 0 and 5% formaldehyde. The measurements were carried out at 30°C, after attempts to make them at 20°C failed owing to the rapidity of gelation at that temperature (Fig. 3).

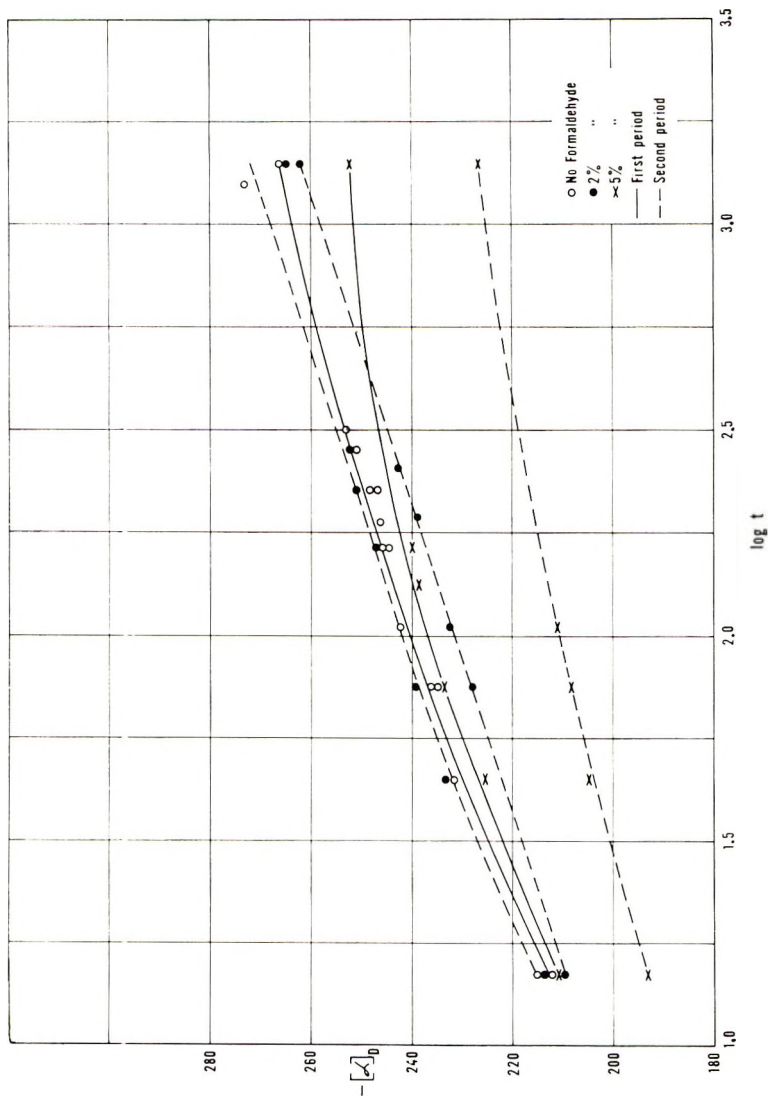


Fig. 1. Variation of specific rotation with logarithm of time (in minutes) for 5% gelatin solution with 0, 2, and 5% formaldehyde for two 24-hr periods at 20°C. Prior to the second period the sample has been heated to 50°C for 30 min. Gelatin 2.

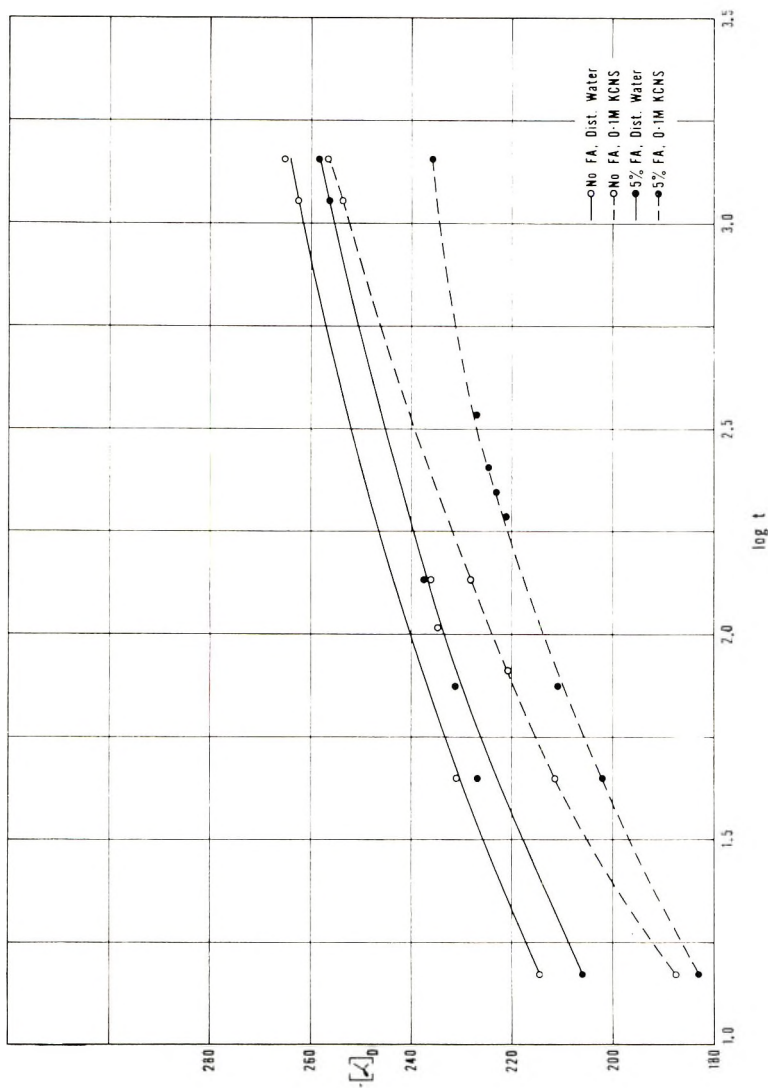


Fig. 2. Variation of specific rotation with logarithm of time (in minutes) for 5% gelatin solutions in water and 0.1M potassium thiocyanate, with 0 and 5% formaldehyde, at 20°C. Gelatin 2.



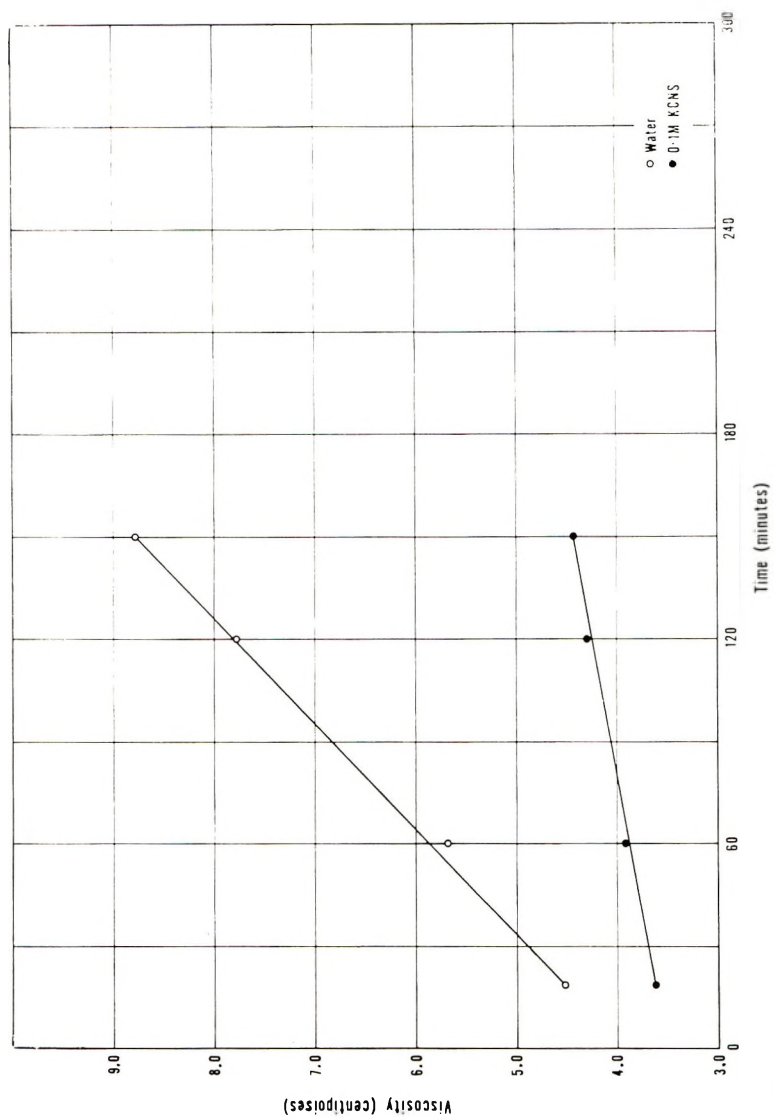
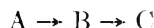


Fig. 3. Variation of viscosity with time for 5% gelatin solutions in water and 0.1M KCNS, at 30°C. Gelatin 2.

## DISCUSSION

## Kinetics of Helix Formation

As the specific rotation of gelatin is a function of the helical content, it might be expected that the change in rotation would be amenable to analysis on the basis of reaction kinetics. Consequently, an attempt was made to fit the experimental data to a variety of reaction mechanisms. A single reaction of first, second, or third order, a reversible equilibrium reaction, and a first-order series reaction



were all tested without success. More complex reactions would be difficult to analyse with the available data. Finally, an empirical approach was adopted and the data fitted to expressions of the form:

$$-[\alpha]_D = b_0 + b_1t + b_2t^2 + b_3t^3 \quad (1)$$

where  $b_0, b_1, b_2, b_3$  are constants,  $[\alpha]_D$  is the specific levorotation in degrees, and  $t$  is the time in hours. The curve fitting was carried out by means of curvilinear regression with the aid of an IBM 360 computer. As some of the

TABLE III  
Values of Constants from the Equation<sup>a</sup>

$$-[\alpha]_D = b_0 + b_1t + b_2t^2 + b_3t^3$$

Sample no.	Temperature, °C	Formal-dehyde concn, %	$b_0$	$b_1$	$b_2$	$b_3$
1	20	0	169.9	31.403	-8.938	0.8561
2	20	2	170.1	22.363	-4.600	0.3160
3	20	5	161.2	28.296	-6.553	0.4907
4	25	0	145.5	10.275	-1.906	0.1243
5	25	2	145.6	8.378	-1.637	0.1270
6	25	5	144.0	7.292	-1.435	0.1045
7	30	0	138.0	1.0011	-0.2355	0.02024
8	30	2	135.4	1.6495	-0.4715	0.04330
9	30	5	136.6	1.2324	-0.2915	0.02226
10	35	0	134.3	0.5128	-0.1227	0.01655
11	35	2	134.6	-0.6228	0.2138	-0.02461
12	35	5	132.3	2.6071	-0.9192	0.09492
13	40	0	134.9	-0.1564	0.07143	-0.00187
14	40	2	133.2	-0.5039	0.2302	-0.02186
15	40	5	131.5	-0.1072	0.04266	-0.00357
16	45	0	130.2	0.3999	0.00588	0
17	45	2	132.1	0.1995	-0.04638	0.00443
18	45	5	130.9	-0.05591	0.02052	-0.00193
19	50	0	130.2	0.3016	-0.00120	0
20	50	2	129.4	0.0787	0.00007	0
21	50	5	128.4	-0.0558	0.00068	0

<sup>a</sup>  $t$  is time in hours, calculated by curvilinear regression by using the data in Table I.

observations were taken only over 8 hours, data covering longer times than this were omitted from the calculations in order to obtain comparable results. Exceptions to this were the 50°C observations, for which the full 4 days data were used. The results are shown in Table III.

The constants in Table III for 20°C to 30°C show a reasonably consistent pattern. In those from the 35, 40, and 45°C series, the rotation changes are so small that the significant pattern may be disguised by experimental error. The 50°C data are not in the same category because they were taken over a much longer period and so show more readily discernible trends.

### Helix Formation in Unhardened Gelatin Solutions

Both the absolute optical rotation and the rate of change fall steadily as the temperature rises. The greatest change occurs between 20°C and 30°C; above the latter temperature the differences between the curves at successive temperature intervals are not great. It is interesting that even at 50°C there is a steady, although very slow, rise in the value of  $[\alpha]_D$  with time. The measurements at 50°C were taken over a much longer time than those at lower temperatures, 4 days instead of 24 hr, in order to confirm this behavior. The growth of optical rotation at 50°C is rather puzzling, since this temperature is higher than the melting point of the gel and viscosity measurements at this temperature and gelatin concentration show no evidence of intermolecular crosslinking over periods of several hours. Apparently, under the stable conditions in the polarimeter observation tube, the interchain interactions are strong enough to slowly establish a low degree of order. In order to survive, a crosslink has to be considerably stronger at 50°C than at temperatures at which gels are stable, i.e., a greater number of hydrogen bonds would have to be established. The probability of these bonds forming is lower, but still significant. It may be noted that the polynomial constants for the 50°C sample indicate a simpler pattern than those at lower temperatures, almost a linear relationship. This seems to indicate that the mechanism of helix formation is less complex than at lower temperatures.

### Effect of Formaldehyde on Helix Formation

The optical rotation data for gelatin solutions with 2 and 5% formaldehyde (expressed as percentages of the amount of gelatin, by weight) show a variation with time similar to that of the unhardened samples.

The lowering of the rate of helix formation by formaldehyde occurs at all temperatures covered by the experiments. Melting the gel by heating, followed by recooling, leads to even greater reductions in optical rotation with 2% and 5% formaldehyde hardened samples (Fig. 1). When the gel is melted, all samples, hardened and unhardened, returned to much the same specific rotation, viz., between  $-131$  and  $-133^\circ$ . The formaldehyde crosslinks between gelatin chains are quite stable at 50°C, and so when the

hardened solutions are recooled there will be an already formed network of formaldehyde crosslinks, which hinder helix formation to a greater degree than they did initially, when few formaldehyde crosslinks had formed.

It is apparent that under normal circumstances formaldehyde hinders helix formation. When the natural crosslinking process is diminished, e.g., by using 0.1*M* potassium thiocyanate solution, the growth of helix structure is also diminished (Fig. 2). This might be expected with unhardened gelatin solutions, but if one compares the 0 and 5% formaldehyde samples in thiocyanate solution, it is interesting that even with the additional crosslinking provided by formaldehyde, which presumably will bring together some natural crosslinking sites, the hardened samples still have lower rotations than the unhardened samples. The degree by which the thiocyanate reduces the natural (hydrogen-bonded) crosslinking is demonstrated by viscosity data (Fig. 3).

The form of the rotation-time relationship for gelatin solutions containing formaldehyde is similar to that of unhardened solutions, except for those cases in which there is very little change in rotation (5% formaldehyde at the higher temperatures). This suggests that formaldehyde crosslinking merely reinforces a mechanism existing in unhardened gelatin solutions, presumably the retarding effect of steric hinderance on helix formation.

### Mechanism of Formaldehyde Crosslinking

Formaldehyde appears to adversely affect the formation of the collagen fold when present in greater quantities than about 1% of the weight of gelatin. It may be instructive therefore to consider the situation resulting from the crosslinking action of this amount of gelatin. The amino acid compositions of the gelatins used in this work are not known at present, but it may be assumed that they are similar to that of ox skin collagen given by Eastoe and Leach<sup>23</sup> with perhaps a somewhat lower arginine content. By using these data it can be calculated that 1% formaldehyde, if all of it reacted, and if only one molecule of it was required per crosslink, would form crosslinks involving 6% of all residues. If two molecules of formaldehyde are required to produce a crosslink,<sup>16</sup> then 3% of all residues would be involved.

If formaldehyde reactions with amino groups are limited to lysine, hydroxylysine, arginine, asparagine, and glutamine, as has been suggested,<sup>18,19</sup> then formaldehyde crosslinks will be somewhat localized. Polar residues, such as the abovementioned tend to be segregated from apolar residues in the gelatin molecule.<sup>24</sup> The second stage of the reaction, i.e., with the hydroxyl group, might take place either with a polar or apolar residue. It has been suggested<sup>7</sup> that the polar segments are the preferred sites for the initial hydrogen-bonded crosslinks, and that from these segments helix formation spreads to neighboring pyrrolidine-rich apolar regions. A substantial proportion of formaldehyde crosslinking could well interfere with this natural aligning process.

Assuming the amino acid composition already mentioned it can be estimated that it would require 2.5% formaldehyde to react with all the lysine, hydroxylysine, and arginine present in the molecules (asparagine and glutamine not being present in significant proportions). However, if an additional molecule of formaldehyde was required to complete each crosslink, then 5% formaldehyde would be absorbed by the crosslinking process before saturation was reached. With 5% formaldehyde in a solution the optical rotation undergoes no rise whatever at 40°C and over. Apparently the reaction rate, which rises with temperature, at 40°C produces enough crosslinks to prevent any significant helix formation. However, with 2% formaldehyde, the rotation still changes at a quite appreciable rate, even at 50°C, and its effect at this temperature appears to be no greater than at 40°C.

Using Robinson's<sup>17</sup> equation relating the crosslinking rate constant  $k_1$  and temperature,

$$k_1 = Ze^{-E_a/RT}$$

where,  $Z$  is the frequency factor,  $T$  is absolute temperature,  $R$  is the gas constant, and  $E_a$  is activation energy, and taking the value of  $E_a$  as 17,350 cal/mole, it can be calculated that at 50°C the crosslinking rate will be more than twice that at 40°C. Consequently, it may be assumed that 2% formaldehyde reacts completely with the gelatin at 40°C. However, it is clear that considerably more formaldehyde is required to completely inhibit helix formation. If two molecules of formaldehyde were involved per crosslink, then 5% formaldehyde would be required to fully react with the available sites. This corresponds to the experimental evidence.

The author wishes to thank A. D. Envall for preparing the computer program and Mrs. Anita Infanti for technical assistance.

### References

1. J. D. Ferry and J. E. Eldridge, *J. Phys. Colloid Chem.*, **53**, 184 (1949).
2. P. H. von Hippel and W. F. Harrington, *Biochim. Biophys. Acta*, **36**, 427 (1959).
3. P. J. Flory and E. S. Weaver, *J. Amer. Chem. Soc.*, **82**, 4518 (1960).
4. J. Engel, *Arch. Biochem. Biophys.*, **97**, 150 (1962).
5. K. A. Piez and A. L. Carrillo, *Biochemistry*, **3**, 908 (1964).
6. K. Altgelt, A. J. Hodge, and F. O. Schmitt, *Proc. Nat. Acad. Sci. U. S.*, **47**, 1914 (1961).
7. A. Veis and J. Schnell, in *Symposium on Fibrous Proteins Australia 1967*, W. G. Crewther, Ed., Butterworths, Australia 1968, p. 193.
8. J. E. Eldridge and J. D. Ferry, *J. Phys. Chem.*, **58**, 992 (1954).
9. H. Boedtker and P. Doty, *J. Phys. Chem.*, **58**, 968 (1954).
10. J. D. Ferry, *Advan. Protein Chem.*, **4**, 1 (1948).
11. J. W. Janus, B. E. Tabor, and R. L. R. Darlow, *Kolloid-Z.*, **205**, 134 (1965).
12. A. Yaron and A. Berger, *Bull. Res. Council Israel*, **A10**, 46 (1961).
13. P. M. Cowan, S. McGavin, and A. C. S. North, *Nature*, **176**, 1062 (1955).
14. J. Pouradier, *J. Chim. Phys.*, **64**, 1616 (1967).
15. H. Fraenkel-Conrat and H. S. Olcott, *J. Amer. Chem. Soc.*, **70**, 2673 (1948).
16. P. Davis and B. E. Tabor, *J. Polym. Sci. A*, **1**, 799 (1963).

17. I. D. Robinson, *J. Appl. Polym. Sci.*, **8**, 1903 (1964).
18. R. A. Milch, *Nature*, **205**, 1108 (1965).
19. A. Veis and M. P. Drake, *J. Biol. Chem.*, **238**, 2003 (1963).
20. I. H. Coopes, *J. Polym. Sci. A-1*, **6**, 1991 (1968).
21. M. F. Johnson and N. Blonowicz, private communication.
22. H. G. Curme, P. Costich, W. Fellows, M. F. Johnson, W. O. Kamm, H. Otto, and E. P. Przytylowicz, private communication.
23. J. E. Eastoe and A. A. Leach, in *Recent Advances in Gelatin and Glue Research*, G. Stainsby, Ed., Pergamon Press, New York, 1958, p. 173.
24. A. Veis, *The Macromolecular Chemistry of Gelatin*, Academic Press, New York-London, 1964, p. 206.

Received October 28, 1969

Revised November 26, 1969

## Polymerization of Sodium 2-Sulfoethyl Methacrylate in Aqueous Solution

D. A. KANGAS, *Edgar C. Britton Research Laboratory, The Dow Chemical Company, Midland, Michigan 48640*

### Synopsis

The rate of sodium 2-sulfoethyl methacrylate ( $\text{SEM}^{\ominus}\text{Na}^{\oplus}$ ) polymerization in aqueous solution was measured as a function of temperature, ionic strength,  $\text{K}_2\text{S}_2\text{O}_8$ , and  $\text{SEM}^{\ominus}\text{Na}^{\oplus}$  concentration. The ratio of rate constants,  $k_p k_t^{-1/2} (fk_d)^{1/2}$ , increases with decreasing ionic strength. Because  $\text{SEM}^{\ominus}\text{Na}^{\oplus}$  is itself an ionic salt, the ratio of polymerization rate constants increases with decreasing monomer concentration. The change in ratio of rate constants as a function of ionic strength can be described by an equation derived from the limiting form of the Debye-Hückel theory. The value of the effective ionic charge on the polymeric growing radical is 3, as calculated by means of the derived equation.

### INTRODUCTION

The anionic vinyl monomer 2-sulfoethyl methacrylate (SEM) easily forms high molecular weight water-soluble polymers and copolymers by free-radical polymerization in water solution.<sup>1</sup> The polymers may be flocculants or surface active depending upon molecular weight and composition.

Since SEM is ionized in aqueous solution, its rate of polymerization may be affected by the anionic charge on the monomer and the growing polymer radical. For example, the decrease in rate of methacrylic acid polymerization with increasing pH<sup>2-4</sup> and the formation of syndiotactic poly(methacrylic acid) at high pH<sup>5</sup> have been attributed to ionic repulsion between monomer and growing polymer radical.

Purified solutions of the sodium salt of SEM,  $\text{SEM}^{\ominus}\text{Na}^{\oplus}$ , at pH 5 were used for rate measurements because SEM undergoes acid-catalyzed hydrolysis in aqueous solutions of the sulfonic acid. Aqueous solutions of SEM salts are stable to hydrolysis at pH's between 3 and 8. Since SEM is a strong acid, its rate of polymerization would not be expected to be a function of pH as is the case with methacrylic acid.

### EXPERIMENTAL

Solutions of  $\text{SEM}^{\ominus}\text{Na}^{\oplus}$  were purified by treatment with hydrous  $\text{ZrO}(\text{OH})_2$  followed by treatment with activated charcoal.<sup>6</sup> Impurities which initiate polymerization are completely removed by the purification process.

The monomer solutions did not contain polymer after heating overnight at 60°C in the absence of O<sub>2</sub>.

Other reagents such as K<sub>2</sub>S<sub>2</sub>O<sub>8</sub>, NaNO<sub>3</sub>, and KCl were reagent-grade chemicals obtained from stock.

Polymerization rate measurements in concentrated solutions of SEM<sup>⊖</sup>Na<sup>⊕</sup>, which become very thick at low conversion, were made in a recording dilatometer as described by Rubens.<sup>7</sup> The procedure for polymerization rate measurement in the dilatometer was as follows.

The SEM<sup>⊖</sup>Na<sup>⊕</sup> solution at the concentration desired was deaerated by evacuating and repressuring with N<sub>2</sub> three times. The deaerated monomer solution was transferred to a poly(vinyl fluoride) film bag. During the transfer the solution was protected from air by a stream of N<sub>2</sub>. The required amount of K<sub>2</sub>S<sub>2</sub>O<sub>8</sub> solution was added, and a sample taken for unsaturation analysis by the bromate-bromide titration method. The film bag containing the polymerization charge was sealed in the dilatometer in such a manner as to exclude all bubbles from the bag.

The dilatometer was filled with mercury through the bottom filling valve by means of a leveling bulb. The filled dilatometer was placed in a water bath which was thermostatted at the desired temperature.

The loading procedure and warm-up time in the bath was accomplished in 5 min. Initial time was taken after the dilatometer reached temperature in the bath. Initial monomer concentration was calculated from the unsaturation analysis.

The drop in mercury level in the capillary was automatically recorded as a function of time. After the polymerization was essentially complete, the film bag containing the polymerization charge was removed from the dilatometer. The final monomer concentration was calculated from unsaturation analysis of the polymerized solution by the bromate-bromide titration method.

A factor to convert the recorded drop of mercury level in the capillary to monomer concentration was calculated by dividing the difference in initial and final monomer concentration by the total drop in mercury level.

The small shrinkage resulting from polymerizing SEM<sup>⊖</sup>Na<sup>⊕</sup> in solutions of less than 0.5*M* concentrations cannot be accurately measured by the recording dilatometer. However, the dilute solutions remain fluid at high conversion of monomer to polymer so that monomer concentration can be determined on samples removed from a flask. Flask polymerizations were carried out in the following manner.

The flask used for polymerizations was 250 ml capacity with three spherical ground glass joints and a glass tubing nipple. The flask was equipped with a glass stirrer, reflux condenser, thermometer and a N<sub>2</sub> sparging tube. The glass tubing nipple was closed with a rubber serum cap through which samples could be removed or catalyst added with a hypodermic needle. A thermostatted water bath was used to control polymerization temperature. For the dilute solutions of SEM<sup>⊖</sup>Na<sup>⊕</sup> polymerized in the flask, there was no increase in temperature during the reaction.



Water and  $\text{SEM}^{\ominus}\text{Na}^{\oplus}$  solution were placed in the flask and purged with  $\text{N}_2$  to remove dissolved  $\text{O}_2$ . The  $\text{N}_2$  used for sparging was washed through alkaline pyrogallol solution to remove traces of  $\text{O}_2$ . Polymerizations were started by adding  $\text{K}_2\text{S}_2\text{O}_8$  solution with a hypodermic syringe. Samples were withdrawn periodically by means of a hypodermic syringe and unsaturation determined by the bromate-bromide titration method. Sample time was measured from the time of injection of  $\text{K}_2\text{S}_2\text{O}_8$  solution to the time of injection of the sample into a flask for determination of unsaturation.

### RATE EXPRESSION FOR $\text{SEM}^{\ominus}\text{Na}^{\oplus}$ POLYMERIZATION

The initial rate of disappearance of  $\text{SEM}^{\ominus}\text{Na}^{\oplus}$  was found to be first-order with respect to  $\text{SEM}^{\ominus}\text{Na}^{\oplus}$  concentration as indicated by linearity of plots of  $\ln[\text{SEM}^{\ominus}\text{Na}^{\oplus}]$  versus time.

From the rate expression for free radical-initiated polymerization of a single monomer,<sup>8a</sup> the following equation can be written:

$$R_0/[\text{SEM}^{\ominus}\text{Na}^{\oplus}]_0 = [(k_p/k_t^{1/2})(fk_d^{1/2})][\text{K}_2\text{S}_2\text{O}_8]_0^{1/2} \quad (1)$$

where  $R_0$  = initial rate of monomer disappearance (mole/l.-sec);  $[\text{SEM}^{\ominus}\text{Na}^{\oplus}]_0$  = initial monomer concentration (mole/l.);  $[\text{K}_2\text{S}_2\text{O}_8]_0$  = initial

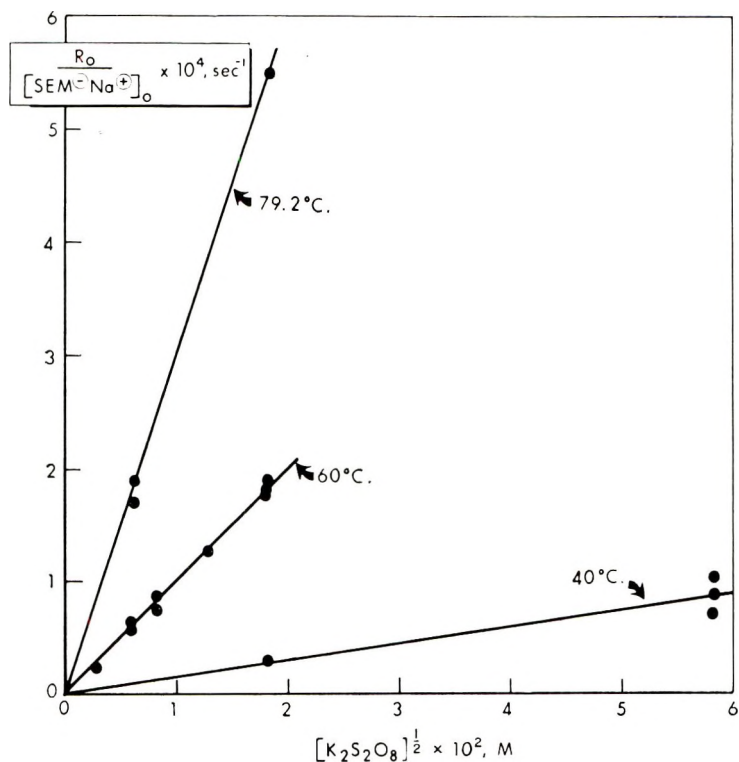


Fig. 1. Rate of  $\text{SEM}^{\ominus}\text{Na}^{\oplus}$  polymerization as a function of  $\text{K}_2\text{S}_2\text{O}_8$  concentration.

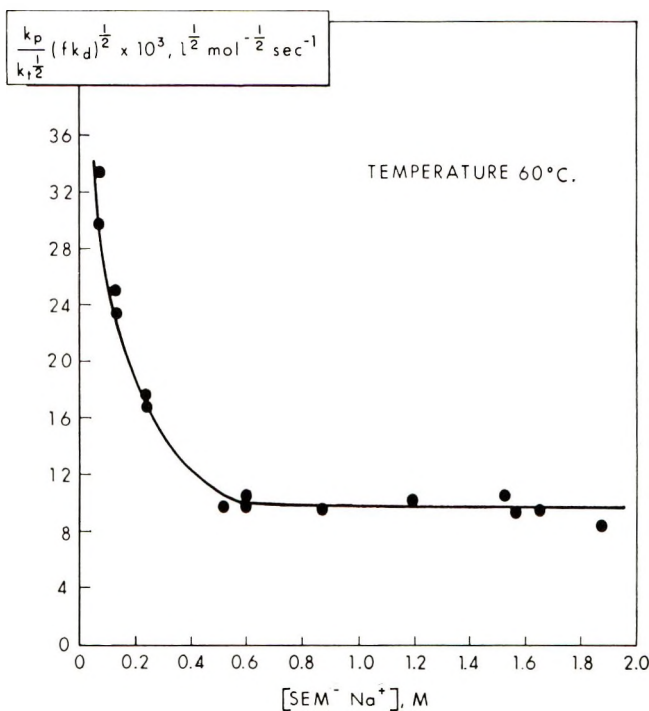


Fig. 2. Ratio of  $\text{SEM}^{\ominus}\text{Na}^{\oplus}$  polymerization rate constants,  $(k_p/k_t)(fk_d)^{1/2}$ , as a function of monomer concentration.

initiator concentration (mole/l.);  $k_p$  = rate constant of propagation reaction (l./mole-sec);  $k_t$  = rate constant of termination reaction (l./mole-sec);  $f$  = fraction of initiator radicals which initiate polymer chains;  $k_d$  = rate constant for initiator decomposition ( $\text{sec}^{-1}$ ).

Graphs of  $R_0/[\text{SEM}^{\ominus}\text{Na}^{\oplus}]_0$  as function of  $[\text{K}_2\text{S}_2\text{O}_8]_0^{1/2}$  are shown in Figure 1 for  $\text{SEM}^{\ominus}\text{Na}^{\oplus}$  polymerizations run at concentrations greater than  $0.5M$  with  $\text{K}_2\text{S}_2\text{O}_8$  initiator at temperatures of 40, 60, and  $79.2^\circ\text{C}$ . Since the plots are linear with intercept at zero initiator concentration, the ratio of rate constants  $k_p k_t^{-1/2} (fk_d)^{1/2}$ , can be calculated by means of eq. (1) by using  $R_0$  from data of  $\text{SEM}^{\ominus}\text{Na}^{\oplus}$  concentration as a function of time and initial  $\text{K}_2\text{S}_2\text{O}_8$  concentration.

The value of the ratio of rate constants for  $\text{K}_2\text{S}_2\text{O}_8$ -initiated polymerizations at  $60^\circ\text{C}$  is plotted as a function of monomer concentration in Figure 2.

TABLE I  
Effect of Ionic Strength on the Ratio of Polymerization Rate Constants

$\text{SEM}^{\ominus}\text{Na}^{\oplus}$ , M	$\text{NaNO}_3$ , M	Ionic strength, $\mu$	$k_p k_t^{-1/2} (fk_d)^{1/2}$ , $\text{l.}^{1/2}/\text{mole}^{1/2}\text{-sec}^{1/2}$
0.120	—	0.120	$23.4 \times 10^{-3}$
0.107	1.00	1.107	$11.9 \times 10^{-3}$
1.195	—	1.195	$10.4 \times 10^{-3}$

Although the initial points for each run produced a linear plot of  $\ln[\text{SEM}^\ominus\text{Na}^\oplus]$  as a function of time, indicating first-order dependence of polymerization rate on monomer concentration, the value of the ratio of rate constants increases with decreasing  $\text{SEM}^\ominus\text{Na}^\oplus$  concentration.

The addition of a neutral salt, such as  $\text{NaNO}_3$ , reduced the rate parameter to approximately the same value as an equivalent amount of  $\text{SEM}^\ominus\text{Na}^\oplus$  as shown in Table I.

The fact that  $\text{NaNO}_3$  is equivalent to  $\text{SEM}^\ominus\text{Na}^\oplus$  in reducing the ratio of polymerization rate constants indicates that solution ionic strength is involved rather than a specific reaction of  $\text{SEM}^\ominus\text{Na}^\oplus$ . Since  $\text{SEM}^\ominus\text{Na}^\oplus$  is itself an ionic salt the ratio of rate constants is also a function of monomer concentration, as shown in Figure 2. Because the ratio of rate constants  $k_p k_t^{-1/2} (f k_d)^{1/2}$  increases in dilute solution, the termination reaction rate constant  $k_t$  must be smaller relative to the propagation reaction rate constant  $k_p$  in dilute solution than it is in concentrated salt solution. This effect is attributed to a greater ionic repulsion between the growing poly( $\text{SEM}^\ominus\text{Na}^\oplus$ ) radical involved in the termination reaction than between the  $\text{SEM}^\ominus\text{Na}^\oplus$  monomer and the growing poly( $\text{SEM}^\ominus\text{Na}^\oplus$ ) involved in the propagation reaction.

An equation describing the effect of ionic strength on the ratio of rate constants can be derived as follows.

The effect of ionic strength on the rate constant for a reaction between two ions in solution is approximately described by the simplified equation, eq. (2), which is derived from the Debye-Hückel theory of dilute electrolyte solutions:<sup>9</sup>

$$\ln k = \ln k_0 + 2Z_a Z_b \alpha \mu^{1/2} \quad (2)$$

where  $k$ ,  $k_0$  are reaction rate constants at ionic strength  $\mu$  and zero ionic strength, respectively;  $Z_a$  and  $Z_b$  are valences of reacting ions,  $\mu$  is the ionic strength, and  $\alpha$  is a constant for a given solvent and temperature.

The ionic reactions involved in each step of  $\text{SEM}^\ominus\text{Na}^\oplus$  polymerization are shown in the eqs. (3)–(5)

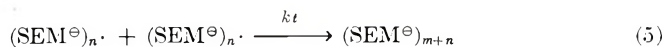
Initiation:



Propagation:



Termination:



The initiation reaction rate constant  $k_i$  appears in the polymerization rate expression, eq. (1), as  $f$ , the fraction of initiator radicals which initiate polymer chains. The effect of ionic strength on the efficiency of initiation is described by the following equation:

$$\ln f = \ln f_0 + 2\alpha\mu^{1/2} \quad (6)$$

where  $f, f_0$  are efficiency factors at ionic strength  $\mu$  and zero ionic strength. Equation (6) was obtained by substituting the valence of  $\text{SEM}^\ominus$  and  $\text{SO}_4^\ominus$  into eq. (2).

The decomposition rate constant,  $k_d$ , for  $\text{K}_2\text{S}_2\text{O}_8$  is independent of ionic strength in acid solution.<sup>10</sup>

It should be noted that it is possible for polymerization to be initiated by hydroxyl radical which is formed by reaction of sulfate ion radical with water.<sup>10</sup> Hydroxyl endgroups have been found in methyl methacrylate polymer prepared with  $\text{K}_2\text{S}_2\text{O}_8$  in the presence of water.<sup>11</sup> Initiation by an uncharged hydroxyl radical would be independent of ionic strength. However, lacking polymerization rate data with a nonionic initiator or an independent endgroup analysis, it is impossible to determine the ratio of polymer chains initiated by hydroxyl radical to those initiated by sulfate ion radical.

The effect of ionic strength on the rate constant of the propagation reaction which involves a univalent monomer and a polyvalent growing polymer chain is described by eq. (7):

$$\ln k_p = \ln k_{p0} + 2Z_p\alpha\mu^{1/2} \quad (7)$$

where  $k_p, k_{p0}$  are the propagation rate constants at ionic strength  $\mu$  and zero ionic strength, respectively, and  $Z_p$  is the charge on the growing polymer radical.

The effect of ionic strength on the rate constant of the termination reaction, is described by eq. (8):

$$\ln k_t = \ln k_{t0} + 2Z_p^2\alpha\mu^{1/2} \quad (8)$$

where  $k_t, k_{t0}$  are the termination rate constants at ionic strength  $\mu$  and zero ionic strength, respectively.

Combining eqs. (6), (7), and (8) results in the following equation:

$$\ln[(k_p/k_t^{1/2})(fk_d)^{1/2}] = \ln[(k_{p0}/k_{t0}^{1/2})(f_0k_d)^{1/2}] + (1 + 2Z_p - Z_p^2)\alpha\mu^{1/2} \quad (9)$$

From eq. (9) it can be seen that a plot of ratio of rate constants as a function of  $\mu^{1/2}$  will increase or decrease dependent on the value of  $Z_p$ , the charge on the growing polymer radical. If the charge on the growing polymer radical is greater than 2.4, the inhibition by ionic repulsion between ionic reactants will have more effect on the termination reaction than on the propagation reaction so that as the effect of ionic charge is diminished by the addition of salt the value of the ratio of rate constants decreases.

Figure 3 is a plot of the ratio of rate constants as a function of  $\mu^{1/2}$ . In solutions of ionic strength greater than  $0.5M$  the ratio of rate constants is essentially constant, indicating that the effective charge on the growing polymer radical  $Z_p$  has a minimum value of 2.4. Since the effect of reactant charges on the propagation and termination reactions are balanced  $\text{SEM}^\ominus\text{Na}^\oplus$  polymerization in aqueous solutions of greater than  $0.5M$  is described by the same kinetic expressions as are nonionic monomers,

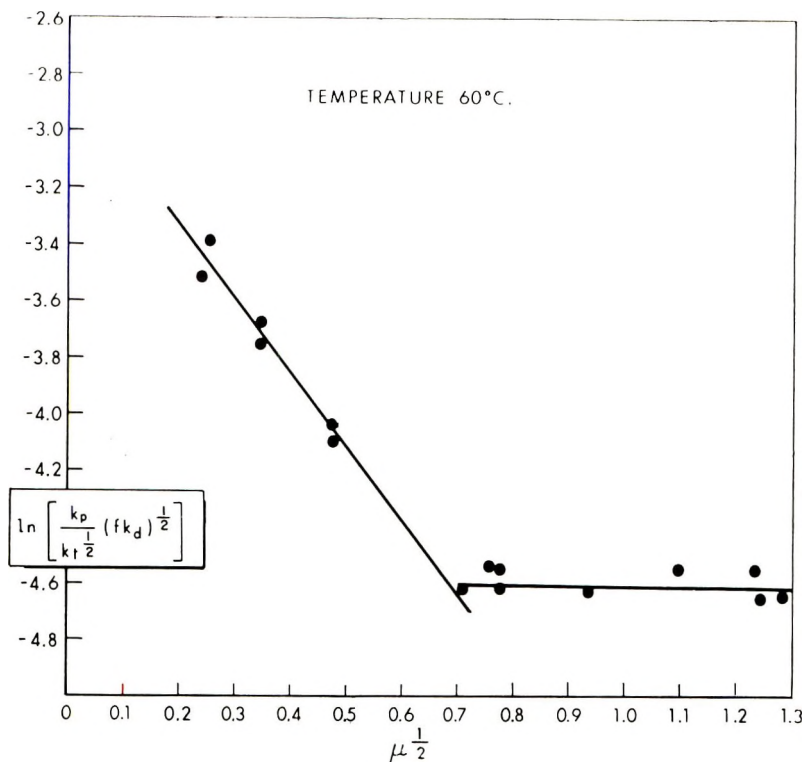


Fig. 3. Ratio of SEM<sup>⊖</sup>Na<sup>⊕</sup> polymerization rate constants,  $(k_p/k_t^{1/2})(fk_d)^{1/2}$ , as a function of ionic strength  $\mu$ .

The points shown in Figure 3 at ionic strengths of less than 0.5M fall on a straight line with negative slope. The value of  $Z_p$ , calculated by means of eq. (9) by using 1.26 as the value for  $\alpha$  for water at 60°C<sup>12</sup> was 3.1. The effective ionic charge on the growing polymer radical,  $Z_p$ , is much less than the degree of polymerization. Poly(SEM<sup>⊖</sup>Na<sup>⊕</sup>) prepared at 0.06M had an intrinsic viscosity of 1.2 dl/g in 4% KCl solution at 30°C, which indicates a molecular weight much greater than about 600 if the degree of polymerization is only 3. The low value of  $Z_p$  calculated by using eq. (9) is the result of having used the limiting form of the Debye-Hückel theory in deriving eq. (9). With this limitation, eq. (9) applies only to solutions of ionic strength approaching infinite dilution. It is expected that the ratio of rate constants for SEM<sup>⊖</sup>Na<sup>⊕</sup> polymerization at concentrations of less than 0.06M will be greater than predicted by extending the straight line drawn in Figure 3.

Because of the low value of  $Z_p$  there is essentially no change in solution ionic strength on conversion of monomer to polymer. Therefore the ratio of rate constants is essentially constant at all conversions, and the rate of monomer disappearance is described by the same equations as derived for nonionic monomers.

The value of  $Z_p$  is 2.8 if calculated by means of an equation derived assuming the efficiency of initiation  $f$  to be independent of ionic strength. Because the difference between the values of  $Z_p$  calculated by means of the two equations is small, using a nonionic initiator would probably have negligible effect on the ratio rate constants.

### EFFECT OF TEMPERATURE ON THE POLYMERIZATION RATE

Values of  $\ln k_p k_t^{-1/2} (f k_d)^{1/2}$  for  $\text{SEM}^\ominus \text{Na}^\oplus$  polymerization runs at concentrations of 0.5 and 0.06M are plotted as a function of  $1/T$  in Figure 4. Since the points are approximately on a straight line, the Arrhenius equation can be used to describe the effect of temperature on the polymerization rate parameter.

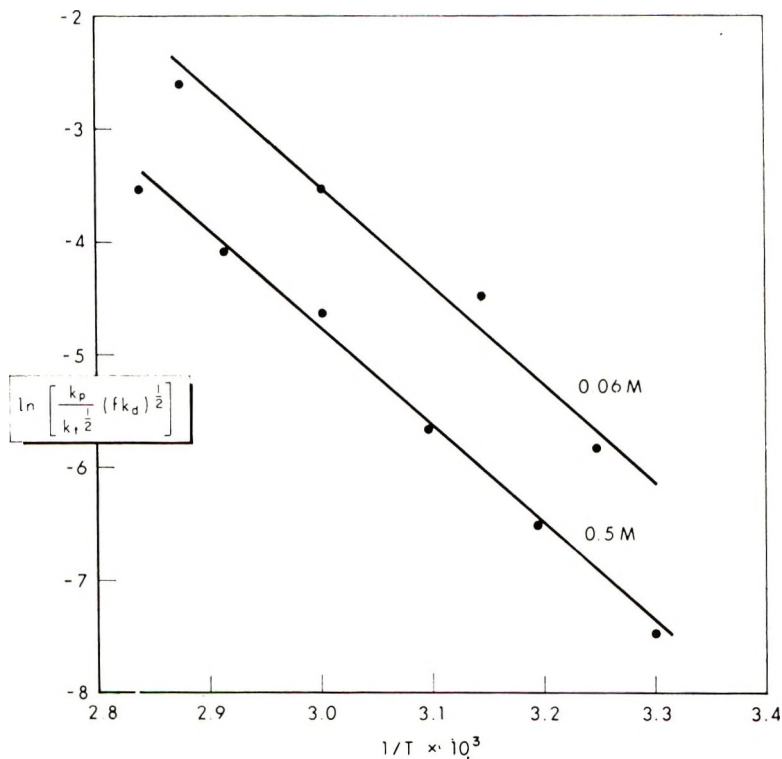


Fig. 4. Ratio of  $\text{SEM}^\ominus \text{Na}^\oplus$  polymerization on rate constants,  $(k_p/k_t^{1/2})(f k_d)^{1/2}$ , as a function of temperature.

The Arrhenius equation is written as follows for  $\text{SEM}^\ominus \text{Na}^\oplus$  polymerization:

$$\ln [(k_p/k_t^{1/2})(f k_d)^{1/2}] = \ln A - (E_a/RT) \quad (10)$$

where  $A$  is a constant,  $R$  is the gas constant (1.987 cal/deg-mole),  $T$  is absolute temperature, and  $E_a$  is the overall activation energy (cal/mole).

From the data shown in Figure 4 the value  $E_a$  is calculated to be 17.2 kcal/mole. Assuming that the temperature dependence of the rate constant of each reaction involved in the polymerization rate parameter is described by the Arrhenius equation, the overall activation energy  $E_a$  is given by the sum of activation energies for each reaction involved in the chain which can be written as follows:<sup>8b</sup>

$$E_a = E_p - (E_t/2) + (E_d/2) \quad (11)$$

Since the value of  $E_d$  for persulfate is 33.5 kcal/mole,<sup>10</sup> it can be calculated from eq. (11) that the activation energy of the termination reaction is about twice as great as that of the propagation reaction in  $\text{SEM}^\ominus\text{Na}^\oplus$  polymerization. This conclusion does not seem unreasonable since the repulsive energy between the two polyvalent electrolytes involved in the termination reaction, must be greater than the repulsive energy between the monovalent and polyvalent electrolytes involved in the propagation reaction.

Approximately the same overall activation energy is calculated from the data shown in Figure 4 for 0.06M  $\text{SEM}^\ominus\text{Na}^\oplus$  as was calculated from the measurements in 0.5M  $\text{SEM}^\ominus\text{Na}^\oplus$ . Since the rate parameter is higher at the lower ionic strength, the effect of increasing ionic charge on the reactants is to decrease the number of effective collisions. The difference in activation energies of propagation and termination reactions is apparently independent of ionic strength.

### References

1. W. J. LeFevre and D. P. Sheetz, U.S. Pat. 3,024,221 (1962); U.S. Pat. 3,033,833 (1962).
2. A. Katchalsky and G. Blauer, *Trans. Faraday Soc.*, **47**, 1360 (1951).
3. S. H. Pinner, *J. Polym. Sci.*, **9**, 282 (1952).
4. G. Blauer, *J. Polym. Sci.*, **11**, 189 (1953).
5. F. A. Bovey, *J. Polym. Sci. A*, **1**, 843 (1963).
6. D. A. Kangas and D. P. Sheetz, U.S. Pat. 3,415,870 (1968).
7. L. C. Rubens and R. E. Skochdopole, *J. Appl. Polym. Sci.*, **9**, 1487 (1965).
8. P. J. Flory, *Principles of Polymer Chemistry*, Cornell Univ. Press, Ithaca, N.Y., 1953, (a) p. 114; (b) p. 124.
9. A. A. Frost and R. G. Pearson, *Kinetics and Mechanism*, Wiley, New York, 1953, p. 138.
10. I. M. Kolthoff and I. K. Miller, *J. Amer. Chem. Soc.*, **73**, 3055 (1951).
11. P. Ghosh, S. C. Chadha, A. R. Mukherjee, and S. R. Palit, *J. Polym. Sci. A*, **2**, 4433 (1964).
12. H. S. Harned and B. B. Owen, *The Physical Chemistry of Electrolytic Solutions*, Reinhold, New York, 1958, p. 165.

Received November 5, 1969

Revised December 8, 1969

## Termination Rate Constants in Radical Polymerization

KATSUKIYO ITO, *Government Industrial Research Institute of Nagoya,  
Kita-ku, Nagoya, Japan*

### Synopsis

A rate constant is generally derived by using Fick's equation corresponding to the spherical interdiffusion of particles. By using this rate constant, chain and primary radical termination rate constants can be approximated to rate constants for the bimolecular reactions between two radical chain ends, and primary radical and radical chain end, respectively. The former is given by  $k_{ss} = 8\pi N_L D_s L_s \exp\{-L_s/R_s\} \times 10^{-3}$  l./mole-sec. The latter is given by  $k_{si} = 4\pi N_L (D_s + D_i) L_{si} \exp\{-L_{si}/R_{si}\} \times 10^{-3}$  l./mole-sec. Here,  $N_L$  is Avogadro's number;  $D_s$  and  $D_i$  are the diffusion constants of radical chain end and primary radical, respectively;  $L_s$  and  $L_{si}$  are, respectively, the distances between two radical chain ends and between a primary radical and a radical chain end at a thermal energy equal to the coulombic energy of interaction of the net charges; and  $R_s$  and  $R_{si}$  are, respectively, the average distances between two radical chain ends and primary radical on a collision.

### INTRODUCTION

In the previous papers,<sup>1-5</sup> chain and primary radical termination rate constants for various solution polymerization systems have been successfully interpreted by using an equation derived on the application of collision theory for reaction in gases.<sup>6</sup> Generally, treatments for the derivation of rate constant in condensed systems as solution are different from treatments for the derivation of rate constant in gases. The rate constant of very rapid reaction is derived by Rabinowitch's treatment<sup>7</sup> and Smoluchowski's treatment.<sup>8</sup> An important boundary condition in the Smoluchowski treatment was physically modified by Collins and Kimball.<sup>9</sup> Collins developed the Smoluchowski treatment by using this modified boundary condition.<sup>10</sup> Furthermore, the Smoluchowski treatment was also developed for the diffusion-controlled rate constant considering the effect of electrical force by Debye<sup>11</sup> and Umberger and Lamer.<sup>12</sup>

In this paper, Fick's equation corresponding to the spherical interdiffusion of particles with electric charge was used for the derivation of rate constant under the modified boundary condition. The chain and primary radical termination rate constants are discussed on the basis of this rate constant.



## GENERAL TREATMENTS

## Derivation of Rate Constant by the Modified Smoluchowski Treatment

Two spherical particles are considered as reactants. One of them exists in the center of a spherical coordinate, and the other is diffusing. On setting the mutual electrical energy between them as  $U$  and the diffusion constant is  $D$  for the sum of the diffusion constants of the above two reactants, Fick's equation corresponding to their spherical interdiffusion is given by<sup>11,12</sup>

$$\frac{\partial \phi}{\partial t} = D \left[ \frac{\partial^2 \phi}{\partial r^2} + \frac{\partial \phi}{\partial r} \left( \frac{2}{r} - \frac{\partial U}{kT \partial r} \right) \right] \quad (1)$$

where  $k$  is Boltzmann's constant,  $T$  is the absolute temperature, and  $\phi$  is the thermodynamic activity at time  $t$  and distance  $r$  and given by

$$\phi = C \exp \{ U/kT \} \quad (2)$$

where  $C$  is the concentration of the diffusing reactant. On denoting a specific reaction rate and the distance to the above approaching reactants for bimolecular reaction by  $k_a$  and  $R$ , respectively, the initial and boundary conditions<sup>7,9,10</sup> are

$$C = {}^*C \quad t > 0, r \rightarrow \infty \quad t = 0, \quad r > R \quad (3a)$$

$$C = (D/k_a)(\partial C/\partial r)_{r=R} \quad t > 0, \quad r = R \quad (3b)$$

In the case of the stationary state, on putting

$$\exp \{ U/kT \} = \exp \{ L/r \} \quad (4)$$

where  $L$  is the distance between two reactants at which the thermal energy equals the coulombic energy of interaction of the net charges, equation (2) becomes

$$d^2\phi/dr^2 + (2/r + L/r^2)d\phi/dr = 0 \quad (5)$$

and eqs. (3a) and (3b), respectively, are reduced to be

$$\phi = {}^*C \quad r \rightarrow \infty \quad (6a)$$

$$\phi = (D/k_a)[(d\phi/dr)_{r=R} + L\phi/R^2] \quad r = R \quad (6b)$$

By using the solution of eq. (5) under the conditions eqs. (6a) and (6b), a reaction rate constant is derived as

$$k_{pt} = 4\pi N_L D \frac{LR^2 \exp\{-L/R\}}{R^2(1 - \exp\{-L/R\}) + L(D/k_a)\exp\{-L/R\}} \times 10^{-3} \text{ l./mole-sec} \quad (7)$$

where  $N_L$  is Avogadro's constant. By first using  $\exp\{-L/R\} \cong 1 - L/R$  at  $L/R \ll 1$  and second putting  $L = 0$ ,  $k_{pt}$  becomes

$$k_{pt} = 4\pi N_L D R^2 / (R + D/k_a) \times 10^{-3} \text{ l./mole-sec} \quad (8)$$

### Definitions of the Specific Reaction Rate $k_a$ and the Diffusion Constant $D$

The mean distance between the centers of particles is  $R + \langle s \rangle$ , where  $R$  is the diameter of particle, and  $\langle s \rangle$  is the mean distance between their surfaces and given by

$$\langle s \rangle = \int_0^{\infty} s\psi(s)ds \quad (9)$$

where  $s\psi(s)$  is the probability of a displacement having a surface distance between  $s$  and  $s + ds$ . Using the same treatment as Cohen and Turnbull's treatment<sup>13</sup> for a diffusion constant in statistical mechanics,  $\psi(s)$  is the most probable distribution satisfying eq. (9), and given by

$$\psi(s) = \frac{1}{\langle s \rangle} \exp\{-s/\langle s \rangle\}. \quad (10)$$

The specific reaction rate was defined for the displacement in the neighborhood of  $r = R$ . Thus, it should be defined as

$$k_a = p\nu \int_0^{\infty} s\psi(s)ds \quad (11)$$

where  $p$  is a reaction probability and  $\nu$  is the mean displacing frequency. The diffusion constant should be not defined for the displacement in the neighborhood of  $r = R$ , but for the displacement in the range  $r \geq *s + R$ , where  $*s$  is the critical length sufficient to permit another particle to displace after displacement. Thus, it should be defined as

$$D = \nu \int_{*s}^{\infty} s^2\psi(s) \quad (12)$$

Using eq. (10),  $k_a$  and  $D$ , respectively, were calculated to be

$$k_a = p\nu\langle s \rangle \quad (13)$$

$$D = \nu(*s^2 + 2\langle s \rangle*s + 2\langle s \rangle^2) \exp\{-*s/\langle s \rangle\} \quad (14)$$

## APPLICATIONS

### Chain-Termination Rate Constant

A rate constant for the bimolecular reaction between two polymeric radicals with the same diameter  $R$  at  $U = 0$  is taken into consideration. When  $R \ll D/k_a$ , this rate constant  $k_t$  can be derived by using eq. (8) and setting the mean velocity of displacement as

$$u = \nu\langle s \rangle \quad (15)$$

$$k_t = 4\pi N_L p u R^2 \times 10^{-3} \text{ l./mole-sec} \quad (16)$$

This rate constant is equivalent to  $S^{1/2}k_c$  where  $k_c$  is a rate constant in the collision theory<sup>6</sup> and given by

$$k_c = 2^{1/2}\pi N_L p u R^2 \times 10^{-3} \text{ l./mole-sec} \quad (17)$$

The rate constant given by eq. (17) was used for the derivation of the chain-termination rate constant by Ito.<sup>1,2</sup> Even if a specific reaction rate is not evaluated by eq. (13), for the condition  $R \ll D/k_a$  for the reaction process as the usual chemical control at low and high conversions, eq. (17) should be applicable over almost the complete conversion range. The chain-termination rate constant obtained is given by

$$k_t' = 2^{1/2} \gamma u_s \mu^3 (3 - \mu)(1 - \mu)^2 \text{ l./mole-sec.} \quad (18)$$

Here,  $\gamma$  is a reactivity constant between radical chain ends,  $u_s$  is the mean velocity of displacement of the radical chain end, and  $\mu$  is the ratio of the maximum overlap length on collision between polymeric radicals to  $R/2$ . In the derivation of eq. (18), the average distance to polymeric radicals approaching during a collision was set as  $R(1 - \mu)$ . If this average distance is correct, the larger the value of  $\mu$  in the neighborhood of  $\mu = 1$ , the smaller the value of  $k_t'$ . However, the increase of the overlap volume should be always equivalent to the increase of the chain-termination rate constant. Thus,  $k_t'$  is not correct, and the average distance must be modified to  $R$ . On this modification, the rate constant is given by

$$k_t = 2^{1/2} \gamma u_s \mu^3 (3 - \mu) \text{ l./mole - sec} \quad (19)$$

The rate for the decrease of radical chain ends in the overlap volume during a collision time  $\tau$  between polymeric radicals is given by

$$-d[S]/dt = k_s[S]^2 \quad 0 \leq t \leq \tau \quad (20)$$

where  $[S]$  and  $k_s$  are the concentration of radical chain ends, and the rate constant for the combination reaction between radical chain ends in overlap volume, respectively. In the previous paper,<sup>2</sup> for convenience, on assuming that  $\tau$  is sufficiently short interval to permit

$$\begin{aligned} tk_s &= ([S]_0 - [S])/[S]_0[S] \\ &\cong ([S]_0 - [S])/[S]_0^2 \end{aligned}$$

(where  $[S] = [S]_0$  at  $t = 0$ ), and taking

$$x = u_s t$$

eq. (20) was treated as the following first-order reaction

$$-d[S] = u_s \gamma [S]_0 [S] dx$$

where  $x$  is the distance of translation of the radical chain end in the overlap volume. Thus  $u_s \gamma$  is equal to  $k_s$ , and eq. (19) becomes

$$k_t = 2^{1/2} \mu^3 (3 - \mu) k_s \text{ l./mole-sec} \quad (21)$$

Because the observed rate constant is the mean value of  $k_t$  at various values of  $\mu$  (assuming that a weighting factor on the various collisions is constant), the mean chain-termination rate constant is given by

$$\bar{k}_t = \int_0^1 k_t d\mu = 0.778 k_s \text{ l./mole-sec} \quad (22)$$

This equation indicates that the mean chain-termination rate constant can be approximated by the rate constant of bimolecular reaction between radical chain ends.

Because of the proportionality<sup>1-5,14-17</sup> of the observed termination rate constant to the diffusion constant of radical chain end  $D_s$ , the following inequality should hold:

$$R_s^2 [1 - \exp\{-L_s/R_s\}] \gg L_s(D_s/k_{as}) \exp\{-L_s/R_s\} \quad (23)$$

where  $L_s$  is the distance between radical chain ends at the thermal energy equaling the coulombic energy of interaction of the net charges,  $R_s$  is the average distance between radical chain ends, and  $k_{as}$  is a specific reaction rate for the combination reaction between radical chain ends. Thus,  $k_s$  becomes

$$k_s = 8\pi N_L D_s L_s [\exp\{-L_s/R_s\} / (1 - \exp\{-L_s/R_s\})] \times 10^{-3} \text{ l./mole-sec} \quad (24)$$

Even if the observed chain termination rate constant is not proportional to the diffusion constant of radical chain end, eq. (7) can be used for the analysis.

On the application of eq. (14) to the diffusion constant of radical chain end, the critical length for the radical chain end should be evaluated by its diameter  $R'_s$ , and the order of the magnitudes of the mean distance  $\langle s_f \rangle$  and  $R_s$  should be given by

$$\langle s_f \rangle \ll R'_s \quad (25)$$

Thus  $D_s$  is given by

$$D_s = \nu R_s'^2 \exp\{-R'_s/\langle s_f \rangle\} \quad (26)$$

The diffusion constant  $D_f$  evaluated by the free volume  $v$  is given by

$$D_f = \frac{1}{6} R'_s u_\theta \exp\{-av^*/v_f\} \quad (27)$$

where  $u_\theta$  is kinetic velocity of a gas,  $a$  is an overlap factor, and  $v^*$  is the critical volume sufficient to permit another particle to jump in after the displacement.<sup>13</sup> When  $u_\theta$  is evaluated by

$$u_\theta = 6 \nu R'_s$$

and  $v_f/a$  is evaluated by the spherical volume for a radius  $\langle s_f \rangle$

$$v_f/a = \frac{4}{3} \pi \langle s_f \rangle^3$$

eq. (27) is equivalent to eq. (26). Thus, because  $D_f$  is so well applicable at high conversion,<sup>4</sup>  $D_s$  is also applicable at high conversion.

### Termination Rate Constant for Primary Radical

On modification of the average distance between primary radical and polymeric radical on a collision to  $R/2$ , the primary radical termination rate constant in the previous paper<sup>2</sup> is modified to

$$k_{ti} = 1.5 \mu_i k_{si} \text{ l./mole-sec} \quad (28)$$

Here,  $k_{st}$  is the rate constant for the bimolecular reaction between primary radical and radical chain end, and  $\mu_i$  is the ratio of the maximum immersing length of primary radical into polymeric radical to  $R/2$ . Assuming that a weighting factor exists for various collisions between primary radical and polymeric radical, the mean primary radical termination rate constant is given by

$$\bar{k}_{ti} = \int_0^1 k_{ti} d\mu_i = 0.750k_{st} \text{ l./mole-sec.} \quad (29)$$

This equation indicates that  $\bar{k}_{ti}$  can be approximated to  $k_{st}$ .

For the proportionality of the primary radical termination rate constant to the diffusion constant

$$D_{st} = D_s + D_i \quad (30)$$

where  $D_i$  is the diffusion constant of primary radical, by using Eq. (7),  $k_{st}$  is given by

$$k_{st} = 4\pi N_L D_{st} L_{st} [\exp\{-L_{st}/R_{st}\} / (1 - \exp\{-L_{st}/R_{st}\})] \times 10^{-3} \text{ l./mole-sec} \quad (31)$$

Here,  $L_{st}$  is the distance between the primary radical and the radical chain end at the thermal energy equaling the coulombic energy of interaction of the net charges, and  $R_{st}$  is the average distance between the radical chain end and primary radical on a collision. On application of eq. (14),  $D_i$  is given by

$$D_i = \nu R_i^2 \exp\{-R_i/\langle s_f \rangle\} \quad (32)$$

where  $R_i$  is the diameter of the primary radical.

## DISCUSSION

On using the rate constant

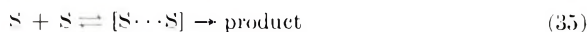
$$k_d = 4\pi N_L D \rho R \times 10^{-3} \text{ l./mole-sec} \quad (33)$$

in the original Smoluchowski's theory,<sup>8</sup> a mean chain-termination rate constant  $\bar{k}_{tm}$  equivalent to a rate constant  $k_{sm}$  of the bimolecular reaction between radical chain ends was derived by Moroni and Schulz.<sup>14</sup>

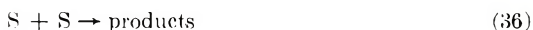
$$\bar{k}_{tm} = k_{sm} = 8\pi N_L D_s R_s \alpha \beta \times 10^{-3} \text{ l./mole-sec} \quad (34)$$

Here,  $\alpha$  is a steric factor, and  $\beta$  is an energetic probability. The experimental result that the observed chain termination rate constant is one hundred times smaller than the typical diffusion-controlled rate constant between small molecules was explained by putting  $\alpha = 1/67$ ,  $R_s = 1.0 \times 10^{-8}$  cm and  $D_s = 4.3 \times 10^{-6}$  cm<sup>2</sup>/sec at  $\beta = 1$ . In their conclusion, because of  $p < 1$ , the chain termination rate constant is not diffusion-controlled.

The distinction between the original Smoluchowski theory and the modified Smoluchowski theory should be understandable in the reaction process:



Here,  $[S \cdots S]$  is a proximate pair as a reaction coordinate in the Rabino-witch's treatment,<sup>7</sup> and the mean distance between two reactants is  $R_s + \langle s_f \rangle$ . The collision number in the proximate pair is larger by a factor of 20–30 than the diffusing collision number in the solution systems ( $R_s \gg \langle s_f \rangle$ ). Thus, the total collision number can be compared with the collision number in the proximate pair. The diffusing collision number is negligible. However, because of the total collision number evaluated by the diffusing collision number in the original Smoluchowski theory, it should not be applicable except under the condition  $p = 1$ , when the reaction process is diffusion-controlled:



In the modified Smoluchowski theory, the contribution of each collision number to the reaction rate constant is treated by the modified boundary condition, eq. (3b). Thus, this theory should be applicable to the general reaction process given by eq. (35). In order to examine both theories in the light of experimental results, the discussion of the difference between the chain-termination rate constant and the propagation rate constant is suitable. Because of  $p = \alpha\beta < 1$ , the original Smoluchowski theory is not applicable to the chain-termination rate constant. Furthermore, because of the independence of the latter of the solvent viscosity, it is not applicable to the propagation rate constant. On the other hand, in the modified Smoluchowski theory, when the inequality (23) is available, the reaction process is diffusion-controlled. The experimental result that the observed chain-termination rate constant is one hundred times smaller than the typical diffusion-controlled rate constant between small molecules can be successfully interpreted by introducing  $\exp\{-L_s/R_s\}$ .

When  $L_s/R_s \geq 4$ ,  $\exp\{-L_s/R_s\} \leq 1/55$  cannot be compared with unit. Thus, eq. (24) becomes

$$k_s = 8\pi N_L D_s L_s \exp\{-L_s/R_s\} \times 10^{-3} \text{ l./mole-sec.} \quad (37)$$

First, taking  $D_s = 4.3 \times 10^{-6} \text{ cm}^2/\text{sec}$ , eq. (37) becomes

$$k_s = 6.5 \times 10^{16} L_s \exp\{-L_s/R_s\} \text{ l./mole-sec.} \quad (38)$$

Second, taking  $R_s = 1.0 \times 10^{-8} \text{ cm}$  and  $L_s = 5.0 \times 10^{-8} \text{ cm}$ ,  $k_s$  was calculated to be  $2.2 \times 10^7 \text{ l./mole-sec}$ . This value is equivalent to the observed chain termination rate constant.

Furthermore, because of the independence of the specific reaction rate of solvent viscosity, on putting  $D/k_a \gg R$  in eq. (8), the modified Smoluchowski theory is also applicable to the propagation rate constant. On the above discussions, the Moroni and Schulz rate constant should be not correct.

In the previous paper,<sup>2</sup> it was pointed out that the termination rate constant in the polymerization of some methacrylates<sup>18</sup> depends on the distance of translation of the radical chain end for a collision between radical chain end and solvent particle. Actually, because this dependence is

very little, it is negligible. Furthermore, in view of eq. (37), it is meaningless.

In the above polymerization, the effect of Taft polar constant on the termination rate constant can be evaluated by  $L_s$  in eq. (37). The net charge of radical chain end decreases with increasing Taft polar constant. Thus, the larger the Taft polar constant, the less the repulsion between radical chain ends. That is, the increasing approach between radical chain ends is equivalent to the increasing chain-termination rate constant. In the above discussion, at  $L_s/R_s \geq 4$ , a change of  $L_s$  can not be compared with a change of  $\exp\{-L_s/R_s\}$ . This is,  $L_s$  is approximated to a constant.

In eq. (34), when  $1 \gg \exp\{-L_{si}/R_{si}\}$ ,  $k_{si}$  becomes

$$k_{si} = 4\pi N_L D_{si} L_{si} \exp\{-L_{si}/R_{si}\} \times 10^{-3} \text{ l./mole-sec} \quad (39)$$

This rate constant should be useful for the analysis of a chain-termination rate constant for copolymerization as well as the analysis of the primary radical-termination rate constant.

### References

1. K. Ito, *J. Polym. Sci. A-1*, **7**, 827 (1969).
2. K. Ito, *J. Polym. Sci. A-1*, **7**, 2247 (1969).
3. K. Ito, *J. Polym. Sci. A-1*, **7**, 2707 (1969).
4. K. Ito, *J. Polym. Sci. A-1*, **7**, 2995 (1969).
5. K. Ito, *J. Polym. Sci. A-1*, **7**, 3387 (1969).
6. M. C. MacLewie, *J. Chem. Soc.* **1918**, 471.
7. E. Rabinowitch, *Trans. Faraday Soc.*, **33**, 1225 (1937).
8. M. V. Smoluchowski, *Z. Physik. Chem.*, **29**, 129 (1917).
9. F. C. Collins and G. E. Kimball, *J. Colloid Sci.*, **4**, 425 (1949).
10. F. Collins, *J. Colloid Sci.*, **5**, 499 (1950).
11. P. Debye, *Trans. Electrochem. Soc.*, **82**, 265 (1942).
12. J. Q. Umberger and V. K. Lamer, *J. Amer. Chem. Soc.*, **67**, 1099 (1945).
13. M. Cohen and T. Turnbull, *J. Chem. Phys.*, **31**, 1164 (1959).
14. A. F. Moroni and G. V. Schulz, *Makromol. Chem.*, **118**, 313 (1968).
15. S. W. Benson and A. M. North, *J. Amer. Chem. Soc.*, **81**, 1339 (1959).
16. A. M. North and G. A. Reed, *Trans. Faraday Soc.*, **57**, 859 (1961).
17. A. M. North and G. A. Reed, *J. Polym. Sci. A*, **1**, 1311 (1963).
18. K. Yokota, M. Kani, and Y. Ishii, *J. Polym. Sci. A-1*, **6**, 1335 (1968).

Received October 10, 1969

Revised December 8, 1969

# Electron Spin Resonance Studies on Graft Copolymerization of Gaseous Styrene onto Preirradiated Polypropylene. I. Preirradiation in the Presence of Oxygen

BUNZO EDA, KEICHI NUNOME, and MACHIO IWASAKI,  
*Government Industrial Research Institute, Nagoya, Hirate-machi, Kita-ku,  
Nagoya, Japan*

## Synopsis

Graft copolymerization of gaseous styrene was carried out onto polypropylene preirradiated in the presence of oxygen at  $-78^{\circ}\text{C}$  and at room temperature, respectively. The origin of the graft initiation activities of these polymers was investigated by means of electron spin resonance (ESR) of trapped radicals. More grafting was found for the polymers irradiated at  $-78^{\circ}\text{C}$  than for those irradiated at room temperature. The difference of grafting between polymers irradiated at  $-78^{\circ}\text{C}$  and those irradiated at room temperature was not explained by the total amounts of trapped radicals, and it was found that all radicals are not effective in the grafting reaction. ESR measurements showed that there exist two kinds of peroxy radicals, one has more effective ability of abstracting hydrogen atoms from the surrounding polymer chains to form carbon radicals, and another is less effective at the temperature of grafting reaction ( $40^{\circ}\text{C}$ ). Although the samples irradiated at  $-78^{\circ}\text{C}$  contain the both types of radicals, those irradiated at room temperature do not contain the former type of radicals. It was shown that the carbon radicals produced by such a hydrogen abstraction reaction are actually the effective centers in the grafting reaction of polymers irradiated in the presence of oxygen.

## INTRODUCTION

The preirradiation method has been given much attention in radiation-induced graft copolymerization because it depresses the formation of homopolymers; thus the grafting reaction can be carried out at any time, away from the radiation source. Two methods of preirradiation in the different atmospheres have been used: irradiation in the presence of air and irradiation *in vacuo*. Usually, the former leads to grafting on radiation-peroxidized polymers<sup>1</sup> which are thermally decomposed at higher temperatures to form oxy radicals, i.e., active centers of grafting reaction, and the latter to the grafting reaction initiated by trapped polymer radicals. The irradiation in the presence of air has the advantage that it does not require the evacuating technique which is attended with some difficulties in practice. As the grafting reaction is carried out at an elevated temperature to decompose the peroxidized polymers, however, considerable amounts of homo-



polymers are still produced in this case by thermal reaction of monomers, chain transfer reaction, and decomposition of hydroperoxides. Therefore, the possibility that the grafting reaction might be induced by trapped peroxy radicals of polymers irradiated in the presence of oxygen was examined. The present authors reported previously<sup>2</sup> that when polypropylene was  $\gamma$ -irradiated at  $-78^{\circ}\text{C}$  in the presence of air, graft copolymerization was effectively initiated, even at temperatures below  $40^{\circ}\text{C}$  at which the decomposition of peroxidized polymers was not likely to occur. In the grafting of styrene onto polytetrafluoroethylene irradiated in air, trapped peroxy radicals were reported to become initiators of grafting.<sup>3</sup> In the system of preirradiated polypropylene-styrene, what species are directly related to grafting activity has not yet been clarified. As peroxy radicals are produced in polypropylene irradiated in the presence of air, they may be supposed to be the primary active centers of the grafting reaction. On the other hand, as it is known that peroxy radicals are transmuted into carbon radicals by abstracting hydrogen atoms from the surrounding polymer chains when annealed *in vacuo*,<sup>4</sup> the possibility that carbon radicals may be the active centers of grafting may not be excluded.

This study was made to investigate the structures and behaviors of radicals trapped in polypropylene  $\gamma$ -irradiated in an oxygen atmosphere by means of electron spin resonance (ESR) and also to elucidate their relation to the origin of grafting activity at a temperature at which the thermal decomposition of peroxidized polymers does not occur. The monomer used in this work was gaseous styrene. Gaseous monomers are suitable for such a study because the formation of homopolymers can be minimized. In addition, gaseous monomers are favorable for the determination of radical concentrations by ESR, for they lower the  $Q$  value of the sample cavity less than liquid monomers do.

## EXPERIMENTAL

The isotactic polypropylene used was an 80–100 mesh powder of Mitsubishi Noblen, a product of Mitsubishi Petrochemical Co., Ltd. Both an 80–100 mesh powder and a 200–250 mesh powder were used for comparison, but no difference was found between these two in the grafting reaction or in the ESR spectra. Styrene was purified according to the usual methods.

Polymer samples were irradiated in an oxygen atmosphere with  $^{60}\text{Co}$   $\gamma$ -rays at  $-78^{\circ}\text{C}$  or at room temperature. The total dose was about 3 MR at a dose rate of about 0.2 MR/hr. An oxygen atmosphere was used instead of air because just after irradiation in air at  $-78^{\circ}\text{C}$ , considerable amounts of carbon radicals which had not yet reacted with oxygen were found in addition to peroxy radicals. Irradiation in an oxygen atmosphere made it possible to ensure that all carbon radicals reacted.

After irradiation, polymer samples were degassed (up to  $10^{-3}$  mm Hg) and sealed, and then styrene vapor was introduced by breaking the seal situated between polymers and styrene reservoir. Polymer samples and

styrene vapor were kept at 39.7–39.8°C to prevent the condensation of styrene on the surface of polymer samples. This temperature difference was easily achieved by putting a diaphragm in a thermo bath.

To examine whether or not decomposition of peroxidized polymers has some role in the initiation of the grafting reaction, the styrene vapor was introduced to polymers at several temperatures in the same way as mentioned above after all the trapped peroxy radicals had been destroyed by the heat treatment in air. Noticeable amounts of graft copolymers were not obtained when the samples were kept at or below 40°C. It is likely that thermal decomposition of peroxidized polymers does not take place to a large extent at this temperature. Therefore, 40°C was chosen as a reaction temperature at which only the trapped radicals are safely assumed to initiate graft copolymerization.

After reaction, polymers were repeatedly washed with cold benzene until no precipitate was observed when methanol was added to the filtrate. The polymers were then dried to constant weight. A weight increase was regarded as due to the grafting polystyrene. The degree of grafting was expressed as a percentage grafting,  $100(\Delta W/W)$ , in which  $W$  is the original weight of polypropylene used and  $\Delta W$  is the weight increase after reaction.

As the grafting reaction was carried out in a long ESR sample tube (5 mm in diameter) in which the polymer sample was filled to a length of 5 cm from the bottom, it was necessary to get some information regarding the difference of the percentage grafting in places. The sensitivity of ESR sample cavity is very much affected by the position of the paramagnetic specimens in the cavity. If the grafting in such a long tube is not homogeneous, the correct correlation between the percentage grafting and the amount of trapped radicals may not be obtained. Therefore, a sample tube was filled with polymers to a length of 10 cm, and then the grafting reaction was carried out according to the above-mentioned procedures. After the reaction, the sample was divided into ten successive portions and the infrared spectrum of a KBr disk of each portion was measured. The comparison of the absorption bands characteristic of polypropylene and polystyrene, showed no remarkable difference of the degree of grafting between the uppermost and the middle portions. Therefore, a glass tube which contains the polymer sample to a length of 5 cm was used in this work. To avoid the interference of the color centers produced in a glass tube, the other end of the sample cell was annealed and then the irradiated polymers were transferred to this end.

ESR measurements were carried out with a Japan Electron Optics JES-3BSX spectrometer at  $-78^\circ\text{C}$  unless otherwise described. The modulation frequency was 100 kcps and the microwave power was kept below 1mW to avoid saturation. Spectra were recorded as a first derivative curve. The determination of the relative radical concentrations was made by using a TE<sub>105</sub> dual-sample cavity which contains the irradiated sample and a Mn<sup>2+</sup> standard sample simultaneously. The ratio of the integrated intensity to the peak height of the signal of Mn<sup>2+</sup> was taken as a measure of

the relative radical concentration. The integrated intensity of the spectrum was obtained by a double integration with a Japan Electron Optics spectrum computer Model JR-5. Synthetic ESR spectra of the mixtures of peroxy radicals and carbon radicals were also obtained for a number of mixing ratios with this computer in order to estimate the amount of carbon radicals produced by the hydrogen abstraction reaction of the peroxy radicals.

## RESULTS AND DISCUSSION

### Degree of Grafting

Figure 1 shows the percentage grafting of styrene vapor (vapor pressure of about 16 mm Hg at 40°C) onto polypropylene preirradiated in an oxygen atmosphere at  $-78^{\circ}\text{C}$  and at room temperature, respectively. A remarkable difference is seen between the two irradiation temperatures employed. Preirradiation at  $-78^{\circ}\text{C}$  gave much more grafting than that at room temperature. For example, the degrees of grafting at 16 hr after the introduction of styrene vapor were found to be 23% and 7%, respectively. Such a difference of the degree of grafting was observed also in grafting of liquid styrene onto preirradiated polypropylene as reported previously.<sup>2</sup> To elucidate the cause of such a difference of grafting between polymers irradiated at different temperatures, ESR spectra were measured for the trapped radicals formed at the two different irradiation temperatures.

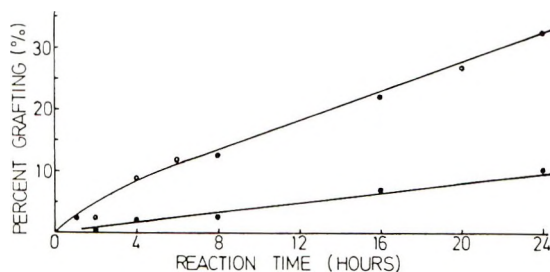


Fig. 1. Grafting of gaseous styrene onto preirradiated polypropylene powders at 40°C, dose 3 MR: (○) preirradiated at  $-78^{\circ}\text{C}$ ; (●) preirradiated at room temperature.

### Electron Spin Resonance Spectra

ESR spectra obtained from the samples irradiated at the two different temperatures exhibited different line shapes in addition to the amount of radicals trapped in polymers, indicating some qualitative difference in trapped radicals. Figures 2a and 2b show the ESR spectra of the peroxy radicals in polypropylene irradiated in the presence of oxygen at  $-78^{\circ}\text{C}$  and at room temperature, respectively. The radicals produced at  $-78^{\circ}\text{C}$  gave a broader spectrum than those produced at room temperature. However, it was found that spectra very similar to each other are obtained when the

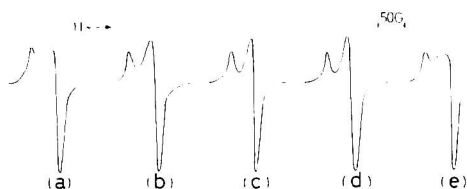


Fig. 2. ESR spectra of peroxy radicals of polypropylene  $\gamma$ -irradiated in the presence of oxygen: (a) irradiated at  $-78^{\circ}\text{C}$  and measured at  $-78^{\circ}\text{C}$ ; (b) irradiated at room temperature and measured at  $-78^{\circ}\text{C}$ ; (c) irradiated at room temperature and measured at  $-78^{\circ}\text{C}$ ; (d) irradiated at room temperature and measured at  $-196^{\circ}\text{C}$ ; (e) irradiated at room temperature and measured at room temperature.

observation temperature is lowered from  $-78^{\circ}\text{C}$  to  $-196^{\circ}\text{C}$ , as shown in Figures 2c and 2d. This spectral change with observation temperature was reversible. It is to be noted that the spectra of the samples irradiated at  $-78^{\circ}\text{C}$  exhibited a marked temperature dependence, while those of the samples irradiated at room temperature showed little temperature dependence and gave a similar line shape at  $-78^{\circ}\text{C}$  and  $-196^{\circ}\text{C}$ . It is well known that peroxy radicals possess an approximately axially symmetric  $g$ -tensor,<sup>5,6</sup> and that the line shape of the spectrum is strongly affected by molecular motions. This was further confirmed by the measurements at more elevated temperature. As shown in Figure 2e, the sharper spectrum in Figure 2b was changed to the broader one at room temperature, resulting from the higher degree for molecular motions at elevated temperature. When the radicals are sufficiently rigid at  $-196^{\circ}\text{C}$ , they give a line shape characteristic of an axially symmetric  $g$ -anisotropy as shown in Figures 2c and 2d. The prominent temperature dependence of spectrum a in Figure 2 indicates that the radicals in the samples irradiated at  $-78^{\circ}\text{C}$  have more motional freedom than those in the samples irradiated at room temperature. Although the difference of ESR spectra between polymers irradiated at  $-78^{\circ}\text{C}$  and at room temperature was thus ascribed to the difference of motional freedom of the trapped radicals, it is not yet clear at the present stage whether the difference is due to a difference in the matrix in which radicals are trapped or a difference of the radical species. This point will be discussed in subsequent papers, since the decision regarding the origin of the difference will not have a serious influence on the conclusion of this paper.

As the difference of motional freedom of trapped radicals should be reflected in the decay of radicals, the isothermal decay was measured.

#### Amounts of Trapped Radicals and Isothermal Decay

The isothermal decay of peroxy radicals at  $40^{\circ}\text{C}$  was examined in the styrene vapor as well as *in vacuo* in order to see the reaction of the trapped radicals with styrene. The decay *in vacuo* (about  $10^{-3}$  mm Hg) is shown in Figure 3, in which the logarithms of the relative radical concentrations

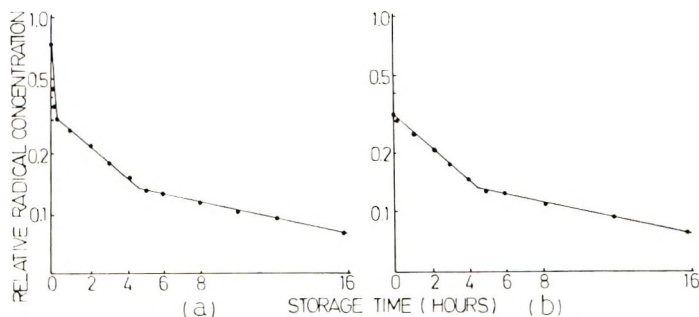


Fig. 3. Isothermal decay of peroxy radicals *in vacuo* at 40°C: (a) sample irradiated in oxygen atmosphere at  $-78^{\circ}\text{C}$ ; (b) sample irradiated in oxygen atmosphere at room temperature.

were plotted against the storage time assuming first-order decay. During the decay of peroxy radicals, the signal due to the carbon radicals formed by the hydrogen abstraction reaction appeared as described in the later section. The radical concentrations plotted in the figure are the sum of those of the peroxy and the carbon radicals. The decay curves seem to be divided into several linear portions. Although first-order decay was assumed here, it is only for the convenience of showing the existence of several stages of different decay rates. The peroxy radicals produced by the irradiation at  $-78^{\circ}\text{C}$  showed a rapid decay of an amount of about  $\frac{2}{3}$  of the initial concentration within the first hour, followed by two steps of relatively slow decay with half lives of about 90 and 840 min, respectively.

On the other hand, the peroxy radicals produced by the irradiation at room temperature did not show rapid decay corresponding to the first step of the former case but show only two steps of nearly the same decay rates and concentrations as those of the second and the third steps in the former case. Therefore, it is evident that the difference between spectra *a* and *b* in Figure 2 comes from the radicals exhibiting a rapid decay. Thus, the peroxy radicals, which showed a temperature-dependent broad spectrum and a rapid decay, are attributed to those having more motional freedom. When irradiated at room temperature, it is believed that the radicals having more motional freedom have decayed during irradiation, leaving the radicals having less motional freedom.

The decay of peroxy radicals in the styrene vapor was also studied. Although it has been reported that the decays of the trapped radicals of polyethylene,<sup>7</sup> polyamide,<sup>8</sup> and polytetrafluoroethylene<sup>3</sup> were accelerated in the presence of styrene vapor, the decay in the present case was not so different from that *in vacuo* within the experimental error. This may be explained by assuming that graft initiation radicals are transferred to the propagating radicals of grafting polystyrene and the rate of termination of the propagating radicals is not so different from the decay rate of graft initiation radicals. It might be expected that the propagating radicals of polystyrene give a broad ESR spectrum, the overall width of which is

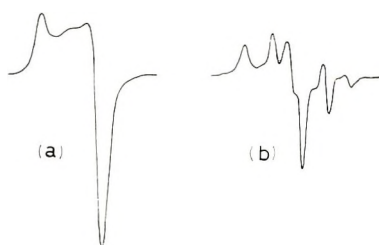


Fig. 4. Change of ESR spectrum after methyl methacrylate vapor was introduced at  $40^{\circ}\text{C}$  to the polypropylene samples irradiated at  $-78^{\circ}\text{C}$  in oxygen atmosphere followed by evacuation: (a) before introducing methyl methacrylate vapor; (b) 2 hr after introducing methyl methacrylate. Spectra were measured at  $-78^{\circ}\text{C}$ .

about 23 G because of the delocalization of the unpaired electron in the phenyl group. Therefore, it may be difficult to discern the broad spectrum from that of graft initiation radicals decaying in the styrene vapor. If the propagating radicals give a sharp spectrum, it will be easy to show the presence of them. Methyl methacrylate is such a case. Figure 4 shows the ESR spectrum 2 hr after methyl methacrylate vapor was introduced at  $40^{\circ}\text{C}$  to polypropylene which was preirradiated at  $-78^{\circ}\text{C}$  in the presence of oxygen followed by evacuation. The overlapping of the well known 9-line spectrum due to the propagating radicals of grafting poly(methyl methacrylate) is seen distinctly.

Now, since the amount of radicals is greater in polymers irradiated at  $-78^{\circ}\text{C}$  than in polymers irradiated at room temperature, by an amount of radicals which gave a temperature-dependent broad spectrum and showed a rapid decay, at a glance the larger percentage of grafting in the former case was thought to be due to the efficient grafting activity of these radicals. However, this supposition was completely denied by the experiment described in the next section. It was found that the radicals effective for the graft initiation are only a minor part of the trapped radicals. Therefore, it is not so surprising that the total concentration of the trapped radicals is not seriously affected by the presence of styrene vapor.

#### Grafting after Thermal Annealing

If the above supposition is correct, nearly the same percentage grafting should be obtained both for polymers irradiated at  $-78^{\circ}\text{C}$  and for polymers irradiated at room temperature when the styrene vapor is introduced after the radicals corresponding to the first step for the low temperature case are destroyed by heat treatment, because the decay curves for the steps with slower decay rates are quite similar to each other. Therefore, the polymers irradiated at  $-78^{\circ}\text{C}$  were annealed *in vacuo* for 1 hr to eliminate the radicals corresponding to the first step and then the styrene vapor was introduced. In spite of the fact that the remaining amount of radicals is only  $1/3$  and is almost the same as that of radicals produced by the room temperature irradiation, the degree of grafting was not diminished at all

within the experimental error. This clearly indicates that the peroxy radicals, which have more motional freedom and show a rapid decay, are not so effective in grafting and the percentage grafting does not depend on the total amount of trapped radicals.

On the other hand, when the polymer sample irradiated at  $-78^{\circ}\text{C}$  was annealed in air instead of *in vacuo* before introduction of the styrene vapor, the percentage grafting for the sample decreased considerably and was nearly equal to that for the polymer sample irradiated at room temperature. It is expected that the annealing *in vacuo* produces carbon radicals which are formed by the hydrogen abstraction reaction of the peroxy radicals,<sup>4</sup> while annealing in air does not produce such carbon radicals. Therefore, the above-mentioned experiments suggest that the carbon radicals might be effectively involved in the grafting reaction. Accordingly, the hydrogen abstraction reaction was examined, and a notable difference was found between polymers irradiated at  $-78^{\circ}\text{C}$  and at room temperature.

### Hydrogen Abstraction

Since the preirradiated samples are degassed before the styrene vapor is introduced, it is important to know something about the behavior of peroxy radicals after degassing. The spectral change during the storage at  $40^{\circ}\text{C}$  *in vacuo* shows that hydrogen abstraction by peroxy radicals took place with decrease of peroxy radicals. It was found that the rate of this reaction was strongly affected by the irradiation condition as was expected. Figure 5 shows the spectra taken after storage *in vacuo* at  $40^{\circ}\text{C}$  for 3 hr. In peroxy radicals formed in polymers irradiated at  $-78^{\circ}\text{C}$ , noticeable overlapping of other spectra was observed as shown in Figure 5a. This spectrum is due to the carbon radical produced by hydrogen abstraction, as already reported by Fischer et al.<sup>4</sup> On the other hand, carbon radicals were not observed in the case of the peroxy radicals formed by the room-temperature irradiation, as shown in Figure 5b. In this case, the carbon radicals did not appear for 10 hr, although they appeared within 10 min in the low temperature case. In addition, when the samples irradiated at  $-78^{\circ}$  were annealed in air for 1 hr at  $40^{\circ}\text{C}$  and then evacuated, the formation of the carbon radicals was extremely depressed. These results indicate that the peroxy

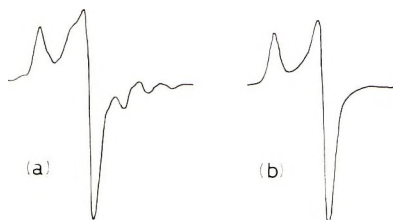


Fig. 5. ESR spectra of irradiated polypropylene measured after storage *in vacuo* at  $40^{\circ}\text{C}$  for 3 hr: (a) sample irradiated in oxygen atmosphere at  $-78^{\circ}\text{C}$ ; (b) sample irradiated in oxygen atmosphere at room temperature. Spectra were measured at  $-78^{\circ}\text{C}$ .

radicals in the first step, which was found only in the low-temperature case, abstract hydrogen atoms more easily than those in the second and third steps. As described in the preceding sections, the peroxy radicals in the first step have more motional freedom, so that higher reactivity with the surrounding polymer chains seems quite reasonable.

If one assumes that the carbon radical is more effective in the grafting reaction, the difference in hydrogen abstraction reaction of the peroxy radicals may be an actual cause of the difference of percentage grafting for the two irradiation temperatures. This idea was further confirmed by the following experiments and the estimates of the carbon radicals produced.

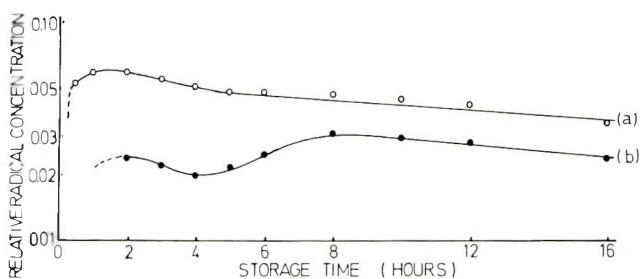


Fig. 6. Relative amounts of carbon radicals produced during storage at 40°C: (a) storage *in vacuo*; (b) storage in styrene vapor.

### Active Species of Grafting Reaction

If the carbon radicals produced by hydrogen abstraction are the active species of the grafting reaction, introduction of oxygen to convert the carbon radicals into peroxy radicals should depress the grafting reaction. To verify this, the polymer sample irradiated at  $-78^{\circ}\text{C}$  was annealed *in vacuo* for 1 hr at  $40^{\circ}\text{C}$  and then oxygen was introduced. After the reaction with oxygen, the sample was degassed and the grafting reaction was carried out according to the usual procedures. In this case, percentage grafting decreased considerably and was not so different from that of the polymer sample irradiated at room temperature. This suggests that the carbon radicals produced by the hydrogen abstraction reaction are very effective in the grafting reaction. This was further confirmed by comparing the amounts of carbon radicals produced during the storage at  $40^{\circ}\text{C}$  *in vacuo* and in the styrene vapor, respectively. Figure 6 shows the relative amounts of these carbon radicals, which were obtained by decomposing the spectrum into the spectrum of peroxy radicals and that of carbon radicals using a spectrum computer. Because of the possibility of overlapping of the spectrum of propagating radicals of grafting polystyrene at the central part of the spectrum, the outer peaks of the spectrum of carbon radicals were used as a measure. Although the total amounts of radicals were nearly the same for both the cases at each storage time as already stated, the amount of carbon radicals for the latter case was tremendously less than



that for the former case. This result strongly indicates that some of carbon radicals reacted with styrene during storage in the styrene vapor.

### CONCLUSION

In polymers irradiated at  $-78^{\circ}\text{C}$ , the peroxy radicals having more motional freedom with a rapid decay are produced, and some of them are converted into carbon radicals through the hydrogen abstraction reaction with the surrounding polymer chains when the samples are kept under vacuum at  $40^{\circ}\text{C}$ . Although these peroxy radicals are completely decayed in about 1 hr, the carbon radicals produced survive in the continued annealing. These carbon radicals effectively react with styrene molecules coming through into the polymers. On the other hand, the irradiation at room temperature produces no peroxy radicals which are converted effectively into the carbon radicals. Then the poor grafting is observed. Thus the difference in graft activity is attributed to the behavior of peroxy radicals trapped in the polymers.

It is to be noted that the efficient activity of grafting is gained by irradiation at low temperature, but the activity is not destroyed when the specimen temperature is raised to  $40^{\circ}\text{C}$  for a fairly long period (several hours), if the samples are kept under vacuum. This is due to the stability of the carbon radicals which are the effective centers of grafting.

The authors wish to express their thanks to Dr. Tatsuo Matsuda for his continued interest and encouragement. They are also grateful to Mitsubishi Petrochemical Co., Ltd. for supplying isotactic polypropylene.

### References

1. A. Chapiro, *Radiation Chemistry of Polymeric System*, Interscience, New York, 1962, p. 601.
2. T. Matsuda, B. Eda, and K. Nunome, *Proc. 5th Conf. Radioisotopes, Japan*, **4-109** (1963).
3. J. Dobo and P. Hedvig, in *Macromolecular Chemistry, Prague 1965 (J. Polym. Sci. C, 16)*, O. Wichterle and B. Sedláček, Eds., Interscience, New York, 1967, p. 2577.
4. H. Fischer, K. H. Hellwege, U. Johnsen, and P. Neudörfl, *Kolloid-Z.*, **195**, 129 (1964).
5. H. Fischer, K. H. Hellwege, and P. Neudörfl, *J. Polym. Sci. A*, **1**, 2109 (1963).
6. R. P. Gupta, *J. Phys. Chem.*, **68**, 1229 (1964).
7. N. Tamura and K. Shinohara, *Repts. Progr. Polym. Phys. Japan*, **6**, 273 (1964).
8. A. I. Kurilenko, L. B. Smetanina, L. B. Aleksandrova, and V. L. Karpov, *Vysokomol. Soedin.*, **7**, 1935 (1965).

Received December 15, 1969

## Poly(4,4'-dipiperidyl)amides\*

J. PRESTON and R. W. SMITH,†  
*Chemstrand Research Center, Inc., Durham,  
North Carolina 27702*

### Synopsis

Polyamides from 4,4'-dipiperidyl, 1,2-ethylene-, and 1,3-propylene- bridged dipiperidyls were prepared via solution and interfacial polycondensation techniques. In sharp contrast to the polyamides from *N,N'*-alkyl-substituted alkylene diamines and aromatic diacids, the polyamides from 4,4'-dipiperidyls are high-melting (up to 455°C) and alcohol-insoluble. Tough films were cast from formic acid solutions of the polymers; fiber of good physical properties was prepared from a formic acid solution of the polyterephthalamide of 1,2-di(4-piperidyl)ethane.

### INTRODUCTION

Prior to their disclosure in Monsanto patents,<sup>1,2</sup> polyamides (A) derived from dipiperidyls apparently were unknown, despite the fact that dipiperidyl and its homologs have been known for many years and despite the fact that analogous polyamides from piperazine and substituted piperazines have been studied extensively<sup>3</sup> (a comprehensive review on the subject has been published by Morgan<sup>4</sup>).

We have been prompted to report our study of the polyamides derived from 4,4'-dipiperidyl and bridged dipiperidyls because of the recent publication of a study by Allport<sup>5</sup> on polyamides and polyureas from 2,2'- and 4,4'-dipiperidyl. None of the polymers discussed here, except I (Table I) which was reported also by Allport, have been reported previously. Polymers (B and C) structurally related to those derived from 4,4'-dipiperidyl have been claimed in recently issued patents.<sup>6,7</sup>

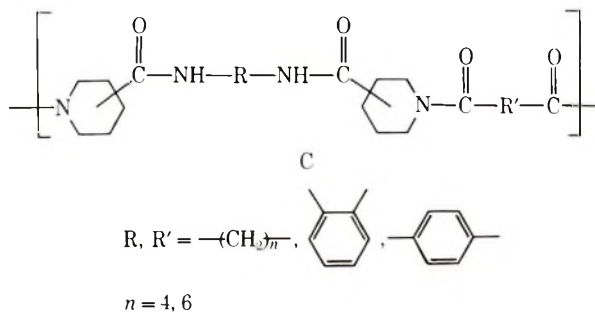
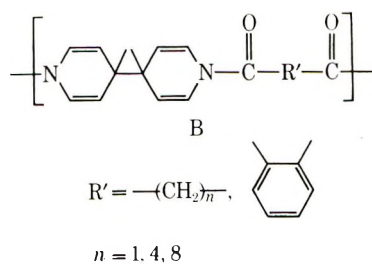
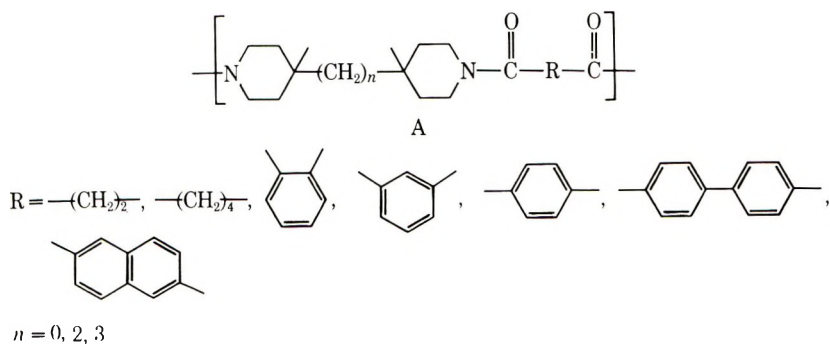
### EXPERIMENTAL

#### Preparation of Diamines

4,4'-Dipiperidyl<sup>8</sup> and 1,2-di(4-piperidyl)ethane<sup>9</sup> were prepared by published procedures. A generous sample of 1,3-di(4-piperidyl)propane was obtained from Reilly Coal Tar Products.

\* Presented in part at the 159th National Meeting, American Chemical Society, Houston, Texas, February 1970.

† Present address: Monsanto Company, Pensacola, Florida 32502.



### Preparation of Diacid Chlorides

Commercially available succinyl, adipyl and *o*-phthaloyl chlorides were redistilled under reduced pressure; a commercial sample of oxalyl chloride was used as received. The other diacid chlorides were distilled under reduced pressure, then recrystallized from *n*-hexane and dried at 25°C under vacuum (nitrogen bleed).

### Polymerizations

All of the polymers except the oxamides were prepared by the interfacial polycondensation technique;<sup>10,11</sup> the polyoxamides were prepared by the solution polycondensation technique<sup>12</sup> because of the very rapid hydrolysis of oxalyl chloride during interfacial polycondensation.

### Interfacial Polycondensation

The procedure employed was similar to that used by Katz for the preparation of the polyphthalamides of piperazine.<sup>3</sup> Into a food blender jar were placed 200 ml of ice-water, 6.30 g (0.03 mole) of 1,3-(4-dipiperidyl)propane, 6.4 g sodium carbonate, 10 ml of chloroform, and 0.25 g Duponol ME (DuPont trademark for sodium lauryl sulfate). The contents of the jar were stirred vigorously and a solution of 6.09 g (0.03 mole) of isophthaloyl chloride in 40 ml chloroform was added all at once. An emulsion was formed which was stirred for 15 min, after which time the contents of the blender jar were transferred to a beaker containing 200 ml hot water. The chloroform was boiled off and the polymer was isolated, washed well with water and dried. The yield of XV (Table I) having an inherent viscosity of 0.86 was 10.2 g (100% of theory).

### Solution Polycondensation

Because chloroform is a suitable solvent for poly(dipiperidyl)amides and because it is inert to the reaction of acid chlorides, it was chosen as solvent for preparing the polyoxamides of 4,4'-dipiperidyls from oxalyl chloride—a monomer too reactive with water to be used for the preparation of high molecular weight polymer in good yield *via* the interfacial polymerization method. The procedure used was essentially that of Kwolek (et al.,<sup>1,2</sup>) except that no triethylamine hydrochloride was added to the chloroform prior to polymerization of the diamines with oxalyl chloride.

### Spinning of Fiber

Polymer VII (Table I) was dissolved in 95% formic acid, deaerated, and wet-spun into a coagulation bath consisting of an aqueous caustic solution. The resulting fiber was hand-drawn.

## RESULTS AND DISCUSSION

### Polymerizations

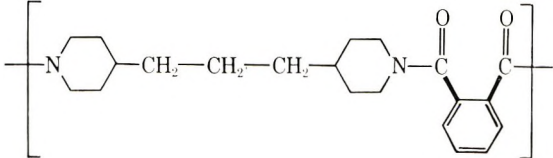
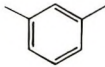
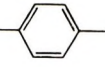
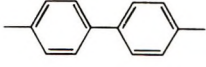
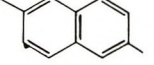
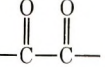


Polymers were readily prepared either by interfacial polymerization or by solution polycondensation. Presumably melt condensations could be carried out for melt stable polymers by employing the salts of the dipiperidyls and diacids or the diamines and diesters as reported by Allport.<sup>5</sup>

It is important to note that polymers of reasonably high molecular weight can readily be prepared from the 4,4'-dipiperidyls and *o*-phthaloyl chloride and succinyl chloride. On the other hand, it is well known that these acid chlorides react with primary diamines to yield low molecular weight polymers which are unstable in the melt because of imide formation. The explanation for the behavior of the 4,4'-dipiperidyls with these acid chlorides lies in the fact that secondary diamines, such as piperazine, cannot undergo the ring-closing reaction (see Katz<sup>3</sup>). The molecular weights of the polymers from succinyl chloride are limited, however, by

TABLE I  
 Poly(4,4'-dipiperidyl)amides

No.	Structure	Polymerization method <sup>a</sup>	$\eta_{inh}^b$
I		I	0.70 <sup>c</sup>
II		I	0.97 <sup>c</sup>
III		I	0.76 <sup>c</sup>
IV		I	0.41
V		I	1.64
VI		I	1.64
VII		I	2.34
VIII		I	0.62
IX		I	0.23
X		I	2.03
XI		S	0.24
XII		I	0.80
XIII		I	0.71

TABLE I (continued)

No.	Structure	Polymerization method <sup>a</sup>	$\eta_{inh}^b$
XIV		I	0.38
XV		I	0.86
XVI		I(S)	0.99 (0.30)
XVII		I	0.29
XVIII		I	0.99
XIX		S	0.37
XX		I	0.49
XXI		I	0.53

<sup>a</sup> I, interfacial polymerization; S, solution polycondensation.

<sup>b</sup> Inherent viscosities were determined at 30°C on a solution of 0.5 g of polymer per 100 ml of *m*-cresol.

<sup>c</sup> Solvent: 90% formic acid.

the fact that short-chain acid chlorides undergo hydrolysis during interfacial polymerization at a rate much higher than that of the longer chain homologs.

### Fabrication of Films and Fibers

All of the polymers prepared were readily soluble in chloroform, 90–95% formic acid, *m*-cresol, and concentrated sulfuric acid. Excellent colorless films were cast from solutions of the polymers in chloroform and formic acid. All of the films could be hot-drawn; several films became opaque upon being drawn several times their original length.

Film of VII (Table I) was studied by means of the penetrometer and found to have transitions at  $-5$ ,  $125$ , and  $203^\circ\text{C}$ ; the latter temperature is thought to be the glass transition temperature. No melting point was

TABLE II  
 Thermal Properties of Poly(4,4'-dipiperidyl)amides

No.	PMT, °C <sup>a</sup>	Glass transition temperature, °C <sup>b</sup>	Decomposition temperature, °C <sup>c</sup>
I	435 (376-380) <sup>d</sup>		460
II	455 <sup>e</sup>	~320 (270) <sup>f</sup>	460
III	455	(270) <sup>f</sup>	465
IV	(215) <sup>d</sup>	(175) <sup>f</sup>	
V	(250-252) <sup>d</sup>		
VI	(254-255) <sup>d</sup>		
VII	340-345 <sup>e</sup> (346-354) <sup>d</sup>	~160 (203) <sup>h</sup>	440
VIII	(320) <sup>d</sup>	200	400
IX	(>300) <sup>d</sup>		
X	270	210-220	455
XI	(245) <sup>d</sup>		
XII	(225) <sup>d</sup>		
XIII	(182-187) <sup>d</sup>	(~150) <sup>f</sup>	
XIV	(215) <sup>a</sup>		
XV	160		445
XVI	290		
XVII	(275) <sup>d</sup>		
XVIII	250	170 (240) <sup>f</sup>	450
XIX	(195) <sup>d</sup>		
XX	(215) <sup>d</sup>		
XXI	(160) <sup>d</sup>		

<sup>a</sup> Polymer melt temperature determined by differential thermal analysis (DTA) in nitrogen (rate = 20°C/min).

<sup>b</sup> Determined from the DTA thermogram.

<sup>c</sup> Decomposition temperature observed by thermogravimetric analysis (TGA) in nitrogen (rate = 15°C/min).

<sup>d</sup> Visual PMT determined in air.

<sup>e</sup> With decomposition.

<sup>f</sup> Visual softening temperature determined in air.

<sup>g</sup> DTA decomposition temperature in nitrogen, 370°C.

<sup>h</sup> Penetrometer determination.

observed for VII in the penetrometer examination which was conducted to a temperature in excess of 275°C.

A fiber was spun from a solution of VII ( $\eta_{inh}$  1.78) in formic acid; the tensile properties of the fiber (denier, 6.9 dpf) were: tenacity, 2.8 g/den and elongation, 16.1%. It was possible to spin I into fiber by means of a syringe; however, no tensile properties were obtained on this rudimentary fiber.

### Thermal Properties

**Melting Points.** The melting points (Table II) of the various polymers were determined by means of differential thermal analysis (DTA) and by visual observation of the polymer on a hot block. DTA melting points (nitrogen atmosphere) were higher than those observed on the hot block

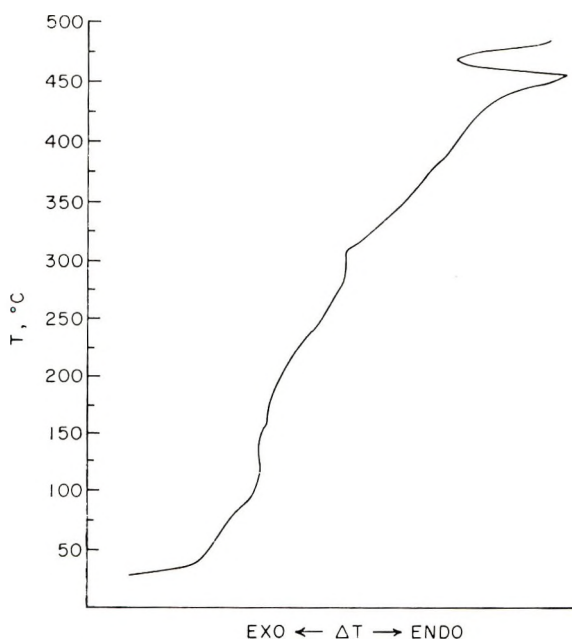


Fig. 1. Programmed DTA (in nitrogen, 15°C/min) of film of II (previously hot-drawn at 250°C).

in air. Possibly the rapid determination in nitrogen by means of DTA gives the "true" melting point of the polymer while the visual method in air yields the melting point of the slightly degraded polymer. Katz<sup>3</sup> also observed this phenomenon for the polyamides of piperazine (DTA mp values of 449–483°C but softening points in the neighborhood of 325°C) and Shashoua<sup>14</sup> observed it for the polyterephthalamides of short chain aliphatic diamines (mp values from x-ray analysis ranged 55–120°C lower than DTA analysis).

A typical DTA thermogram is shown in Figure 1.

Although the softening points (Table II) in air of films from polymers I, II, and VII were rather low when these films were in the relaxed state on a heated surface, no softening was observed to 300°C and no decomposition was seen up to 350°C when the films were held taut.

Fabrication by fusion techniques was not effective except for the lowest-melting polymers of the series; the polymers of high melting point suffered degradation when held at the melt for appreciable periods of time.

**Decomposition Temperatures.** Thermogravimetric analysis (TGA) in a nitrogen atmosphere of the poly(4,4'-dipiperidyl)amides showed them to be fairly resistant to thermal degradation (Table II). In fact, the TGA decomposition temperatures in nitrogen for certain of these polymers were comparable to those of some of the wholly aromatic polyamides.<sup>15,16</sup>

Despite the variations in structure and the wide spread in melting points of several poly(4,4'-dipiperidyl)amides, their weight-loss curves (Fig. 2)



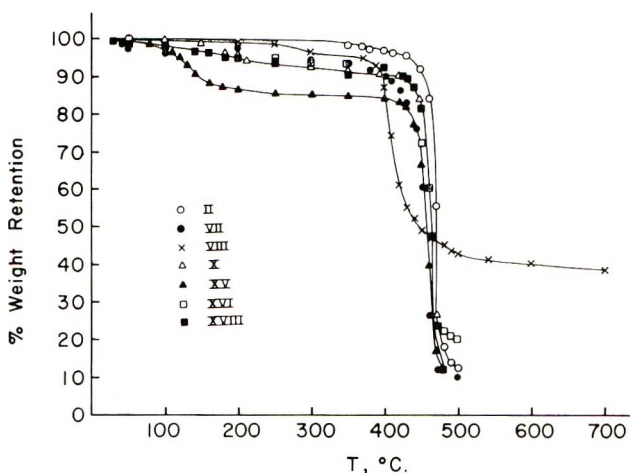


Fig. 2. Programmed TGA (in nitrogen, 15°C/min) of poly(4,4'-dipiperidyl)amides. Note: the relatively large drop in weight for XV above 100°C is presumed to be due to loss of adsorbed water, since the sample of film used for the TGA determination had been previously hot-drawn at 150°C.

determined by means of TGA were remarkably similar. Thus, decomposition occurred for most of these polymers in the range of 440–460°C, and very little residue was obtained. A notable exception was the polyamide from tetrachloroterephthaloyl chloride, which decomposed at a lower temperature (~400°C) but gave a relatively high char yield (40%).

**Resistance to Air Oxidation.** The well-recognized sensitivity of polyamides derived from primary aliphatic diamines to air oxidation at elevated temperatures is also observed for the polyamides from dipiperidyl and its homologs. Oxidation apparently occurs upon the piperidyl ring, for Allport<sup>5</sup> reports that the infrared spectra of the degraded products obtained by heating the model compounds *N,N'*-diacetyl- and *N,N'*-dibenzoyl-4,4'-dipiperidyl at 200°C in air indicated the presence of additional oxygenated materials.

### Structure–Property Relationships

It is well known that substitution of methyl or ethyl groups for hydrogen on the nitrogen in carboxamide groups of polyamides leads to greatly enhanced solubility and to a drastic lowering of melting point. Thus, the polyterephthalamide of tetramethylenediamine has a melting point of 436°C while the melting point of the polymer from the corresponding *N,N'*-dimethyl substituted diamine has a melting point of only 270°C.<sup>14</sup> The latter polymer is soluble in ethanol, chloroform, and acetone, whereas the former is quite insoluble in these solvents.

It is not surprising, therefore, that polyamides of secondary diamines, such as piperazine and substituted piperazines and dipiperidyl and its homologs exhibit good solubility in solvents such as chloroform. What is

surprising is the rather high melting points of these polymers which lack hydrogen bonding. It is to be expected that polyterephthalamides of secondary diamines should have considerably lower melting points than polyterephthalamides of primary diamines of the same chain length. However, in the case of the polyterephthalamides of piperazine and 4,4'-dipiperidyls apparently the lack of hydrogen bonding is compensated for by the stiffness of the heterocyclic rings.

An interesting observation may be made by comparing the structures and melting points of the polyterephthalamides of short-chain alkylene-diamines with those of the polyterephthalamides of some 4,4'-dipiperidyls (Table III). One observes that the melting points of the polyterephthalamides of primary straight-chain diamines are directly comparable to those of the polyterephthalamides from 4,4'-dipiperidyls containing the same number of *methylene groups* in that continuous segment of the polymer

TABLE III  
Comparison of Polyterephthalamides of Dipiperidyls and Alkylendiamines

Structure	$T_m$ , °C <sup>a</sup>
	435 (450-490) <sup>b</sup>
	436
	370
	371 <sup>c</sup>
	290
	341 <sup>c</sup>

<sup>a</sup> Determined by differential thermal analysis.

<sup>b</sup> Data of Allport.<sup>5</sup>

<sup>c</sup> Data of Shashoua and Eareckson.<sup>14</sup>

repeat unit derived from the heterocyclic diamines. A similar comparison may be made for the melting point of the polyterephthalamide of piperazine with that of the polyterephthalamide of ethylene diamine; thus, the former polymer has mp 350°C (dec., 478°C)<sup>3</sup> and the latter polymer has an mp (determined by x-ray analysis) of 400°C (455°C by DTA).<sup>14</sup>

### Solubility

Solubility of the poly(4,4'-dipiperidyl)amides is directly proportional to the length of the bridge in the diamine moiety. This is in agreement with the usual observation that solubility increases with decreasing melting point for a series of polymers of the same class.

The authors wish to express their appreciation to Dr. L. G. Kasbo for the preparation of one of the monomers and to Dr. T. L. Tolbert for another. We also wish to thank Messrs. W. L. Smith and W. L. Hofferbert, Jr. for their excellent technical assistance.

The encouragement of this work by the late Dr. W. A. H. Huffman is gratefully acknowledged.

### References

1. Belg. Pat. 629,358 (1963); Brit. Pat. (to Monsanto Company), 970,145 (1964).
2. J. Preston and R. W. Smith (to Monsanto Company), U.S. Pat. 3,371,068 (1968).
3. M. Katz, *J. Polym. Sci.*, **40**, 337 (1959).
4. P. W. Morgan, *Condensation Polymers by Interfacial and Solution Methods*, Interscience, New York, 1965.
5. D. C. Allport, in *Advances in Polymer Science and Technology*, (S. C. I. Monograph No. 26) Soc. of Chem. Ind., London, 1967, p. 143.
6. W. E. Kramer and L. A. Joo (to Pure Oil Co.), U.S. Pat. 3,197,442 (1965).
7. F. E. Cislak, U.S. Pat. 3,297,655 (1957).
8. C. R. Smith, *J. Am. Chem. Soc.*, **50**, 1928 (1936).
9. T. L. Tolbert and J. Preston, *J. Heterocyclic Chem.*, **6**, 963 (1969).
10. E. L. Wittbecker and P. W. Morgan, *J. Polym. Sci.*, **40**, 289 (1959).
11. P. W. Morgan and S. L. Kwolek, *J. Polym. Sci.*, **40**, 299 (1959).
12. P. W. Morgan, in *Macromolecular Chemistry, Paris 1963 (J. Polym. Sci. C, 4)*, M. Magat, Ed., Interscience, New York, 1963, p. 1075.
13. S. L. Kwolek, P. W. Morgan, and W. R. Sorenson, U.S. Pat. 3,063,766 (1962).
14. V. E. Shashoua and W. M. Eareckson, *J. Polym. Sci.*, **40**, 343 (1959).
15. J. Preston, *J. Polym. Sci. A-1*, **4**, (1966).
16. F. Dobinson and J. Preston, *J. Polym. Sci. A-1*, **4**, 2093 (1966).

Received December 16, 1969

## Kinetics of Polymerization of *N*-Carboxy Amino Acid Anhydride in Dimethyl Sulfoxide

MASANAO OYA, *College of Technology, University of Gunma, Kiryu-shi Gunma-ken, Japan*, and KEIKICHI UNO and YOSHIO IWAKURA, *Department of Synthetic Chemistry, Faculty of Engineering, University of Tokyo, Bunkyo-ku Hongo, Tokyo, Japan*

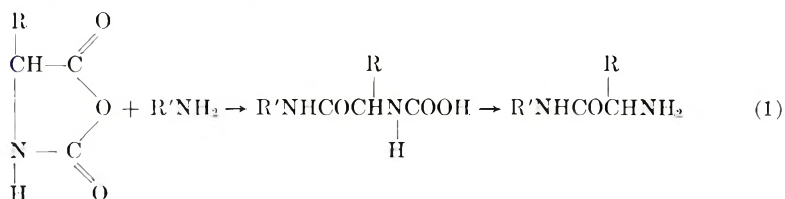
### Synopsis

Various kinds of NCA's were polymerized in dimethyl sulfoxide (DMSO). DL-Alanine NCA polymerized at a fast rate without initiator, the rate being represented by  $R_{p1} = k[M]^{1/2}$ . When the polymerization was carried out in chloroform in the presence of DMSO, the rate was represented by the equation,  $R_{p2} = K_2[M][DMSO]^{1/2}$ .

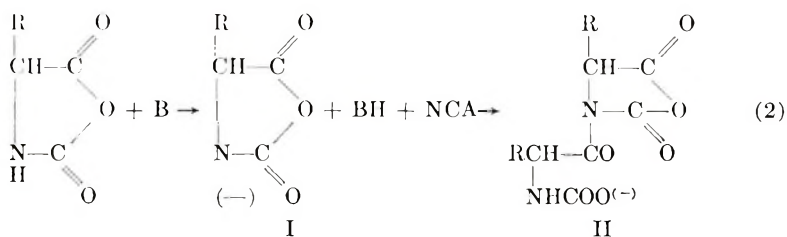
Glycine NCA and DL- $\alpha$ -amino-*n*-butyric acid NCA also polymerized at a fast rate in DMSO without initiator. On the other hand, *N*-methylglycine NCA, DL- and L-valine NCA and DL- and L-leucine NCA did not polymerize in DMSO without initiator.

### INTRODUCTION

The mechanism of amine-initiated polymerization of *N*-carboxy amino acid anhydrides has been studied extensively.<sup>1-9</sup> Primary amines initiate the polymerization of  $\gamma$ -benzyl L-glutamate NCA in DMF and of DL-alanine NCA in acetonitrile<sup>3</sup> by nucleophilic attack of an amino group on C-5 carbonyl of NCA. The propagation reaction is considered to proceed by repetition of the reaction (1). When the polymerization proceeds by this mechanism, the degree of polymerization of the polymer obtained agreed with  $[M_0]/[I_0]$ , where  $[M_0]$  and  $[I_0]$  are concentrations of the monomer and initiator, respectively.<sup>4-6</sup>



Tertiary amines, which are strong bases, initiate the polymerization by proton abstraction from the nitrogen of the NCA.<sup>6-8</sup> The resulting NCA<sup>-</sup> (I) attacks the C-5 carbonyl of an additional NCA to give the product (II). In such a case the degree of polymerization of the polymer obtained was found to be larger than  $[M_0]/[I_0]$ . It is well known that the polymerizations initiated by primary and secondary amines in dioxane, tetrahydro-



furan, and chloroform are considered to involve both mechanisms (1) and (2).<sup>6</sup>

When the polymerization was carried out in acetonitrile, the polymer formed was insoluble in the solvent, and the propagation proceeded between solid polymer and liquid monomer. As the initiation reaction was faster than the propagation reaction at this time, the rate of polymerization is determined by the propagation rate.<sup>3</sup>

The polymerization of NCA in DMSO was found to give polymer of quite different appearance from that in acetonitrile. The polymerization of some NCA proceeded at a fast rate in DMSO without initiator.<sup>1</sup> It is clear that DMSO is related to the NCA in the polymerization.

## RESULTS AND DISCUSSION

When NCA was dissolved in purified DMSO, polymerization began immediately and the solution turned into a colloidal suspension. At this time, chlorine content in the NCA affected the polymerization reaction.

The polymerization of DL-alanine NCA was carried out in purified DMSO under various conditions. The results are shown in Figures 1 and 2.

As shown in Figures 1 and 2, the induction period lengthened with increasing chlorine content in the NCA. The polymerization rate and degree of polymerization of the polymer were slightly decreased with the increase of chlorine content in the NCA. The rate of the polymerization and number-average degree of polymerization of the polymer obtained were not affected by increasing of water content in the DMSO, however. It is well known that water initiates the polymerization of NCAs to produce polypeptide. These results, however, indicate that the water in DMSO did not affect the rate of polymerization of NCAs.

The plot in Figure 1 shows that the kinetics of the polymerization of DL-alanine NCA in DMSO obey eq. (3):

$$R_p = k[M]^{1/2} \quad (3)$$

This suggests that the NCAs are aggregated to produce a type of micelle in DMSO, and the concentration of the monomer around the micelle does not decrease in proportion to the decrease of the overall monomer concentration. Accordingly the apparent rate of polymerization must be proportional to  $[M]^{1/2}$ . The rate did not slow down at 15–20% conversion, in spite of the fact that the solution became viscous at this point. This further supported the above consideration.

The relationships between the degree of polymerization and conversion to the polymer are shown in Table I. The degree of polymerization of the polymer was not affected by the monomer concentration and polymerization temperature. If the polymerization were a stepwise reaction, the degree of polymerization of the polymer formed would increase with increasing conversion to the polymer. But as Table I shows, a high degree of polymerization of the polymer was obtained at the low conversion of the

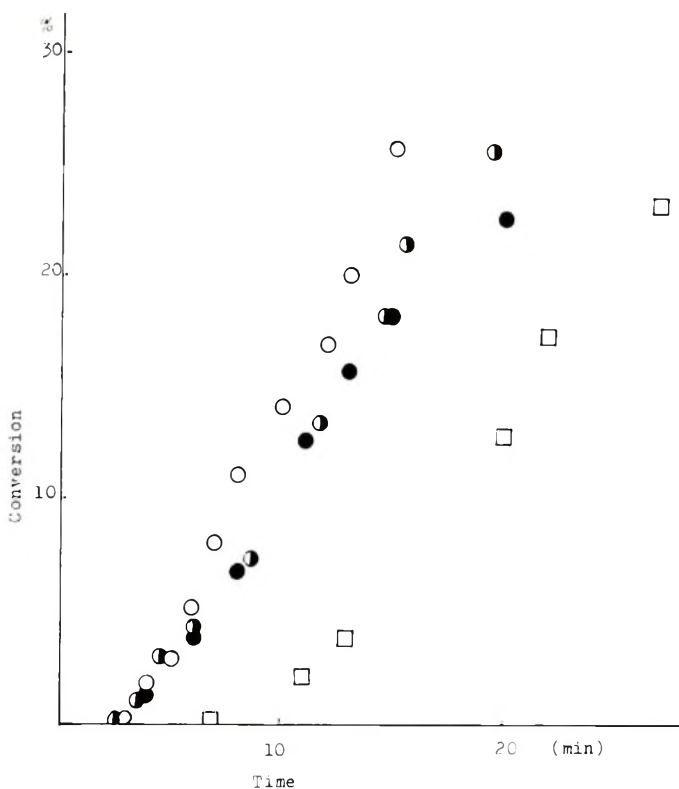


Fig. 1. Polymerization of *DL*-alanine NCA in DMSO at 30°C: (○) 0.434 mole/l.,  $[M] = 0.434$  mole/l.,  $R = 2.17\%$ /min; (●) 0.289 mole/l.,  $[M] = 0.309$  mole/l.,  $R = 1.75\%$ /min; (◐) 0.217 mole/l.,  $[M] = 0.233$  mole/l.,  $R = 1.57\%$ /min; (□) 0.173 mole/l.,  $[M] = 0.187$  mole/l.,  $R = 1.44\%$ /min. Cl content 0.015%.

monomer. This may indicate that the propagation reaction is faster than the initiation reaction.

DMSO must affect the initiation of the polymerization. Two mechanisms are considered as follows.

DMSO is known to be a good aprotic solvent.<sup>10</sup> However, it is known that DMSO is a reactive compound.<sup>11</sup> For example, DMSO can react with acid anhydride (Pummer reaction).<sup>12</sup> DMSO can react with acetic anhydride to produce  $\alpha$ -acetoxy thioether at 80% yield.<sup>13</sup> Since NCA is a kind of intermolecular acid anhydride, it is possible that it would react with

TABLE I  
 Polymerization of DL-Alanine NCA in DMSO<sup>a</sup>

Cl content of NCA, %	Temp, °C	Polymerization time, min	Conversion, %		H <sub>2</sub> O in DMSO, mg	[ $\eta$ ] in DCA	Degree of polymeri- zation	Sulfur in polymer, %
			By CO <sub>2</sub>	By weight				
0.015	30	11.0	13.55	16.78	0.61	0.314	93	0
	"	19.5	25.37	28.00	0.61	0.326	98	0
	"	30.0	44.00	49.00	0.61	0.335	101	0
0.082	21	16.0	17.80	20.00	0.61	0.353	109	0
	25	15.0	18.91	21.91	0.61	0.346	106	0
	30 <sup>b</sup>	36.0	28.40	30.50	0.61	0.353	109	0
	30	41.0	25.30	26.60	0.17	0.307	90	0
	30	41.0	24.30	23.40	1.27	0.302	88	0
	25.5	14.5	18.90	21.10	0.17	0.377	119	0
	20	34	11.40	14.00	0.17	0.326	98	0

<sup>a</sup> Initial monomer concentration 0.23 mole

<sup>b</sup> (0.17 mole/l.), about 20 cc.

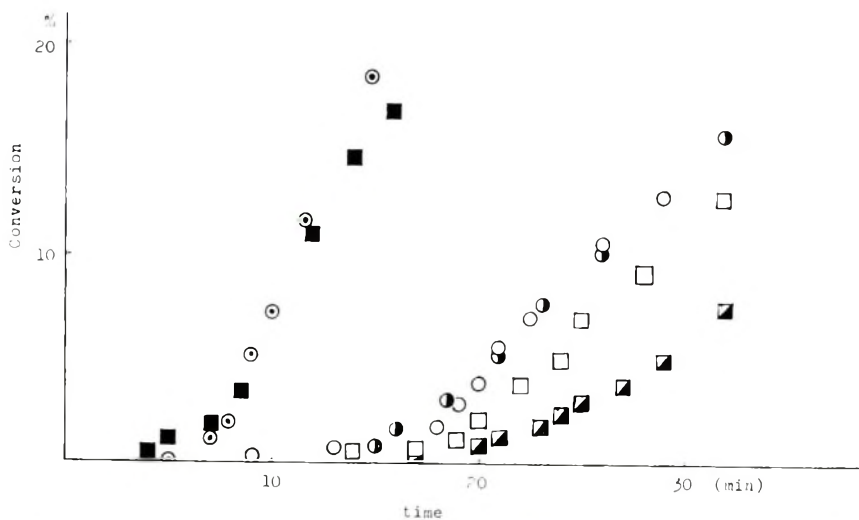
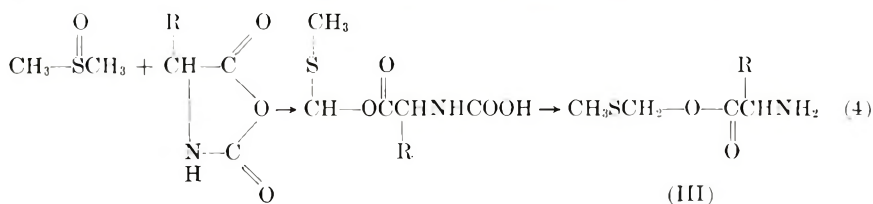
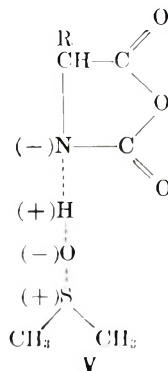
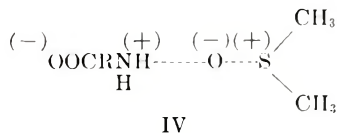


Fig. 2. Polymerization of DL-alanine NCA in DMSO: (○) Cl content 0.015%, H<sub>2</sub>O in DMSO, 0.169 mg/cc, 25°C; (■) Cl content, 0.015%, H<sub>2</sub>O in DMSO, 0.169 mg/cc, 21°C; (○) Cl content 0.082%, H<sub>2</sub>O in DMSO, 0.169 mg/cc, 30°C; (●) Cl content 0.082%, H<sub>2</sub>O in DMSO, 1.27 mg/cc, 30°C; (□) Cl content 0.082%, H<sub>2</sub>O in DMSO, 0.169 mg/cc, 25.5°C; (◐) Cl content 0.082%, H<sub>2</sub>O in DMSO, 0.169 mg/cc, 21°C. Monomer concentration, 0.217 mole/l.

DMSO to give an amino compound such as product III. The amino compound III may initiate the polymerization of NCA to produce polypeptide.

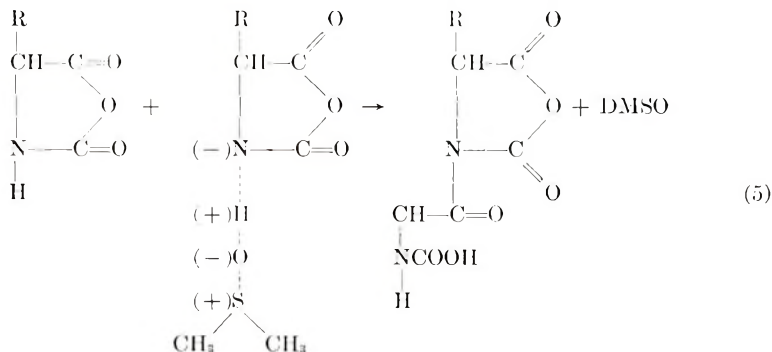


A complex of NCA with DMSO may be produced. It is well known that DMSO produces complex with amino compounds because DMSO is able to form hydrogen bonds with the amino group, as shown by the structures IV.<sup>14</sup>





DMSO is known to accelerate addition of an amino group ( $\alpha$ -amino acid) to an  $\alpha,\beta$ -unsaturated compound by hydrogen-bonding interaction.<sup>14</sup> Accordingly, DMSO may hydrogen-bond with NCA as shown in structure V. This complex would be more active than the NCA, and a propagation mechanism by this intermediate species can be postulated. This involves nucleophilic attack by NCA complex on the C-5 carbonyl of an NCA molecule. This propagation mechanism is similar to that of activated monomer by tertiary amines shown in eq. (2).



When the polymerization is considered to proceed by mechanism (1), the degree of polymerization of the polymer must agree with  $[M_0]/[I_0]$ , and the polymer must have a methyl sulfide group as an endgroup of the polymer. As Table I shows, the molecular weight of the polymer obtained by the polymerization in DMSO was not affected by the conversion of the monomer.

Since DMSO seems to affect the initiation, polymerization of DL-alanine NCA was carried out in chloroform and tetrahydrofuran with addition of a small amount of DMSO. DMSO was the initiator for the polymerization. The results are shown in Table II and Figure 3. The rate of polymerization in chloroform was first-order when the concentration of DMSO was constant. The apparent rate of polymerization relative to the concentration of DMSO was calculated. It was found that the rate was proportional to

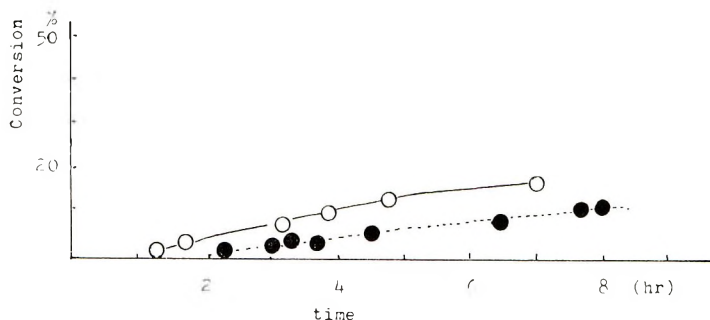


Fig. 3. Polymerization of DL-alanine NCA with DMSO in chloroform: (O) DMSO 50%; (●) DMSO 10%. Monomer concentration 0.435 mole/l., 30°C.

TABLE II  
 Polymerization of DL-Alanine NCA in Some Solvents with DMSO<sup>a</sup>

Solvent	Polymerization time, hr	Conversion, % (by weight)	[ $\eta$ ] in DCA	Degree of polymerization		Sulfur in polymer, %
				Osmometric	Calcd	
Chloroform-DMSO 10% (vs. NCA)	8.3	11.4	0.372	118	1.2	0
	19.0	66.0	0.398	136	6.6	0
	23.0	82.0	0.355	113	18.2	0
Tetrahydrofuran-DMSO 5.0% (vs. NCA)	44.0	100.0	0.382	112	10.0	0
	69.5	3.2	0.470	164	0.65	0
	141.5	8.1	0.530	180	1.60	0
Tetrahydrofuran-DMSO 10% (vs. NCA)	220.0	89.0	0.489	170	18.0	0
	48.0	9.7	0.277	78	0.95	0
	72.0	77.0	0.188	37	7.7	0

<sup>a</sup> Initial monomer concentration, 0.23% mole/l. (20 cc); DCA = dichloroacetic acid.

$[\text{DMSO}]^{1/2}$ . Then the initial rate of polymerization will be represented as follows:

$$R_p = d[-M]/dt = k[\text{NCA}][\text{DMSO}]^{1/2} \quad (6)$$

with  $k = 1.1 \times 10^{-3}$

This equation is very similar to that for vinyl polymerization and shows that the initiation is very slow and the propagation is very fast.

Polymerization of DL-alanine NCA was initiated with *n*-butylamine and triethylamine in THF and chloroform for comparison with the polymerization in the presence of DMSO. The results are shown in Figure 4 and Table III. The rate of polymerization initiated with *n*-butylamine (A,B)

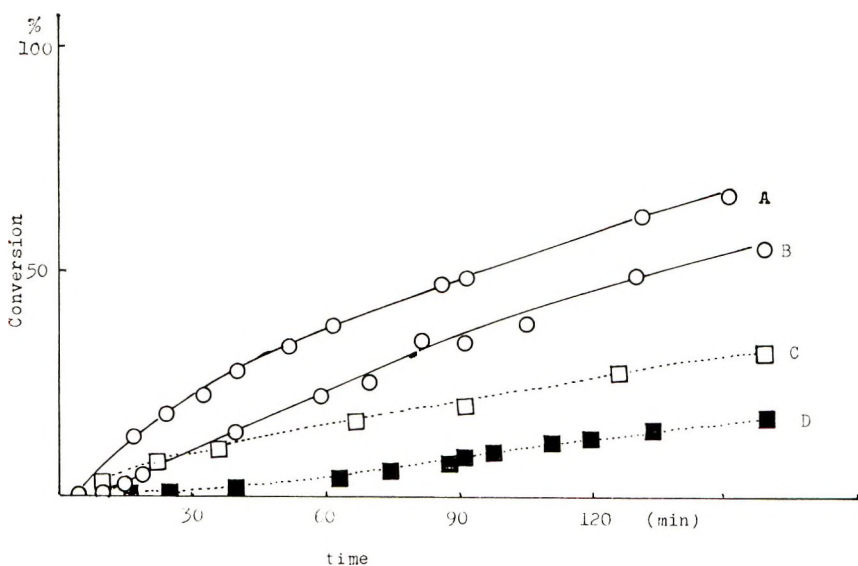


Fig. 4. Polymerization of DL-alanine NCA in chloroform and tetrahydrofuran initiated with *n*-butylamine and triethylamine: (A) *n*-butylamine, in chloroform; (B) *n*-butylamine, in THF; (C) triethylamine, in chloroform; (D) triethylamine, in THF. Monomer, 0.435 mole/l., 30°C.

was faster than that initiated with triethylamine (D,C). However the degree of polymerization of the polymer obtained with initiation with *n*-butylamine was less than that of the polymer obtained with triethylamine at the same conversion. In the polymerization initiated with triethylamine the molecular weight of the polymer was not affected by the conversion of the monomer. This may mean that the rate of propagation for triethylamine-initiated polymerization was faster than that for *n*-butylamine-initiated reaction. These results agreed with the polymerization of  $\gamma$ -benzyl L-glutamate NCA initiated by primary and tertiary amines, respectively.

In the polymerization in the presence of DMSO, the fast rate of propagation and high molecular weight of the polymer at low conversion were

TABLE III  
 Polymerization of DL-Alanine NCA in Chloroform and Tetrahydrofuran Initiated with *n*-Butylamine and Triethylamines<sup>a</sup>

A	Solvent	Initiator (0.5 mole-%)	Polymerization time, min	Conversion, %		$[\eta]$	$\bar{P}$ (osmometric)
				By CO <sub>2</sub>	By weight		
A	Chloroform	<i>n</i> -Butylamine	15	16.8	12.8	0.162	37
			30	23.5	27.5	0.222	51
			135	67.6	81.0	0.363	106
B	Tetrahydrofuran	<i>n</i> -Butylamine	24	15.9	16.2	0.153	34
			60	26.2	30.4	0.235	66
			120	44.0	45.0	0.206	51
C	Chloroform	Triethylamine	335	87.6	90.9	0.467	173
			60	14.2	10.4	0.431	152
			145	28.1	25.4	0.407	131
D	Tetrahydrofuran	Triethylamine	340	42.2	37.9	0.467	124
			110	11.7	9.1	0.166	37
			357	42.6	39.8	0.102	19
			535	50.5	50.3	0.147	34

<sup>a</sup> Initial monomer concentration, 0.435 mole/l. (20 cc).

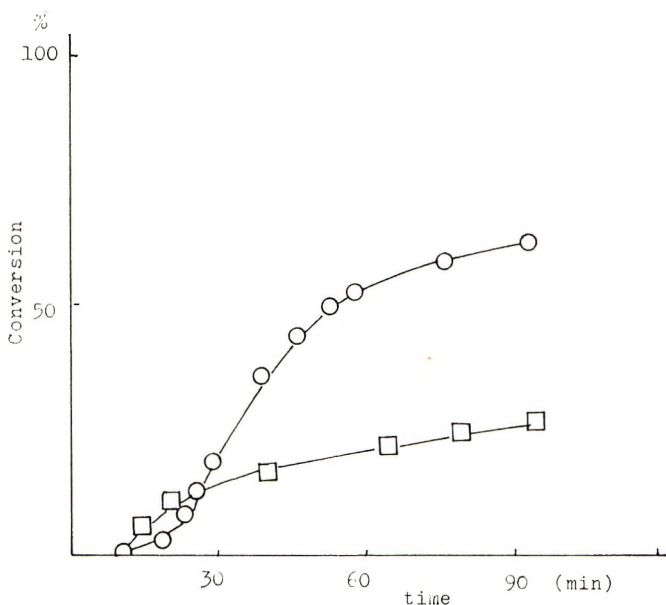


Fig. 5. Polymerization of glycine NCA and DL- $\alpha$  amino-*n*-butyric acid NCA in DMSO: (O) DL- $\alpha$  amino-*n*-butyric acid NCA, 0.141 mole/l.; (□) glycine NCA, 0.217 mole/l.

similar to those of the polymerization with triethylamine, and the degree of polymerization of the polymer was higher than the value of  $[M_0]/[I_0]$ .

Analysis of sulfur in the polymer was carried out by a special method using silver particles and by a sodium nitroprusside method,<sup>15,16</sup> but no sulfur was found in the polymers.\*

In conclusion, the polymerization of DL-alanine NCA in DMSO may be considered to proceed in a similar way as that initiated by tertiary amine, mainly by the mechanism (2) of the activated complex system.

Glycine NCA and  $\alpha$ -amino-*n*-butyric acid NCA were polymerized in DMSO without initiator. The results are shown in Table IV and Figure 5.

The polymerization of these NCAs proceeded at a high rate. The intrinsic viscosity of these polymers was high at low conversion of NCA. These results are similar to those in the polymerization of DL-alanine NCA in DMSO.

L- and DL-valine NCA, L- and DL-*n*-leucine NCA, L- and DL-*n*-valine NCA, and L- and DL-leucine NCA did not polymerize in DMSO without initiator but did polymerize with initiator (Table V). These facts may be explained as follows: the DMSO-NCA complex could not attack at the C-5 carbonyl of these NCAs because of steric hindrance of the large substituent on the NCA carbonyl.

*N*-Methylglycine NCA and *N*-phenylglycine NCA also did not polymerize in DMSO without initiator. They could not participate in complex formation because they have no hydrogen on 3-N of the NCA.

\* As the molecular weights of these polymers were 2600-12000, there should be sulfur contents of 1.27-0.27% if the sulfur existed as endgroups of the polymers.

TABLE IV  
 Polymerization of Some NCAs in DMSO without Initiator

NCAs	Polymerization time, min	Conversion % <sup>a</sup>		[ $\eta$ ]	Sulfur in polymer
		By CO <sub>2</sub>	By weight		
Glycine NCA <sup>a</sup>	24	8.0	7.2	0.170 (TFA)	0
	60	19.0	18.2	0.164	0
	90	19.2	19.0	0.156	0
DL- $\alpha$ -Amino- <i>n</i> -butyric acid NCA <sup>b</sup>	24	9.6	11.0	0.189	0
	45	41.8	44.0	0.225	0
	4800	59.6	60.0	0.205	0

<sup>a</sup> Monomer concentration 1 g/22.8 cc, no initiator.

<sup>b</sup> Monomer concentration, 0.5 g/20 cc, no initiator.

 TABLE V  
 Polymerization of Some NCAs in DMSO with Initiator<sup>a</sup>

NCA	Poly- merization time, hr	Conversion (by weight), %	[ $\eta$ ] <sup>b</sup>	Sulfur in polymer
L-Leucine NCA	54	3.5	1.40 (TFA)	0
	114	12.9	0.53	0
	180	16.0	0.35	0
DL- <i>n</i> -Leucine NCA <sup>c</sup>	42	12.9	0.164 (DCA)	0
	102	19.1	0.177	0
	182	20.2	0.181	0
DL- <i>n</i> -Valine NCA	18	7.5	0.382 (DCA)	0
	60	20.7	0.355	0
	240	37.1	0.437	0

<sup>a</sup> Monomer concentration, 1 g/20 cc; 0.5 mole-% *n*-butylamine was used as an initiator. All polymerizations (Tables I-V) run at 30°C without stirring.

<sup>b</sup> DCA = dichloroacetic acid; TFA = trifluoroacetic acid.

<sup>c</sup> Monomer concentration, 0.5 g/20 cc.

If the polymerization of NCA in DMSO were to proceed by mechanism (1), the polymerization of these NCAs would proceed without initiator in DMSO. These results also confirm that the polymerization of DL-alanine NCA in DMSO proceeded by means of an activated complex.

## EXPERIMENTAL

DMSO was dried over CAH<sub>2</sub> and molecular sieves and distilled *in vacuo*. The water content was determined by Karl Fisher titration.

Very pure DL- and L-alanine NCA (4-methyl oxazolidine dione) (chlorine contents less than 0.02%) were prepared as reported previously.<sup>1</sup> The other NCAs in highly pure form were prepared under the conditions shown in Table VI. Polymerization was carried out as reported previously,<sup>1</sup> but acetonitrile was used instead of diethyl ether as the precipitation solvent for the polymers.

TABLE VI  
 Conditions for Synthesis of NCAs

Starting material	Amt, g	Phosgenation		Recrystallization solvents	
		Amt solvent (THF), cc	Temp, °C	First	Second
Glycine	8	400	40-50	Ethyl acetate (hot)	Ethyl acetate
DL- $\alpha$ -Amino <i>n</i> -butyric acid	10	400	"	Chloroform (hot)	Ethyl acetate
L- $\alpha$ -Amino- <i>n</i> -butyric acid	5	200	"	Diethyl ether	Isopropyl ether
L-Valine	10	400	"	Diethyl ether	Isopropyl ether
DL-Valine	10	400	"	Diethyl ether	Isopropyl ether
L- <i>n</i> -Valine	10	200	"	Diethyl ether	Isopropyl ether
DL- <i>n</i> -Valine	10	400	"	Diethyl ether	Isopropyl ether
L-Leucine	10	400	"	Diethyl ether	Isopropyl ether
DL-Leucine	10	400	"	Diethyl ether	Isopropyl ether
L- <i>n</i> -Leucine	5	200	"	Diethyl ether	Isopropyl ether
DL- <i>n</i> -Leucine	5	200	"	Diethyl ether	Isopropyl ether
N-Phenylglycine	10	400	"	Diethyl ether	Acetonitrile
N-Methylglycine	10	400	"	Diethyl ether	Acetonitrile

The rate of polymerization was obtained by measuring the amount of CO<sub>2</sub> evolved by the method of Katchalski and Shalitin.<sup>9</sup>

The molecular weight of the poly-DL-alanine was determined by the equation as reported previously.<sup>3</sup>

Sulfur in polymer was determined by a special procedure involving the use of Ag particles and by a sodium nitroprusside method.<sup>15,16</sup> The sample used in this analysis was above 50 mg.

### References

1. Y. Iwakura, K. Uno, and M. Oya, *Kogyo Kagaku Zasshi*, **69**, 741 (1966).
2. Y. Iwakura, K. Uno, and M. Oya, *J. Polym. Sci. A-1*, **5**, 2867 (1967).
3. Y. Iwakura, K. Uno, and M. Oya, *J. Polym. Sci. A-1*, **6**, 2165 (1968).
4. M. Szwarc, *Fortschr. Hochpolym. Forsch.*, **4**, 1 (1968).
5. C. H. Bamford, in *Polyamino Acids, Polypeptides and Proteins*, M. A. Stahmann, Ed., Univ. Wisconsin Press, Madison, Wisc., 1965.
6. M. Goodman and J. Hutchison, *J. Amer. Chem. Soc.*, **88**, 3627 (1965).
7. M. Goodman, *J. Amer. Chem. Soc.*, **86**, 2284 (1964).
8. M. Goodman and U. Aron, *Biopolymers*, **1**, 500 (1963).
9. E. Katchalski, *J. Amer. Chem. Soc.*, **82**, 1630 (1960).
10. D. Martin, *Angew. Chem.*, in press.
11. E. J. Corey and M. Chaykooski, *J. Amer. Chem. Soc.*, **84**, 866 (1962).
12. R. Pummer, *Ber.*, **43**, 1401 (1910).
13. L. Horner and Kaiser, *Ann.*, **626**, 19 (1959).
14. M. Friedman, *J. Amer. Chem. Soc.*, **89**, 4709 (1967).
15. Nippon Kagakukai, *Jikkenkagaku Koza*, **16**, 229 (1959).
16. T. Uno, *Kisobunsekikagaku Koza*, Kyoritsu, Japan, 1966, p. 33.

Received September 4, 1968

Revised December 17, 1969

## Studies on Monomer Reactivity Ratios. III. Comparison of Various Mathematical Models

JAMES R. HOYLAND, *Battelle Memorial Institute,  
Columbus Laboratories, Columbus, Ohio 43201*

### Synopsis

Seven mathematical models for the treatment of monomer reactivity ratios in free-radical copolymerization are compared from the viewpoint of their relative simplicity, accuracy, and the number of parameters necessary for their use. It is concluded that the electronegativity and charge-transfer models proposed in previous papers represent the best compromise for routine usage if quantitative accuracy is the primary concern.

### INTRODUCTION

Two new mathematical models for the treatment of monomer reactivity ratios in free-radical bulk copolymerization have recently been introduced.<sup>1,2</sup> It was shown that these models are generally capable of giving a quantitative description of experimental data except for certain copolymer systems involving acrylonitrile. This is in contrast to the older  $Q-e$  scheme<sup>3</sup> which, while giving a qualitative description of reactivity ratios, fails to give quantitative accuracy even if the relatively large experimental errors are taken into account. In spite of these shortcomings, however, the  $Q-e$  scheme is exceedingly useful because of its simplicity and its ability to give a fair overall picture of the trends of reactivity ratios. It is perhaps for this reason that studies leading to better mathematical models have not previously been undertaken.

This paper represents an effort to develop further mathematical models and to discuss the relative merits of these and existing formulations. Such a systematic investigation should be of great utility in defining the limitations and advantages of the various methods and to enable the proper choice of model best suited to the needs of the user.

### THE MATHEMATICAL MODELS

The models discussed in this paper can be divided into three major classifications depending on the number of parameters per monomer required for their use. Each of these will be defined briefly in this section beginning with the two-parameter models, which are the simplest, and then proceeding to the three- and four-parameter formulations.



**Model I.** The first model considered is the familiar  $Q-e$  scheme<sup>3</sup> of Alfrey and Price. The equation utilized for the calculation of reactivity ratios is

$$r_1 = (Q_1/Q_2) \exp \{ -e_1 (e_1 - e_2) \} \quad (1)$$

**Model II.** The second model is also a two-parameter scheme which we designate as the "average charge-transfer" method, or ACT scheme. This model arises from the observation that in the charge-transfer model (Model III discussed below), the radical parameter  $E_R$  is usually quite close to the average of the parameters  $E_U$  and  $E_O$ . We therefore assume this relationship, and the expression for the reactivity ratio  $r_1$  can be written as

$$\log r_1 = \Delta E_{CT}(1 \cdot 2) - \Delta E_{CT}(1 \cdot 1) \quad (2)$$

where

$$\Delta E_{CT}(1 \cdot 2) = \min \left\{ \begin{array}{l} E_U(2) - [E_U(1) + E_O(1)]/2 \\ [E_U(1) + E_O(1)]/2 - E_O(2) \end{array} \right\} \quad (3)$$

$$\Delta E_{CT}(1 \cdot 1) = [E_U(1) - E_O(1)]/2 \quad (4)$$

**Model III.** The charge-transfer model, or CT scheme, is the next formulation considered.<sup>2</sup> This is a scheme in which the three necessary parameters can be construed as being related to the highest occupied orbital energy level,  $E_O$ , and the lowest lying unoccupied energy level,  $E_U$ , of the monomer, and the energy level of the singly occupied radical level,  $E_R$ . The expression for  $r_1$  is the same as eq. (2) but we now define

$$\Delta E_{CT}(i \cdot j) = \min \left\{ \begin{array}{l} E_U(j) - E_R(i) \\ E_R(i) - E_O(j) \end{array} \right\} \quad (5)$$

**Model IV.** Another three-parameter model which has been proposed is the electronegativity, or EN, scheme.<sup>1</sup> The parameters required are the electronegativity of the monomer and radical  $X_M$  and  $X_R$ , and a quantity  $L$  which is presumably related to resonance stabilization. The reactivity ratios are computed for the relationship

$$\log r_1 = L(2) - L(1) + |X_R(1) - X_M(1)| - |X_R(1) - X_M(2)| \quad (6)$$

**Model V.** The final three-parameter model considered is the  $Q-e-e^*$  scheme proposed by Wall<sup>4</sup> in which different polar parameters  $e$  and  $e^*$  are assigned to the monomer and radical. The expression for the reactivity ratio  $r_1$  is

$$r_1 = (Q_1/Q_2) \exp[-e^*_1(e_1 - e_2)] \quad (7)$$

**Model VI.** The first four-parameter model considered can be thought of as a combination of the  $Q-e$  and CT schemes. It is postulated that polar effects and charge transfer are both important factors in determining the relative transition state energies. Thus in addition to the parameters

$E_O$ ,  $E_U$ , and  $E_R$ , a parameter  $e$  is also assigned to each monomer, leading to the following expression for  $r_1$ :

$$\log r_1 = \Delta E_{CT}(1\cdot 2) - \Delta E_{CT}(1\cdot 1) - e_1(e_1 - e_2) \quad (8)$$

where  $\Delta E_{CT}(i\cdot j)$  is given by eq. (5). This model is designated as the CTE scheme.

**Model VII.** The final model considered in this paper is a four-parameter scheme similar to the previous formulation, but combining the  $Q-e$  and EN schemes. The required parameters are  $L$ ,  $X_M$ ,  $X_R$ , and  $e$ , and the equation for  $r_1$  is as follows:

$$\log r_1 = L(2) - L(1) + |X_R(1) - X_M(1)| - |X_R(1) - X_M(2)| - e_1(e_1 - e_2) \quad (9)$$

We designate this model by the acronym ENE.

### CALCULATIONS

Seventeen monomers for which extensive copolymerization data, preferably at 60°C, is available were chosen for study. These monomers are the same ones used previously for the study of the CT and EN models.<sup>1,2</sup> It was immediately apparent, however, that the  $Q-e$ , ACT, and  $Q-e-e^*$  models were incapable of sensible prediction for copolymers involving vinylidene chloride as one comonomer, and for these schemes only 16 monomer systems were studied. Furthermore, none of the models studied here is able to predict good values for  $r_1$  in systems in which  $M_1$  is a vinylpyridine and  $M_2$  is acrylonitrile. Wide scatter in experimental data seems to indicate that these systems are particularly troublesome, so that any computed  $r_1$  value for these copolymers was considered correct. One further particularly troublesome system, acrylonitrile and vinylidene chloride, was not considered. Otherwise all copolymer systems involving the 16 or 17 monomers for which experimental data have been reported were taken into account.

Parameter values for each model were generated by a method given previously.<sup>1</sup> The technique is a numerical least-squares formulation which takes into account experimental errors. The basic procedure is the numerical minimization of the function

$$f = \Sigma \Delta^2 \quad (10)$$

where  $\Delta$  is defined as

$$\Delta = \min \left\{ \begin{array}{l} |r_{\text{calc}} - r_{\text{exp}} - \epsilon| \\ |r_{\text{calc}} - r_{\text{exp}} + \epsilon| \end{array} \right\} \quad (11)$$

$\epsilon$  being the probable experimental error. The quantity  $\Delta$  is taken to be zero if  $r_{\text{calc}}$  lies between  $r_{\text{exp}} - \epsilon$  and  $r_{\text{exp}} + \epsilon$ . The calculations were made by using the pattern search method of Hooke and Jeeves.<sup>5</sup> It is now apparent why copolymer systems for which the various schemes are

unsuitable by their inherent nature should not be included since a few relatively large errors can mask an otherwise relatively satisfactory performance and completely disrupt the minimization calculation. The final minimized value of  $f$  is taken as a measure of the relative goodness of the various models.

## RESULTS AND DISCUSSION

Table I is a summary of the minimized values of the function  $f$  for the various models considered. Results for the four models capable of prediction for vinylidene chloride copolymers are given for both the case in which these copolymers are included in calculating  $f$  and also for the case in which they are excluded so that a more meaningful comparison between all methods can be made. It is apparent from the consideration of the results of Table I that two parameter models are inherently poor for quantitative prediction. The  $Q-e$  scheme is slightly better in overall predictive value than the ACT model so that there is no reason to give further consideration to this latter formulation. It is further noted that the  $Q-e-e^*$  method is extremely poor in comparison with the other three-parameter models. It is also noted that the values of the parameters which minimize the function  $f$  bear no orderly resemblance to the  $Q-e$  parameters, as shown in Table II, and the simple interpretation of the  $e$  values as related to electron withdrawing or donating properties of the vinyl group substituents is lost. We therefore believe that the  $e$  and  $e^*$  parameters probably bear little correlation to any physical or chemical property of the monomers or radicals and that the  $Q-e-e^*$  scheme should be regarded only as a mathematical model whose parameters cannot be related to any simple molecular property.

The CT and EN models, on the other hand, are great improvements over the two-parameter schemes. The function  $f$  assumes a relatively small value for either formulation and both are capable of satisfactorily treating vinylidene chloride copolymers. Furthermore, the parameters included in these models can be related, at least qualitatively, to simple physical properties of the molecules and radicals, as shown previously.<sup>1,2</sup> It would appear that the CT scheme is slightly better in overall performance

TABLE I  
Minimized Values of  $f$

Model	$f$ , VCl <sub>2</sub> excluded	$f$ , VCl <sub>2</sub> included
$Q-e$	0.2441	—
ACT	0.3108	—
CT	0.0080	0.0089
EN	0.0119	0.0122
$Q-e-e^*$	0.0994	—
CTE	0.0026	0.0027
ENE	0.0028	0.0029

TABLE II  
 Best Parameter Values for the  $Q-e$  and  $Q-e-e^*$  Models

Monomer	$Q-e$ model		$Q-e-e^*$ model		
	$Q$	$e$	$Q$	$e$	$e^*$
Styrene (ST)	1.000	-0.784	1.000	-2.475	-0.280
Methyl acrylate (MA)	0.388	0.714	0.573	0.732	0.458
Methyl methacrylate (MM)	0.805	0.380	1.095	0.127	0.417
2-Vinylpyridine (2VP)	1.128	-0.490	1.158	-1.482	-0.097
4-Vinylpyridine (4VP)	0.856	-0.170	0.964	-1.046	0.057
Acrylonitrile (AN)	0.756	1.260	1.197	1.241	1.453
<i>p</i> -Methoxystyrene (PMXS)	1.417	-1.232	1.136	-3.154	-0.410
<i>p</i> -Chlorostyrene (PCLS)	0.990	-0.450	1.065	-1.791	-0.010
<i>p</i> -Methylstyrene (PMES)	1.105	-0.970	0.888	-2.771	-0.237
Methyl vinyl ketone (MVK)	0.812	0.777	1.736	1.097	0.466
2-Methyl-5-vinyl-pyridine (2M5VP)	1.080	-0.726	1.016	-1.799	-0.235
Vinyl acetate (VAC)	0.031	-0.101	0.050	0.060	0.259
Methacrylonitrile (MAN)	1.364	1.112	1.744	0.789	1.252
Methacrylic acid (MACD)	1.610	0.660	2.625	0.666	0.449
Methacryloxymethylpenta- methylsiloxane (MMPD)	0.735	0.124	0.860	-0.830	0.281
5-Ethyl-2-vinylpyridine (5E2VP)	1.260	-0.728	1.133	-1.939	-0.195

but the EN model is more satisfying insofar as physical interpretation is concerned.

The four-parameter models further reduce the value of  $f$  significantly, but this reduction may be more apparent than real. The number of

 TABLE III  
 Parameter Values for the CTE Model

Monomer <sup>a</sup>	$E_U$	$E_R$	$E_O$	$e$
ST	2.989	0.000	-3.349	0.154
MA	2.950	-0.549	-4.479	-0.280
MM	2.733	-0.501	-3.651	-0.166
2VP	2.770	-0.213	-3.279	-0.262
4VP	2.776	-0.300	-3.386	-0.276
AN	2.710	-0.816	-4.480	-0.376
PMXS	3.062	0.005	-3.190	0.283
PCLS	2.837	-0.300	-3.308	0.206
PMES	3.022	0.000	-3.343	0.233
MVK	2.486	-0.595	-4.222	-0.323
2M5VP	2.953	-0.100	-3.342	0.038
VAC	4.001	-0.515	-5.030	-0.230
MAN	2.386	-0.759	-3.870	-0.280
MACD	2.187	-0.660	-3.857	-0.057
MMPD	2.910	-0.525	-3.584	-0.084
5E2VP	2.917	-0.160	-3.278	-0.047
VCl2	3.600	-0.659	-4.340	-0.150

<sup>a</sup> Abbreviations given in Table II except for vinylidene chloride, VCl2.

TABLE IV  
 Parameter Values for the ENE Model

Monomer	$L$	$X_R$	$X_M$	$e$
ST	0.000	0.000	0.148	0.071
MA	0.588	0.542	0.817	-0.267
MM	0.010	0.494	0.458	-0.125
2VP	-0.155	0.220	0.252	-0.218
4VP	-0.082	0.300	0.290	-0.210
AN	0.397	0.789	0.870	-0.420
PMXS	-0.029	-0.069	0.033	0.175
PCLS	-0.092	0.270	0.203	0.118
PMES	0.012	-0.088	0.130	0.188
MVK	0.189	0.580	0.817	-0.250
2M5VP	-0.020	0.160	0.170	-0.051
VAC	1.338	0.480	0.480	-0.231
MAN	-0.003	0.670	0.690	-0.311
MACD	-0.209	0.598	0.688	-0.172
MMPD	0.075	0.497	0.316	-0.086
5E2VP	-0.072	0.180	0.156	-0.041
VC12	0.800	0.662	0.360	-0.080

freely varying parameters in the CTE case is 67 ( $E_R$  for styrene is fixed at zero), and 66 in the ENE case ( $L$  and  $X_R$  for styrene are fixed at zero), and the number of reactivity ratios available for parameter calculation is only 96, several of these having large uncertainties associated with them. We are therefore approaching the situation in which there are only a few more equations than unknowns and one expects nearly perfect fitting in this case. Ideally, we would like to have perhaps 20-30 more reactivity ratios for the monomers considered to better judge whether the increased flexibility inherent in the four-parameter models is really significant or a mathematical artifact. A further questionable feature of these models is the relatively large variation of the  $e$ -values computed for each model as shown by inspection of Tables III and IV. It is expected that if these parameters have some real physical significance that closer agreement would be obtained between the two sets of results. It should be pointed out, however, that again this variation may be more apparent than real due to the difficulty of locating a true minimum on such a complicated mathematical hypersurface as we are dealing with here. The parameters are closely coupled, so that errors in one parameter can be nearly compensated by errors in others, leading to a local false minimum on the hypersurface from which there is no "down-hill" path to the true minimum. It is almost impossible to avoid these local minima and it is expected that a very large number of parameter sets exist which will give minimized  $f$  values to within  $\pm 0.0002$  of those found here.

In view of the relatively large uncertainties in experimental data, it is felt that either the CT or EN model represents a good compromise between quantitative accuracy, number of parameters per monomer, and ease of routine usage. The other three-parameter model tested, namely the

$Q-e-e^*$  scheme, appears to have only a small advantage over the  $Q-e$  formulation and should not be seriously considered as a working model in view of the success of the CT and EN methods.

The  $Q-e$  scheme still appears to be a relatively important model for rapid calculation of qualitative data. It is significantly better than the ACT method and is familiar to most polymer chemists, which is a definite advantage. The revised parameters given in Table II allow somewhat better overall agreement with experiment than the older values and will enable a more consistent set of  $Q-e$  data to be computed for monomers not considered in this study.

### References

1. J. R. Hoyland, *J. Polym. Sci. A-1*, **8**, 885 (1970).
2. J. R. Hoyland, *J. Polym. Sci. A-1*, **8**, 901 (1970).
3. T. Alfrey, Jr., and C. C. Price, *J. Polym. Sci.*, **2**, 101 (1947).
4. L. A. Wall, *J. Polym. Sci.*, **2**, 542 (1947).
5. R. Hooke and T. A. Jeeves, *J. Assoc. Comput. Mach.*, **8**, 212 (1961).

Received December 24, 1969

## Statistical Study of the Effect of Variation of Bimolecular Rate Constant in Condensation Polymerization

V. S. NANDA and S. C. JAIN, *Centre for Advanced Study in Physics,  
University of Delhi, Delhi 7, India*

### Synopsis

We investigate the effect of variation of bimolecular rate constant with chain length on condensation polymerization by a statistical approach. The variation of reactivity with chain length is simulated in the present study by assigning appropriate weight factors to different species. Formal expressions for the size distribution and various averages of interest have been obtained. Some simple cases are then analyzed and comparisons with the experimental results of Taylor and Howard are carried out.

In an earlier paper,<sup>1</sup> using the kinetic approach, we investigated the effect of the variation of the bimolecular reaction rate constant with chain length on the statistical character of condensation polymers. The expressions for the size distribution and various averages of interest were obtained for the case when the reaction rate constant varies linearly with chain length. No general solution of the problem seemed possible.

In the present study, we employ a statistical approach to gain further insight into the problem. The technique of the generating function is employed, and the variation of reactivity with chain length is taken into account by assigning appropriate weight factors to different species. Formal expressions for various quantities of interest are first derived and some simple cases are then analyzed. Finally comparisons with the experimental results of Taylor<sup>2</sup> and Howard<sup>3</sup> are carried out in the light of our theoretical results.

Let  $N_0$  and  $N$ , respectively, denote the number of monomers and the polymer molecules at any stage of the reaction. The constraints to which the polymerization process is subjected obviously are

$$\sum_{i=1}^{\infty} N_i = N \quad (1)$$

and

$$\sum_{i=1}^{\infty} i \cdot N_i = N_0 \quad (2)$$

where  $N_i$  denotes the number of  $i$ -mers.

Consider first the case of the functional groups which are equally reactive, irrespective of the chain lengths. The number of complexions corresponding to a particular set of  $\{N_i\}$  is given by

$$\omega_{\{N_i\}} = N! / \prod_i N_i! \quad (3)$$

The total number of complexions

$$\Omega = \sum_{\{N_i\}} \omega_{\{N_i\}}$$

corresponding to the formation of  $N$  polymers from  $N_0$  monomers, is obtained from the G.F. (Generating Function)

$$\begin{aligned} \sum_{N_0} \Omega x^{N_0} &= (x' + x^2 + \dots)^N \\ &= \left( \frac{x}{1-x} \right)^N \end{aligned} \quad (4)$$

Since all the complexions here are equally likely to occur, the number of  $i$ -mers in the sample is given by the relation

$$\bar{N}_i = \frac{\sum_{\{N_i\}} N_i \omega_{\{N_i\}}}{\sum_{\{N_i\}} \omega_{\{N_i\}}} \quad (5)$$

The G.F. for  $\Omega_i$  (which stands for the term in the numerator) is

$$\sum_{N_0} \Omega_i x^{N_0} = N x^i \left( \frac{x}{1-x} \right)^{N-1} \quad (6)$$

as has been shown in our earlier work.<sup>4</sup> The expression for  $\bar{N}_i$  may be obtained by following the exact combinatorial treatment<sup>4</sup> or by the help of the method of steepest descents in complex variable. The procedure for the more general case is outlined in the Appendix. In either case for  $N \gg 1$ , we find

$$\bar{N}_i = N x^{i-1} (1-x) \quad (7)$$

where  $x$  here denotes the value of the variable at the saddle point and is given by the relation

$$x = 1 - (N/N_0)$$

Equation (7) represents the well known most probable distribution of Flory.

If the reactivity of a functional group varies with chain length, the polymerization process becomes nonrandom. In our statistical analysis, we assume that the occurrence of an  $i$ -mer has *a priori* probability\*  $g_i$  which depends upon prevailing distribution. Accordingly, to weigh suitably the different species, the number of complexions corresponding to different

\* The probability factors may have to be considered as time-dependent. The eventual problem would be to relate these to the various rate constants and the extent of the reaction.



set of  $\{N_i\}$  of eq. (3) is multiplied by  $\prod_i g_i^{N_i}$ . Consequently, the average number of  $i$ -mers in a polymer sample is given by the equation

$$\bar{N}_i = \sum_i N_i \omega_{i,N_i} \prod_i g_i^{N_i} / \sum_i \omega_{i,N_i} \prod_i g_i^{N_i} \quad (8)$$

The generating functions for the denominator ( $= \Omega$ ) and the numerator ( $= \Omega_i$ ) are easily found to be

$$\sum_{N_0} \Omega x^{N_0} = \left( \sum_i g_i x^i \right)^N \quad (9)$$

$$\sum_{N_0} \Omega_i x^{N_0} = N g_i x^i \left( \sum_i g_i x^i \right)^{N-1} \quad (10)$$

As is shown in the Appendix, the application of the method of steepest descents to eqs. (9) and (10) and substitution in eq. (8) gives

$$\bar{N}_i = N g_i x^{i-1} / \sum_i g_i x^{i-1} \quad (11)$$

where  $x$  here is the value of the variable at the saddle point and is given by the equation

$$\sum_i i g_i x^i / \sum_i g_i x^i = N_0 / N \quad (12)$$

Using eq. (11), the following formal expressions for the number-average chain length  $i_n$  and the weight-average chain length  $i_w$  can be put down.

$$i_n = \langle i^1 \rangle / \langle i^0 \rangle = \sum_i i g_i x^{i-1} / \sum_i g_i x^{i-1} \quad (13)$$

$$i_w = \langle i^2 \rangle / \langle i^1 \rangle = \sum_i i^2 g_i x^{i-1} / \sum_i i g_i x^{i-1} \quad (14)$$

where

$$\langle i^s \rangle = \sum_i i^s N_i / \sum_i N_i$$

denotes the  $s$ -th moment.

We now evaluate the expressions for the various statistical quantities for a few simple cases. Consider first the case

$$g_i = i^{-s} \quad (15)$$

Taking  $s < 1$  and making use of the relation

$$\lim_{n \rightarrow \infty} \left( \sum_i i^{-s} x^{i-1} \right) = \Gamma(1-s) / (1-x)^{1-s} \quad (16)$$

we find the number fraction

$$n_i = N_i / N = i^{-s} x^{i-1} (1-x)^{1-s} / \Gamma(1-s) \quad (17)$$

where  $x$ , by using eq. (12), is given by

$$x = 1 - (1-s) N / N_0 \quad (18)$$

and  $\Gamma s$  is the gamma function of order  $s$ .

By using eq. (17), the expression for the cumulative weight fraction can be put in the form

$$\begin{aligned} c_i &= (1/i_n) \int_0^i i n_i d_i \\ &\simeq \frac{1}{i_n} [\Gamma(1-s)]^{-1} \int_0^i \left\{ \frac{i(1-s)}{i_n} \right\}^{1-s} e^{-(i/i_n)(1-s)} di \\ &= I(u, p) \end{aligned} \quad (19)$$

where  $I(u, p)$  is the incomplete gamma function

$$u = \frac{i}{i_n} \frac{p}{\sqrt{1+p}}$$

and

$$p = 1 - s$$

For  $s = 1$ , the procedure outlined already leads to the expressions

$$n_i = -x^i [i \log(1-x)]^{-1} \quad (20)$$

$$i_n = -x [(1-x) \log(1-x)]^{-1} \quad (21)$$

$$i_w = (1-x)^{-1} \quad (22)$$

Thus the inhomogeneity index

$$R = i_w/i_n = -x^{-1} \log(1-x) \quad (23)$$

It seems reasonable to enquire about the upper limit to the  $s$  value which is consistent with the formation of high polymers. An inspection of eq. (13) with  $g_i = i^{-s}$  indicates that for  $i_n$  to be large, we must have  $s \leq 2$ . The following set of equations apply for  $s < 2$ .

$$n_i = i^{-s} x^{i-1} / \zeta(s) \quad (24)$$

$$i_n = \frac{\Gamma(s-1)}{\zeta(s)} (1-x)^{1-s} \quad (25)$$

$$i_w = (s-1) (1-x)^{-1} \quad (26)$$

and

$$R = \frac{(s-1) \zeta(s)}{(1-x)^{2-s} \Gamma(s-1)} \quad (27)$$

where  $\zeta(s)$  stands for the Reimann zeta function of order  $s$ . For  $s = 2$ , on the other hand, we find

$$n_i = i^{-2} x^{i-1} / \zeta(2) \quad (28)$$

$$i_n = -\frac{1}{\zeta(2)} \log(1-x) \quad (29)$$

$$i_w = -x [(1-x) \log(1-x)]^{-1} \quad (30)$$

and

$$R = \frac{x \zeta(2)}{(1-x) [\log(1-x)]^2} \quad (31)$$

It appears interesting to study the variation of inhomogeneity with  $s$ . In Figure 1, we have shown the variation of  $R$  with  $s$  for  $s < 1$  when  $i_n \gg 1$ . For this range of  $s$  values, the inhomogeneity seems to have a limiting value (see, however, Nanda<sup>5</sup>). For  $1 \leq s \leq 2$ , the value of  $R$  depends strongly on the degree of polymerization and has no finite limit when  $i_n$  becomes infinitely large. For this range of  $s$  values, we show in Figure 2 the variation of  $R$  with the average chain length  $i_n$  for  $s = 1$  and  $s = 1.5$ .

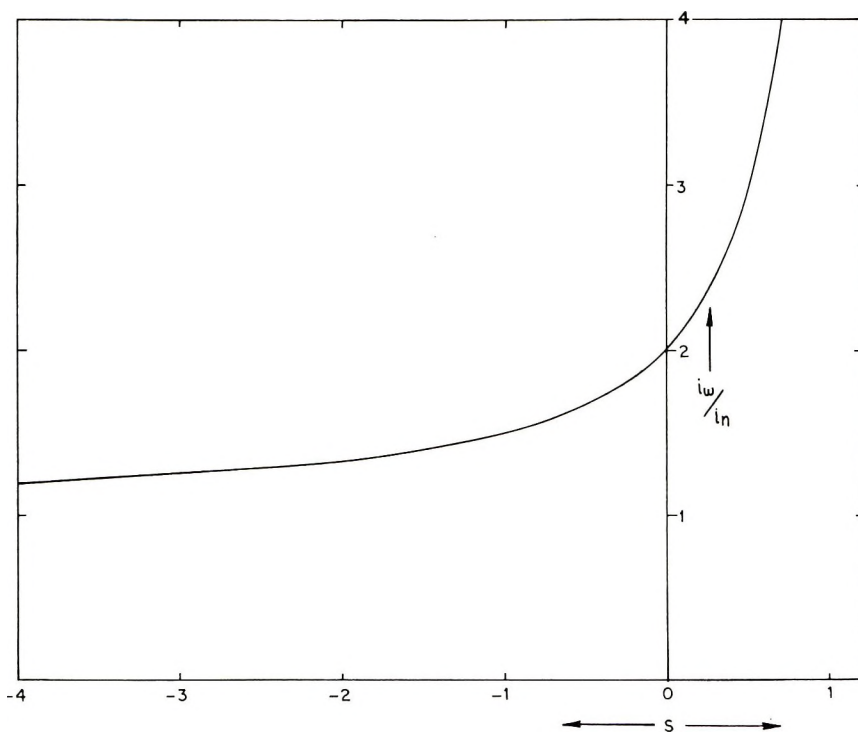


Fig. 1. Variation of the inhomogeneity index  $R$  with the parameter  $s$  of eq. (15) for  $s < 1$  and  $i_n \gg 1$ .

The foregoing choice of  $g_i$  would be appropriate for the study of polymerization process when the bimolecular rate constant varies appreciably with chain length even for long chains. It appears, however, more reasonable to assume that the rate constant varies appreciably with chain length for small chains but takes up a practically constant value for larger ones. Such a situation in the statistical approach would be simulated by taking

$$g_i = 1 + (c/i^s) \quad (32)$$

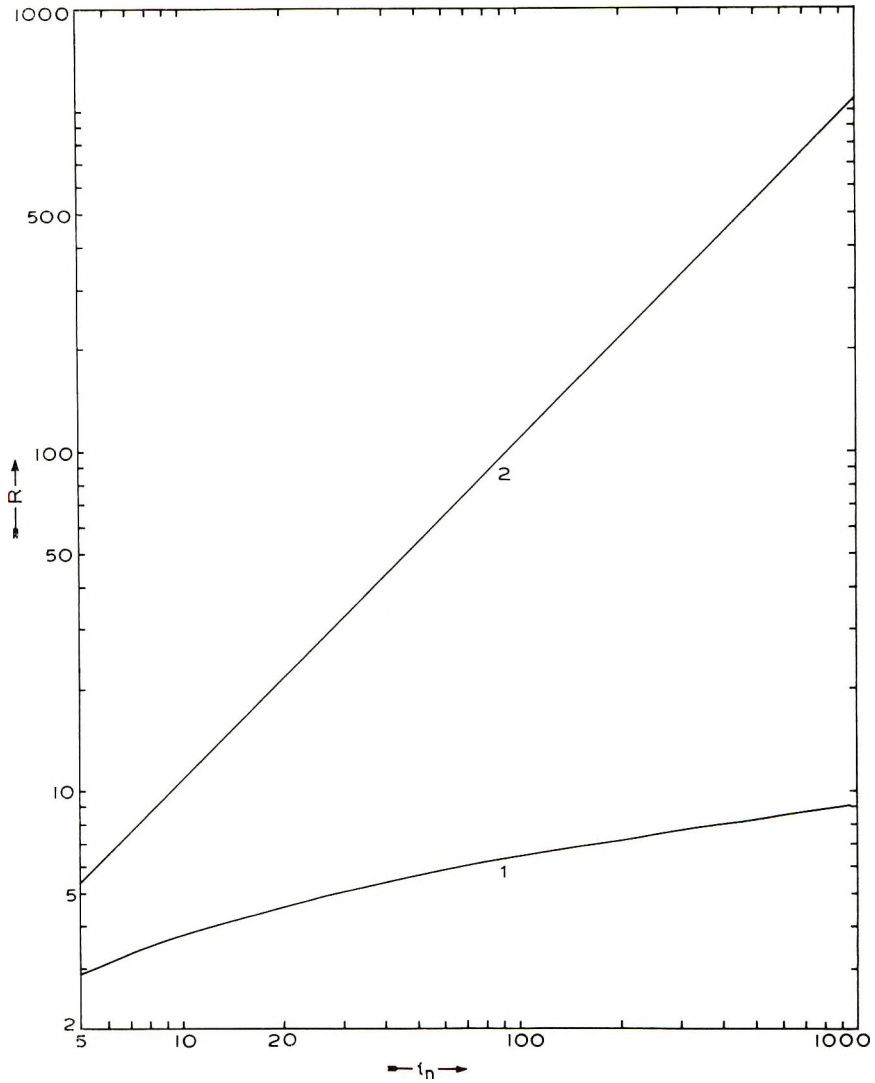


Fig. 2. Variation of  $R$  with  $i_n$ : (1)  $s = 1$ ; (2)  $s = 1.5$ .

where  $c$  and  $s$  are arbitrary parameters and  $s$  takes only positive values. Using eqs. (11), (13), and (14), we can write

$$n_i = \frac{[1 + (c/i^s)]x^{i-1}}{\left[ \frac{1}{1-x} + c \frac{\Gamma(1-s)}{(1-x)^{1-s}} \right]} \quad (33)$$

$$i_n = \left[ \frac{x}{(1-x)^2} + \frac{c\Gamma(2-s)}{(1-x)^{2-s}} \right] / \left[ \frac{x}{1-x} + \frac{c\Gamma(1-s)}{(1-x)^{1-s}} \right] \quad (34)$$

$$i_w = \left[ \frac{x(1+x)}{(1-x)^3} + \frac{c\Gamma(3-s)}{(1-x)^{3-s}} \right] / \left[ \frac{x}{(1-x)^2} + \frac{c\Gamma(2-s)}{(1-x)^{2-s}} \right] \quad (35)$$

and

$$R = \frac{\left[ \frac{x(1+x)}{(1-x)^3} + \frac{c\Gamma(3-s)}{(1-x)^{3-s}} \right] \left[ \frac{x}{1-x} + \frac{c\Gamma(1-s)}{(1-x)^{1-s}} \right]}{\left[ \frac{x}{(1-x)^2} + \frac{c\Gamma(2-s)}{(1-x)^{2-s}} \right]^2} \quad (36)$$

For  $s = 1$ , on the other hand, the following expressions for the size distribution and the averages are obtained:

$$n_i = [1 + (c/i)x^{i-1} \{1/(1-x)\} - (c/x) \log(1-x)] \quad (37)$$

$$i_n = \frac{x + c(1-x)}{(1-x)[x - c(1-x) \log(1-x)]} \quad (38)$$

$$i_w = \frac{x(1+x) + c(1-x)}{(1-x)[x + c(1-x)]} \quad (39)$$

and

$$R = \frac{[x(1+x) + c(1-x)][x - c(1-x) \log(1-x)]}{[x + c(1-x)]^2} \quad (40)$$

We shall now investigate how the statistical character of the polymer changes with increase in the degree of polymerization when  $g_i$  follows eq. (32) and  $s$  is positive. We first take  $c = 1$  and  $s = 1$ . In Table I, the

TABLE I

$x$	$i_n$	$i_w$	$R$	$R/R_F$
0.98106	50	103.6	2.073	1.047
0.99034	100	205.1	2.050	1.030
0.99802	500	1008.4	2.017	1.009
0.99901	1000	2009.9	2.010	1.005

results of calculation from eqs. (38) to (40) are shown. For the indicated values of  $i_n$ , the corresponding values of  $x$  are determined from eq. (38). These values are then used in the calculation of  $i_w$  and  $R$ . In the fifth column of Table I,  $R_F$  refers to the  $R$  value obtained from the most probable distribution of Flory. It is observed that initially the inhomogeneity is greater than the most probable value and approaches it as the reaction progresses. Such a behavior may be generally expected when  $c$  and  $s$  are positive. In terms of the kinetic language this implies increase of reaction rate constant with chain length and the eventual attainment of a practically constant value for sufficiently long chains.

Next we consider the opposite case when the reaction rate decreases initially with chain length before acquiring an effectively constant value. This behavior can be represented in the statistical approach by taking  $s$  positive and  $c$  negative in the  $g_i$  expression (32). For the sake of simplicity

TABLE II

$x$	$i_n$	$i_w$	$R$	$R/R_F$
0.9786	50	93.7	1.873	0.946
0.9896	100	192.4	1.924	0.967
0.9980	500	990.1	1.979	0.990
0.9990	1000	1998.0	1.988	0.995

we take  $c = -1$  and  $s = 1$ .<sup>\*</sup> The results of our calculations are given in Table II. As the increase in  $g_i$  with  $i$  implies decrease in the bimolecular rate constant with increasing chain length, we find as expected,  $R$  values

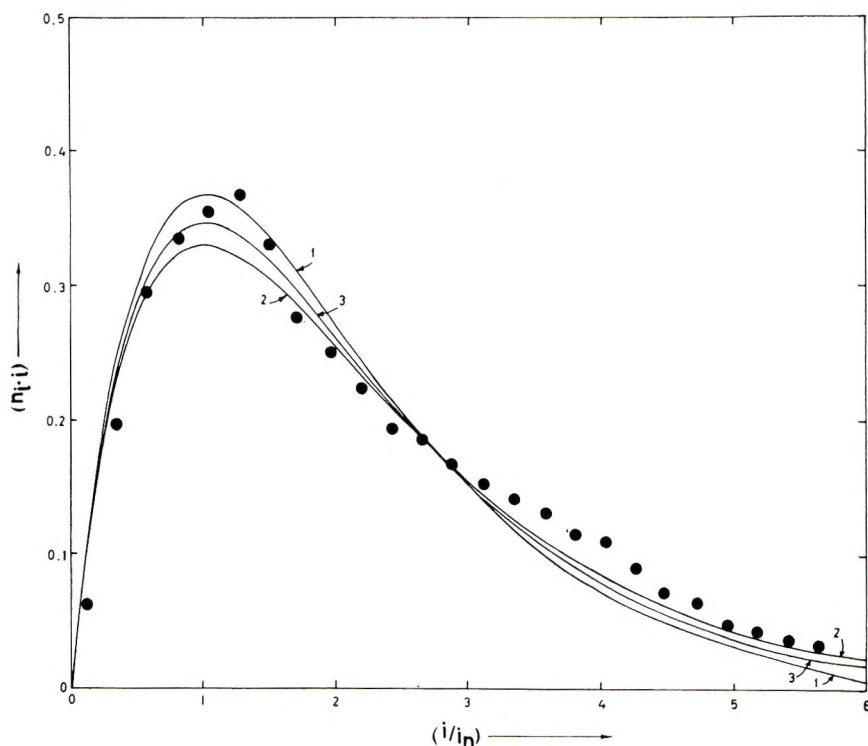


Fig. 3. Variation of  $in_i$  with  $i/i_n$ : (1) Flory distribution; (2) by eq. (17), with  $R = 2.10$ ,  $i_n = 100$ ,  $s = 1/11$ ; by eq. (17) (3) with  $R = 2.20$ ,  $i_n = 100$ ;  $s = 1/6$ . Dots are the experimental results of Taylor.

lower than the most probable distribution. However, as  $i_n$  increases  $R$  approaches  $R_F$ .

In the foregoing sections, we have given a formulation in which the effect of variation of reactivity with chain length is taken into account by assigning appropriate weight factors to different species. In principle it should

<sup>\*</sup> This choice results in  $g_1 = 0$  which implies infinitely fast rate constant involving reaction with monomers.

be possible to treat any case of nonrandom polymerization by this procedure. However, closed form expressions for the various quantities of interest can be worked out in cases where the assigned weight factors vary with chain length according to some simple relation. A few such cases have been analyzed here. These cover both the categories in which the resulting polymer is either more homogeneous or less homogeneous than the Flory distribution.

We now turn to comparison with the experimental results and take up first the consideration of Taylor's data.<sup>2</sup> Since  $i_w/i_n$  here is greater than the most probable value, we attempt the representation of the size distribution results by eq. (17) with suitable positive values of  $s$ . Here  $i_n = 100$  and  $R \simeq 2.10$ . Making use of eqs. (13) and (14), we find  $s = 1/11$  and  $x = 109/110$ . In Figure 3, plots of  $(in_i)$  versus  $(i/i_n)$  are shown along with the experimental results. Curve 2 represents the theoretical results with the indicated choice of parameters. We find that this curve shows a better agreement with experiment than the Flory distribution (shown as curve 1). Since Taylor has calculated  $R$  from the cumulative weight fraction plots, this may be subject to some errors. Therefore, we plot another curve, 3, which corresponds to  $R = 2.20$ . Then, using eqs. (13) and (14), we get  $s = 1/6$  and  $x = 119/120$ . It may be noted that curve 3 shows a better representation of the experimental size distribution curve especially on the side of longer chains.

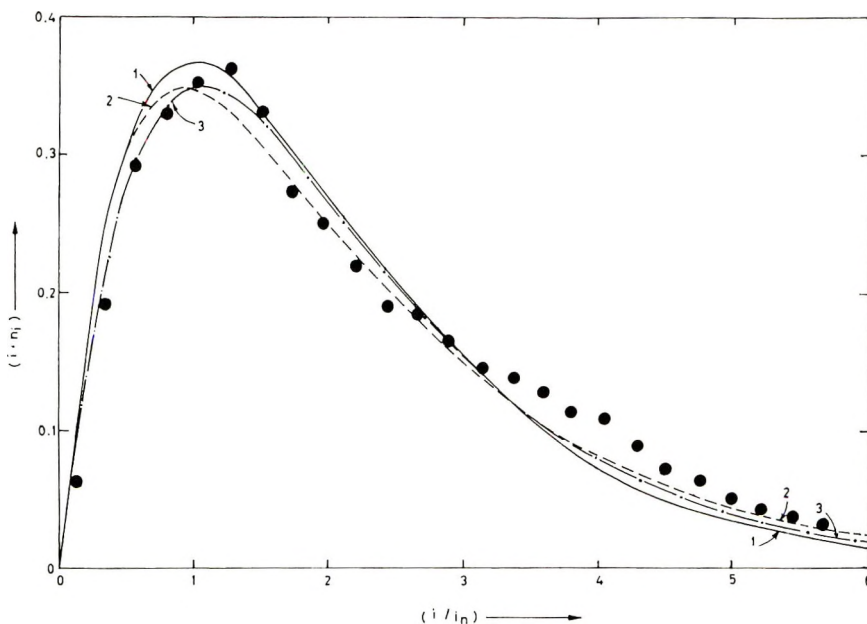


Fig. 4. Variation of  $in_i$  with  $i/i_n$ : (1) Flory distribution; (2) by eq. (42), with  $R = 2.10$ ,  $i_n = 100$ ,  $C_2/C_1 = -0.01$ ,  $i_0 = 200$ ,  $i_0' = 3.82$ ; (3) by eq. (2) with  $R = 2.15$ ,  $i_n = 100$ ,  $C_2/C_1 = -0.003$ ,  $i_0 = 200$ ,  $i_0' = 166$ . Dots are the experimental results of Taylor.

In order to obtain improvement over the lower chain length side of the curve, we try for  $g_i$  the form

$$g_i = c_1 + c_2(i - i_0)e^{-i/i'_0} \tag{41}$$

where  $c_1, c_2, i_0,$  and  $i'_0$  are four numerical parameters to be assigned. Making use of eq. (41) in eq. (11), we get the expression for the number-fraction

$$n_i = \frac{\{c_1 + c_2(i - i'_0) e^{-i/i'_0}\} x^{i-1}}{\frac{c_1}{(1-x)} + \frac{c_2 e^{-1/i'_0}}{(1 - xe^{-1/i'_0})^2} [1 - i_0(1 - xe^{-1/i'_0})]} \tag{42}$$

The corresponding expressions for the number-average and the weight-average chain lengths are

$$i_n = \frac{\frac{c_1}{(1-x)^2} + \frac{c_2 e^{-1/i'_0}}{(1 - xe^{-1/i'_0})^3} [1 + xe^{-1/i'_0} - i_0(1 - xe^{-1/i'_0})]}{\frac{c_1}{(1-x)} + \frac{c_2 e^{-1/i'_0}}{(1 - xe^{-1/i'_0})^2} [1 - i_0(1 - xe^{-1/i'_0})]} \tag{43}$$

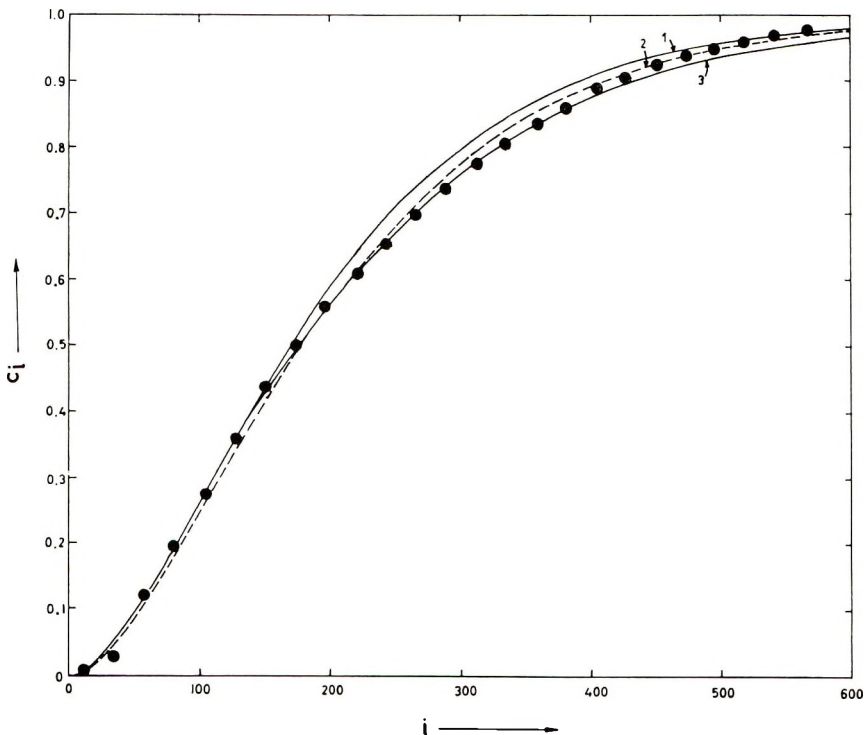


Fig. 5. Variation of cumulative weight fraction  $c_i$  with  $i$ : (1) Flory distribution; (2) based on eq. (42), with  $R = 2.10, i_n = 100, C_2/C_1 = -0.01, i_0 = 200, i'_0 = 3.82$ ; (3) by eq. (42), with  $R = 2.15, i_n = 100, C_2/C_1 = -0.003, i_0 = 200, i'_0 = 166$ . Dots are the experimental points of Taylor.



and

$$i_w = \frac{\frac{c_1(1+x)}{(1-x)^3} + \frac{c_2 e^{-1/i'_0}}{(1-xe^{-1/i'_0})^4} [1 + 4xe^{-1/i'_0} + x^2 e^{-2/i'_0} - i_0(1-x^2 e^{-2/i'_0})]}{\frac{c_1}{(1-x)^2} + \frac{c_2 e^{-1/i'_0}}{(1-xe^{-1/i'_0})^3} [1 + xe^{-1/i'_0} - i_0(1-xe^{-1/i'_0})]}} \quad (44)$$

In Figure 4, we have plotted  $(in_i)$  versus  $(i/i_n)$  for  $i_n = 100$  with  $R = 2.10$  and  $R = 2.15$  as curves 2 and 3, respectively, along with the experimental points of Taylor. It may be noted that curve 3 passes through the initial experimental points nicely, while curve 2 shows a better agreement with the experimental results on the long chain length side.

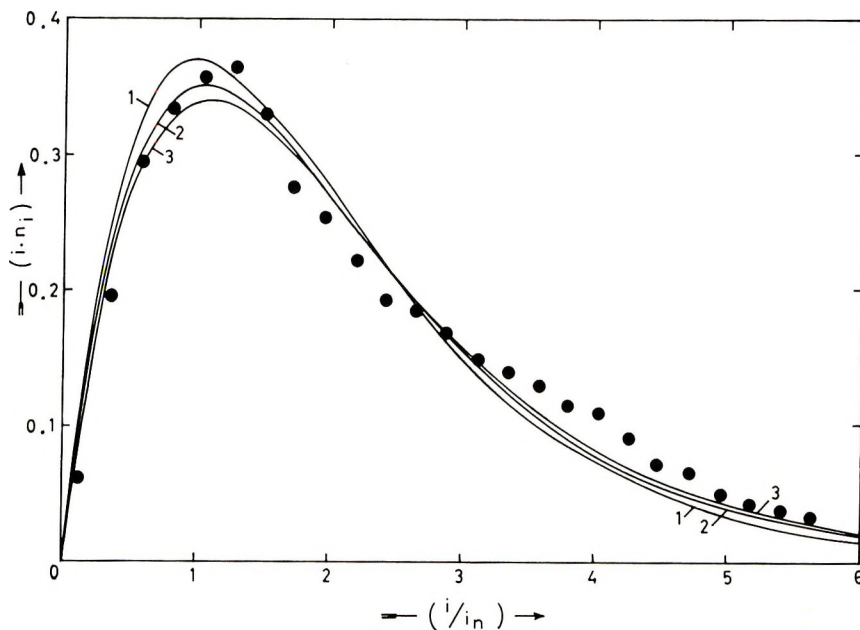


Fig. 6. Variation of  $in_i$  with  $i/i_n$ : (1) Flory distribution; (2) by eq. (45) for  $i_n = 100$ , with  $R = 2.10$ ,  $c = 0.753$ ,  $y = 0.89$ ,  $x = 0.99048$ ; (3) by eq. (45) for  $i_n = 100$ , with  $R = 2.15$ ,  $c = 0.92$ ,  $y = 0.92$ ,  $x = 0.99073$ . Dots are the experimental points of Taylor.

Since Taylor has constructed the  $(in_i)$  curve from the cumulative weight fraction data, it was considered worthwhile to make a direct comparison between experiment and the corresponding theoretical results. In Figure 5 we have shown the variation of cumulative weight fraction  $c_i$  with chain length  $i$  according to the Flory distribution (curve 1) along with the results obtained by using eq. (41) (curves 2 and 3 correspond to  $R = 2.10$  and  $R =$

2.15, respectively). We find that curve 3 provides here the best fit with the experimental points.

From the foregoing analysis, it seems that the various choices of  $g_i$  result in better agreement with the experimental size distribution curve as compared to the Flory distribution either on the longer chain length side or on the shorter chain length side. In order to achieve improvement simultaneously over the two extremes, we try another form

$$g_i = 1 + cy^i \quad (45)$$

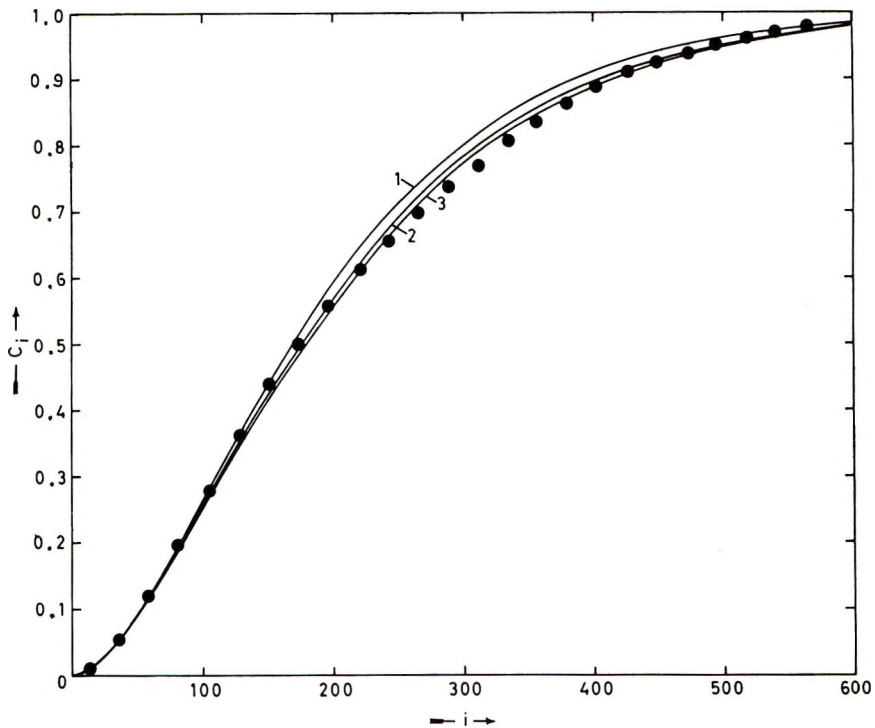


Fig. 7. Variation of  $c_i$  with  $i$ : (1) Flory distribution; (2) based on eq. (45) for  $i_n = 100$ , with  $R = 2.10$ ,  $C = 0.753$ ,  $y = 0.89$ , and  $x = 0.99048$ ; (3) based on eq. (45) for with  $R = 2.15$ ,  $c = 0.92$ ,  $y = 0.92$ , and  $x = 0.99073$ . Dots are the experimental points of Taylor.

where  $c$  and  $y$  are numerical constants. We further assume  $y < 1$ . Using eqs. (11), (13) and (14) we obtain

$$n_i = (1 + cy^{i-1})x^{i-1} \left\{ \frac{1}{1-x} + \frac{cy}{1-xy} \right\} \quad (46)$$

$$i_n = \left[ \frac{x}{(1-x)^2} + \frac{cxy}{(1-xy)^2} \right] \left[ \frac{x}{1-x} + \frac{cxy}{1-xy} \right]^{-1} \quad (47)$$

$$i_w = \left[ \frac{1+x}{(1-x)^3} + \frac{c(1+xy)}{(1-xy)^3} \right] \left[ \frac{x}{(1-x)^2} + \frac{cxy}{(1-xy)^2} \right]^{-1} \quad (48)$$

and

$$R = \left[ \frac{1+x}{(1-x)^3} + \frac{c(1+xy)}{(1-xy)^3} \right] \left[ \frac{x}{1-x} + \frac{cxy}{1-xy} \right] \left[ \frac{x}{(1-x)^2} + \frac{cxy}{(1-xy)^2} \right]^{-2} \quad (49)$$

It is clear from eq. (49) that both the cases  $R > [2 - (1/i_n)]$  or  $R < [2 - (1/i_n)]$  can be represented by the present choice of  $g_i$  by taking  $c$  positive or negative.

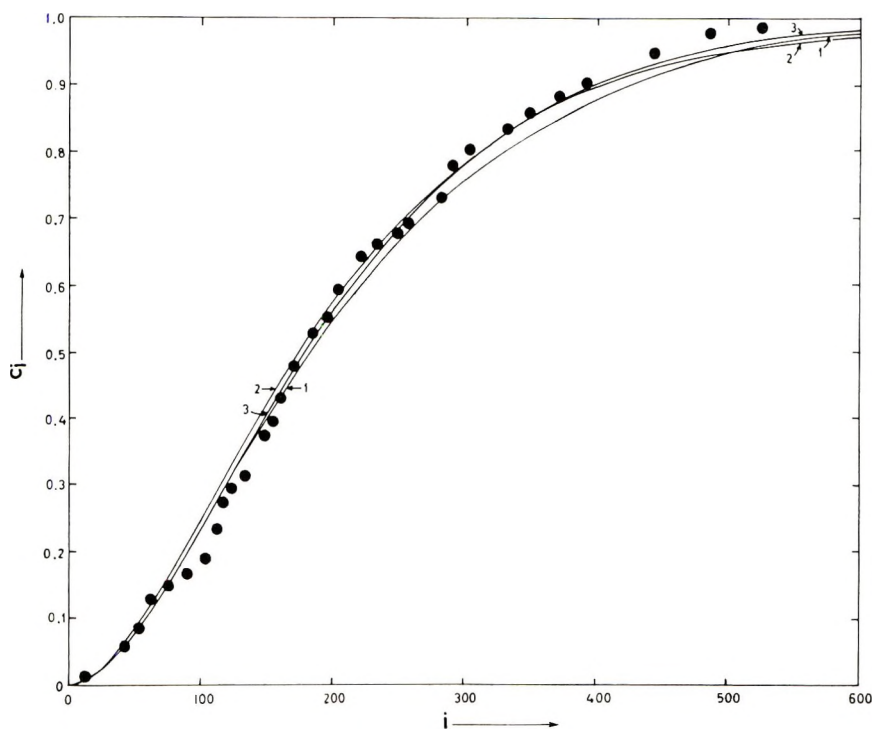


Fig. 8. Variation of  $c_i$  with  $i$ : (1) Flory distribution; (2) based on eq. (42), with  $R = 1.90$ ,  $i_n = 110$ ,  $s = -1/9$ ; (3) based on eq. (42), with  $R = 1.9$ ,  $i_n = 110$ ,  $c_2/c_1 = 0.003$ ,  $i_o = 20$ ,  $i_o' = 234$ . Dots represent the experimental results of Howard.

In Figure 6, plots between  $(in_i)$  and  $(i/i_n)$  are shown for  $i_n = 100$  with  $R = 1.99$ , 2.10, and 2.15 along with the experimental points of Taylor. We find that curve 3 for  $R = 2.15$  provides the best representation of experimental results.

In Figure 7 we have shown the comparison between the theoretical results based on eq. (46) and the data of Taylor for the cumulative weight fraction  $c_i$  as a function of the chain length  $i$  for the  $R$  values used for Figure 6. Once again the curve for  $R = 2.15$  is found to provide the best

representation of the experimental data. An appreciable improvement in the representation of the experimental data over Figure 6 may be noted.

Finally we take up the comparison with the experimental results of Howard for nylon 66 in *m*-cresol-cyclohexane as solvent at 25°C. Here  $i_n = 110$ , and the value of  $R$  is less than the Flory value. From our study, corresponding to cases given by eqs. (15), (41), and (45) this corresponds to negative  $s$ , positive  $c_2/c$  and negative  $c_1$  respectively. Curves 2 and 3 in

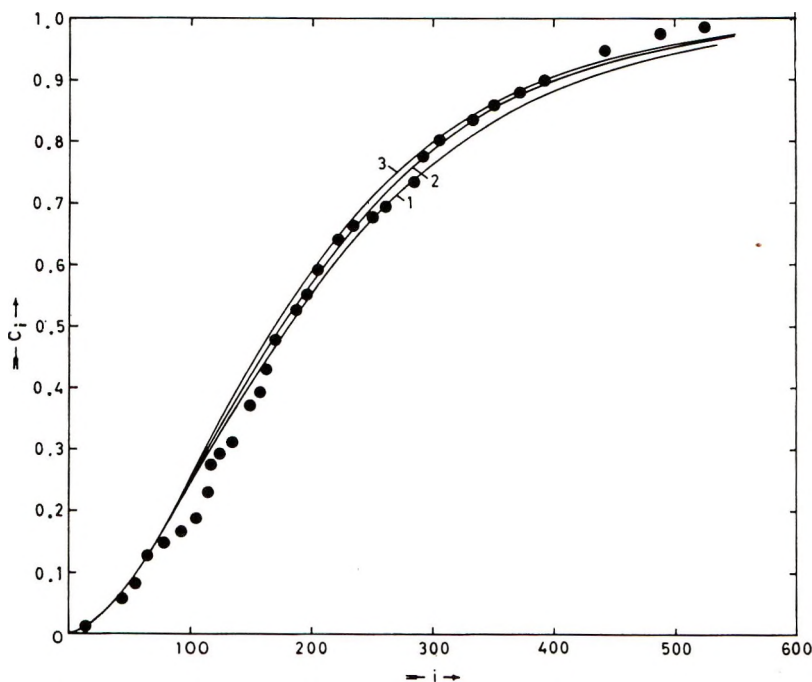


Fig. 9. Variation of  $c_i$  with  $i$ : (1) Flory distribution; (2) based on eq. (45) for  $i_n = 110$ , with  $R = 1.90$ ,  $C = -0.71$ ,  $y = 0.915$ ,  $x = 0.99033$ ; (3) based on eq. (45) for  $i_n = 110$ , with  $R = 1.85$ ,  $C = -1.151$ ,  $y = 0.9001$ ,  $x = 0.99004$ . Dots represent the experimental results of Howard.

Figure 8 are drawn for the first two cases. We find that curve 3 provides the best representation of the experimental results. In Figure 9, the results based on eq. (45) with  $R = 1.99$  (Flory case),  $R = 1.90$ , and  $R = 1.85$  are drawn. It appears that curve 3 provides a representation of the experimental results which shows only marginal improvements over curve 3 of Figure 8.

It would seem from the foregoing analysis that a better understanding of the dependence of bimolecular rate constant on chain length should be possible if more extensive and accurate data on the size distribution for various polymers at different stages of reaction are made available.

## APPENDIX

Here we outline the intermediate steps necessary to obtain eq. (11) of the text.

Regarding  $x$  in eq. (9) as a complex variable and making use of Cauchy's theorem we may write

$$\Omega = \frac{1}{2\pi j} \oint e^{G(x)} dx \quad (\text{A-1})$$

where  $j = \sqrt{-1}$  and

$$G(x) = N \log f(x) - (N_0 + 1) \log x$$

The integral in eq. (A-1), may be evaluated approximately by the method of steepest descents. Following the standard procedure,<sup>6</sup> we get

$$\Omega \simeq \frac{e^{G(x)}}{\sqrt{2\pi G''(x)}} = \frac{[f(x)]^N}{x^{N_0+1} \sqrt{[2\pi N f''(x)/f(x)]}} \quad (\text{A-2})$$

where  $x$  here [as also in eq. (7) and following eq. (10) in the text] stands for the value of the variable at the saddle point while  $G''(x)$  denotes the value of the second derivative of  $G(x)$  at this point. The saddle point is obtained by putting the first derivative of  $G(x)$  equal to zero. This gives

$$x f'(x)/f(x) \simeq N_0/N \quad (\text{A-3})$$

Starting from eq. (10) and following the same procedure we find

$$\Omega_i \simeq \frac{[f(x)]^{N-1}}{x^{N_0+1-i}} \frac{1}{\sqrt{2\pi N f''(x)/f'(x)}} \quad (\text{A-4})$$

Using eqs. (A-2) and (A-4) and eq. (8), we get eq. (11) of the text.

One of us (S. C. J.) is thankful to the C.S.I.R. (India) for the grant of a fellowship during the course of this work.

## References

1. V. S. Nanda and S. C. Jain, *J. Chem. Phys.*, **49**, 1318 (1968).
2. G. B. Taylor, *J. Amer. Chem. Soc.*, **69**, 638 (1947).
3. G. J. Howard, *J. Polym. Sci.*, **37**, 310 (1959).
4. V. S. Nanda and R. K. Pathria, *J. Chem. Phys.*, **30**, 27 (1959).
5. V. S. Nanda, *J. Polym. Sci. A*, **2**, 2275 (1964).
6. E. Schrödinger, *Statistical Thermodynamics*, Cambridge Univ. Press, London, 1957, Chap. VI.

Received July 22, 1969

Revised December 30, 1969

# High-Temperature Pyrolysis of Poly(vinyl chloride): Gas Chromatographic-Mass Spectrometric Analysis of the Pyrolysis Products from PVC Resin and Plastisols

MICHAEL M. O'MARA, *B. F. Goodrich Chemical Company,  
Avon Lake, Ohio 44012*

## Synopsis

A pyrolysis-gas chromatographic-mass spectrometric technique for analyzing the pyrolysis products from polymers in an inert atmosphere is described. Initial studies encompassing the pyrolysis of poly(vinyl chloride) homopolymer and a series of PVC plastisols (based on *o*-phthalate esters) have provided a complete qualitative and semi-quantitative analysis of the pyrolysis products from these materials. PVC resin yields a series of aliphatic and aromatic hydrocarbons when pyrolyzed at 600°C; the amount of aromatic products is greater than the amount of aliphatic products. Benzene is the major organic degradation product. A typical PVC plastisol [PVC/*o*-dioctyl phthalate (100/60)] yields, upon pyrolysis, products that are characteristic of both the PVC matrix and the phthalate plasticizer. The pyrolysis products from the plasticizer dilute those from the PVC portion of the plastisol and are, in turn, the major degradation products. There are no degradation products resulting from an interaction of the PVC with the plastisol. The pyrograms resulting from pyrolysis of the various plastisols of PVC can be used for purposes of "fingerprinting." Identification of the major peaks in a typical plastisol pyrogram provides information leading to a precise identification of the plasticizer. The pyrolysis data from this study were related to a special case of flammability and toxicity.

## INTRODUCTION

The mechanism of the thermal dehydrochlorination of poly(vinyl chloride) has been the subject of many studies in the general area of polymer degradation. A number of the important contributions in this area have been reviewed by Levy in two excellent publications.<sup>1,2</sup> The present paper deals with the identification of the volatile, hydrocarbon pyrolysis products resulting from the thermal degradation of PVC at 600°C in an inert (helium) atmosphere.

The objective of the current study was to obtain a complete profile of the degradation products from PVC resin and PVC plastisols. This study has acted as a starting point in an overall study of thermal degradation, combustion, and flammability of chlorinated polymers.

## PREVIOUS WORK

Stromberg<sup>3</sup> has studied the thermal degradation of PVC in vacuum by first stripping the resin of HCl at temperatures up to 350°C for 30 min. The resulting residue was then heated at 400°C for 30 min and the volatile hydrocarbon products resulting from this second heating were identified via mass spectrometry. In this particular study, Stromberg identified approximately 25 hydrocarbon products.

Ohtani and Ihikawa<sup>4</sup> pyrolyzed PVC at 425°C in a nitrogen atmosphere and studied the resulting degradation products by infrared and ultraviolet spectroscopy. Their findings showed that: (1) the pyrolysis products (other than HCl) consisted of aliphatic and aromatic hydrocarbons, and (2) the types of pyrolysis products from PVC were a function of the stereoregularity (tacticity) in the undegraded polymer. Additional qualitative or quantitative measurements were not made.

Noffz et al.<sup>5</sup> degraded PVC in a high-frequency pyrolyzer and separated the degradation products by gas chromatography. Their findings revealed that the hydrocarbon degradation products consisted of only aromatic compounds; a volatile aliphatic hydrocarbon fraction was not identified.

Coleman and Thomas<sup>6</sup> have studied the combustion of PVC by thermally degrading the polymer in an excess of oxygen. Under the experimental conditions employed, the hydrocarbons formed as a result of polymer degradation were completely oxidized to carbon oxides. In addition to HCl, CO, and CO<sub>2</sub>, a very trace amount (5 ppm) of carbonyl chloride was also identified.<sup>7</sup>

In a more recent study of the degradation of PVC in air, Boettner et al.<sup>8,9</sup> found that when PVC homopolymer and compounds were heated in air from ambient to 600°C, approximately 95% of the PVC was reacted to HCl, CO, and CO<sub>2</sub> (no phosgene above 0.1 ppm). The 5% hydrocarbon fraction consisted of 18 aliphatic and aromatic hydrocarbons.

Analogous degradation experiments of PVC plastisols (PVC plus a phthalate ester) revealed that the hydrocarbon fraction of the pyrolyzate increased due to products from thermal breakdown of the plasticizer. Characteristic degradation products derivable from the plasticizer alone were not formed.

## INSTRUMENTATION AND PYROLYSIS TECHNIQUES

Thermolysis of PVC resin (Geon 103, Cl = 57.4%) was carried out by two general techniques. The first method involved heating the resin in the heated (325°C) inlet of our mass spectrometer (CEC model 21-103C) in order to obtain a mass spectrum of the total pyrolyzate.

The second, more detailed method consisted of degrading the resin in a pyrolysis-gas chromatograph-mass spectrometer (PGM) tandem system. Briefly, our PGM unit consists of an F & M Model 700 temperature-programmed gas chromatograph interfaced to the mass spectrometer through a molecular enricher.<sup>10</sup> A pyrolysis unit consisting of a radiant

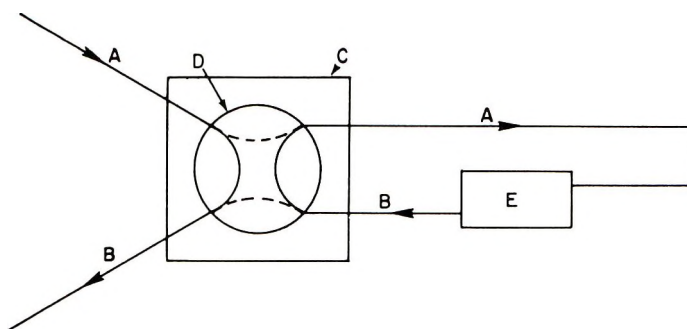


Fig. 1. Schematic of pyrolysis unit illustrating relative position of (A) carrier gas (helium) lines; (B) heated effluent lines; (C) oven containing; (D) F and M gas-sampling valve and (E) quartz pyrolysis chamber and radiant heat pyrolyzer. Arrows indicate the direction of gas flow.

type furnace (Sargent & Co., Model S-36400), quartz chamber, and heated F & M gas sampling valve (Model GV-11) was constructed. Function of the gas sampling valve was to interface the pyrolysis chamber to the gas chromatograph and to permit on-line or off-line operation of the pyrolysis unit. The two gas chromatographic carrier gas lines were "looped" outside the body of the chromatograph through Tygon tubing connectors. In this way, carrier gas could be directed from the chromatograph to the pyrolysis chamber and the effluent line from the pyrolysis chamber could then be directed to either of the injection ports of the gas chromatograph. A diagram of the pyrolysis chamber, gas chromatograph, and gas sampling valve is presented in Figure 1.

The results from the pyrolysis experiments carried out in the heated inlet of the mass spectrometer indicated that in order to obtain a complete chromatographic separation of the pyrolysis products from PVC, two chromatographic columns would be required. Light gases ( $C_1$ - $C_4$ ) were separated on an 8-ft Porapak QS while the higher-boiling components ( $C_4$  to acenaphthalene) were analyzed on a 20-ft  $\times$   $3/16$  in. SE52 (10% on 80/100 CRG) column. This same combination of gas chromatographic columns was also used for the analyses of degradation products from PVC plastisols. The plastisols were prepared by fusing 100 parts of PVC resin with 60 parts of plasticizer (i.e., *o*-dioctyl phthalate) at 350°F for 5 min.

Samples of PVC resin and plastisols were pyrolyzed at 600°C in a carrier gas flow of 60-70 ml/min; sample sizes ranged from 10 to 20 mg.

### HCl EVOLUTION DURING PYROLYSIS

Since a stoichiometric amount of HCl is released (58.3%) from PVC when heated at 600°C, over half of the degradation products, by weight, is HCl. The problem of chromatographic analysis of HCl was dealt with in the following manner. It was found that for analyses performed on the SE52 chromatographic column, the retention time of the HCl peak corresponded



approximately to the dead time of the column. This peak was fairly symmetrical and did not exhibit excessive bleeding.

However, with the Porapak column, HCl was found to bleed excessively. In order to correct this, the pyrolyzate was scrubbed of HCl by placing 4 Å molecular sieves in the heated (150°C) effluent line (Fig. 1, B) to the chromatograph. This eliminated the HCl and did not seem to remove any of the other gases. It was found, as a result of other work, that the sieves did have an affinity for short chain chloroalkanes under these conditions.

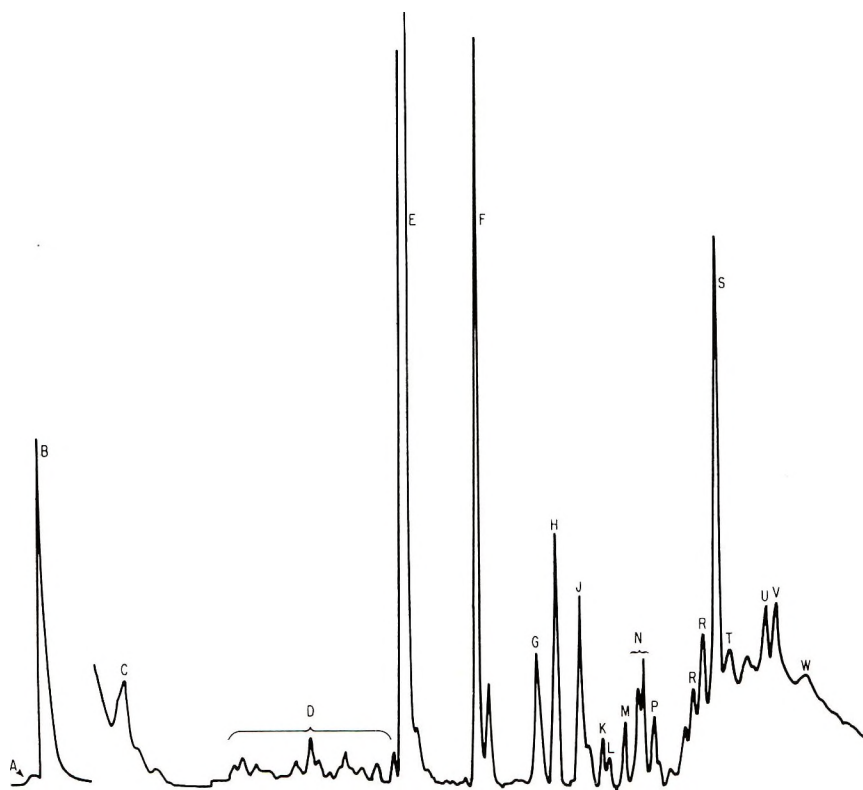


Fig. 2. Pyrogram of PVC resin from 20 ft  $\times$   $\frac{3}{16}$  in. 10% SE52 on 80/100 CRW chromatographic column. Lettered peaks refer to identifications in Table I.

Since these types of compounds are not evolved during the pyrolysis of PVC, this selectivity for chloroalkanes did not interfere with the results of the analysis.

In a typical pyrolysis experiment, 10–20 mg of PVC resin were precisely weighed into a 5.0 mm  $\times$  10 mm porcelain boat and loaded into the pyrolysis chamber along with a small magnet. The chamber was closed, the gas sampling valve was so positioned that the pyrolysis unit was on-line with the chromatograph, and the furnace was turned on. Once the temperature of the furnace reached 600°C (calibrated), the boat was moved, with the aid of

the magnet, into the hot zone of the pyrolysis chamber. In this way a typical pyrogram was recorded.

After the remains of the sample cooled down, the gas sampling valve was positioned for off-line operation.

While the gas-chromatographic analysis was being completed, the chamber (now off-line) was opened, and the sample boat was removed and weighed. This operation permitted the percentage char formation to be calculated. The measurement was not corrected for minor amounts of material which condensed at the end of the pyrolysis chamber.

### PYROLYSIS OF PVC RESIN

Pyrolysis of PVC at 600°C in a helium atmosphere results in the complete removal of Cl as HCl (58.3%) from the backbone of the polymer. The resulting carbonaceous ash, devoid of chlorine, represents approximately 3-4% of the original polymer.

TABLE I  
Identification of Components in Pyrogram (Fig. 2) of PVC

Peak identification	Components
A	CH <sub>4</sub> , <sup>a</sup> CO, <sup>a</sup> CO <sub>2</sub> , <sup>a</sup> C <sub>2</sub> H <sub>4</sub> , <sup>a</sup> C <sub>2</sub> H <sub>6</sub> <sup>a</sup>
B	HCl, C <sub>3</sub> H <sub>6</sub> , <sup>a</sup> C <sub>3</sub> H <sub>8</sub> <sup>a</sup>
C	Butane, <sup>a</sup> butene, <sup>a</sup> butadiene, <sup>a</sup> diacetylene <sup>a</sup>
D	C <sub>5</sub> and C <sub>6</sub> aliphatic and olefinic hydrocarbons
E	Benzene
F	Toluene
G	Chlorobenzene
H	Xylene
J	Allylbenzene
K	C <sub>9</sub> H <sub>12</sub>
L	C <sub>9</sub> H <sub>12</sub>
M	Indane
N	Indene, ethyltoluene
P	Methylindane
R	Methylindenes
S	Naphthalene
T	Dimethylindane
U	Methylnaphthalene
V	Methylnaphthalene, acenaphthalene
W	Dimethylnaphthalene

<sup>a</sup> Separated and identified on an 8-ft Porapak QS.

Aside from a stoichiometric amount of HCl, the PVC pyrolyzate consists of a series of aliphatic, olefinic, and aromatic hydrocarbons. Only one chlorinated hydrocarbon, chlorobenzene, was found, and the yield of this component was well below 1 wt-%.

A typical pyrogram of PVC (SE52 column) is presented in Figure 2; component identifications are summarized in Table I. A similar analysis

was also carried out on the Poropak QS column. The components separated and identified in this analysis are noted in Table I.

The major components resulting from the pyrolysis of PVC are HCl, benzene, toluene, and naphthalene. In addition to these major products, an homologous series of aliphatic and olefinic hydrocarbons ranging from C<sub>1</sub> to C<sub>6</sub> are formed. This finding is in direct contrast to the results obtained by Noffz. This difference may be attributed to differences in techniques since Noffz degraded his samples with rf energy.

### GAS CHROMATOGRAPHIC ANALYSIS OF HCl

The chromatographic peak from HCl can be used to quantify the amount of HCl released during the pyrolysis of PVC if the pyrolysis and chromatographic system is first "seasoned" with a slug of HCl gas. For example, in one experiment a series of PVC samples (10–20 mg) were pyrolyzed at 600°C and the gas-chromatographic areas of the resulting HCl peaks were recorded. (The gas chromatography column and pre-column were maintained at ambient temperatures throughout this experiment. Usually six to seven pyrolyses could be carried out before benzene began to

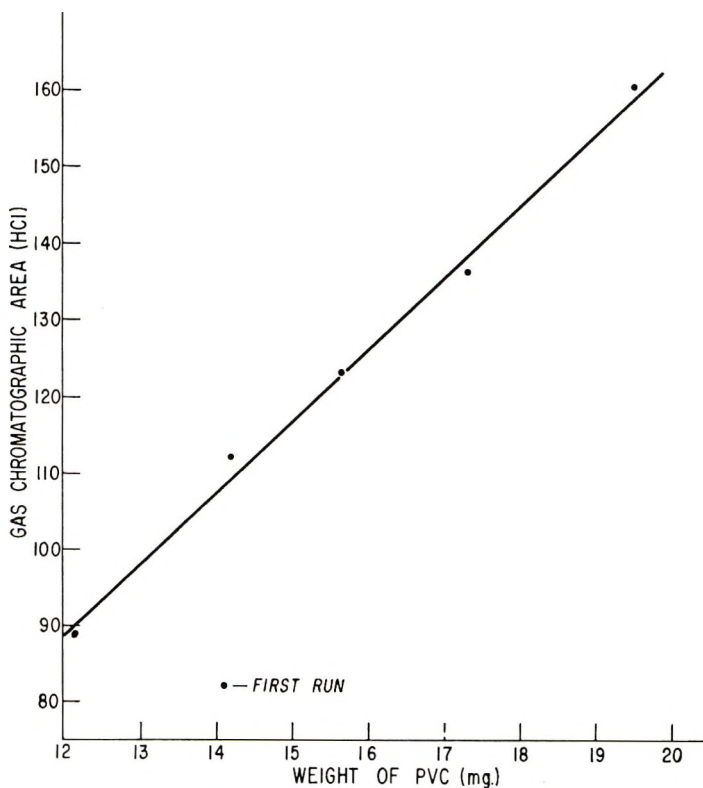


Fig. 3. Plot of HCl (gas-chromatographic area) vs. weight of PVC resin pyrolyzed at 600°C.

bleed from the column. Bleeding of minor amounts of other more volatile hydrocarbons did not interfere with the analyses).

A plot of HCl content (peak area) versus weight of resin pyrolyzed at 600°C is presented in Figure 3. Aside from the first run, all subsequent analyses provided a linear relationship between the two variables of HCl area and amount of resin pyrolyzed. The first run of HCl through the column seems to condition the apparatus by coating the walls with gaseous HCl. In subsequent runs, all of the HCl formed during pyrolysis, reaches the detector with little or no adsorption on the chromatographic walls.

This aspect of the pyrolysis of PVC is being further investigated in the direction of optimizing the technique for measuring the amount of HCl produced when PVC compounds and other chlorinated polymers are thermally degraded.

### PYROLYSIS REPRODUCIBILITY

The demonstration of reproducibility in pyrolysis work is an important aspect of this technique. In order to meet this requirement, three pyrolysis

TABLE II  
Composition (Gas-Chromatographic Area) of PVC Hydrocarbon Pyrolyzate

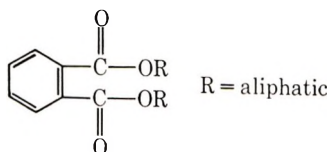
Component	Area, %		
	Run 1	Run 2	Run 3
CO	0.6	2.2	0.8
Methane	8.8	7.8	9.3
CO <sub>2</sub>	0.4	0.3	0.2
Ethylene	3.5	3.5	3.8
Ethane	4.8	5.1	5.5
Propylene	2.9	2.6	3.0
Propane	3.0	1.9	2.3
Butane, butene	2.5	2.1	2.1
Butadiene, diacetylene			
C <sub>5</sub> and C <sub>6</sub> hydrocarbons	1.9	1.8	1.3
Benzene	51.2	50.8	50.1
Toluene	5.3	5.9	5.8
Chlorobenzene	1.1	1.1	1.3
Xylene	1.9	2.1	2.3
Allylbenzene	1.3	1.4	1.6
C <sub>9</sub> H <sub>12</sub>	0.4	0.5	0.5
C <sub>9</sub> H <sub>12</sub>	0.2	0.2	0.3
Indane	0.2	0.3	0.3
Indene	0.9	1.4	0.9
Ethyltoluene			
Methylindane	0.5	0.5	0.5
Methylindenes	1.1	1.3	1.0
Naphthalene	4.8	4.6	4.5
Dimethylindane	0.7	0.8	0.8
Methylnaphthalene	0.8	0.7	0.7
Methylnaphthalene	1.2	1.0	1.1
Acenaphthalene			

experiments were carried out in which various PVC (resin) samples were pyrolyzed at 600°C. (A dual analysis was carried out in each case, one for analysis on the SE52 chromatographic column, the other for analysis on the Porapak QS column.) The resulting gas-chromatographic peak areas of all components were recorded for the three pyrolysis experiments. These three analyses, summarized in Table II, demonstrate the quantitative and qualitative reproducibility of the technique.

The gas chromatographic peak areas reported in Table II closely reflect the mole per cent contents, thus an approximate quantitative analysis of the pyrolyzate from thermally degraded PVC is possible. It should be noted that the total hydrocarbon fraction corresponds to approximately 38% (weight) of the original PVC sample; the remaining 62% consists of HCl and a carbonaceous, chlorine-free ash. Benzene is the component of greatest concentration in the entire hydrocarbon fraction.

### PYROLYSIS OF POLY(VINYL CHLORIDE) PLASTISOLS

Initial pyrolysis of PVC plastisols centered about a plastisol prepared by fusing 100 parts of PVC and 60 parts of *o*-(2-ethylhexyl) phthalate (DOP) at 350°F for 5 min. The scope of this initial study was then expanded to include a number of other PVC plastisols. The plasticizers used throughout this study were derived from *o*-phthalic acid:



The results of the initial study (PVC/DOP) revealed that the degradation products reflected both polymer and plasticizer thermolysis. Thus, the pyrogram could be used as a finger printing tool for identifying the specific plasticizer present in the plastisol.

The pyrolysis of the PVC/DOP plastisol was carried out at 600°C in a helium atmosphere; the resulting pyrogram (SE52 gas chromatography column) from this pyrolysis is presented in Figure 4. Peak identifications are summarized in Table III.

As previously mentioned, the pyrolysis products reflect polymer degradation (HCl, benzene, toluene, etc.) and plasticizer degradation ( $C_8$  hydrocarbon,  $C_8$  aldehyde, and phthalic anhydride). It is the presence of those components due to DOP fragmentation that provides the basis for using the plastisol pyrogram as a "fingerprinting" aid.

This fingerprinting capacity of pyrograms from typical PVC plastisols is illustrated in Figure 4. A series of seven pyrograms resulting from the pyrolysis of the following PVC plastisols is presented: (*B*) *o*-dihexylphthalate (DHP), (*C*) *o*-di-2-ethylhexyl-phthalate (DOP), (*D*) *o*-dicapryl phthalate (DCP), (*E*) *o*-diisodecyl phthalate (DDP), and (*F*) the mixed

ester butyl benzyl *o*-phthalate (BuBzP). The first pyrogram in Figure 4 is that of the resin without plastisol and is included for purposes of comparison. It should be noted that much of the detail (i.e., minor components) of these

TABLE III  
Comparison of Gas-Chromatographic Areas of Degradation Products  
from PVC Resin and PVC Plastisol (DOP, 100/60)<sup>a</sup>

Degradation product	Area, %	
	Resin	DOP Plastisol
CO	0.6	1
Methane	8.8	3.3
CO <sub>2</sub>	0.4	6.5
Ethylene	3.5	2.8
Ethane	4.8	4.6
Propylene	2.9	4.7
Propane	3.0	1.5
Butane, butene	2.5	5.2
C <sub>5</sub> and C <sub>6</sub> hydrocarbons (total) <sup>b</sup>	1.9	—
C <sub>5</sub> H <sub>10</sub>	—	1.0
Isoprene	—	1.1
2-Methyl-1-butene	—	2.0
3-Penten-1-yne	—	0.4
C <sub>6</sub> olefin (total)	—	1.6
Benzene	51.2	11.8
C <sub>7</sub> olefins	—	1.3
Toluene	5.3	2.6
C <sub>8</sub> olefins	—	24.7
Chlorobenzene	1.1	0.4
Xylene	1.9	0.7
Allylbenzene	1.3	—
C <sub>9</sub> H <sub>12</sub>	0.4	—
C <sub>9</sub> H <sub>12</sub>	0.2	—
2-Ethyl hexanal	—	1.4
Indane	0.2	—
Indene	—	—
Ethyltoluene	0.9	0.5
Methylindane	0.5	—
Methylindene	1.1	0.8
Naphthalene	4.8	1.2
Dimethylindane	0.7	—
Methylnaphthalene	0.8	—
Acenaphthalene	1.2	—
Methylnaphthalene	—	19.9
Phthalic anhydride	—	(minor)
		(major)

<sup>a</sup> Area related to mole-%.

<sup>b</sup> Applicable only to degradation of resin.

pyrograms has been omitted through a judicious choice of attenuation settings on the gas-chromatographic recorder. This was done for reasons of simplicity as the major peaks in each of the pyrograms provided adequate differences for purposes of fingerprinting.

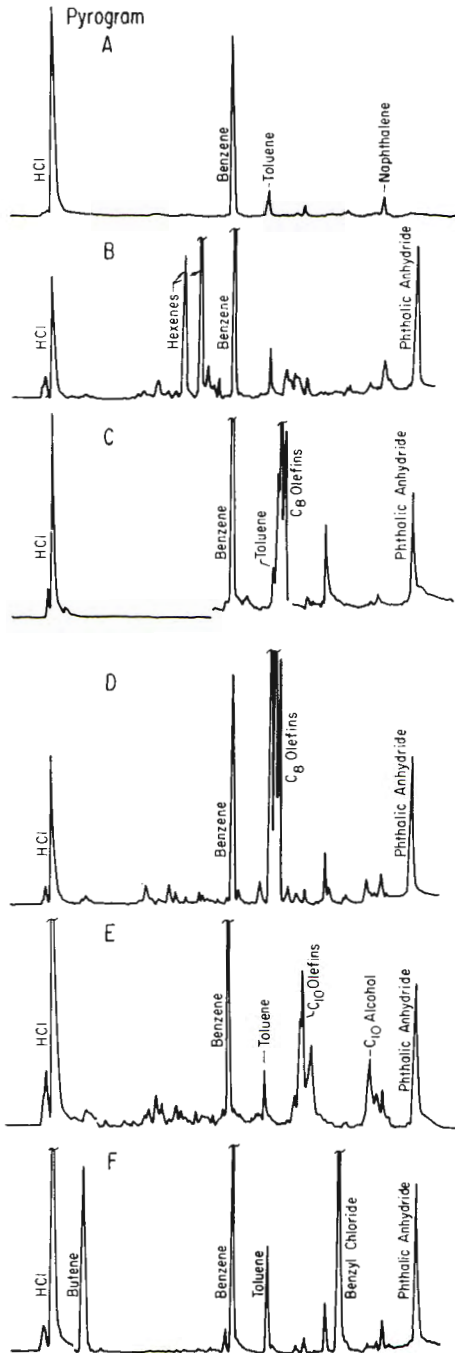


Fig. 4. Pyrograms of (A) PVC resin; (B) PVC/*o*-dihexyl phthalate; (C) PVC/*o*-di-2-ethylhexyl phthalate; (D) PVC/*o*-dicapryl phthalate; (E) PVC/*o*-diisodecyl phthalate; (F) PVC/*o*-butyl benzyl phthalate.

Detailed qualitative analyses of all degradation products from the five plastisols (*B-F*) were not carried out; only the major degradation products have been identified.

The first pyrogram in the series (Fig. 4) indicates the relative location of the major degradation from PVC resin (i.e., HCl, benzene, toluene and naphthalene).<sup>\*</sup> The second pyrogram (*B*), PVC/*o*-dihexyl phthalate, contains those peaks representing thermolysis of the plasticizer (hexene and phthalic anhydride) in addition to those from degradation of the polymer. The pyrogram of *o*-diisodecyl phthalate/PVC (*F*) is analogous to that of the dihexyl phthalate pyrograms: the presence of phthalic anhydride identifies the aromatic portion of the plasticizer while the position (and presence) of the olefin moiety (C<sub>10</sub> in this case) identifies the aliphatic portion of the plasticizer.

Olefinic degradation products result from the thermal de-esterification and subsequent dehydration of the plasticizer. In one case (diisodecyl phthalate), an alcohol (C<sub>10</sub>) was found among the degradation products.

The pyrograms of the two C<sub>8</sub> plastisols (DOP and DCP) provide an interesting case. Both pyrograms contain a C<sub>8</sub> aldehyde peak, the expected phthalic anhydride peak, and three C<sub>8</sub> olefin peaks. However, the ratio of the three olefin peaks is different in each of the two cases. Since it has already been demonstrated that the reproducibility of pyrolysis, as employed in this study, is excellent, this difference in isomer distribution reflects the difference in the two C<sub>8</sub> plasticizers. Further investigation of these two plastisols directed toward the identification of the specific C<sub>8</sub> olefins in each case was not carried out. The important point was that pyrolysis-gas chromatography could be used to distinguish the two isomeric plasticizers.

If it had been necessary to completely characterize these two C<sub>8</sub> plasticizers with respect to the aliphatic portion, it is obvious that pyrolysis-gas chromatography offers many advantages over a technique involving acid hydrolysis of the plasticizer followed by an analysis of the alcoholic hydrolysis products.

The pyrogram of the mixed ester (BuBzP) plastisol reveals the presence of an unexpected secondary reaction occurring during pyrolysis or during the resulting chromatographic analysis.

A C<sub>4</sub> olefin due to fragmentation of the butoxy portion of the ester is present, as expected. Pyrolysis of the -OCH<sub>2</sub>C<sub>6</sub>H<sub>5</sub> portion however, provides a unique case in that olefin formation via dehydration is not possible.

The pyrolysis products from this fragment (-OBz) were toluene† and benzyl chloride. Independent work in our laboratory, involving the pyrolysis of dibenzyl ether (HCl not rigorously excluded from gas-chromatograph lines or pyrolysis chamber) showed that this material produces the

\* Lower-chain aliphatic products (CH<sub>4</sub>, C<sub>2</sub>H<sub>4</sub>, etc.) are buried under the HCl peak.

† The ratio of benzene/toluene (peak height:peak height) in all of the pyrograms, except that of DBzP, was 6.5 ± 0.4; in the BuBzP pyrogram the ratio was 3.6, thereby reflecting an increase in toluene.





"on-line" position and the pyrolysis products were swept from the chamber to the chromatograph. Under these conditions, the  $C_8$  olefins underwent complete cracking to lower chain olefins.

### TOXICITY OF DEGRADATION PRODUCTS

Boettner<sup>8</sup> has shown that when plasticized PVC is degraded in air under programmed temperature conditions a number of organic molecules (In addition to a stoichiometric amount of HCl), very similar to the lower molecular weight hydrocarbons identified in the present study, are released. The overall toxicity, however, is related to the gross quantity of CO, CO<sub>2</sub> and HCl, the first of these having the greatest effect.<sup>11</sup>

The present pyrolysis work, having been carried out in the absence of air, is applicable to only one particular set of fire conditions: that case where the plastic is subjected to "shock" heating conditions where plasticizer undergoes thermal degradation rather than evaporation and oxidation. Thus, in this particular instance, the degradation products would contain phthalic anhydride, the level of which would be dependent upon the plasticizer's degradation to evaporation/oxidation ratio. This product would not grossly affect the toxicity of the degradation products since the particular quantity of CO<sub>2</sub>, HCl, and most importantly CO determines this parameter.

Boettner's work most closely simulates actual burning conditions, that is, as the plastic is heated, HCl and plasticizer are boiled off, the plasticizer may flame (depending on the HCl content) and CO and CO<sub>2</sub> are produced.

The findings of the present study representing a special case of flammability are offered as a corollary to Boettner's work.

The author wishes to acknowledge the technical comments of L. B. Crider and M. L. Dannis, the instrument modifications suggested by R. A. Yount and J. Deliman, and the technical assistance of J. A. Nikora.

### References

1. D. W. Levi, "Literature Survey on Thermal Degradation, Thermal Oxidation, and Thermal Analysis of High Polymers," June, 1963. Clearinghouse for Fed. Scien. and Tech. Info., U. S. Dept. of Commerce, AD423546.
2. D. A. Teetsel and D. W. Levi, "Literature Survey on Thermal Degradation, Thermal Oxidation and Thermal Analysis of High Polymers II," January 1966, Clearinghouse for Fed. Scien. and Tech. Info., U. S. Dept. of Commerce, AD631655.
3. Stromberg et al., *J. Polym. Sci.*, **35**, 355 (1959).
4. S. Ohtani and T. Ishikawa, *Kogyo Kagaku Zasshi*, **65**, 1617-22 (1962).
5. D. Noffz, W. Benz, and W. Pfab, *Z. Anal. Chem.*, **235**, 121 (1968).
6. E. H. Coleman and C. H. Thomas, *J. Appl. Chem.*, **4**, 379 (1954).
7. E. H. Coleman, *Plastics*, **24**, 416 (1959).
8. E. A. Boettner and B. Weiss, *Amer. Ind. Hyg. Assoc. J.*, **28**, 535 (1967).
9. E. A. Boettner et al., *J. Appl. Polym. Sci.*, **13**, 377 (1969).
10. J. T. Watson and K. Biemann, *Anal. Chem.*, **36**, 1135 (1964).
11. H. H. Cornish, paper presented at Polymer Conference Series on Flammability Characteristics of Polymeric Materials, University of Detroit, June 19, 1969.

Received December 1, 1969

Revised December 31, 1969

## Stereospecific Polymerization of Methacrylonitrile. V. Formation of the Carbonyl in the Polymer

YASUSHI JOH, TOSHIO YOSHIHARA, SEIKI KURIHARA,  
TOSHIO SAKURAI, and TATSUNORI TOMITA, *Research Laboratories,  
Mitsubishi Rayon Co., Ltd., Otake City, Hiroshima, Japan*

### Synopsis

The isotactic polymethacrylonitrile prepared by the organometallic catalysts has carbonyl groups in the polymer. Thus, the carbonyl formation during the polymerization by diethylmagnesium was carefully studied by infrared spectrometry. It was found that the imino anion formed by monomolecular termination of the propagating chain end in the cyclization reaction successively attacks the vicinal pendent nitriles in the polymer so as to form the conjugated cyclic imines, which are hydrolyzed to acid amines during the catalyst decomposition with acidic methanol.

### INTRODUCTION

In this series we have reported the successful synthesis of isotactic polymethacrylonitrile<sup>1-7</sup> which has a different infrared spectrum from that for the conventional polymer. In addition to crystalline-sensitive bands, the crystalline polymethacrylonitrile has an absorption band at 1697  $\text{cm}^{-1}$  which indicates the presence of the carbonyl group in the polymer.

The aim of the present paper is to elucidate the formation of the carbonyl during the polymerization by diethylmagnesium catalyst. It is found that the imino anion formed by a monomolecular termination of the propagating chain end in a cyclization reaction successively attacks the vicinal pendent nitrile groups in the polymer chain so as to form conjugated cyclic imines, which are hydrolyzed to acid amides during catalyst decomposition with acidic methanol.

### EXPERIMENTAL

#### Polymerization

The polymerization of methacrylonitrile was carried out by using diethylmagnesium in toluene at 70°C. The details of the procedure were described in previous papers.<sup>6,7</sup> One portion of the reaction mixture was terminated by methanol acidified with HCl. Another portion of the reaction mixture was terminated by a mixture of methanol and a small amount of  $\text{CH}_3\text{COOH}$ . The polymer obtained with  $\text{CH}_3\text{OH-HCl}$  was colorless, whereas that obtained with  $\text{CH}_3\text{OH-CH}_3\text{COOH}$  was red-brown. The pre-

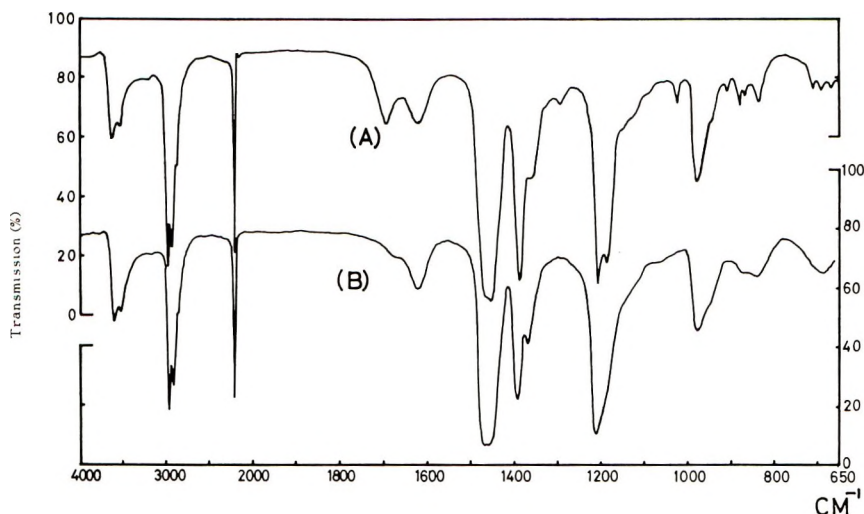


Fig. 1. Infrared spectra for polymethacrylonitriles: (A) crystalline polymer; (B) conventional polymer obtained with radical initiator.

epitates were filtered, washed with a large amount of methanol, and dried *in vacuo* at room temperature.

### Isotactic Polymethacrylonitrile

A 1-g portion of the crude polymer precipitated with  $\text{CH}_3\text{OH-HCl}$  was placed in a flask, and to this, 100 ml of dimethyl sulfoxide was introduced. The flask was then warmed to  $70^\circ\text{C}$  with stirring. After 2 hr the polymer was extremely swollen. The swollen polymer could be isolated by centrifugation. The white precipitate obtained by an addition of methanol to the swollen polymer was washed with a sufficient amount of methanol, dried and weighed; 0.7 g of highly crystalline material was isolated. The infrared spectrum for this material is shown in Figure 1.

#### Treatment of the Crystalline Polymethacrylonitrile by Alkali Reagent

**Treatment with  $\text{NH}_3$ .** Crystalline polymethacrylonitrile (1 g) was suspended in 28% aqueous  $\text{NH}_3$  solution at room temperature for 48 hr. The polymer was then washed successively with plenty of water followed by methanol and dried.

**Treatment with Organometallic Compounds in Nonaqueous Media.** Crystalline polymethacrylonitrile (1 g) was suspended in toluene and the reaction vessel was placed in a water bath adjusted at a given temperature.

To this, 0.001 mole of *n*-butyllithium or diethylmagnesium was introduced, then the mixture was maintained at a constant temperature with stirring for 1 hr. This treatment caused the polymer to turn red. The reaction mixture was then diluted with a large amount of methanol, filtered, and washed with an excess of methanol. The products obtained were dried and then used for the infrared spectral measurement.

### Measurement of Infrared Spectra

The infrared spectra were measured by using a Hitachi EPI G-2 spectrophotometer. The samples were in the form of KBr disks, except those for Figures 1, 9, and 10 for which spectra were measured for films cast from  $\text{CF}_3\text{COOH}$  solutions. The solvent retained in the film was removed by keeping them in boiling water for 3 hr.

### RESULTS AND DISCUSSION

Typical infrared spectra for the isotactic polymethacrylonitrile and for the conventional one prepared with azobisisobutyronitrile are shown in Figure 1. The absorption band at  $1697\text{ cm}^{-1}$ , which was not observed in the radical-initiated polymethacrylonitrile, should be attributed to  $-\text{CONH}_2$ , since samples with strong absorption at  $1697\text{ cm}^{-1}$  also show strong absorption at  $3200\text{ cm}^{-1}$  (Fig. 2).

Possible routes for the formation of the carbonyl during the polymerization might be as follows.

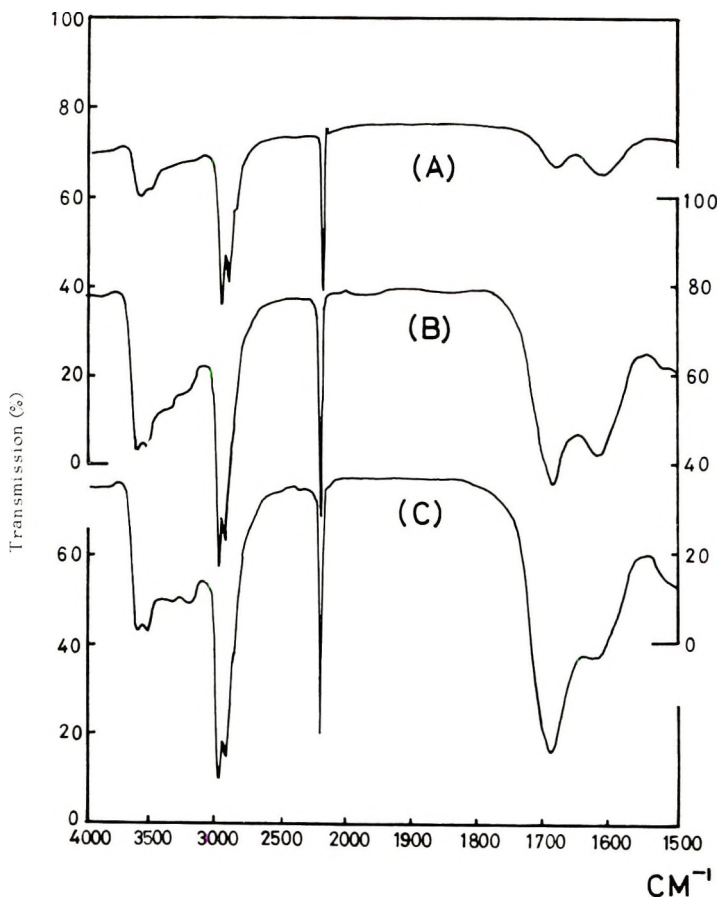


Fig. 2. Infrared spectra for polymethacrylonitriles obtained by organometallic catalyst: (A) DMF-insoluble; (B) DMF-soluble and acetone-insoluble; (C) acetone-soluble.





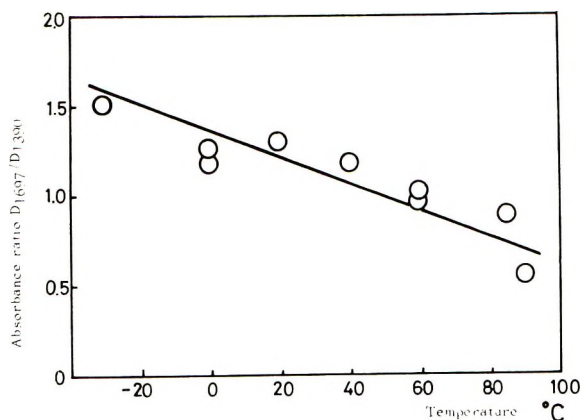


Fig. 3. Relation of the absorbance ratio  $D_{1697}/D_{1390}$  to polymerization temperature.

The relation between the polymerization temperature and the absorbance ratio ( $D_{1697}/D_{1390}$ ), which corresponds to the ratio of the absorbance from carbonyl to that from methyl group is a useful evidence for the route of the carbonyl formation.

Figure 3 shows the plots of the absorbance ratio against polymerization temperature. Obviously, the ratio decreased with increasing polymerization temperature; in other words, the amount of the carbonyl in the polymer decreased with increasing polymerization temperature. This observation is conflict with the explanation by the route of eqs. (1) or (2), since the reaction between the nitrile and diethylmagnesium is faster at higher temperatures. Furthermore, as already described, the samples with a strong absorption at  $1697\text{ cm}^{-1}$  also give an absorption band at  $3200\text{ cm}^{-1}$ , which is considered to be due to the N-H stretching vibrations. This fact indicates the carbonyl is present in the form of primary acid amide, and the explanation for the carbonyl formation through the reaction of nitrile groups with catalyst is ruled out.

The route involving monomolecular termination of the propagating chain [eq. (3)] can also be excluded from the experimental fact that the carbonyl is present in the form of acid amide.

Direct hydrolysis of the nitriles in the polymer during the catalyst decomposition by acidic methanol seems incompatible with the fact that the polymer obtained at higher temperature has a lower carbonyl content because it has been shown by many authors<sup>10-14</sup> that the rate of hydrolysis is considerably influenced by chain configuration, and the polymers with predominantly isotactic units are more easily hydrolyzed than atactic or syndiotactic polymers. As we have already reported,<sup>1,6</sup> the polymer obtained at higher temperature has higher stereoregularity. If the carbonyl were formed through the hydrolysis route, the absorbance ratio  $D_{1697}/D_{1390}$  should be the same or higher for the polymer obtained at higher temperatures at which more isotactic polymers are formed. This is incom-



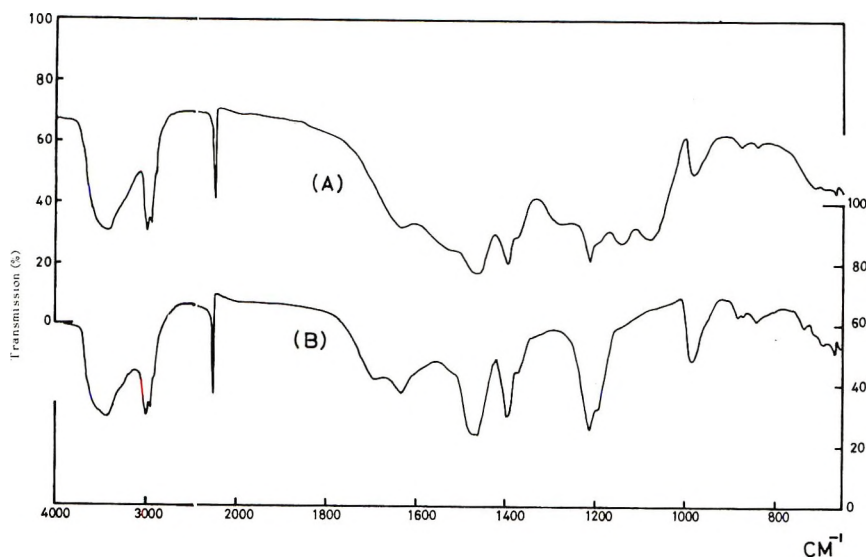


Fig. 4. Infrared spectra for polymethacrylonitriles obtained with  $MgEt_2$ : (A) decomposed by  $CH_3OH-CH_3COOH$  system; (B) decomposed by  $CH_3OH-HCl$  system.

patible with the experimental results, and the route involving direct hydrolysis is not acceptable.

In the polymerization of methacrylonitrile by diethylmagnesium<sup>1,6</sup> or other stereospecific catalysts,<sup>2,7</sup> the polymerization started by an addition of the monomer with a simultaneous precipitation of red polymer. The color has been explained as a result of the formation of a charge transfer complex<sup>1,15</sup> between the catalyst and the nitrile group of the monomer. Natta and Dall'Asta<sup>15</sup> reported that when methanol was added to the colored reaction mixture, the color disappeared at once and the polymerization stopped. However, according to our findings, treatment with methanol acidified by HCl resulted in white polymer, but when the reaction mixture was treated with methanol alone or with a methanol-acetic acid mixture the color did not disappear, but only faded to red-brown.

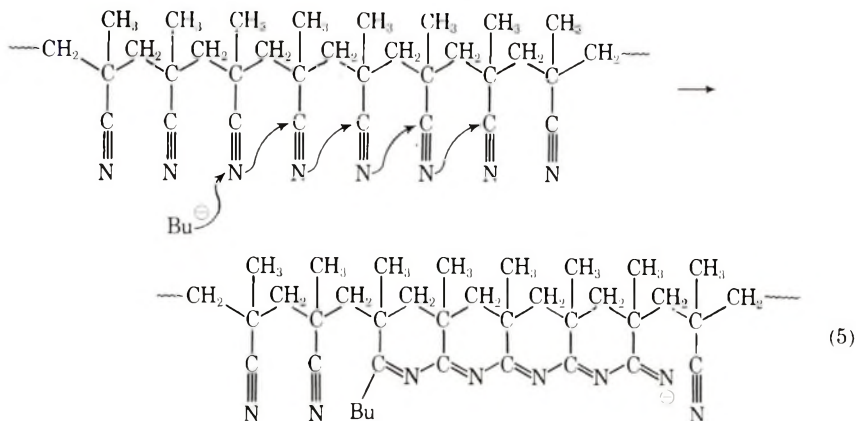
Figure 4 shows the infrared spectra for the polymers terminated by methanol acidified by HCl and by methanol-acetic acid mixture. The former was white but the latter was still colored red-brown. The spectrum in Figure 4B has an absorption at  $1697\text{ cm}^{-1}$  which is not observed in the spectrum of Figure 4A. On the other hand, spectrum A in Figure 4 has absorbance bands at  $1540$ ,  $1280$ ,  $1145$ , and  $1075\text{ cm}^{-1}$ .

If the carbonyl in the polymer is formed through the hydrolysis route of eq. (4), the cyclic conjugated imine structure might be detected in the infrared spectrum. The fact that the spectrum A in Figure 4 seems quite similar to that of the heat-treated polymethacrylonitrile<sup>16-19</sup> prompted us to attempt the following several experiments to identify the cyclic conjugated imine structure.

### Alkali Treatment of the Crystalline Polymethacrylonitrile

**Treatment by Aqueous  $\text{NH}_3$ .** Since it is known that an alkali reagent attacks the nitrile group of polymethacrylonitrile to form the cyclic conjugated imines which bring about coloration, a typical crystalline polymethacrylonitrile was treated by aqueous ammonia solution. This treatment caused new weak absorptions to appear at 1540, 1280, 1145, and 1075  $\text{cm}^{-1}$  which disappeared again on treatment with  $\text{CH}_3\text{OH}-\text{HCl}$  as shown in Figure 5.

**Treatment by BuLi.** Figure 6 shows the infrared spectra for the polymethacrylonitrile treated by butyllithium in toluene at 70°C for 2 hr. New absorption bands appeared at 1540  $\text{cm}^{-1}$ , 1280  $\text{cm}^{-1}$ , 1145  $\text{cm}^{-1}$  and 1075  $\text{cm}^{-1}$ . In Figure 6, a great decrease of the absorption at 2240  $\text{cm}^{-1}$  in the spectrum *B*, which is due to  $\text{C}\equiv\text{N}$  stretching vibrations, together with a reverse in intensity at 2960 and at 2870  $\text{cm}^{-1}$  between the two spectra indicates the introduction of an *n*-butyl group in the polymer accompanying the attack of *n*-butyl anion to a positive carbon of the nitrile group. These results indicate the formation of cyclic conjugated imines as has been explained<sup>20,21</sup> as follows [eq. (5)].



From the results mentioned above, the absorption bands at 1540, 1280, 1145, and 1075  $\text{cm}^{-1}$  are considered to be ascribed to  $(\text{C}=\text{N})_n$ .

A pronounced difference between the spectrum *A* in Figure 4 and the spectrum *B* in Figure 6 is that the latter has a weaker absorption at around 1075  $\text{cm}^{-1}$ ; in addition, there are differences in intensity of the absorption due to nitrile, methyl, and methylene stretching vibrations.

**Treatment by Diethylmagnesium.** Figure 7 shows the infrared spectrum for the polymethacrylonitriles treated with diethylmagnesium at 70 and 0°C in toluene. Spectrum *B* in Figure 7 is quite similar to that of the polymer catalyzed by diethylmagnesium and terminated by  $\text{CH}_3\text{OH}-\text{CH}_3\text{COOH}$ , as shown in Figure 4*A*, except for the absorption bands due to  $\text{C}=\text{N}$  stretching vibrations at 2240  $\text{cm}^{-1}$  and methyl and methylene stretching vibrations at 2960 and 2870  $\text{cm}^{-1}$ . A great decrease of the absorption

at  $2240\text{ cm}^{-1}$  (Fig. 7) shows that the nitrile of the polymer underwent a chemical change on treatment with diethylmagnesium, and the change in intensity at  $2960$  and  $2870\text{ cm}^{-1}$  shows that the ethyl groups were introduced into the polymer by this treatment. It should be noted that the polymethacrylonitrile treated by diethylmagnesium at  $0^\circ\text{C}$  shows no ap-

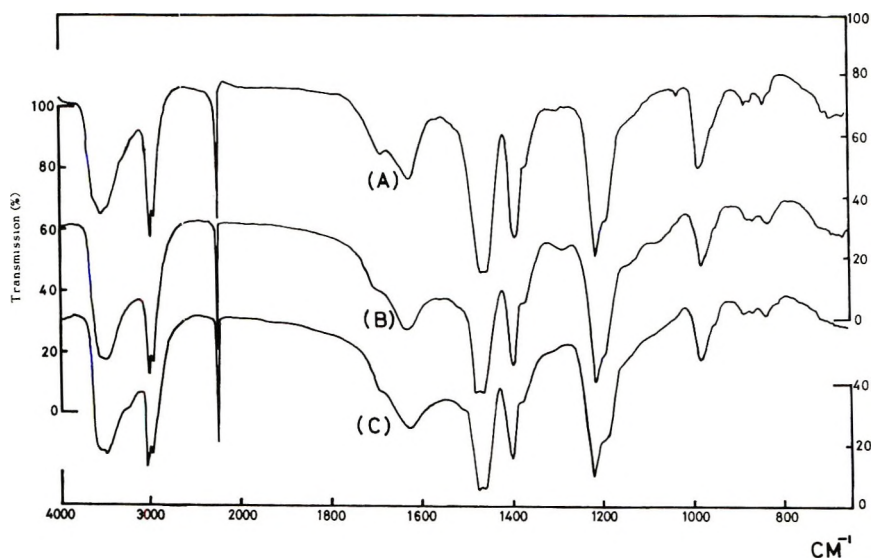


Fig. 5. Infrared spectra for polymethacrylonitriles: (A) original polymer; (B) polymer treated with 28% aqueous  $\text{NH}_3$  at room temperature for 48 hr; (C) sample B treated with  $\text{CH}_3\text{OH-HCl}$ .

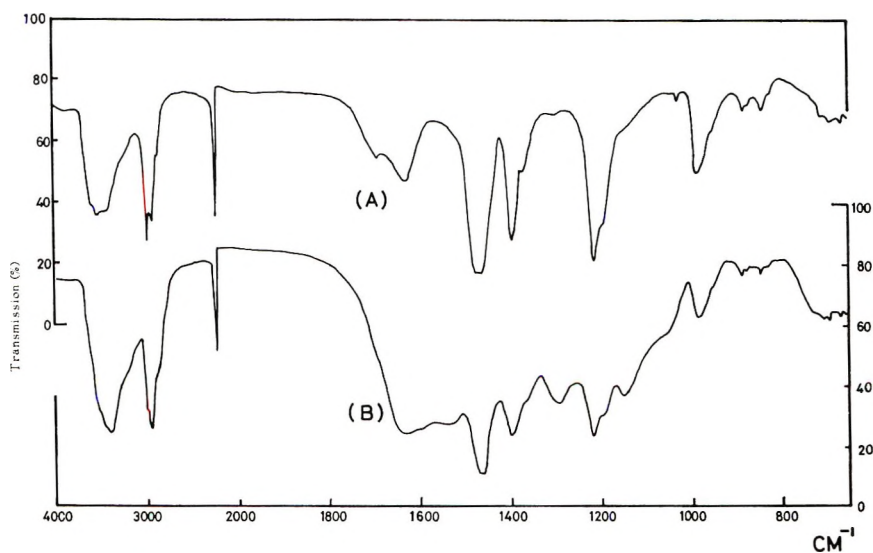


Fig. 6. Infrared spectra of polymethacrylonitriles: (A) original polymer; (B) polymer treated with  $n$ -butyllithium at  $70^\circ\text{C}$  for 2 hr.

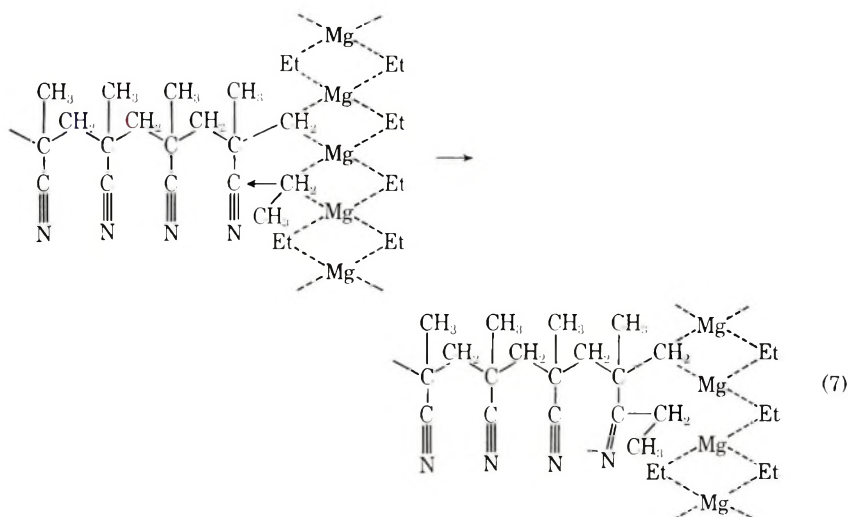


result shows the reaction between the nitrile and diethyl magnesium stopped at the stage shown in eq. (6) at 0°C.

Thus although on this evidence the formation of carbonyl by the reaction between nitrile groups and diethylmagnesium seems possible, it is eliminated by the experimental fact, illustrated in Figure 3, that the polymer obtained at high temperature has a lower carbonyl content.

As carefully discussed above, the cyclic conjugated imine structure after polymerization is certainly present.

The cyclic conjugated imine during the polymerization might be formed by other routes. Diethylmagnesium<sup>22</sup> would be present in the reaction medium in a polymeric form with a tetrahedral arrangement of four ethylene groups around magnesium atom, and the propagating chain end might be simply visualized as shown in eq. (7).



The cyclization reaction might be initiated through eq. (7), which involves no cyclic termination of the propagating chain. However, if  $(C=N)_n$  were formed in this monomer, the content of  $(C=N)_n$  and the subsequent formation of the carbonyl should be higher at higher temperatures.

Thus this route can be eliminated from the incompatibility with the experimental data in Figure 3.

Putting all the experimental results and discussions together, the route for carbonyl formation involving hydrolysis of  $(C=N)_n$  seems to be the most probable explanation. The infrared spectrum after polymerization shown in Figure 4 A has a strong peak at around  $1075\text{ cm}^{-1}$ . This suggests the presence of  $C=NH$  groups in addition to the cyclic conjugated imine structure.

The  $C=NH$  group would form  $C=O$  group by acid hydrolysis. The presence of a small amount of ketone carbonyl was suggested in the infrared spectra of the crystalline polymethacrylonitrile which were treated by HCl-acidified methanol, namely, a trail of the absorption at  $1969\text{ cm}^{-1}$

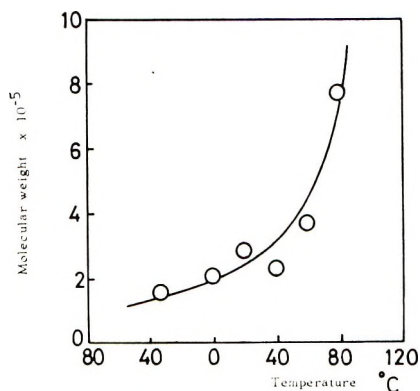


Fig. 8. Influence of polymerization temperature on the molecular weight of the polymer obtained with diethylmagnesium catalyst.

towards  $1720\text{ cm}^{-1}$  was observed in the infrared spectra shown in Figures 1A and 4B.

When the  $\text{C}=\text{N}^-$  was once formed by the cyclic termination, a successive cyclization reaction would occur faster at higher temperature. The experimental fact that the polymer obtained at higher temperature has less carbonyl content indicates that the activation energy of the propagation is considerably higher than that of the monomolecular termination. This is fully substantiated by the fact that the molecular weight of the

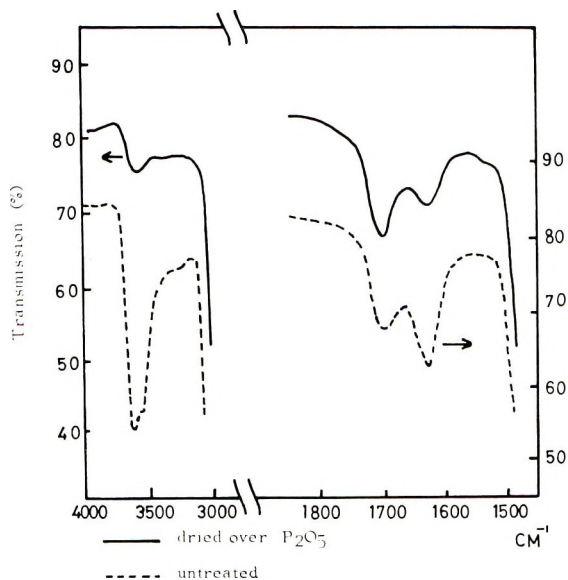


Fig. 9. Infrared spectra for polymethacrylonitrile (—) dried over  $\text{P}_2\text{O}_5$  and (---) untreated polymer.

polymers increased markedly with increasing polymerization temperature, as shown in Figure 8.

All the crystalline polymethacrylonitriles obtained by the various stereospecific catalysts have the carbonyl in the polymers. The formation mechanism by other stereospecific catalysts is probably the same as in the case of diethylmagnesium catalyst.

### Other Comments on the Infrared Spectra

The absorption at around  $1620\text{ cm}^{-1}$  for polymethacrylonitrile has been ascribed to the cyclic conjugated imines,<sup>17,20,21</sup> but as we briefly reported,<sup>5</sup> the band at  $1630\text{ cm}^{-1}$  is certainly due to water retained in the polymer.

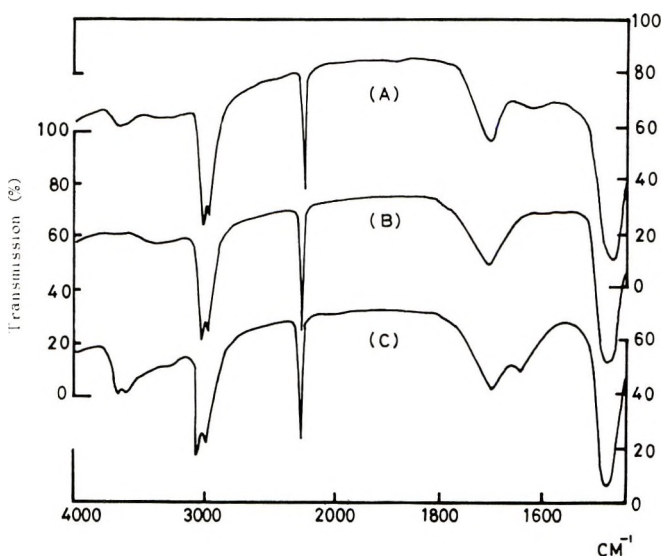


Fig. 10 Infrared spectra for polymethacrylonitriles: (A) sample B (below) after standing at ambient conditions for 2 hr; (B) spectrum taken at  $90^{\circ}\text{C}$ ; (C) spectrum taken at room temperature.

The absorption along with the absorption at  $3500\text{ cm}^{-1}$  decreased on drying the sample over  $\text{P}_2\text{O}_5$ , as shown in Figure 9. Additional evidence was given by the spectra of Figure 10, in which the absorption at  $1620\text{ cm}^{-1}$  and at  $3500\text{ cm}^{-1}$  completely disappeared at  $90^{\circ}\text{C}$  and appeared again after the polymer was allowed to stand at ambient conditions. Crystalline-sensitive bands for the isotactic polymethacrylonitrile are seen in the spectrum of Figure 1A at 1370, 1192, 1025, 910, 882, 873, 839, 711, and  $690\text{ cm}^{-1}$ .

### CONCLUSION

The formation of the carbonyl during the stereospecific polymerization of methacrylonitrile by diethylmagnesium was carefully studied by the infrared spectroscopy.

It was concluded that the most probable explanation for carbonyl formation is that imino anion formed by the monomolecular termination of the propagating chain end in a cyclization reaction successively attacked the vicinal nitrile in the chain so as to form cyclic conjugated imines which were hydrolyzed to acid amides.

### References

1. Y. Joh, T. Yoshihara, Y. Kotake, F. Ide, and K. Nakatsuka, *J. Polym. Sci. B*, **3**, 933 (1965).
2. Y. Joh, T. Yoshihara, Y. Kotake, F. Ide, and K. Nakatsuka, *J. Polym. Sci. B*, **4**, 673 (1966).
3. Y. Kotake, T. Yoshihara, H. Sato, N. Yamada, and Y. Joh, *J. Polym. Sci. B*, **5**, 163 (1967).
4. T. Yoshihara, Y. Kotake, and Y. Joh, *J. Polym. Sci. B*, **5**, 459 (1967).
5. Y. Joh, Y. Kotake, T. Yoshihara, F. Ide, and K. Nakatsuka, *J. Polym. Sci. A-1*, **5**, 593 (1967).
6. Y. Joh, Y. Kotake, T. Yoshihara, F. Ide, and K. Nakatsuka, *J. Polym. Sci. A-1*, **5**, 605 (1967).
7. Y. Joh, T. Yoshihara, Y. Kotake, Y. Imai, and S. Kurihara, *J. Polym. Sci. A-1*, **5**, 2503 (1967).
8. C. G. Swain, *J. Amer. Chem. Soc.*, **69**, 2306 (1947).
9. A. Ottolenghi and A. Zilkha, *J. Polym. Sci. A*, **1**, 687 (1963).
10. F. J. Glavis, *J. Polym. Sci.*, **36**, 547 (1959).
11. C. B. Chapman, *J. Polym. Sci.*, **45**, 238 (1960).
12. G. Smets and W. DeLoecker, *J. Polym. Sci.*, **45**, 461 (1960).
13. E. Gaetjens and H. Morawetz, *J. Amer. Chem. Soc.*, **83**, 1738 (1961).
14. K. Butler, P. R. Thomas, and G. J. Tyler, *J. Polymer Sci.*, **48**, 357 (1960).
15. G. Natta, and G. Dall'Asta, *Chim. Ind. (Milan)*, **46**, 1429 (1964).
16. N. Grassie, and I. C. McNeil, *J. Chem. Soc.*, **1956**, 3929.
17. N. Grassie and I. C. McNeil, *J. Polym. Sci.*, **27**, 207 (1958).
18. N. Grassie and I. C. McNeil, *J. Polym. Sci.*, **33**, 171 (1958).
19. N. Grassie, *J. Polym. Sci.*, **48**, 79 (1960).
20. C. G. Overberger, E. M. Pearce, and N. Mayes, *J. Polym. Sci.*, **34**, 109 (1959).
21. C. G. Overberger, H. Yuki, and N. Urakawa, *J. Polym. Sci.*, **45**, 127 (1960).
22. E. Weiss, *J. Organometal. Chem.*, **4**, 101 (1965).

Received December 1, 1969

Revised December 31, 1969

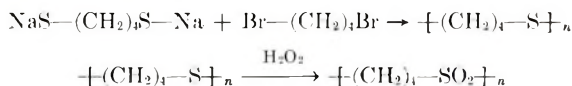


## NOTE

***Diene Polysulfones. I. Structure of the Butadiene-Sulfur Dioxide Copolymer***

The copolymer of butadiene and sulfur dioxide was first described by Staudinger and Ritzenthaler<sup>1</sup> in 1935, and has since been studied by several investigators.<sup>2-5</sup> These studies have established that the product obtained from butadiene and sulfur dioxide over a broad range of temperatures and compositions of starting materials always has a 1:1 butadiene/sulfur dioxide ratio, indicating a regular alternating 1:1 copolymer.

However, the exact mode of enchainment of the butadiene has not been clearly defined, apparently because of the intractable nature of the polymer. A 1,4-structure was proposed, without proof, in 1955 by Grouch and Wicklatz.<sup>2</sup> Two years later, Naylor and Anderson<sup>4</sup> suggested, on the basis of the polymer's infrared spectrum that, "the structure of the butadiene-sulfur dioxide copolymer was perhaps as high as 95% 1,4-adduct." We now want to report that we have confirmed the 1,4-structure of the copolymer by hydrogenation and comparison with a polytetramethylene sulfone prepared by the following unambiguous route.<sup>6</sup>



The 1:1 copolymer of butadiene and sulfur dioxide was prepared by emulsion polymerization at 38°C, using Duponol ME as emulsifier and ammonium nitrate as the initiator. This polymer is insoluble in all common solvents; the lack of solubility can be ascribed to the high degree of crystallinity (as shown by the x-ray diffraction pattern) and to the high melting point (>300°C). It can be dissolved, however, in phenolic solvents at elevated temperatures. We used *p*-chlorophenol, in which the polymer swells sufficiently at 120°C to permit hydrogenation with the soluble tris(triphenylphosphine)-rhodium chloride as catalyst.\* The hydrogenated polymer is soluble in *p*-chlorophenol at this temperature.

The hydrogenated polymer is recovered from *p*-chlorophenol solution by addition of methanol. It has a melting point of 285°C, the same as that of the poly(tetramethylene sulfone) prepared via the polythioether. The essentially complete hydrogenation of the unsaturated polymer is evidenced by the disappearance of the infrared absorption band at 975 cm<sup>-1</sup> (Fig. 1) due to the 1,4-*trans* double bond. Comparison of the infrared spectra of the hydrogenated polymer and the poly(tetramethylene sulfone) obtained from the oxidation of poly(tetramethylene sulfide) (Figs. 2 and 3) indicates that the two polymers have identical structures. In addition, the NMR spectrum of the hydrogenated polymer, as that of the other poly(tetramethylene sulfone), shows only two absorption peaks at 2.9 ppm and 1.7 ppm, which are indicative of the protons adjacent to the sulfur dioxide group, and the protons on the two central carbons, respectively. The absorption peaks characteristic for the unsaturated polysulfone cannot be detected.

The thermal stability of the polymer was improved considerably by hydrogenation. Figure 4 shows the thermogravimetric curves for the unhydrogenated polymer, the hydrogenated polymer, and the poly(tetramethylene sulfone) prepared via the polythioether route. As can be seen, the thermal stability of the hydrogenated polysulfone actually exceeds that of the polymer derived from the polythioether. We believe that

\* Suggested and prepared by K. C. Dewhirst of these laboratories.<sup>6</sup>

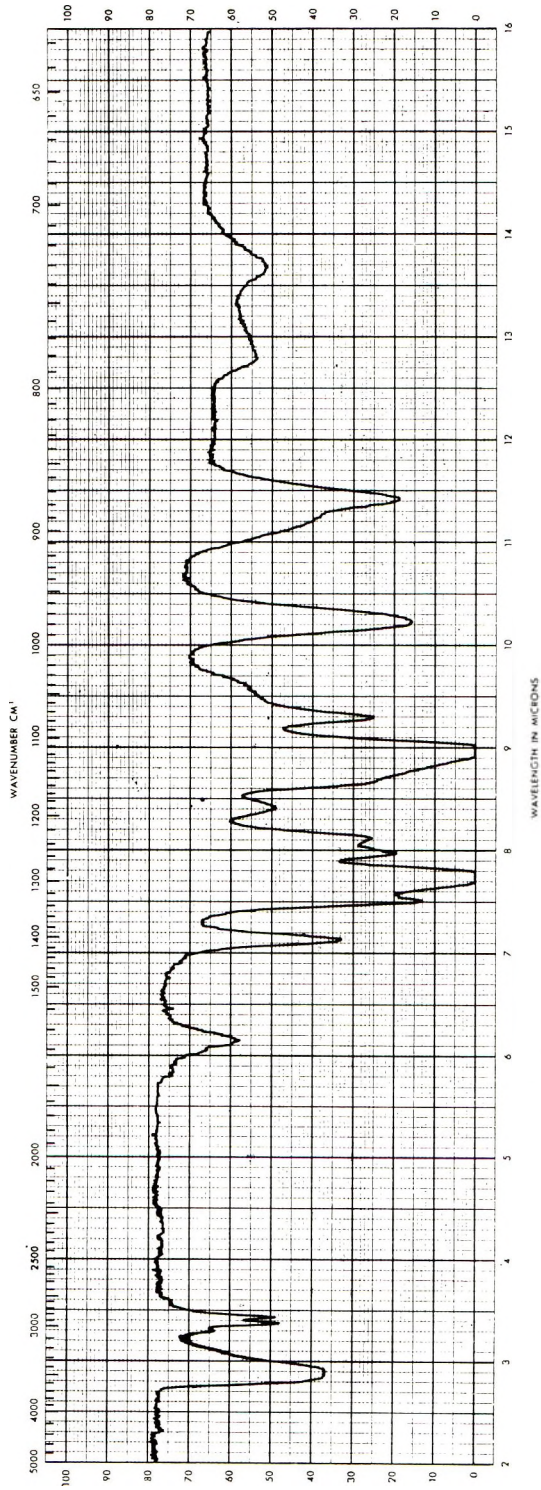


Fig. 1. Infrared spectrum of the butadiene-SO<sub>2</sub> copolymer. Run in KBr.

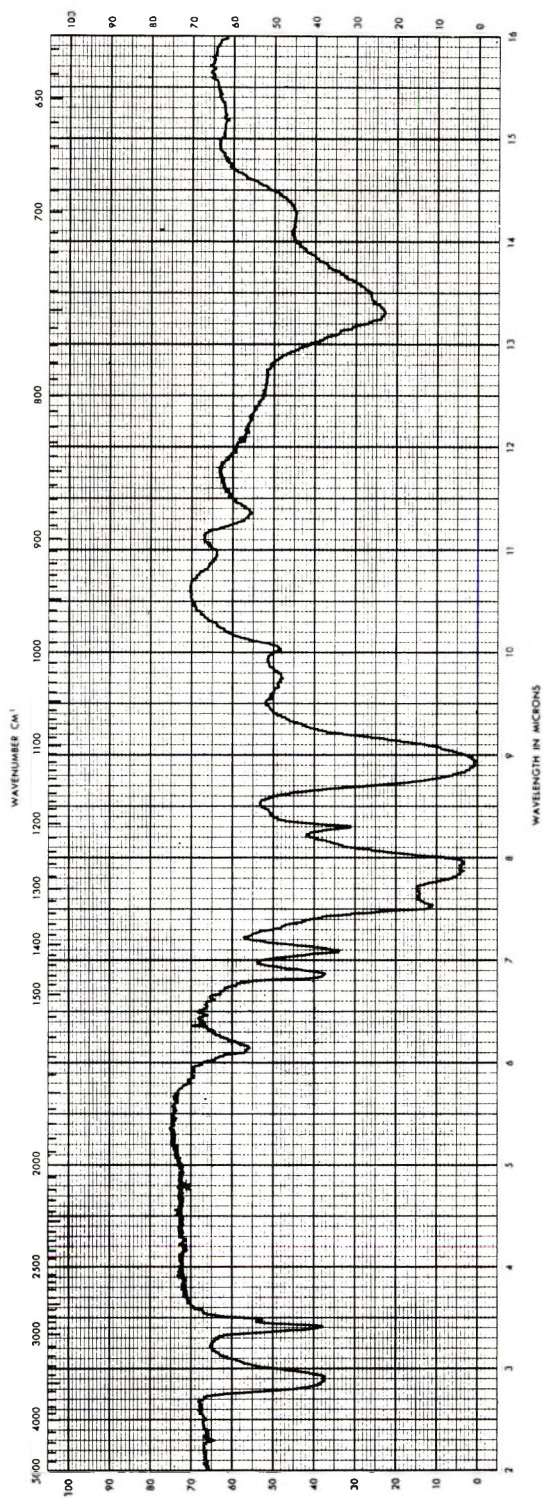


Fig. 2. Infrared spectrum of the hydrogenated butadiene-SO<sub>2</sub> copolymer. Run in KBr.

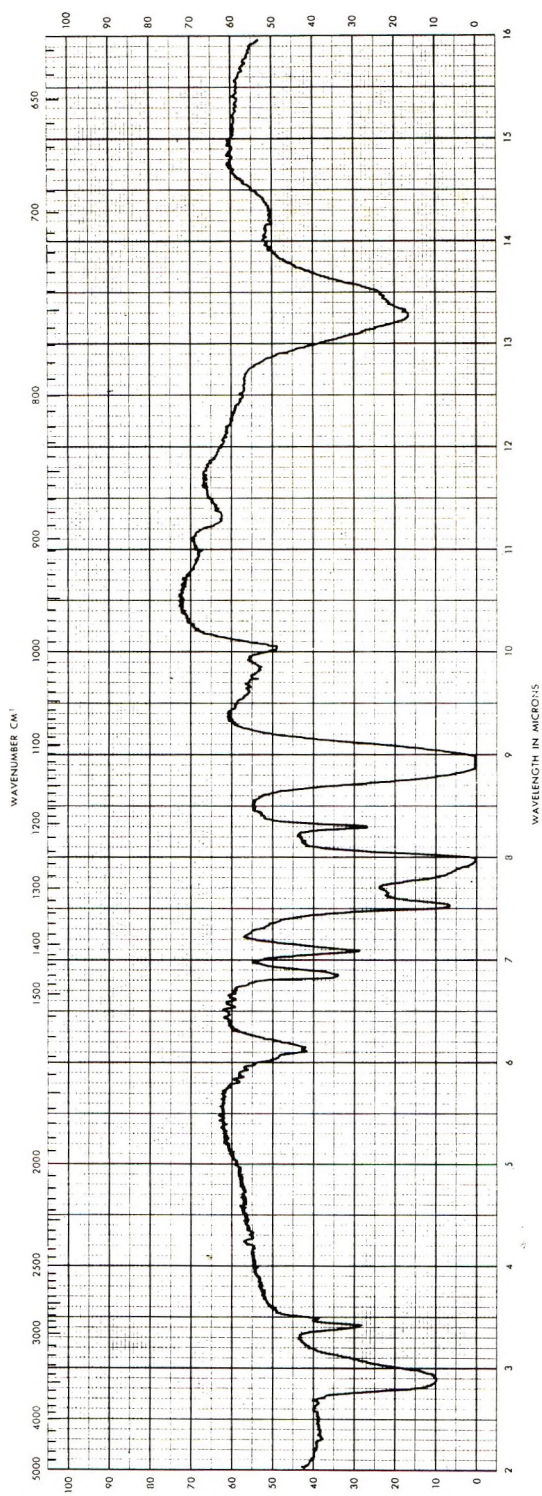


Fig. 3. Infrared spectrum of poly(tetramethylene sulfone) obtained by the oxidation of poly(tetramethylene sulfide). Run in KBr.

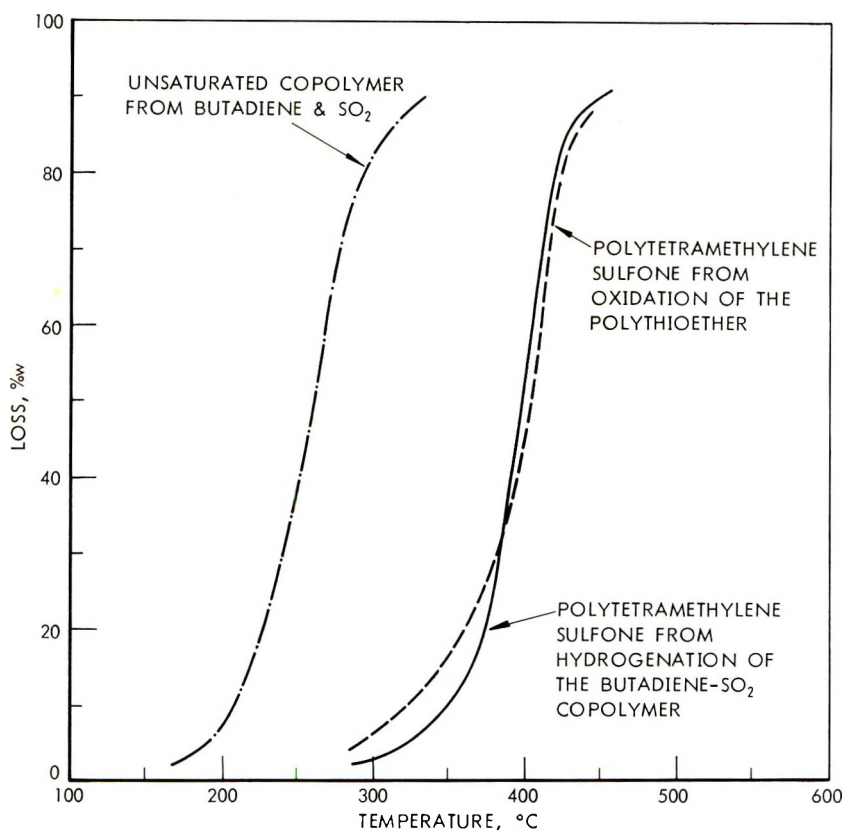


Fig. 4. Thermogravimetric curves for poly(tetramethylene sulfone) obtained by oxidation of the polythioether and by hydrogenation of the butadiene- $\text{SO}_2$  copolymer compared with that for the unsaturated polymer from butadiene and  $\text{SO}_2$ . Heating rate =  $2.5^\circ\text{C}/\text{min}$ .

the higher initial rate of degradation of the latter is due to sulfoxide groups which are likely to be present because the oxidation of the polythioether is in part heterogeneous<sup>7</sup> and therefore difficult to carry to completion.

## References

1. H. Staudinger and B. Ritzenthaler, *Ber.*, **68**, 455 (1935).
2. W. W. Crouch and J. E. Wicklatz, *Ind. Eng. Chem.*, **47**, 160 (1955).
3. H. M. d'Emaus, B. G. Bray, J. J. Martin, and L. C. Anderson, *Ind. Eng. Chem.*, **49**, 1891 (1957).
4. M. A. Naylor and A. W. Anderson, *J. Amer. Chem. Soc.* **76**, 3962 (1954).
5. J. J. Kearney, V. Stannett, and H. G. Clark, in *Macromolecular Chemistry, Prague 1965* (*J. Polym. Sci. C*, **16**), O. Wichterle and B. Sedláček, Eds., Interscience, New York, 1968, p. 3441.
6. This compound has been obtained independently by several workers: K. C. Dewhirst, U. S. Patent 3,489,786, Jan. 13, 1970; M. A. Bennett and P. A. Longstaff, *Chem. Ind. (London)*, 846 (1956); J. F. Young, J. A. Osborn, F. H. Jardine, and G.

Williamson, *Chem. Commun.*, 131 (1965); L. Vaska and R. E. Rhodes, *J. Amer. Chem. Soc.*, **87**, 4970 (1965).

7. H. D. Noether, *Text. Res. J.*, **28**, 533 (1958).

R. S. BAUER  
H. E. LUNK  
E. A. YOUNGMAN

Shell Development Company  
Emeryville, California 94608

Received October 24, 1969

Revised January 19, 1970

*Contents (continued)*

MICHAEL M. O'MARA: High-Temperature Pyrolysis of Poly(vinyl chloride): Gas Chromatographic-Mass Spectrometric Analysis of the Pyrolysis Products from PVC Resin and Plastisols.....	1887
YASUSHI JOH, TOSHIO YOSHIHARA, SEIKI KURIHARA, TOSHIO SAKURAI, and TATSUNORI TOMITA: Stereospecific Polymerization of Methacrylonitrile. V. Formation of the Carbonyl in the Polymer.....	1901
NOTE	
R. S. BAUER, H. E. LUNK, and E. A. YOUNGMAN: Diene Polysulfones. I. Structure of the Butadiene-Sulfur Dioxide Copolymer.....	1915

The *Journal of Polymer Science* publishes results of fundamental research in all areas of high polymer chemistry and physics. The *Journal* is selective in accepting contributions on the basis of merit and originality. It is not intended as a repository for unevaluated data. Preference is given to contributions that offer new or more comprehensive concepts, interpretations, experimental approaches, and results. Part A-1 *Polymer Chemistry* is devoted to studies in general polymer chemistry and physical organic chemistry. Contributions in physics and physical chemistry appear in Part A-2 *Polymer Physics*. Contributions may be submitted as full-length papers or as "Notes." Notes are ordinarily to be considered as complete publications of limited scope.

Three copies of every manuscript are required. They may be submitted directly to the editor: For Part A-1, to C. G. Overberger, Department of Chemistry, University of Michigan, Ann Arbor, Michigan 48104; and for Part A-2, to T. G. Fox, Mellon Institute, Pittsburgh, Pennsylvania 15213. Three copies of a short but comprehensive synopsis are required with every paper; no synopsis is needed for notes. Books for review may also be sent to the appropriate editor. Alternatively, manuscripts may be submitted through the Editorial Office, c/o H. Mark, Polytechnic Institute of Brooklyn, 333 Jay Street, Brooklyn, New York 11201. All other correspondence is to be addressed to Periodicals Division, Interscience Publishers, a Division of John Wiley & Sons, Inc., 605 Third Avenue, New York, New York 10016.

Detailed instructions in preparation of manuscripts are given frequently in Parts A-1 and A-2 and may also be obtained from the publisher.

# Selected Titles in Molecular Composition from Wiley-Interscience

## TESTING OF POLYMERS Volume 4

Edited by William E. Brown, *The Dow Chemical Company*

"... this volume is a stimulating addition to the library of those familiar with polymer testing as well as those who have but little experience and wish to learn more. The fourth volume is a worthy member of the *Testing of Polymers* series."—K. B. Goldblum, *General Electric Co.*

Volume 4 of *Testing of Polymers* deals principally in tests for engineering analysis and design and the theoretical foundations for certain prominent aspects of mechanical and chemical behavior. Topics from the eight contributors include: deformation data, tensile creep testing, adhesion tests, fatigue measurements, and exposure testing. Prediction techniques for mechanical and chemical behavior, and the development of rubber components from tests on models, are also considered.

### CONTENTS:

Deformation Data for Engineering Design—*S. Turner*. Experimental Technique in Uniaxial Tensile Creep Testing—*D. A. Thomas* and *S. Turner*. Prediction Techniques for Mechanical and Chemical Behavior—*S. Goldfein*. Development of Rubber Components from Tests on Models—*R. E. Morris*. Tests for Adhesion of Polymers—*J. J. Bikerman*. Fatigue in Polymers—*E. H. Andrews*. Theoretical Stress Analysis—*I. M. Daniel*. Measurement of Tensile Properties of Polymers—*W. D. Harris*. Appendices. Author Index. Subject Index.

1969 480 pages \$22.50

## STATISTICAL MECHANICS OF CHAIN MOLECULES

By P. J. Flory, *Stanford University*

New methods for discerning the equilibrium properties of chain molecules developed by the author and his collaborators during the past five years are presented in this volume. These methods for evaluating statistical mechanical averages of the moments of the chain vector distribution and of related invariants are logically and coherently presented. Derivations are given in full with utmost mathematical simplicity. Artificial models so much in use for this purpose can now be abandoned in favor of a more realistic approach.

### CONTENTS:

Analysis of the Spatial Configurations of Chain Molecules and Treatment of Simplified Model Chains. Random Coil Configurations and Their Experimental Characterization. Configurational Statistics of Chain Molecules with Interdependent Rotational Potentials. Moments of Chain Molecules. Symmetric Chains. Asymmetric Vinyl Chains. Polypeptides, Proteins, and Analogs. The Statistical Distribution of Configurations. Optical Properties and Radiation Scattering. Appendix A. The Theorem of Lagrange. Appendix B. The Axis Transformation Matrix  $T_i$  Relating Coordinate Systems of Consecutive Skeletal Bonds and Diagonalization of its Average for Bonds Subject to Independent Rotational Potentials. Appendix C. An Alternative Reduction of the Configuration Partition Function. Appendix D. Macrocyclization Equilibrium. Appendix E. Expansion of the Chain Vector Distribution Function in Hermite Polynomials. Appendix F. The Chain Vector Distribution of Freely Jointed Chains. Appendix G. The Porod-Kratky Chain. Appendix H. The Average Orientation of a Vector within a Chain of Specified End-to-End Vector  $r$ . Glossary of Principal Symbols. Author Index. Subject Index.

1969 432 pages \$17.50



WILEY-INTERSCIENCE

a division of JOHN WILEY & SONS, Inc.

605 Third Avenue • New York, N. Y. 10016

In Canada: 22 Worcester Road, Rexdale, Ontario